frontiers | Research Topics

EEG / MEG based diagnosis for psychiatric disorders

Edited by
Junpeng Zhang, Jing Xiang and Lizhu Luo

Published in
Frontiers in Psychiatry
Frontiers in Human Neuroscience

ISSN 1664-8714
ISBN 978-2-83251-565-5
DOI 10.3389/978-2-83251-565-5

About Frontiers

Frontiers is more than just an open access publisher of scholarly articles: it is a pioneering approach to the world of academia, radically improving the way scholarly research is managed. The grand vision of Frontiers is a world where all people have an equal opportunity to seek, share and generate knowledge. Frontiers provides immediate and permanent online open access to all its publications, but this alone is not enough to realize our grand goals.

Frontiers journal series

The Frontiers journal series is a multi-tier and interdisciplinary set of open-access, online journals, promising a paradigm shift from the current review, selection and dissemination processes in academic publishing. All Frontiers journals are driven by researchers for researchers; therefore, they constitute a service to the scholarly community. At the same time, the *Frontiers journal series* operates on a revolutionary invention, the tiered publishing system, initially addressing specific communities of scholars, and gradually climbing up to broader public understanding, thus serving the interests of the lay society, too.

Dedication to quality

Each Frontiers article is a landmark of the highest quality, thanks to genuinely collaborative interactions between authors and review editors, who include some of the world's best academicians. Research must be certified by peers before entering a stream of knowledge that may eventually reach the public - and shape society; therefore, Frontiers only applies the most rigorous and unbiased reviews. Frontiers revolutionizes research publishing by freely delivering the most outstanding research, evaluated with no bias from both the academic and social point of view. By applying the most advanced information technologies, Frontiers is catapulting scholarly publishing into a new generation.

What are Frontiers Research Topics?

Frontiers Research Topics are very popular trademarks of the *Frontiers journals series*: they are collections of at least ten articles, all centered on a particular subject. With their unique mix of varied contributions from Original Research to Review Articles, Frontiers Research Topics unify the most influential researchers, the latest key findings and historical advances in a hot research area.

Find out more on how to host your own Frontiers Research Topic or contribute to one as an author by contacting the Frontiers editorial office: frontiersin.org/about/contact

EEG / MEG Based diagnosis for psychiatric disorders

Topic editors

Junpeng Zhang — Sichuan University, China

Jing Xiang — Cincinnati Children's Hospital Medical Center, United States

Lizhu Luo — University of Electronic Science and Technology of China, China

Citation

Zhang, J., Xiang, J., Luo, L., eds. (2023). *EEG / MEG based diagnosis for psychiatric disorders*. Lausanne: Frontiers Media SA. doi: 10.3389/978-2-83251-565-5

Table of contents

04 Editorial: EEG/MEG based diagnosis for psychiatric disorders
Junpeng Zhang, Jing Xiang, Lizhu Luo and Rui Shui

07 Machine Learning-Based Electroencephalographic Phenotypes of Schizophrenia and Major Depressive Disorder
Kuk-In Jang, Sungkean Kim, Soo Young Kim, Chany Lee and Jeong-Ho Chae

15 EEG Microstates and Its Relationship With Clinical Symptoms in Patients With Schizophrenia
Qiaoling Sun, Jiansong Zhou, Huijuan Guo, Ningzhi Gou, Ruoheng Lin, Ying Huang, Weilong Guo and Xiaoping Wang

22 Atypical Resting State Functional Neural Network in Children With Autism Spectrum Disorder: Graph Theory Approach
Daiki Soma, Tetsu Hirosawa, Chiaki Hasegawa, Kyung-min An, Masafumi Kameya, Shoryoku Hino, Yuko Yoshimura, Sou Nobukawa, Sumie Iwasaki, Sanae Tanaka, Ken Yaoi, Masuhiko Sano, Yuka Shiota, Nobushige Naito and Mitsuru Kikuchi

36 Abnormalities in Electroencephalographic Microstates Among Adolescents With First Episode Major Depressive Disorder
Yuqiong He, Qianting Yu, Tingyu Yang, Yaru Zhang, Kun Zhang, Xingyue Jin, Shuxian Wu, Xueping Gao, Chunxiang Huang, Xilong Cui and Xuerong Luo

46 Repetitive Transcranial Magnetic Stimulation Modulates Frontal and Temporal Time-Varying EEG Network in Generalized Anxiety Disorder: A Pilot Study
Penghui Song, Han Tong, Luyan Zhang, Hua Lin, Ningning Hu, Xin Zhao, Wensi Hao, Peng Xu and Yuping Wang

53 From Sound Perception to Automatic Detection of Schizophrenia: An EEG-Based Deep Learning Approach
Carla Barros, Brian Roach, Judith M. Ford, Ana P. Pinheiro and Carlos A. Silva

70 Detection of Schizophrenia Cases From Healthy Controls With Combination of Neurocognitive and Electrophysiological Features
Qing Tian, Ning-Bo Yang, Yu Fan, Fang Dong, Qi-Jing Bo, Fu-Chun Zhou, Ji-Cong Zhang, Liang Li, Guang-Zhong Yin, Chuan-Yue Wang and Ming Fan

80 Bibliometric Analysis of Quantitative Electroencephalogram Research in Neuropsychiatric Disorders From 2000 to 2021
Shun Yao, Jieying Zhu, Shuiyan Li, Ruibin Zhang, Jiubo Zhao, Xueling Yang and You Wang

96 Predictions of tDCS treatment response in PTSD patients using EEG based classification
Sangha Kim, Chaeyeon Yang, Suh-Yeon Dong and Seung-Hwan Lee

frontiers | Frontiers in Human Neuroscience

TYPE Editorial
PUBLISHED 02 November 2022
DOI 10.3389/fnhum.2022.1061176

OPEN ACCESS

EDITED AND REVIEWED BY
Mingzhou Ding,
University of Florida, United States

*CORRESPONDENCE
Junpeng Zhang
junpeng.zhang@gmail.com

SPECIALTY SECTION
This article was submitted to Brain Imaging and Stimulation, a section of the journal Frontiers in Human Neuroscience

RECEIVED 04 October 2022
ACCEPTED 20 October 2022
PUBLISHED 02 November 2022

CITATION
Zhang J, Xiang J, Luo L and Shui R (2022) Editorial: EEG/MEG based diagnosis for psychiatric disorders. *Front. Hum. Neurosci.* 16:1061176. doi: 10.3389/fnhum.2022.1061176

Editorial: EEG/MEG based diagnosis for psychiatric disorders

Junpeng Zhang[1]*, Jing Xiang[2], Lizhu Luo[3] and Rui Shui[1]

[1]Department of Automation, College of Electrical Engineering, Sichuan University, Chengdu, China, [2]Departments of Pediatrics and Neurology, Cincinnati Children's Hospital Medical Center, Cincinnati, OH, United States, [3]School of Life Science and Technology, University of Electronic Science and Technology of China, Chengdu, China

KEYWORDS

psychiatric disorders, magnetoencephalography (MEG), EEG, machine learning, artificial intelligence

Editorial on the Research Topic
EEG/MEG based diagnosis for psychiatric disorders

For a long time, the diagnosis and evaluation of psychiatric disorders are mainly based on clinical symptoms and signs, but the understanding of the etiology and pathogenesis of these psychiatric disorders such as schizophrenia and depression is still not completely clear. At present, there is a lack of objective neurobiological markers that can be used in clinical routine work such as clinical diagnosis, curative effect evaluation and prognosis evaluation of psychiatric disorders. Therefore, it is of great clinical significance to find biomarkers to improve the diagnosis level and evaluate the curative effect. Electroencephalogram (EEG) is a non-invasive technique to record the potential activity of biological brain, through which researchers can analyze the mechanisms underlying psychiatric disorders. In addition, machine learning can be used to further verify the role of these electrophysiological indicators in clinical diagnosis and curative effect evaluation of psychiatric disorders. The goal of this Research Topic is to advance research on neurobiomarkers and EEG/MEG-based diagnostic methods for mental disorders. We hope to conduct in-depth research on the pathogenesis and diagnostic measures of mental diseases such as schizophrenia and depressive disorder through EEG/MEG, in order to improve the performance of artificial intelligence for mental diseases diagnosing. Under this research theme, the following is a brief overview of nine published articles, which, respectively, studied the diagnosis, treatment, and future research of psychiatric disorders by using EEG/MEG.

In this issue, some work are about the research of diagnosis methods of mental disorders. The paper titled "Machine Learning-Based Electroencephalographic Phenotypes of Schizophrenia and Major Depressive Disorder" by Jang et al. investigates brain phenotyping in patients with schizophrenia (SZ) and major depressive disorder (MDD) using EEG and conducted machine-learning-based classification of the two diseases, using these EEG components.

Although EEG microstates have been suggested as a potential endophenotype for schizophrenia, no clear dynamic pattern of microstates has been found. The paper titled "EEG Microstates and Its Relationship With Clinical Symptoms in Patients With Schizophrenia" by Sun et al. demonstrates that patients with schizophrenia have abnormal EEG microstates, especially the microstate class C, through the method of grouping patients into subgroups according to the level of positive and negative symptoms.

Little research has explored EEG differences between adolescents with major depressive disorder (MDD) and healthy controls, particularly EEG microstates differences. The paper titled "Abnormalities in Electroencephalographic Microstates Among Adolescents With First Episode Major Depressive Disorder" by He et al. is the first study to explore the dynamic activity of resting-state large-scale brain networks among adolescents with MDD indicating that adolescents with MDD show EEG alterations in temporal scale of subsecond across the whole brain.

The paper titled "Detection of Schizophrenia Cases From Healthy Controls With Combination of Neurocognitive and Electrophysiological Features" by Tian et al. develops a comprehensive machine learning pipeline based on neurocognitive (contains seven specific areas of cognition) and electrophysiological [PPI, EEG power spectrum, detrended fluctuation analysis, and fractal dimension (FD)] features by using logistics, random forest, and extreme gradient boosting (XGBoost) algorithms and evaluated their classification capabilities separately.

Deep learning techniques have been applied to electroencephalogram (EEG) signals, with promising applications in the field of psychiatry. The paper titled "From Sound Perception to Automatic Detection of Schizophrenia: An EEG-Based Deep Learning Approach" by Barros et al. researches the altered patterns in electrical brain activity during auditory processing and their potential to discriminate schizophrenia and healthy subjects. Their results show the potential of deep learning methods in the study of impaired auditory processing in schizophrenia with implications for diagnosis.

Results of more recent studies have suggested that ASD is a dysfunction of coordination over widely distributed brain regions. To meet this challenge, the paper titled "Atypical Resting State Functional Neural Network in Children With Autism Spectrum Disorder: Graph Theory Approach" by Soma et al. examines the resting-state MEG-derived functional network in children with and without ASD using graph theory and demonstrates a difference between children with and without ASD in MEG-derived resting-state functional brain networks. Their study indicates that combining graph theory and MEG might be a promising approach to establish a biological marker for ASD.

Secondly, it is about exploring the treatment methods of these diseases. Transcranial direct current stimulation (tDCS) is an emerging therapeutic tool for treating posttraumatic stress disorder (PTSD). The paper titled "Predictions of tDCS treatment response in PTSD patients using EEG based classification" by Kim et al. investigates tDCS treatment responsiveness in patients with PTSD using EEG spectral power and machine learning-based prediction methods. These results can provide important information and provide meaningful methods for early identification of patients who may be clinically affected by tDCS treatment, thus reducing the cost and time spent by these patients in the treatment process. Their findings provide information for future research directions, and if confirmed, it is expected that they will eventually provide information for medical guidelines.

The paper titled "Repetitive Transcranial Magnetic Stimulation Modulates Frontal and Temporal Time-Varying EEG Network in Generalized Anxiety Disorder: A Pilot Study" by Song et al. investigates the effect of low-frequency rTMS targeting the right DLPFC on clinical symptoms and TMS-evoked time-varying brain network connectivity in patients with GAD. Their study demonstrates that rTMS does have potential as an effective augmentative treatment in GAD.

One of the work is about the analysis of the development status and trends of these research fields. The paper titled "Bibliometric Analysis of Quantitative Electroencephalogram Research in Neuropsychiatric Disorders From 2000 to 2020" by Yao et al. integrates bibliometric information on the current status, the knowledge base, and future directions of QEEG studies in neuropsychiatric disorders from a macroscopic perspective. It suggests that in the past 20 years, QEEG has been used to reveal the pathological mechanism of various neuropsychiatric diseases, to assist clinical diagnosis and to promote the selection of effective treatment methods. Besides, future studies should focus on cross-validation of promising QEEG biomarkers, development of noval biomarkers, and extraction of biomarkers by machine learning.

The work in this special issue may fall into three categories of research: (1) methods designed for diagnosis of psychiatric disorders; (2) methods for the treatment of psychiatric disorders; (3) trends in this field. AI techniques, including machine learning and deep learning, have been widely applied to improve diagnosis performance and treatment effectiveness. This issue will facilitate to deepen the understanding of the underlying mechanisms of psychiatric disorders from the aspects of neuroelectrophysiology and neuromagnetic-physiology with AI assistance, to improve the accuracy and convenience of treatment

and also to inspire the development of better diagnostics and treatments.

Author contributions

JZ and RS wrote the draft manuscript. JX and LL edited and improved it. All authors contributed to the article and approved the submitted version.

Funding

This work was funded by Key Project of National Science of China (No. 12126606) and Sichuan Science and Technology Agency Project (No. 21ZDYF3607).

Conflict of interest

The authors declare that the research was conducted in the absence of any commercial or financial relationships that could be construed as a potential conflict of interest.

Publisher's note

frontiers in Psychiatry

ORIGINAL RESEARCH
published: 13 October 2021
doi: 10.3389/fpsyt.2021.745458

Machine Learning-Based Electroencephalographic Phenotypes of Schizophrenia and Major Depressive Disorder

Kuk-In Jang[1], *Sungkean Kim*[2], *Soo Young Kim*[3], *Chany Lee*[1]* *and Jeong-Ho Chae*[3]*

[1] Department of Cognitive Science Research, Korea Brain Research Institute (KBRI), Daegu, South Korea, [2] Department of Human-Computer Interaction, Hanyang University, Ansan, South Korea, [3] Department of Psychiatry, College of Medicine, The Catholic University of Korea, Seoul, South Korea

OPEN ACCESS

Edited by:
Junpeng Zhang,
Sichuan University, China

Reviewed by:
Peng Xie,
Chongqing Medical University, China
Kyung Mook Choi,
Daejeon Korean Medicine Hospital of Daejeon University, South Korea

***Correspondence:**
Chany Lee
chanylee@kbri.re.kr
Jeong-Ho Chae
alberto@catholic.ac.kr

Specialty section:
This article was submitted to Neuroimaging and Stimulation, a section of the journal Frontiers in Psychiatry

Received: 22 July 2021
Accepted: 14 September 2021
Published: 13 October 2021

Citation:
Jang K-I, Kim S, Kim SY, Lee C and Chae J-H (2021) Machine Learning-Based Electroencephalographic Phenotypes of Schizophrenia and Major Depressive Disorder. Front. Psychiatry 12:745458. doi: 10.3389/fpsyt.2021.745458

Background: Psychiatric diagnosis is formulated by symptomatic classification; disease-specific neurophysiological phenotyping could help with its fundamental treatment. Here, we investigated brain phenotyping in patients with schizophrenia (SZ) and major depressive disorder (MDD) by using electroencephalography (EEG) and conducted machine-learning-based classification of the two diseases by using EEG components.

Materials and Methods: We enrolled healthy controls (HCs) ($n = 30$) and patients with SZ ($n = 34$) and MDD ($n = 33$). An auditory P300 (AP300) task was performed, and the N1 and P3 components were extracted. Two-group classification was conducted using linear discriminant analysis (LDA) and support vector machine (SVM) classifiers. Positive and negative symptoms and depression and/or anxiety symptoms were evaluated.

Results: Considering both the results of statistical comparisons and machine learning-based classifications, patients and HCs showed significant differences in AP300, with SZ and MDD showing lower N1 and P3 than HCs. In the sum of amplitudes and cortical sources, the findings for LDA with classification accuracy (SZ vs. HCs: 71.31%, MDD vs. HCs: 74.55%), sensitivity (SZ vs. HCs: 77.67%, MDD vs. HCs: 79.00%), and specificity (SZ vs. HCs: 64.00%, MDD vs. HCs: 69.67%) supported these results. The SVM classifier showed reasonable scores between SZ and HCs and/or MDD and HCs. The comparison between SZ and MDD showed low classification accuracy (59.71%), sensitivity (65.08%), and specificity (54.83%).

Conclusions: Patients with SZ and MDD showed deficiencies in N1 and P3 components in the sum of amplitudes and cortical sources, indicating attentional dysfunction in both early and late sensory/cognitive gating input. The LDA and SVM classifiers in the AP300 are useful to distinguish patients with SZ and HCs and/or MDD and HCs.

Keywords: electroencephalographic phenotyping, machine learning, auditory P300, schizophrenia, major depressive disorder

INTRODUCTION

Although psychiatric diagnosis is based on phenomenological distinction of overt features such as behavior, mood, and thought, determination of the neuropathological mechanisms with electroencephalography (EEG) remains challenging. Among the neurophysiologic phenotypes determined using EEG, there is no consistently recommended brain model for schizophrenia (SZ) and major depressive disorder (MDD). Previous EEG studies have focused on pathophysiological distinctions and symptomatic relationships (1–3). The clinical variations in SZ and MDD are very heterogeneous (4–6). Beyond clinical diagnosis based on phenomenological distinctions between SZ and MDD, the definition of EEG endophenotypes using machine learning could provide insights facilitating therapeutic breakthroughs for a variety of pathologic phenotypes (7–10). Especially, classification performance in psychiatric disorders was assured by applying linear discriminant analysis (LDA) and support vector machine (SVM) (11).

Auditory P300 (AP300) is a representative neurophysiological indicator in patients with SZ and depression (12–15); however, some studies provided inconsistent findings for this indicator in depression (16). AP300 includes the N1 and P3 components, which represent the most negative potential at around 100 ms and the most positive potential at around 300 ms following the onset of an auditory stimulus, respectively. Changes in P3 and N1 amplitudes in the midline electrodes are commonly observed (17, 18). Furthermore, the highest peak potential within defined time ranges for each component shows large variations across individuals because each component includes several neurobiological attributes (19, 20). Alternatively, the width of amplitudes within the defined time ranges can also indicate a pathological state (21).

AP300 reflects cognitive processes in auditory responses as well as working memory and attention process (22, 23). N1 has been defined as the neural allocation for early sensory input from the target stimulus (24, 25), and decreased N1 could reflect abnormal early selective attention in SZ and mood disorder (26–29). P3 is a major component of AP300 that is generated by late positive potential from information processing, such as an inputting rare event under ordinary situations (30, 31). N1 and P3 deficiencies are commonly observed in patients with SZ (32, 33). Several studies have also reported delayed latencies and decreased amplitudes of both N1 and P3 in patients with MDD (13, 34–36).

Here, we compared AP300 between healthy controls (HCs) and patients with SZ and MDD. To identify brain phenotypes of SZ and depression, changes in the N1 and P3 components were expressed in three dimensions, namely, peak with latency, sum of amplitudes, and cortical sources, by using radar charts. In addition, we applied machine learning techniques with linear discriminant analysis (LDA) and support vector machine (SVM) classifiers for each two-group classification.

MATERIALS AND METHODS

Participants

We enrolled 34 patients with SZ (13 men and 21 women), 33 patients with MDD (11 men and 22 women), and 30 HCs (15 men and 15 women). The mean ages of the participants with SZ and MDD and the HCs were 37.21 ± 14.94, 40.03 ± 11.08, and 43.63 ± 12.80 years, respectively. The ages of all participants ranged from 19 to 82 years (mean: 40.15 ± 13.19 years). Participants who had vision or hearing problems, drug and/or alcohol abuse, traumatic brain injury, and a lifetime history of neurological disorders were excluded. Healthy participants with a lifetime history of psychiatric disorders were also excluded. All participants were native Koreans diagnosed using the MINI International Neuropsychiatric Interview of the *Diagnostic and Statistical Manual of Mental Disorders, 5th Edition*. The Positive and Negative Syndrome Scale (PANSS) (37) was evaluated in patients with SZ, while the Hamilton Depression and Anxiety rating scales (HAMD and HAMA) (38, 39) were evaluated in patients with MDD. The Beck Depression Inventory (BDI) was also evaluated in patients with MDD and HCs (40). All symptomatic evaluations were performed by a trained psychiatrist. Written informed consent was obtained from all the participants. This study followed the relevant guidelines and regulations of the Institutional Review Board of Seoul St. Mary's Hospital College of Medicine, The Catholic University of Korea (approval number: KC09FZZZ0211).

EEG Measurements

All the participants were seated in a comfortable chair in a sound-attenuated room. The EEG recording was performed using the NeuroScan SynAmps amplifier (Compumedics USA, El Paso, TX, USA) with a 62-channel head cap mounted with AgCl electrodes according to the international extended 10–20 system (FP1, FPz, FP2, AF3, AF4, F7, F5, F3, F1, Fz, F2, F4, F6, F8, FT7, FC5, FC3, FC1, FCz, FC2, FC4, FC6, FT8, T7, C5, C3, C1, Cz, C2, C4, C6, T8, TP7, CP5, CP3, CP1, CPz, CP2, CP4, CP6, TP8, P7, P5, P3, P1, Pz, P2, P4, P6, P8, PO7, PO5, PO3, POz, PO4, PO6, PO8, CB1, O1, Oz, O2, and CB2). Eye movements were detected by electrooculography (EOG) sensors placed above and below the left eye and the outer canthus of both eyes. Bandpass filters ranged from 1 to 100 Hz with a sampling rate of 1000 Hz. The reference and ground channels were located on both the mastoids and forehead, respectively. The impedance was maintained below 5 kΩ during the recording session.

AP300 Protocol and Analyses

AP300 with an auditory oddball task was conducted in the response-contingent behavior paradigm comprising 200 stimuli delivered using MDR-XB500 headphones (Sony, Tokyo, Japan) at 85 dB SPL with 2,000-ms fixed inter-stimulus intervals. A total of 160 standard tones of 1,000 Hz and 40 target tones of 1,500 Hz were presented randomly. The duration of the tone was 100 ms, and the rise and fall times were 10 ms. The STIM2 system (Compumedics USA, El Paso, TX, USA) was used to synchronize

the auditory stimuli and EEG signals. All participants were instructed to press a button promptly when the target tones of 1,500 Hz were presented. A fixation cross was displayed in the middle of the screen during all recording sessions. Above 30-artifact free and -accurate epochs were used in the analyses. Gross artifacts were removed through visual inspection by a trained evaluator who had no information about the origin of the data. Artifacts related to eye blinks and/or movements were rejected in accordance with established mathematical procedures by using SCAN 4.5 and CURRY 8.0 software (41). Based on vertical EOG, positive and negative components exceeding 300 μV from the before- and after-onset stimuli (−100 to 300 ms) were rejected. The data were epoched from before-onset 100 ms to after-onset 700 ms on target stimuli. Pre-stimulus baseline correction was applied, and artifacts exceeding ±100 μV were rejected for all electrodes. The data were bandpass-filtered with a zero-phase shift ranging from 1 to 55 Hz. In the peak with latency, N1 was extracted between 50 and 150 ms post-stimulus. P3 was extracted between 250 and 500 ms. The width of the amplitudes was calculated by summation of all the amplitudes within the defined time ranges.

Cortical Source Analyses and Regions of Interest (ROIs)

Cortical source estimation was performed using standardized low-resolution brain electromagnetic tomography (sLORETA) software. Estimation of the EEG inverse problem was conducted at the cortical source regions based on the 6,239 voxels (42). The source densities of N1 and P3 were calculated using mean values within the defined time ranges. ROIs in the cortical source level were selected to examine changes in the default mode network regions and cognitive control network (43, 44). The source activities of ROIs were extracted from the mean voxel values of the selected areas. The selected 14 regions were the left/right superior frontal gyri (SFGs), left/right middle frontal gyri (MFGs), left/right medial frontal gyri (MeFGs), left/right inferior frontal gyri (IFGs), left/right superior temporal gyri (STGs), left/right inferior parietal lobes (IPLs), and left/right precuneus.

Machine Learning Analyses

Features were selected based on three dimensions: peak with latency ($n = 12$), sum of amplitudes ($n = 7$), and cortical sources ($n = 28$). Dimension-based feature selection was applied. The present study lacked a suitable sample size. Reducing dimension should be performed when the sample sizes and features were sufficiently large to secure acceptable classification performance (45). The classification accuracy, sensitivity, and specificity were evaluated using the 10-by-10-fold cross-validation technique with LDA (46) and linear SVM classifiers (47). Analysis in machine learning was conducted using MATLAB 2019 software with add on toolbox the Bioinformatics and the Statistics and Machine learning (Mathworks, Inc, USA).

Statistical Analyses

Descriptive statistics were analyzed using multivariate analysis of variance (MANOVA), chi-square test, and *t*-test, as appropriate (**Table 1**). Age, education, and accepted AP300 trials among the groups were compared using MANOVA. Differences in sex were also examined using the chi-square test. BDI scores between patients with MDD and HCs were compared using *t*-test. For multivariate analysis with covariance, 49 variables of AP300 were examined as dependent variables among all groups, with age, sex, and education as covariates. Statistical significance was set at $p < 0.05$, two-tailed. Main-effect comparison was performed using the Bonferroni correction from the original *p*-values (48). All statistical analyses were performed using IBM SPSS software (version 20.0; IBM Corp., Armonk, NY, USA).

TABLE 1 | Demographic data of the present study.

Variables	SZ ($n = 34$) (a)	MDD ($n = 33$) (b)	HCs ($n = 30$) (c)	Statistics
Age	37.21 (14.94)	40.03 (11.08)	43.63 (12.80)	f = 1.930, $p = 0.151$
Sex (m/f)	13/21	11/22	15/15	χ^2, $p = 0.387$
Education	13.21 (3.37)	13.70 (2.30)	15.27 (1.57)	f = 5.553, $p = 0.008$ a < c
Duration of illness (Missing value)	29.09 (12.11) (0)	37.29 (7.83) (26)	-	-
Positive	29.26 (6.23)	-	-	-
Negative	19.97 (7.14)	-	-	-
General	52.94 (8.66)	-	-	-
Total	102.18 (15.08)	-	-	-
HAM-D	-	20.15 (5.65)	-	-
HAM-A	-	22.48 (7.77)	-	-
BDI	-	28.06 (12.33)	9.33 (7.49)	T = 7.357, $p < 0.001$
AP300 accepted trials	37.71 (2.51)	37.27 (2.83)	37.73 (2.78)	F = 0.297, $p = 0.744$
Drug administration (*n*)	29	6	-	-
Antipsychotics				
Amisulpride	6	-	-	-
Aripiprazole	4	-	-	-
Blonanserin	1	-	-	-
Clozapine	1	-	-	-
Olanzapine	11	-	-	-
Paliperidone	5	-	-	-
Quetiapine	7	-	-	-
Risperidone	1	-	-	-
Antidepressants				
Alprazolam	-	1	-	-
Lorazepam	-	2	-	-
Mirtazapine	-	1	-	-
Paroxetine	-	1	-	-
Sertraline	-	1	-	-
Venlafaxine	-	3	-	-

RESULTS

Descriptive statistics are presented in **Table 1**. We found no significant differences in age (F = 1.930, $p = 0.151$) and sex (χ^2, $p = 0.387$) among the three groups. Level of education was

significant between patients with SZ and HCs (SZ < HCs, F = 5.553, $p = 0.008$). The BDI scores significantly differed between HCs and patients with MDD (t = 7.357, $p < 0.001$). The number of accepted AP300 trials did not differ significantly among the three groups (F = 0.297, $p = 0.744$).

The present study found significant differences in AP300 among HCs and patients with SZ and MDD [$F_{(2, 91)} = 1.704$, $p = 0.006$, $\eta^2 = 0.645$]. In the assessment of the sum of amplitudes of AP300 (**Table 2** and **Figure 1A**), significant differences were found among patients with SZ, MDD, and HCs (SZ < MDD < HCs, N1-Fz, $p < 0.001$; SZ < MDD, SZ < HCs, N1-Cz, $p = 0.005$; SZ < MDD, N1-Pz, $p < 0.037$; SZ < MDD, SZ < HC, Total value, $p = 0.014$).

On evaluating the peak with latency of AP300 (**Table 2** and **Figures 1B,C**), differences were significant (SZ < HCs, N1-Fz-Peak, $p = 0.027$; SZ < MDD, SZ < HCs, P3-Pz-Peak, $p = 0.043$). On evaluating the cortical source activities of AP300 (**Table 2** and **Figure 2**), significant differences were found (SZ < HCs, MDD < HCs, N1-R-IPL, $p = 0.012$; N1-L-Precuneus, $p = 0.004$; N1-R- Precuneus, $p < 0.001$; P3-R-STG, $p = 0.003$; P3-L-IPL, $p < 0.001$; P3-R-IPL, $p < 0.001$; P3-L-Precuneus, $p < 0.001$; P3-R-Precuneus, $p < 0.001$). There were no significant differences in the assessments of AP300 behavior. Meanwhile, correlations between clinical symptoms and AP300 were not significant (**Figure 3**).

The machine learning results with LDA and SVM are presented in **Table 3**. The results of the two-group classification are as follows:

Accuracy for sum of amplitudes: SZ vs. MDD, LDA, 59.71%, SVM, 54.48%; SZ vs. HCs, LDA, 71.31%, SVM, 57.81%; and MDD vs. HCs, LDA, 74.55%, SVM, 58.89%. Sensitivity for sum of amplitudes: SZ vs. MDD, LDA, 65.08%, SVM, 56.18%; SZ vs. HCs, LDA, 77.67%; SVM, 56.77%; and MDD vs. HCs, LDA, 79.00%, SVM, 57.58%. Specificity for sum of amplitudes: SZ vs. MDD, LDA, 54.83%, SVM, 52.73%; SZ vs. HCs, LDA, 64.00%, SVM, 59.00%; and MDD vs. HCs, LDA, 69.67%, SVM, 60.33%.

Accuracy for peak with latency: SZ vs. MDD, LDA, 55.75%, SVM, 53.88%; SZ vs. HCs, LDA, 70.74%, SVM, 67.35%; and MDD vs. HCs, LDA, 70.60%, SVM, 70.95%. Sensitivity for peak with latency: SZ vs. MDD, LDA, 57.25%, SVM, 55.00%; SZ vs. HCs, LDA, 69.42%; SVM, 70.00%; and MDD vs. HCs, LDA, 75.17%, SVM, 72.12%. Specificity for peak with latency: SZ vs. MDD, LDA, 55.00%, SVM, 52.73%; SZ vs. HCs, LDA, 72.33%; SVM, 64.33%; and MDD vs. HCs, LDA, 65.33%, SVM, 69.67%.

Accuracy for cortical sources: SZ vs. MDD, LDA, 54.28%, SVM, 54.78%; SZ vs. HCs, LDA, 65.41%, SVM, 71.88%; and MDD vs. HCs, LDA, 55.50%, SVM, 65.87%. Sensitivity for cortical sources: SZ vs. MDD, LDA, 58.25%, SVM, 66.77%; SZ vs. HCs, LDA, 69.25%, SVM, 74.41%; and MDD vs. HCs, LDA, 64.00%, SVM, 81.21%. Specificity for cortical sources: SZ vs. MDD, LDA, 50.08%, SVM, 42.42%; SZ vs. HCs, LDA, 60.67%, SVM, 69.00%; and MDD vs. HCs, LDA, 46.67%, SVM, 49.00%.

DISCUSSION

The present study demonstrated differences in AP300 between HCs and patients with SZ and MDD. AP300 with N1 deficiency in patients with SZ and MDD was predominantly found in the sum of the amplitudes. Machine learning-based classification

TABLE 2 | Comparisons of AP300 between patients and HCs.

Variables	SZ ($n = 34$)	MDD ($n = 33$)	HCs ($n = 30$)	Statistics			
	(a)	(b)	(c)	Pairwise comparison	Original p-value	Bonferroni corrected p-value	Effect size (η^2)
Sum of amplitudes							
N1-Fz	278.18 (131.35)	375.58 (137.70)	471.05 (159.07)	a < b < c	<0.001	<0.001	0.226
N1-Cz	334.39 (117.94)	449.97 (162.03)	490.52 (144.58)	a < b, a < c	<0.001	0.005	0.182
N1-Pz	294.24 (121.56)	421.81 (164.11)	354.74 (102.65)	a < b	0.001	0.037	0.146
Total	2583.68 (1114.06)	3591.49 (1583.27)	3879.94 (1245.18)	a < b, a < c	<0.001	0.014	0.165
Peak(μV) with latency (ms)							
N1-Fz-Peak	6.00 (2.50)	7.37 (2.26)	8.46 (2.65)	a < c	0.001	0.027	0.152
P3-Pz-Peak	6.88 (3.33)	8.87 (3.72)	9.95 (3.52)	a < b, a < c	0.001	0.043	0.143
Cortical sources							
N1-Right IPL	0.41 (0.38)	0.39 (0.42)	0.82 (0.67)	a < c, b < c	<0.001	0.012	0.168
N1-Left Precuneus	0.89 (0.59)	0.91 (0.96)	1.67 (1.20)	a < c, b < c	<0.001	0.004	0.187
N1-Right Precuneus	0.80 (0.51)	0.88 (0.72)	1.51 (0.97)	a < c, b < c	<0.001	<0.001	0.223
P3-Right STG	0.86(0.52)	1.29 (0.87)	1.73 (0.88)	a < c, b < c	<0.001	0.003	0.194
P3-Left IPL	0.45(0.43)	0.50 (0.45)	1.12 (0.90)	a < c, b < c	<0.001	<0.001	0.245
P3-Right IPL	0.38(0.28)	0.35 (0.31)	0.97 (0.77)	a < c, b < c	<0.001	<0.001	0.250
P3-Left Precuneus	0.91(0.65)	1.14 (1.08)	2.66 (2.12)	a < c, b < c	<0.001	<0.001	0.276
P3-Right Precuneus	0.90(0.58)	1.09 (0.98)	2.38 (1.94)	a < c, b < c	<0.001	<0.001	0.244

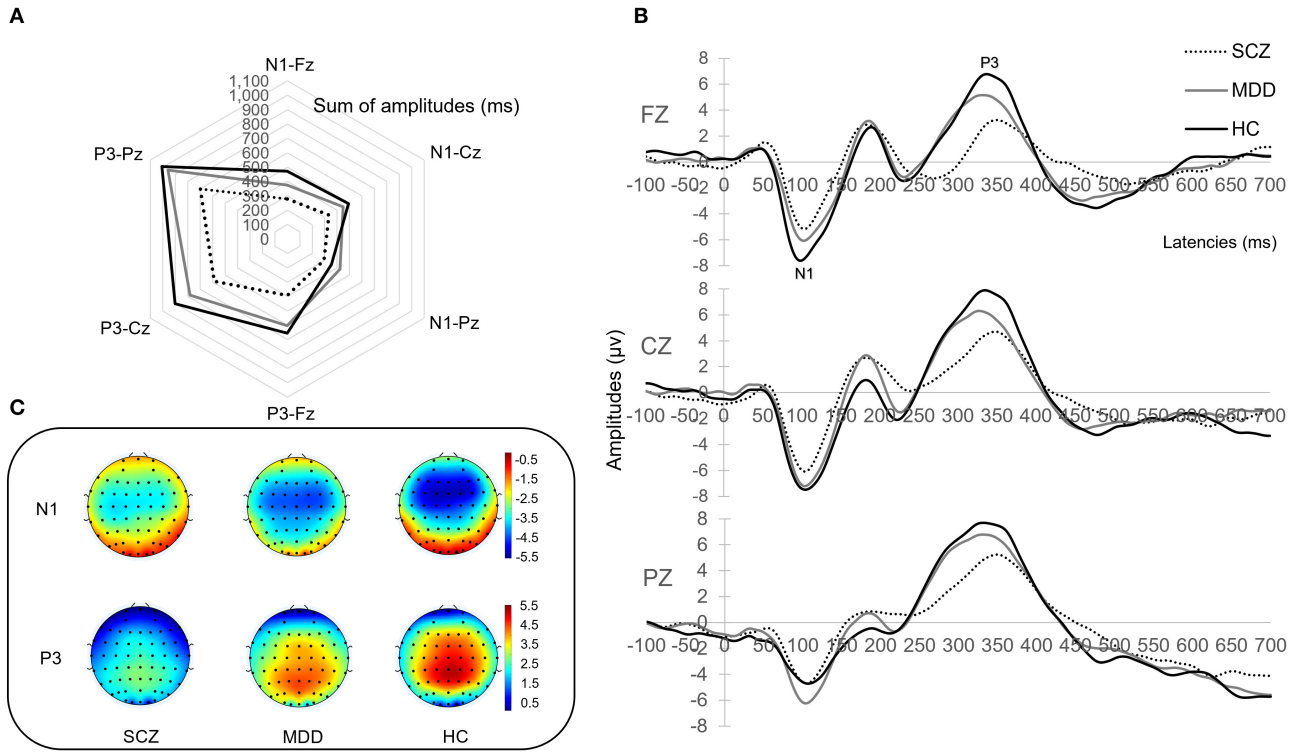

FIGURE 1 | AP300 with brain phenotyping. **(A)** is the radar chart with sum of amplitudes. **(B)** is the peak and latency. **(C)** illustrates topographical map of N1 and P3 between patients and healthy controls.

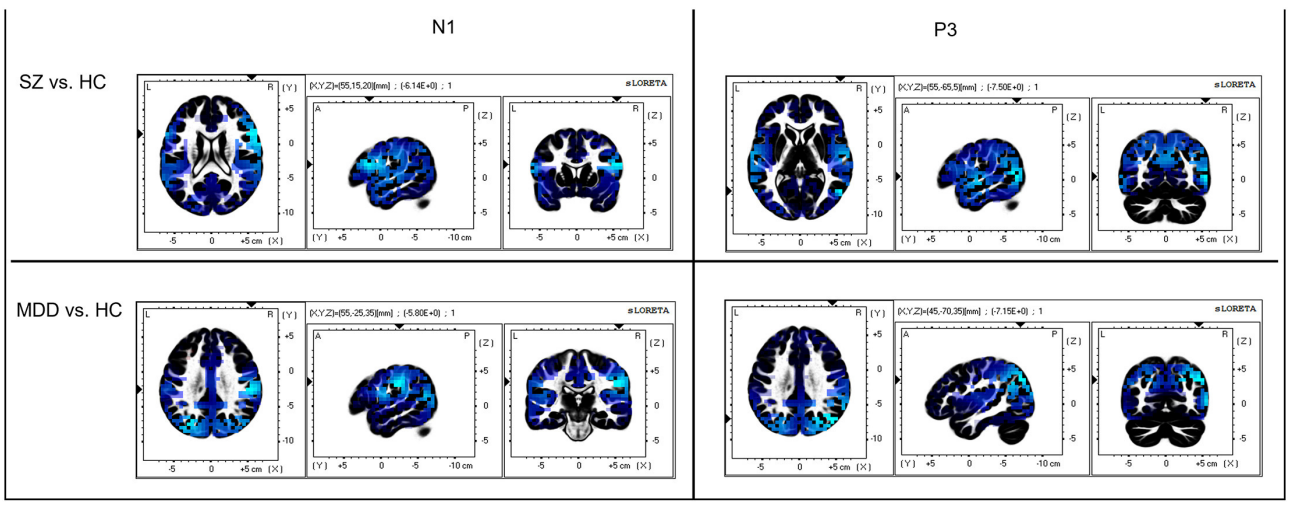

FIGURE 2 | Comparison of AP300 at cortical source level. Blue color indicates cortical source deactivations in patients, compared to healthy controls. The sLORETA has a low-resolution anatomical distribution.

with LDA showed reasonable accuracy and sensitivity between SZ and HCs and/or MDD and HCs. Considering the results of both statistical comparisons and machine learning-based classification, patients with SZ showed defective EEG phenotypes in N1-Fz, N1-Cz, N1-Pz, and total value in the sum of amplitudes. Patients with MDD showed an impaired EEG phenotype in N1-Fz in the sum of amplitudes. In cortical sources, patients with SZ and MDD showed decreased N1 and P3. The SVM classifier showed reasonable sensitivity between SZ and HCs and/or MDD and HCs.

The impaired N1 component in patients with SZ reflects early sensory gating deficits, which lead to a dysfunctional process

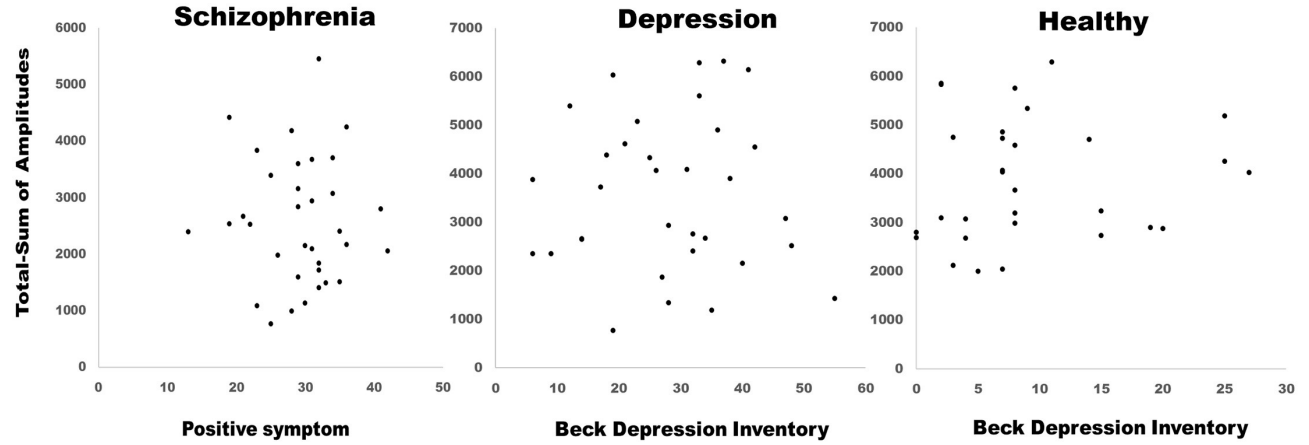

FIGURE 3 | Correlations between clinical symptoms and AP300. Correlations were not significant.

TABLE 3 | Classification using LDA and SVM.

Two sample classifications	Accuracy (%)		Sensitivity (%)		Specificity (%)		Number of features	Selected features
	LDA	SVM	LDA	SVM	LDA	SVM		
SZ vs. MDD	59.71	54.48	65.08	56.18	54.83	52.73	7	Sum of amplitudes
SZ vs. HCs	71.31	57.81	77.67	56.77	64.00	59.00		
MDD vs. HCs	74.55	58.89	79.00	57.58	69.67	60.33		
SZ vs. MDD	55.75	53.88	57.25	55.00	55.00	52.73	12	Peak with latency
SZ vs. HCs	70.74	67.35	69.42	70.00	72.33	64.33		
MDD vs. HCs	70.60	70.95	75.17	72.12	65.33	69.67		
SZ vs. MDD	54.28	54.78	58.25	66.77	50.08	42.42	28	Cortical sources
SZ vs. HCs	65.41	71.88	69.25	74.41	60.67	69.00		
MDD vs. HCs	55.50	65.87	64.00	81.21	46.67	49.00		

of attentional information (49). This impaired phenotype is associated with aberrant neural plasticity in SZ patients showing clinical high-risk factors (50). Patients with depression showed delayed latency of N1 and a lower P3 amplitude (36). Deficits in early sensory gating are related to maladaptive initial directions of sensory information, resulting in delayed N1 latency and lower amplitude (49). P3 is an index of the late sensory gating that decodes whether the stimulus is significant or unnecessary (51).

The present study showed significant differences in N1 and P3 between patients with SZ and those with MDD. Compared to patients with MDD, patients with SZ had lower N1 and P3 amplitudes. However, this difference lacked power because classification with machine learning has low accuracy, sensitivity, and specificity. Previous studies reported that high classification performance was identified when sensor and source level EEG features were used together (10). EEG microstate features had higher classification performance than conventional EEG features in patients with SZ (52). In MDD, EEG band frequency features showed a good performance classifying patients and healthy individuals (53). In the present study, the mean and standard deviation in the EEG data could influence the results in statistical comparison, while distributional similarity of the used features between groups could have a possible effect on the lacking power in classification with machine learning. In addition, sociodemographic factors could influence the results. Further studies are warranted in patients with several clinical phenotypes and EEG features.

This study had a few limitations. First, the sample size was small; thus, future studies with large sample sizes should be conducted to verify the results. Second, several clinical phenotypes, such as affective or mood-specific types and psychosis with mood symptoms, need to be considered. Nevertheless, determination of the neuropathological mechanism via EEG phenotyping could provide useful information for the fundamental treatment of psychiatric disorders. This study identified that in sum of amplitude, a neurophysiologic phenotype with an N1 deficit featured in patients with MDD and SZ, indicating a dysfunctional process of early sensory attentional information. Supporting this result was that the LDA classifier showed reasonable accuracy and sensitivity. In cortical sources, a phenotype with deficits in both N1 and P3 was observed in patients with MDD and SZ, reflecting maladaptive early and/or late sensory/cognitive gating inputs. The SVM classifier with sensitivity showed reasonable scores.

DATA AVAILABILITY STATEMENT

The data presented in the current study are available from the first author (K-IJ) or corresponding author (J-HC) upon reasonable request. Requests to access these datasets should be directed to K-IJ.

ETHICS STATEMENT

The studies involving human participants were reviewed and approved by Institutional Review Board of Seoul St. Mary's Hospital College of Medicine, The Catholic University of Korea (approval number: KC09FZZZ0211). The patients/participants provided their written informed consent to participate in this study.

AUTHOR CONTRIBUTIONS

K-IJ, CL, and J-HC contributed to the conception and design of the study. K-IJ, SYK, and CL contributed to the acquisition and analysis of data. K-IJ contributed to drafting the article. K-IJ, SK, CL, SYK, and J-HC contributed to the review of the article. J-HC and CL contributed to the supervision of the study. All authors approved the final version of the article.

FUNDING

This study was supported by a grant from the Korea Health Technology R&D project through the Korea Health Industry Development Institute (KHIDI) (HI17C2272), as well as by the KBRI basic research program through the Korea Brain Research Institute, which is funded by the Ministry of Science and ICT (21-BR-01-13). This study was also supported by Basic Science Research Program through the National Research Foundation of Korea (NRF) funded by the Ministry of Education (2021R1A6A3A01086699).

SUPPLEMENTARY MATERIAL

The Supplementary Material for this article can be found online at: https://www.frontiersin.org/articles/10.3389/fpsyt.2021.745458/full#supplementary-material

REFERENCES

1. Earls HA, Curran T, Mittal V. A meta-analytic review of auditory event-related potential components as endophenotypes for schizophrenia: perspectives from first-degree relatives. *Schizophrenia Bulletin*. (2016) 42:1504-16 doi: 10.1093/schbul/sbw047
2. Singh R, Shukla R, Dalal PK, Sinha PK, Trivedi KJ. P 300 event related potential in depression. *Indian J Psychiat.* (2000) 42:402–9.
3. O'Donnell BF, McCarley RW, Potts GF, Salisbury DF, Nestor PG, Hirayasu YMA, et al. Shenton. Identification of neural circuits underlying P300 abnormalities in schizophrenia. *Psychophysiology*. (1999) 36:388–98. doi: 10.1017/s0048577299971688
4. Liang SG, A T. Greenwood. The impact of clinical heterogeneity in schizophrenia on genomic analyses. *Schizophrenia Res.* (2015) 161:490–5. doi: 10.1016/j.schres.2014.11.019
5. Wolfers T, Doan NT, Kaufmann T, Alnæs D, Moberget TI, Agartz M, et al. Mapping the heterogeneous phenotype of schizophrenia and bipolar disorder using normative models. *JAMA Psychiat*. (2018) 75:1146–55. doi: 10.1001/jamapsychiatry.2018.2467
6. D. Goldberg. The heterogeneity of "major depression". *World Psychiat. (WPA).* (2011) 10:226–8 doi: 10.1002/j.2051-5545.2011.tb00061.x
7. Levitt J, Edhi MM, Thorpe RV, Leung JW, Michishita M, Koyama SS, et al. Pain phenotypes classified by machine learning using electroencephalography features. *NeuroImage*. (2020) 223:117256. doi: 10.1016/j.neuroimage.2020.117256
8. N. Hackett. QEEG phenotypes, depression and TMS. *Progress Neurology Psychiatry*. (2018) 22:23—6. doi: 10.1002/pnp.510
9. Mumtaz W, Ali SSA, Yasin MAM, Malik AS. A machine learning framework involving EEG-based functional connectivity to diagnose major depressive disorder (MDD). *Med Biol Eng Comput*. (2018) 56:233–46. doi: 10.1007/s11517-017-1685-z
10. Shim M, Hwang HJ, Kim DW, Lee SH, Im HC. Machine-learning-based diagnosis of schizophrenia using combined sensor-level and source-level EEG features. *Schizophr Res*. (2016) 176:314–9. doi: 10.1016/j.schres.2016.05.007
11. Quaak M, L. van de Mortel. Thomas RM, van Wingen G. Deep learning applications for the classification of psychiatric disorders using neuroimaging data: Systematic review and meta-analysis. *NeuroImage Clinical*. (2021) 30:102584. doi: 10.1016/j.nicl.2021.102584
12. Zhou L, Wang G, Nan C, Wang H, Liu Z, Bai H. Abnormalities in P300 components in depression: an ERP-sLORETA study. *Nord J Psychiatry*. 73:1–8 (2019) doi: 10.1080/08039488.2018.1478991
13. Klawohn J, Santopetro NJ, Meyer AG. Hajcak. Reduced P300 in depression: Evidence from a flanker task and impact on ERN, CRN, and Pe. *Psychophysiology*. (2020) 57:e13520. doi: 10.1111/psyp.13520
14. Chang W-H, Chen K-C, Yang Y-K, Chen P-S, Lu R-B, Yeh T-L, et al. Association between auditory P300, psychopathology, and memory function in drug-naïve schizophrenia. *Kaohsiung J Med Sci*. (2014) 30:133–8. doi: 10.1016/j.kjms.2013.10.003
15. D. Blackwood. P300, a state and a trait marker in schizophrenia. *Lancet*. (2000) 355:771–2. doi: 10.1016/s0140-6736(99)00261-5
16. Sara G, Gordon E, Kraiuhin C, Coyle S, Howson A, Meares R. The P300 ERP component: an index of cognitive dysfunction in depression? *J Affect Disord*. (1994) 31:29–38 doi: 10.1016/0165-0327(94)90124-4
17. Johnson R Jr. On the neural generators of the P300 component of the event-related potential. *Psychophysiol.* (1993) 30:90–7. doi: 10.1111/j.1469-8986.1993.tb03208.x
18. Simons CJP, Sambeth A, Krabbendam L, S. Pfeifer, van Os J, Riedel WJ. Auditory P300 and N100 components as intermediate phenotypes for psychotic disorder: Familial liability and reliability. *Clinical Neurophysiology*. (2011) 122:1984–90. doi: 10.1016/j.clinph.2011.02.033
19. Won K, Kwon M, Jang S, Ahn M, Jun SC. P300 Speller Performance Predictor Based on RSVP Multi-feature. *Front Hum Neurosci*. (2019) 13:261. doi: 10.3389/fnhum.2019.00261
20. Pfabigan D, Seidel E, Sladky R, Hahn A, Paul KA. Grahl, et al. P300 amplitude variation is related to ventral striatum BOLD response during gain and loss anticipation: An EEG and fMRI experiment. *Neuroimage*. (2014) 96:12–21. doi: 10.1016/j.neuroimage.2014.03.077
21. MacGregor LJ, Pulvermüller F, van Casteren M, Shtyrov Y. Ultra-rapid access to words in the brain. *Nat Commun*. (2012) 3:711. doi: 10.1038/ncomms1715
22. Chayasirisobhon WV, Chayasirisobhon S, Tin SN, Leu N, Tehrani K, McGuckin JS. Scalp-recorded auditory P300 event-related potentials in new-onset untreated temporal lobe epilepsy. *Clin EEG Neurosci*. (2007) 38:168–71. doi: 10.1177/155005940703800314
23. Donchin E, Coles HMG. Is the P300 component a manifestation of context updating? *Behavioral Brain Sci*. (1988) 11:357–74 doi: 10.1017/S0140525X00058027

24. Citherlet D, Boucher O, Tremblay J, Robert M, Gallagher A, Bouthillier A, et al. Spatiotemporal dynamics of auditory information processing in the insular cortex: an intracranial EEG study using an oddball paradigm. *Brain Struct Funct*. (2020) 225:1537–59 doi: 10.1007/s00429-020-02072-z
25. Thoma L, Rentzsch J, Gaudlitz K, Tänzer N, Gallinat J, Kathmann N, et al. P50, N100, and P200 Sensory Gating in Panic Disorder. *Clin EEG Neurosci*. (2020) 51:317–24 doi: 10.1177/1550059419899324
26. Baskaran, Milev R. S R. McIntyre. A review of electroencephalographic changes in diabetes mellitus in relation to major depressive disorder. *Neuropsychiatr Dis Treat*. (2013) 9:143–50. doi: 10.2147/ndt.S38720
27. Sumich, Harris A, Flynn G, Whitford T, Tunstall N, V. Kumari, et al. Event-related potential correlates of depression, insight and negative symptoms in males with recent-onset psychosis. *Clin Neurophysiol*. (2006) 117:1715–27 doi: 10.1016/j.clinph.2006.04.017
28. Strik WK, Dierks T, Böning J, Osterheider M, Caspari A, Körber J. Disorders of smooth pursuit eye movement and auditory N100 in schizophrenic patients. *Psychiatry Res*. (1992) 41:227–35. doi: 10.1016/0165-1781(92)90004-m
29. Ford JM, Mathalon DH, Kalba S, Marsh L. Pfefferbaum: N1 A, and P300 abnormalities in patients with schizophrenia, epilepsy, and epilepsy with schizophrenialike features. *Biol Psychiat*. (2001) 49:848–60 doi: 10.1016/s0006-3223(00)01051-9
30. Linden DEJ. The P300: where in the brain is it produced and what does it tell us? *Neuroscientist*. (2005) 11:563–76. doi: 10.1177/1073858405280524
31. Polich J, Eischen SE, G. E. Collins. P300 from a single auditory stimulus. *Electroencephalography and Clinical Neurophysiology/Evoked Potentials Section*, 92: 253-261 (1994) doi: 10.1016/0168-5597(94)90068-X
32. Huang M-W, Chou H-CF, Lo P-Y, Cheng K-S. A comparative study on long-term evoked auditory and visual potential responses between Schizophrenic patients and normal subjects. *BMC Psychiat*. (2011) 11:74. doi: 10.1186/1471-244X-11-74
33. Jeon YW, Polich J. Meta-analysis of P300 and schizophrenia: patients, paradigms, practical implications. *Psychophysiol*. (2003) 40:684–701. doi: 10.1111/1469-8986.00070
34. Kawasaki T, Tanaka S, Wang J, Hokama H, Hiramatsu K. Abnormalities of P300 cortical current density in unmedicated depressed patients revealed by LORETA analysis of event-related potentials. *Psychiatry Clin Neurosci*. (2004) 58:68-75. doi: 10.1111/j.1440-1819.2004.01195.x
35. Santopetro NJ, Brush CJ, Bruchnak A, Klawohn J, Hajcak G. A reduced P300 prospectively predicts increased depressive severity in adults with clinical depression. *Psychophysiol*. (2021) 58:e13767. doi: 10.1111/psyp.13767
36. Urretavizcaya M, Moreno I, Benlloch L, Cardoner N, Serrallonga J, Menchón JM, et al. Auditory event-related potentials in 50 melancholic patients: increased N100, N200 and P300 latencies and diminished P300 amplitude. *J Affect Disord*. (2003) 74:293–7 doi: 10.1016/s0165-0327(02)00016-2
37. Kay SR, Fiszbein A, Opler LA. The Positive and Negative Syndrome Scale (PANSS) for Schizophrenia. *Schizophrenia Bulletin*. (1987) 13:261–76. doi: 10.1093/schbul/13.2.261
38. Hamilton M. The assessment of anxiety states by rating. *Br J Med Psychol*. (1959) 32:50–5. doi: 10.1111/j.2044-8341.1959.tb00467.x
39. Hamilton M. A rating scale for depression. *J Neurology, Neurosurgery, Psychiatry*. (1960) 23:56–62 doi: 10.1136/jnnp.23.1.56
40. Song Y-M, Lee H-K, Kim JW, Lee K. Reliability and validity of the Korean version of beck depression inventory-II via the internet: results from a University Student Sample. *J Korean Neuropsychiatr Assoc*. (2012) 51: 402-8. doi: 10.4306/jknpa.2012.51.6.402
41. Semlitsch HV, Anderer P, Schuster PO. Presslich. A solution for reliable and valid reduction of ocular artifacts, applied to the P300 ER. *Psychophysiol*. (1986) 23:695–703.
42. Pascual-Marqui RD, Michel CM, Lehmann D. Low resolution electromagnetic tomography: a new method for localizing electrical activity in the brain. *Int J Psychophysiol*. (1994) 18:49–65. doi: 10.1016/0167-8760(84)90014-X
43. Harrison J, Pujol J, López-Solà M, Hernández-Ribas R, Deus J, Ortiz H, et al. Consistency and functional specialization in the default mode brain network. *Proceedings of the National Academy of Sciences*. (2008) 105:9781. doi: 10.1073/pnas.0711791105
44. Januszko P, Gmaj B, Piotrowski T, Kopera M, Klimkiewicz A, Wnorowska A, et al. Delta resting-state functional connectivity in the cognitive control network as a prognostic factor for maintaining abstinence: An eLORETA preliminary study. *Drug Alcohol Dependence*. (2021) 218:108393. doi: 10.1016/j.drugalcdep.2020.108393
45. Althnian, AlSaeed D, Al-Baity H, Samha A, Dris AB, Alzakari N, Abou Elwafa A, Kurdi H. Impact of dataset size on classification performance: an empirical evaluation in the medical domain. *Applied Sci*. (2021) 11. doi: 10.3390/app11020796
46. R. A. Fisher. The use of multiple measurements in taxonomic problems. *Ann Eugenics*. (1936) 7:179–88. doi: 10.1111/j.1469-1809.1936.tb02137.x
47. Schlögl, Lee F, Bischof H, Pfurtscheller G. Characterization of four-class motor imagery EEG data for the BCI-competition 2005. *J Neural Eng*. (2005) 2:L14–22. doi: 10.1088/1741-2560/2/4/l02
48. Y. Hochberg. A sharper bonferroni procedure for multiple tests of significance. *Biometrika*. (1988) 75:800–2. doi: 10.2307/2336325
49. Shen C-L, Chou T-L, Lai W-S, Hsieh MH, Liu C-C, Liu C-M, Hwu H-G. P50, N100, and P200 auditory sensory gating deficits in schizophrenia patients. *Front Psychiat*. (2020) 11:868. doi: 10.3389/fpsyt.2020.00868
50. Gonzalez-Heydrich J, Enlow MB, D'Angelo E, Seidman LJ, Gumlak S, Kim A, et al. N100 repetition suppression indexes neuroplastic defects in clinical high risk and psychotic youth. *Neural plasticity*. (2016) 2016:4209831. doi: 10.1155/2016/4209831
51. Micoulaud-Franchi JA, Lopez R, Cermolacce M, Vaillant F, Péri P, Boyer L, et al. Sensory gating capacity and attentional function in adults with adhd: a preliminary neurophysiological and neuropsychological study. *J Atten Disord*. (2019) 23:1199–209. doi: 10.1177/1087054716629716
52. Kim K, Duc NT, Choi M, Lee B. EEG microstate features for schizophrenia classification. *PLoS ONE*. (2021) 16:e0251842. doi: 10.1371/journal.pone.0251842
53. Qiao Y, Duan L, Duan H, Wang C, Zhang X, Sha S. Machine learning approaches for MDD detection and emotion decoding using EEG signals. *Front. Hum. Neurosci*. (2020) 14:284. doi: 10.3389/fnhum.2020.00284

Conflict of Interest: The authors declare that the research was conducted in the absence of any commercial or financial relationships that could be construed as a potential conflict of interest.

Publisher's Note: All claims expressed in this article are solely those of the authors and do not necessarily represent those of their affiliated organizations, or those of the publisher, the editors and the reviewers. Any product that may be evaluated in this article, or claim that may be made by its manufacturer, is not guaranteed or endorsed by the publisher.

frontiers in Psychiatry

ORIGINAL RESEARCH
published: 28 October 2021
doi: 10.3389/fpsyt.2021.761203

EEG Microstates and Its Relationship With Clinical Symptoms in Patients With Schizophrenia

Qiaoling Sun[1,2], *Jiansong Zhou*[1,2], *Huijuan Guo*[1,2], *Ningzhi Gou*[1,2], *Ruoheng Lin*[1,2], *Ying Huang*[1,2], *Weilong Guo*[1,2] *and Xiaoping Wang*[1,2*]

[1] Department of Psychiatry, The Second Xiangya Hospital of Central South University, Changsha, China, [2] National Clinical Research Center for Mental Disorders, The Second Xiangya Hospital of Central South University, Changsha, China

Schizophrenia is a complex and devastating disorder with unclear pathogenesis. Electroencephalogram (EEG) microstates have been suggested as a potential endophenotype for this disorder. However, no clear dynamic pattern of microstates has been found. This study aims to identify the dynamics of EEG microstates in schizophrenia and to test whether schizophrenia patients with altered clinical symptoms severity showed different microstates abnormalities compared with healthy controls. Resting-state EEG data in 46 individuals who met the ICD-10 diagnostic criteria for schizophrenia and 39 healthy controls was recorded. The patients with schizophrenia were divided into subgroups based on the level of their negative or positive symptoms assessed using the Positive and Negative Syndrome Scale. Microstate parameters (contribution, occurrence, and duration) of four prototypical microstate classes (A–D) were investigated. Compared with healthy controls, individuals with schizophrenia showed increased duration and contribution of microstate class C, decreased contribution and occurrence of microstate class B. Different microstate patterns were found between subgroups and healthy controls. Results in this study support the consistent observation of abnormal EEG microstates patterns in patients with schizophrenia and highlight the necessity to divide subjects into subgroups according to their clinical symptoms.

Keywords: schizophrenia, clinical symptoms, resting-state, electroencephalogram (EEG), microstates

OPEN ACCESS

Edited by:
Junpeng Zhang,
Sichuan University, China

Reviewed by:
Meng Zhang,
Xinxiang Medical University, China
Qinglin Zhao,
Lanzhou University, China
Zhang Li Peng,
Zhengzhou University, China

****Correspondence:***
Xiaoping Wang
xiaop6@csu.edu.cn

Specialty section:
This article was submitted to Neuroimaging and Stimulation, a section of the journal Frontiers in Psychiatry

Received: *19 August 2021*
Accepted: *08 October 2021*
Published: *28 October 2021*

Citation:
Sun Q, Zhou J, Guo H, Gou N, Lin R, Huang Y, Guo W and Wang X (2021) EEG Microstates and Its Relationship With Clinical Symptoms in Patients With Schizophrenia. Front. Psychiatry 12:761203. doi: 10.3389/fpsyt.2021.761203

INTRODUCTION

Schizophrenia is a complex and devastating mental illness which has affected multiple aspects of patients. Despite numerous long-term studies, its pathogenesis still remains poorly understood. The synchronization models within or between numerous brain regions play an essential role in understanding the psychopathology of schizophrenia. Therefore, recent studies have been focusing on the involvement of the global brain functions in this disorder (1–3). To this end, the use of resting electroencephalogram (EEG) microstates is highly valued to investigate the endophenotypes for schizophrenia (4, 5). Microstates reflect the global brain function by instantly configuring the electrical field of the scalp (6); they remain stable for about 60–120 ms and quickly change into another class of microstates, and then become stable again, showing the semi-simultaneity of the brain network activity on a large scale (7). Besides, microstate sequences and the patterns of these sequences are related to the subsequent switching between these integrated

states (7). Studies also reported that the microstates might be associated with different mental states and represent the collaborative activities in certain brain networks (8), therefore, they can be considered as the "atoms of thought." A large body of evidence showed that the microstate time series could provide insight into the brain's neural activity at the rest state (9–11). Some studies using functional magnetic resonance imaging (fMRI) and EEG methods have shown significant correlations between microstate maps and fMRI resting-state networks (11). Although some studies argued that the attribution patterns of microstates to fMRI brain functions must be more complex (10), the microstates class A, B, C, and D were related closely with auditory, visual, saliency, and attention network, respectively (9). Therefore, microstate analysis of EEG is a helpful and powerful neurophysiological approach to study the global brain function; it is also inexpensive, and might be clinically translatable.

The microstates detected with EEG are highly replicable, and thus can be grouped into different sets according to their topographical similarity with the use of clustering algorithms. It is generally believed that the optimal number of microstate classes is closely related to the dataset studied. To date, there has been no consensus or unified standard on how to determine the optimal number of microstate classes (7). However according to pioneering studies, four major microstate classes, namely class A, B, C, and D, have been found. These four classes of microstates are highly consistent in resting-state EEG and can explain around 80% of the global variance of EEG data (12).

In some studies, patients with schizophrenia exhibited temporal dynamic abnormalities of EEG microstates, such as increased duration and occurrence of microstates class C (13, 14) and decreased duration and occurrence of microstates class D (15), as compared to healthy controls. A meta-analysis on studies of EEG microstates from 1999 to 2015 showed moderate alterations of two classes of microstates in patients with schizophrenia: higher frequency of microstate class C and shorter duration of microstate class D (16); there is also evidence for a slight shortening of microstate class B. Similar to the above study, a recent meta-analysis included studies published before November 29, 2019 (4) found that compared with healthy controls, individuals with schizophrenia showed consistently increased time coverage and occurrence of microstate class C, as well as decreased time coverage of microstate class D. Although the consistency regarding class C and D is remarkable, there are still inconsistent findings in studies (17, 18). As for microstate class A and B, the findings are inconsistent and more complicated (19–22).

A factor leading to the variation in previous findings might be the differences in clinical symptoms in patients with schizophrenia. Individuals with this disease often have different levels of positive or negative symptoms, which might be associated with different prognosis, cognition, medication, and psychophysiology (23, 24). Some studies have explored the relationship between specific abnormalities in EEG microstates and different clinical symptoms of schizophrenia. An early study in patients with chronic schizophrenia showed that the mean microstate duration was positively correlated with the total scores of the Scale for Assessment of Negative Symptoms and the Brief Psychiatric Rating Scale (25). According to some other studies, the duration of microstate class D was shorter in periods with hallucinations (26) and the degree of shortening was significantly correlated with the severity of paranoid hallucination (15). On the contrary, recent studies did not find any correlation between microstates and clinical symptoms in patients with chronic schizophrenia (4). Taken together, the above results might suggest a potential relationship between microstates and clinical symptoms. However, in previous studies, schizophrenia patients are usually considered as a unitary group and no conclusions could be drawn due to the inconsistent results. Therefore, studies on microstate patterns based on different symptoms of patients might provide insights for understanding the dynamics of microstates in schizophrenia.

To our knowledge, findings in previous researches did not propose a clear model for microstates in schizophrenia and inconsistent results may be related to different levels of psychopathological symptoms. In this study, to identify differences between schizophrenia patients and healthy controls with regard to microstates, we will first take the patients with schizophrenia as a unitary group. Further, we will divide the patients into subgroups based on the severity of their positive or negative symptoms, in order to investigate whether schizophrenia patients with altered clinical symptoms severity showed different microstates abnormalities compared with healthy controls.

MATERIALS AND METHODS

Participants

Forty-six patients with schizophrenia (SCZ) aged between 18 and 60 years were enrolled in this study. All the patients were diagnosed with schizophrenia according to the ICD-10 criteria and the Mini-International Neuropsychiatric Interview. Thirty-nine healthy controls (HC) with matched gender and age were recruited from the community, according to the inclusion criterion of having no current or lifetime Axis I or II diagnoses. The exclusion criteria for all the participants were as follows: history of serious medical conditions, severe intellectual disability, previous episode of psychosis due to substance abuse, use of alcohol or benzodiazepine within 24 h, and inability to complete the test. Socio-demographic information such as age, gender, and education level was recorded for all the subjects. All the participants were fully informed of the procedures and signed the written informed consent form. The study was approved by the Clinical Research Ethics Committee of the Second Xiangya Hospital, Central South University.

To assess the clinical symptoms in schizophrenia patients, the Positive and Negative Syndrome Scale (PANSS) (27) was used. The PANSS scale consists of 30 items and is divided into three subscales, i.e., positive, negative, and general psychopathology subscales. All the items are scored with a 7-point scale. The 7 items in the subscale for positive symptoms were summed up to get a score for positive symptoms, which ranged from 7 to 49; the score for negative symptoms was calculated in the same way.

Patients with schizophrenia were classified as having high or low level of positive symptoms according to the median of the

overall severity of positive symptoms (Median = 15.5, Range = 7–30); patient with a higher score for positive symptoms than the median were assigned into the group with high level of positive symptoms (HP) and those with a score lower than or equal to the median were assigned into the group with low level of positive symptoms (LP). Similarly, patients were assigned into the group with high level of negative symptoms (HN) or the group with low level of negative symptoms (LN), according to the median of the overall severity of negative symptoms (Median = 12, Range = 7–33). After classification, there were 23 patients in the HP group, 23 patients in the LP group 26 in the LN group and 20 in the HN group.

Among the 46 patients, 20 were receiving antipsychotic medication; there was no difference in the medication status between the subgroups ($\chi 2 = 0.354$, $p = 0.552$, $\chi 2 = 0.174$, $p = 0.676$; when divided according to positive and negative symptoms respectively). No significant correlation between positive and negative symptoms scores were found ($r = -0.087$, $p = 0.565$).

EEG Recordings

The EEG data were acquired using a 64 BrainAmp cap (BrainProducts GmbH, Munich, Germany), with electrodes positioned according to the 10–20 International System. An additional electrode was used as the ground. The linked mastoid (TP9 and TP10) served as the reference for all the electrodes. The vertical electro-oculogram (VEOG) was recorded from the electrode below the right eye. The signals recorded were filtered with a bandpass of 0.1–1,000 Hz, and all impedances of the electrodes were kept below 10 kΩ. During the recording, the participants was instructed to sit comfortably in a chair, keep relaxed with eyes closed.

Data Pre-processing

Offline pre-processing was performed using the software EEGLAB. The VEOG channel were removed, therefore 61 channels were retained left for the further analyses. The EEG data were filtered with a bandpass of 0.1–70 Hz and then with a notch filter of 48–52 Hz. Bad EEG periods were removed through visual inspection, and interpolation of bad channels with severe artifacts across the whole recording. The data were then divided into 2 s segments and an infomax-based independent component analysis (ICA) was conducted with residual eye- and muscular-artifacts were removed (28). Finally, the data were re-referenced to the common average reference and filtered with a bandpass of 2–20 Hz.

Microstate Analysis

Microstate analysis was performed with the Microstate Analysis plugin developed by Thomas Koenig (http://www.thomaskoenig.ch/index.php/software/). Individual microstate maps for each subject were calculated from original momentary maps. To extract EEG microstates, the peaks of the global field power (GFP) were firstly extracted, and topographic maps occurring at the peaks of the GFP curve were then submitted to a modified k-means clustering algorithm to isolate map topographies. According to the most common (12) and reproducible (7) classification, the number of microstates classes were defined as four. The number of repetitions was set at 20 and the maximum number of iterations was set at infinite. The group-level microstate classes were then identified for SCH and HC patients separately. Using the mean microstate classes across all the participants as the template, individual and group-level maps were sorted out, and the following parameters were extracted for the four microstate classes: globally explained variance, contribution (the proportion of time spent for each microstate), occurrence (the total number of the microstate of a given class per second), and duration (the mean duration of a microstate class in milliseconds).

Statistics Analyses

For continuous variables, inter-group comparisons were performed using *t-test*. Gender difference between group was tested using Pearson's $\chi 2$ test. Inter-group differences in microstate parameters between SCZ subgroups or between SCZ patients and HC were tested using repeated measure analysis of variance (rm-ANOVA), with group (SCZ or LP or HP or LN or HN and HC) as between-subject factor, and microstate classes (A-D) and microstate parameters (contribution, occurrence, and duration) as within-subject factors. The Greenhouse-Geisser correction was applied for multiple comparisons. *Post hoc* tests were performed only when statistical significance was indicated in the rm-ANOVA. Pairwise inter-group comparisons for microstate classes and parameters were corrected for multiple comparisons with Bonferroni correction. All the analyses were conducted using the SPSS Version 23.0.

RESULTS

Subject Characteristics

The demographic and clinical characteristics of SCZ patients and HC are presented in **Table 1**. There was no significant difference in gender, age and education level between groups. There was no significant difference in the score of PANSS negative symptoms between the LP and HP subgroups (**Supplementary Table 1**), and no significant difference in the score of PANSS positive symptoms between the LN and HN subgroups (**Supplementary Table 2**). PANSS general psychopathology significantly differed between the LP and HP subgroups as well as between the LN and HN subgroups, with HP group showed higher PANSS general psychopathology score than LP group, and HN group showed higher PANSS general psychopathology score than LN group.

Data Quality

After the rejection of artifacts, the numbers of 2-sec segments included in the analysis for each group was 100.10 ± 36.358 for HC, 94.8 ± 24.414 for patients with SCH, 97.87 ± 21.663 for the HP group, 91.74 ± 27.022 for the LP group, 99.60 ± 25.525 for the HN group, and 91.12 ± 23.348 for the HN group.

Microstate Parameters: Overall Results

The overall maps, and the maps for patients with SCH and HC are shown in **Figure 1**. The spatial configuration of the four microstate classes for each subgroup was presented

TABLE 1 | Demographic and clinical characteristics of all the participants.

	HC ($n = 39$)	SCZ ($n = 46$)	$t/\chi 2$	P
Gender (M/F)	25/14	36/10	2.088	0.148
Age (years, mean ± SD)	27.21 ± 6.92	28.72 ± 7.44	0.964	0.338
Education (years, mean ± SD)	14.08 ± 2.28	13.16 ± 3.01	1.588	0.116
Age at onset (years, mean ± SD)		24.64 ± 6.93		
Medication (yes/no)		20/23		
Illness duration (years, mean ± SD)		4.11 ± 5.82		
PANSS positive		15.91 ± 5.86		
PANSS negative		14.41 ± 7.74		
PANSS general psychopathology		30.98 ± 7.38		
PANSS total		61.30 ± 16.28		

SCH, individuals with schizophrenia; HC, healthy controls; PANSS, Positive and Negative Syndrome Scale.

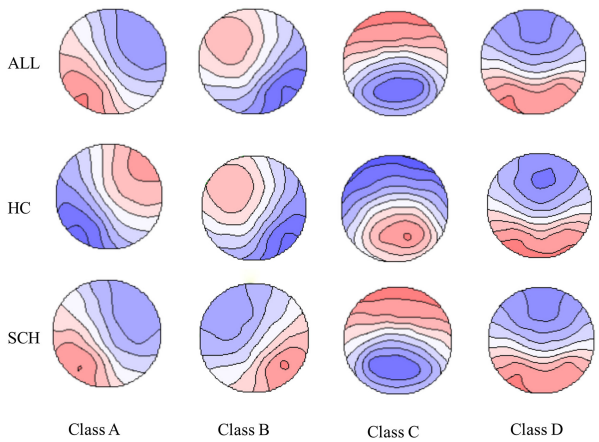

FIGURE 1 | The spatial configuration of the four microstate claasses for the two groups and all the participants. Polarity was ignored. SCH, individuals with schizophrenia; HC, healthy controls; ALL, all the participants in this study.

in **Supplementary Figures 1**, **2**. The four microstate classes explained 76 and 78% of the global variance for the SCH group and the HC, respectively. For each subgroup, the four microstate classes explained 78% of the global variance in the HP group, and the percentage was 77% in the LP group, 77% in the HN group, and 79% in the LN group.

Inter-group Differences in Microstate Parameters

The four parameters for SCH, subgroups (HP, LP, HN, LN) and healthy controls are presented in **Figure 2**. For SCH vs. HC, main effect was found ($F = 4.177$, $p = 0.044$), and rm-ANOVA showed an interaction of group × microstate parameters × microstate class [$F_{(6, 498)} = 4.008$, $p = 0.009$]. *Post hoc* analysis revealed that the interaction effect was related to differences in microstate class B and class C. Compared with HC, patients with SCH showed increased mean duration and contribution of microstate class C and decreased mean contribution and occurrence of microstate class B. No statistically significant inter-group difference was found for microstate class A and D. The means and standard deviations for all considered parameters and microstate classes are reported in **Supplementary Table 3**. Detailed results of rm-ANOVA are presented in **Supplementary Table 4** and *Post hoc* results in **Supplementary Table 5**.

For HP vs. HC, an interaction of group × microstate parameters × microstate class [$F_{(6, 360)} = 2.860$, $p = 0.049$] was found. *Post hoc* analysis revealed that, compared with HC, the HP group showed increased duration and contribution of microstate class C and decreased occurrence and contribution of microstate class B (**Figure 2B**). Detailed results of rm-ANOVA and *Post hoc* results for HP vs. HC are presented in **Supplementary Tables 6**, **7**.

For LP vs. HC, an interaction of group × microstate parameters [$F_{(6, 120)} = 4.059$, $p = 0.048$] and an interaction of microstate parameters × microstate class [$F_{(6, 360)} = 8.224$, $p = 0.001$] were found. *Post hoc* analysis showed that the LP group had decreased occurrence of microstate class A and B, and increased duration of microstate class C, as compared with HC (**Figure 2B**). Detailed results of rm-ANOVA and *Post hoc* results for LP vs. HC are presented in **Supplementary Tables 8**, **9**.

For LN vs. HC, rm-ANOVA revealed an interaction of group × microstate parameters × microstate class [$F_{(6, 378)} = 4.155$, $p = 0.015$]. Simple effect analysis revealed that compared with HC, LN group showed decreased occurrence and contribution of microstate class A and B, and increased duration and contribution of microstate class C (**Figure 2C**). Detailed results of rm-ANOVA and *Post hoc* results for LN vs. HC are presented in **Supplementary Tables 11**, **12**.

For HN vs. HC, no main effect or interaction was found (**Figure 2C**). Detailed results of rm-ANOVA for HN vs. HC are presented in **Supplementary Table 10**.

DISCUSSION

In this study, we have found that patients with SCH showed increased duration and contribution of microstate class C, decreased contribution and occurrence of microstate class B. Nevertheless, different patterns were found when we divided the SCH patients into subgroups according to the level of positive and negative symptoms. Specifically, both HP and LP showed increased duration and contribution of microstate class C, decreased occurrence and contribution of microstate class B, as compared to HC. Besides, the LP group also showed decreased occurrence and contribution of microstate class A. The LN group showed increased duration of microstate class C, decreased occurrence of microstate class A and B, but no difference was found between the HN group and HC group.

In patients with schizophrenia, altered temporal dynamics of EEG microstates had been found in several studies (4, 15, 21). Similar patterns were also found in high-risk populations of psychosis (18, 22), such as siblings of schizophrenia patients (4). Consistent with these studies, our findings demonstrated altered microstate class C in SCH as well as most subgroups. As patients with schizophrenia usually exhibit abnormal assignment of

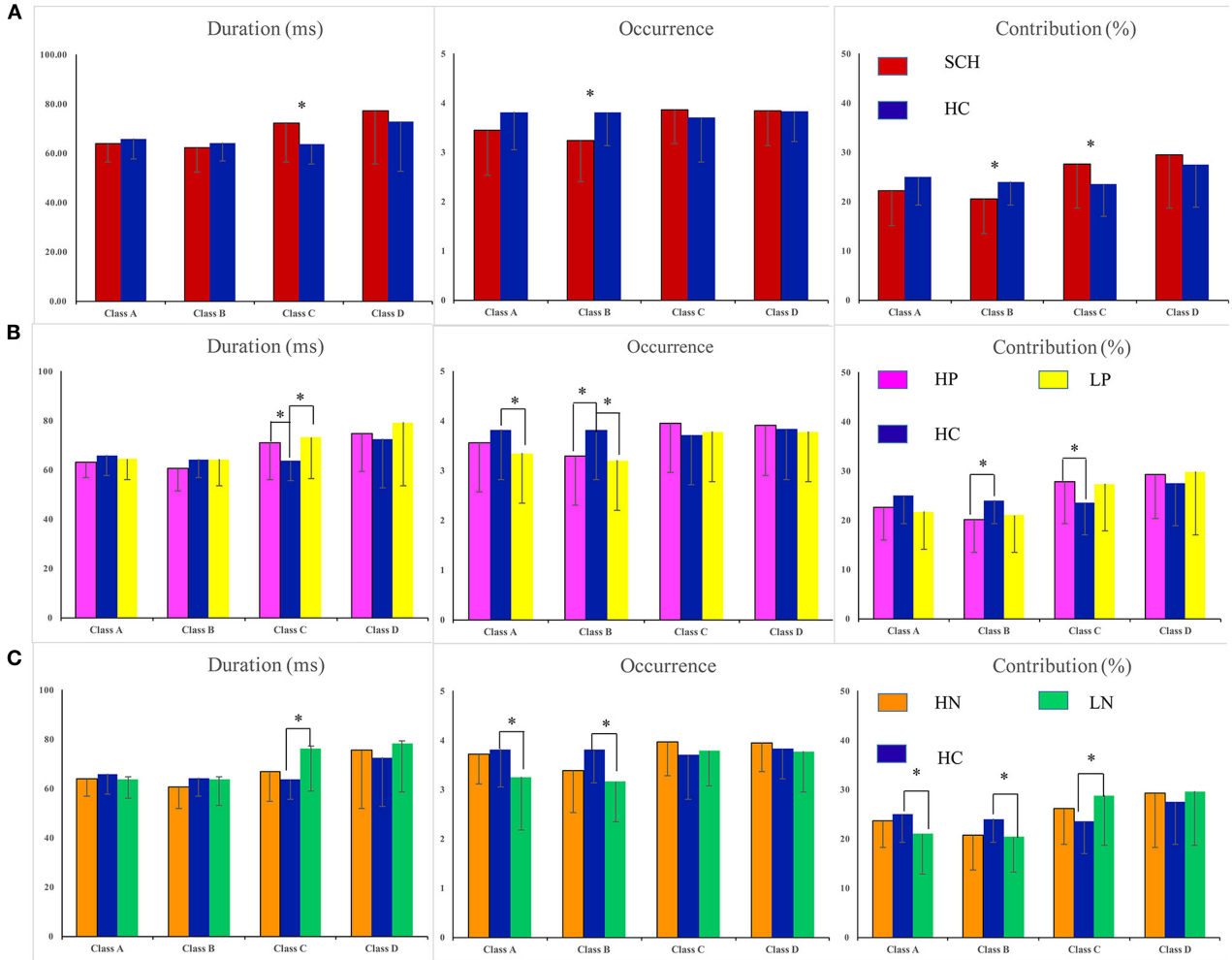

FIGURE 2 | Statistics of the microstate parameters: duration, contribution, and occurrence. *$P < 005$. Errror bars represent standard error. SCH, individuals with schizophrenia; HC, healthy controls; HP, schizophrenia patients with high levels of postive symptoms; LP, schizophrenia patients with low levels of postive symptoms; HN, schizophrenia patients with high level of negative symptoms; LN, schizophrenia patients with low lwvwl of negative symptoms. **(A)** SCH vs. HC. **(B)** Comparisions were made between groups (HP vs. HC, LP vs. HC). **(C)** Comparisons were made between groups (HN vs. HC, LN vs. HC).

saliency (29) as well as dysfunction of attentional processing and executive control (30, 31), the increased occurrence of microstate class C in schizophrenia might be a sign of imbalance across processes involved in saliency. A fMRI-EEG study suggested that microstate class C was correlated with the cerebral activations in the posterior part of the anterior cingulate gyrus, the left claustrum, bilateral inferior frontal gyrus, as well as the right anterior insula (9), which have been found to be part of the saliency-network (32, 33) and to play a critical role in switching between the default mode and executive function mode (34).

Previous studies found a decrease in microstate class B in medication-free schizophrenia patients, as compared to healthy controls (20, 35). In addition, a study found that microstate class B could be used to distinguish patients with first-episode psychosis from high-risk individuals with and without later transition to psychosis (36) and proposed that microstate class B might be a state biomarker underlying the progression of psychosis. However, some studies had shown the opposite effect (18, 37) in medicated patients, which was attributed to the effect of antipsychotic drugs on microstates. This effect can also be used to explain our findings, since more than half of the subjects with schizophrenia were medication-free. As for microstate class A, inconsistent and complicated results have been yielded. Similar to a recent study on first-episode psychosis (21), our study also identified decreased occurrence of microstate class A, while some other studies found an increase (18, 20). No consistent inter-group difference between patients with schizophrenia and healthy controls was found for microstate class A in a recent meta-analysis (4).

We did not find any abnormalities in microstate class D in patients with SCZ, which was inconsistent with literature reports (4). But this difference could explain by medication,

as antipsychotic drugs might have a normalization effect on microstate dynamics (i.e., increasing the occurrence of microstate class D) (14). Besides, from a general perspective, the maps assigned to a certain microstate class varied in different studies, especially for microstate classes C and D (12), which might be one of the reasons for the inconsistencies between the present study and some provious studies in terms of microstate class D in patients with SCZ.

In this study, we observed different microstate patterns when compared subgroups and healthy controls, although it is difficult to explain the functional significance of microstate changes showed in these subgroups, it highlighted the necessity to distinguish patients according to their clinical symptoms. Our findings also provided another explanation for the inconsistent results in studies on microstates in patients with schizophrenia. In future works, patients with schizophrenia could be grouped on the basis of their clinical symptoms, in order to reduce the heterogeneity of subjects and obtain results which may be more consistent.

One of the main limitations of this study is the psychometric measure we used to divide schizophrenia patients into different subgroups. The results are likely to be different if we used another scale such as the Brief Psychiatric Rating Scale. In addition, individuals with high levels of both positive and negative symptoms may show different microstate patterns compared to those with high levels of positive or negative symptoms alone. However, we were only able to investigate positive or negative symptoms independently by dividing the SCZ patients according to the subscale scores of PANSS. Treatments, especially drug therapy, are highly likely to affect the microstate parameters. In this study, some patients were on medication, which might be one of the reasons for some differences observed in this study. Another limitation in this study is that four microstate classes were selected as they had been established in most previous studies (6). Although the four microstate classes explained more than 76% of the variance for each group, it is possible that the abnormalities in SCZ patients are undetected in the remaining 20% of the components. Nevertheless, the four microstate classes allowed direct comparison between this study and previous researches. Lastly, with the relatively small number of patients, especially the small number of subjects included in each subgroup, the results might be less accurate due to sampling error.

In summary, our results suggested that patients with schizophrenia have abnormal EEG microstates, especially the microstate class C. However, different patterns were found when we divided the schizophrenia patients into subgroups according to the level of positive and negative symptoms, which may suggest different neural mechanisms underling positive and negative symptoms and highlight the necessity to differentiate patients according to their clinical symptoms.

DATA AVAILABILITY STATEMENT

The original contributions presented in the study are included in the article/**Supplementary Material**, further inquiries can be directed to the corresponding author/s.

ETHICS STATEMENT

The studies involving human participants were reviewed and approved by Clinical Research Ethics Committee of The Second Xiangya Hospital, Central South University. The patients/participants provided their written informed consent to participate in this study.

AUTHOR CONTRIBUTIONS

XW and JZ conceived and design the research, and revised the paper. QS contributed to the data collection and analysis and wrote the first draft of the manuscript. HG, NG, RL, YH, and WG contributed to the data collection. All authors have approved the final manuscript.

FUNDING

This work was supported by the National Natural Science Foundation of China (82071543), Science and Technology Program of Hunan Provience (2019SK2334), and Natural Science Foundation of Hunan Province (2019JJ40424).

ACKNOWLEDGMENTS

We thank all the patients and healthy controls who volunteered to participate in this study.

SUPPLEMENTARY MATERIAL

The Supplementary Material for this article can be found online at: https://www.frontiersin.org/articles/10.3389/fpsyt.2021.761203/full#supplementary-material

REFERENCES

1. Friston KJ. Schizophrenia and the disconnection hypothesis. *Acta Psychiatr Scand Suppl.* (1999) 395:68–79. doi: 10.1111/j.1600-0447.1999.tb05985.x
2. Uhlhaas PJ, Singer W. Abnormal neural oscillations and synchrony in schizophrenia. *Nat Rev Neurosci.* (2010) 11:100–13. doi: 10.1038/nrn2774
3. Phillips W, Silverstein S. Convergence of biological and psychological perspectives on cognitive coordination in schizophrenia. *Behav Brain Sci.* (2003) 26:65–82. doi: 10.1017/S0140525X03000025
4. da Cruz JR, Favrod O, Roinishvili M, Chkonia E, Brand A, Mohr C, et al. EEG microstates are a candidate endophenotype for schizophrenia. *Nat Commun.* (2020) 11:3089. doi: 10.1038/s41467-020-16914-1
5. Soni S, Muthukrishnan SP, Sood M, Kaur S, Sharma R. Hyperactivation of left inferior parietal lobule and left temporal gyri shortens resting EEG microstate in schizophrenia. *Schizophr Res.* (2018) 201:204–7. doi: 10.1016/j.schres.2018.06.020
6. Koenig T, Prichep L, Lehmann D, Sosa PV, Braeker E, Kleinlogel H, et al. Millisecond by millisecond, year by year: normative

EEG microstates and developmental stages. *Neuroimage.* (2002) 16:41–8. doi: 10.1006/nimg.2002.1070
7. Khanna A, Pascual-Leone A, Michel CM, Farzan F. Microstates in resting-state EEG: current status and future directions. *Neurosci Biobehav Rev.* (2015) 49:105–13. doi: 10.1016/j.neubiorev.2014.12.010
8. Lehmann D, Strik WK, Henggeler B, Koenig T, Koukkou M. Brain electric microstates and momentary conscious mind states as building blocks of spontaneous thinking: I. Visual imagery and abstract thoughts. *Int J Psychophysiol.* (1998) 29:1–11. doi: 10.1016/S0167-8760(97)00098-6
9. Britz J, Van De Ville D, Michel CM. BOLD correlates of EEG topography reveal rapid resting-state network dynamics. *Neuroimage.* (2010) 52:1162–70. doi: 10.1016/j.neuroimage.2010.02.052
10. Yuan H, Zotev V, Phillips R, Drevets WC, Bodurka J. Spatiotemporal dynamics of the brain at rest—exploring EEG microstates as electrophysiological signatures of BOLD resting state networks. *Neuroimage.* (2012) 60:2062–72. doi: 10.1016/j.neuroimage.2012.02.031
11. Musso F, Brinkmeyer J, Mobascher A, Warbrick T, Winterer G. Spontaneous brain activity and EEG microstates. a novel EEG/fMRI analysis approach to explore resting-state networks *Neuroimage.* (2010) 52:1149–61. doi: 10.1016/j.neuroimage.2010.01.093
12. Michel CM, Koenig T. EEG microstates as a tool for studying the temporal dynamics of whole-brain neuronal networks: a review. *Neuroimage.* (2018) 180:577–93. doi: 10.1016/j.neuroimage.2017.11.062
13. Tomescu MI, Rihs TA, Roinishvili M, Karahanoglu FI, Schneider M, Menghetti S. et al. Schizophrenia patients and 22q112 deletion syndrome adolescents at risk express the same deviant patterns of resting state EEG microstates: a candidate endophenotype of schizophrenia. *Schizophr Res Cogn.* (2015) 2:159–65. doi: 10.1016/j.scog.2015.04.005
14. Kikuchi M, Koenig T, Wada Y, Higashima M, Koshino Y, Strik W, et al. Native EEG and treatment effects in neuroleptic-nave schizophrenic patients: Time and frequency domain approaches. *Schizophr Res.* (2007) 97:163–72. doi: 10.1016/j.schres.2007.07.012
15. Koenig T, Lehmann D, Merlo M, Kochi K, Hell D, Koukkou M, et al. deviant EEG brain microstate in acute, neuroleptic-naive schizophrenics at rest. *Euro Archiv Psychiatry Clinic Neurosci.* (1999) 249:205–11. doi: 10.1007/s004060050088
16. Rieger K, Diaz Hernandez L, Baenninger A, Koenig T. 15 Years of microstate research in schizophrenia—where are we? a meta-analysis. *Front Psychiatry.* (2016) 7:22. doi: 10.3389/fpsyt.2016.00022
17. Giordano GM, Koenig T, Mucci A, Vignapiano A, Amodio A, Di Lorenzo G, et al. Neurophysiological correlates of Avolition-apathy in schizophrenia: a resting-EEG microstates study. *Neuroimage Clin.* (2018) 20:627–36. doi: 10.1016/j.nicl.2018.08.031
18. Andreou C, Faber PL, Leicht G, Schoettle D, Polomac N, Hanganu-Opatz IL, et al. Resting-state connectivity in the prodromal phase of schizophrenia: insights from EEG microstates. *Schizophr Res.* (2014) 152:513–20. doi: 10.1016/j.schres.2013.12.008
19. Lehmann D, Faber PL, Galderisi S, Herrmann WM, Kinoshita T, Koukkou M, et al. EEG microstate duration and syntax in acute, medication-naive, first-episode schizophrenia: a multi-center study. *Psychiatry Res.* (2005) 138:141–56. doi: 10.1016/j.pscychresns.2004.05.007
20. Nishida K, Morishima Y, Yoshimura M, Isotani T, Irisawa S, Jann K, et al. EEG microstates associated with salience and frontoparietal networks in frontotemporal dementia, schizophrenia and Alzheimer's disease. *Clin Neurophysiol.* (2013) 124:1106–14. doi: 10.1016/j.clinph.2013.01.005
21. Murphy M, Stickgold R, Ongur D. Electroencephalogram microstate abnormalities in early-course psychosis. *Biol Psychiatry Cogn Neurosci Neuroimaging.* (2020) 5:35–44. doi: 10.1016/j.bpsc.2019.07.006
22. Tomescu MI, Rihs TA, Becker R, Britz J, Custo A, Grouiller F. et al. Deviant dynamics of EEG resting state pattern in 22q112 deletion syndrome adolescents: a vulnerability marker of schizophrenia? *Schizophr Res.* (2014) 157:175–81. doi: 10.1016/j.schres.2014.05.036
23. Harvey RC, James AC, Shields GE, A. Systematic review and network meta-analysis to assess the relative efficacy of antipsychotics for the treatment of positive and negative symptoms in early-onset schizophrenia. *CNS Drugs.* (2016) 30:27–39. doi: 10.1007/s40263-015-0308-1
24. Andreasen NC. Positive vs. negative schizophrenia: a critical evaluation. *Schizophr Bull.* (1985) 3:380–9. doi: 10.1093/schbul/11.3.380
25. Stevens A, Lutzenberger W, Bartels DM, Strik W, Lindner K. Increased duration and altered topography of EEG microstates during cognitive tasks in chronic schizophrenia. *Psychiatry Res.* (1997) 66:45–57. doi: 10.1016/S0165-1781(96)02938-1
26. Kindler J, Hubl D, Strik WK, Dierks T, Koenig T. Resting-state EEG in schizophrenia: auditory verbal hallucinations are related to shortening of specific microstates. *Clin Neurophysiol.* (2011) 122:1179–82. doi: 10.1016/j.clinph.2010.10.042
27. Kay SR, Fiszbein A, Opler LA. The positive and negative syndrome scale (PANSS) for schizophrenia. *Schizophr Bull.* (1987) 13:261–76. doi: 10.1093/schbul/13.2.261
28. Jung TP, Makeig S, Westerfield M, Townsend J, Courchesne E, Sejnowski TJ. Removal of eye activity artifacts from visual event-related potentials in normal and clinical subjects. *Clin Neurophysiol.* (2000) 111:1745–58. doi: 10.1016/S1388-2457(00)00386-2
29. Kapur S. Psychosis as a state of aberrant salience: a framework linking biology, phenomenology, and pharmacology in schizophrenia. *Am J Psychiatry.* (2003) 160:13–23. doi: 10.1176/appi.ajp.160.1.13
30. Green MF, Horan WP, Lee J. Nonsocial and social cognition in schizophrenia: current evidence and future directions. *World Psychiatry.* (2019) 18:146–61. doi: 10.1002/wps.20624
31. Beck AT, Rector NA. Cognitive approaches to schizophrenia: theory and therapy. *Annu Rev Clin Psychol.* (2005) 1:577–606. doi: 10.1146/annurev.clinpsy.1.102803.144205
32. Seeley WW, Menon V, Schatzberg AF, Keller J, Glover GH, Kenna H, et al. Dissociable intrinsic connectivity networks for salience processing and executive control. *J Neurosci.* (2007) 27:2349–56. doi: 10.1523/JNEUROSCI.5587-06.2007
33. Mantini D, Perrucci M, Del GC, Romani G, Corbetta M. Electrophysiological signatures of resting state networks in the human brain. *Proc Natl Acad Sci U S A.* (2007) 104:13170–5. doi: 10.1073/pnas.0700668104
34. Sridharan D, Levitin DJ, Menon V, A. critical role for the right fronto-insular cortex in switching between central-executive and default-mode networks. *Proc Natl Acad Sci U S A.* (2008) 105:12569–74. doi: 10.1073/pnas.0800005105
35. Irisawa S, Isotani T, Yagyu T, Morita S, Nishida K, Yamada K, et al. Increased omega complexity and decreased microstate duration in nonmedicated schizophrenic patients. *Neuropsychobiology.* (2006) 54:134–9. doi: 10.1159/000098264
36. de Bock R, Mackintosh AJ, Maier F, Borgwardt S, Riecher-Rossler A, Andreou C, et al. microstates as biomarker for psychosis in ultra-high-risk patients. *Transl Psychiatry.* (2020) 10:300. doi: 10.1038/s41398-020-00963-7
37. Mackintosh AJ, Borgwardt S, Studerus E, Riecher-Rossler A, de Bock R, Andreou C, et al. Microstate differences in medicated vs. medication-naive first-episode psychosis patients. *Front Psychiatry.* (2020) 11:600606. doi: 10.3389/fpsyt.2020.600606

Conflict of Interest: The authors declare that the research was conducted in the absence of any commercial or financial relationships that could be construed as a potential conflict of interest.

frontiers in Psychiatry

ORIGINAL RESEARCH
published: 14 December 2021
doi: 10.3389/fpsyt.2021.790234

Atypical Resting State Functional Neural Network in Children With Autism Spectrum Disorder: Graph Theory Approach

Daiki Soma[1], Tetsu Hirosawa[1,2], Chiaki Hasegawa[2], Kyung-min An[2], Masafumi Kameya[1], Shoryoku Hino[3], Yuko Yoshimura[2,4], Sou Nobukawa[5], Sumie Iwasaki[2], Sanae Tanaka[2], Ken Yaoi[2], Masuhiko Sano[1], Yuka Shiota[2], Nobushige Naito[1] and Mitsuru Kikuchi[1,2]*

[1] Department of Psychiatry and Neurobiology, Graduate School of Medical Science, Kanazawa University, Kanazawa, Japan, [2] Research Center for Child Mental Development, Kanazawa University, Kanazawa, Japan, [3] Department of Neuropsychiatry, Ishikawa Prefectural Takamatsu Hospital, Kahoku, Japan, [4] Faculty of Education, Institute of Human and Social Sciences, Kanazawa University, Kanazawa, Japan, [5] Department of Computer Science, Chiba Institute of Technology, Narashino, Japan

OPEN ACCESS

Edited by:
Lizhu Luo,
University of Electronic Science and Technology of China, China

Reviewed by:
Lisa Mash,
Baylor College of Medicine, United States
Heng Chen,
Guizhou University, China
Juan Kou,
Sichuan Normal University, China

***Correspondence:**
Tetsu Hirosawa
hirosawatetsu1982@yahoo.co.jp

Specialty section:
This article was submitted to Neuroimaging and Stimulation, a section of the journal Frontiers in Psychiatry

Received: 06 October 2021
Accepted: 19 November 2021
Published: 14 December 2021

Citation:
Soma D, Hirosawa T, Hasegawa C, An K-m, Kameya M, Hino S, Yoshimura Y, Nobukawa S, Iwasaki S, Tanaka S, Yaoi K, Sano M, Shiota Y, Naito N and Kikuchi M (2021) Atypical Resting State Functional Neural Network in Children With Autism Spectrum Disorder: Graph Theory Approach. Front. Psychiatry 12:790234. doi: 10.3389/fpsyt.2021.790234

Measuring whole brain networks is a promising approach to extract features of autism spectrum disorder (ASD), a brain disorder of widespread regions. Objectives of this study were to evaluate properties of resting-state functional brain networks in children with and without ASD and to evaluate their relation with social impairment severity. Magnetoencephalographic (MEG) data were recorded for 21 children with ASD (7 girls, 60–89 months old) and for 25 typically developing (TD) control children (10 girls, 60–91 months old) in a resting state while gazing at a fixation cross. After signal sources were localized onto the Desikan–Killiany brain atlas, statistical relations between localized activities were found and evaluated in terms of the phase lag index. After brain networks were constructed and after matching with intelligence using a coarsened exact matching algorithm, ASD and TD graph theoretical measures were compared. We measured autism symptoms severity using the Social Responsiveness Scale and investigated its relation with altered small-worldness using linear regression models. Children with ASD were found to have significantly lower small-worldness in the beta band ($p = 0.007$) than TD children had. Lower small-worldness in the beta band of children with ASD was associated with higher Social Responsiveness Scale total t-scores ($p = 0.047$). Significant relations were also inferred for the Social Awareness ($p = 0.008$) and Social Cognition ($p = 0.015$) sub-scales. Results obtained using graph theory demonstrate a difference between children with and without ASD in MEG-derived resting-state functional brain networks, and the relation of that difference with social impairment. Combining graph theory and MEG might be a promising approach to establish a biological marker for ASD.

Keywords: autism, MEG, graph theory, small-worldness, social communication

INTRODUCTION

The etiology of autism spectrum disorder (ASD), a neurodevelopmental disorder characterized by stereotypic or repetitive behaviors with impaired social cognition and communication disorders (1), remains largely unknown. However, impaired social cognition and communication can be improved by early and appropriate interventions (2, 3). Its early diagnosis is nevertheless difficult in many cases because no biological marker has been established (4, 5). Consequently, clinicians must rely on symptoms.

In the field of brain imaging, researchers have characterized the functions of individual brain regions affected by ASD. However, results of more recent studies have suggested that ASD is a dysfunction of coordination over widely distributed brain regions (5–7). Assessing relations between brain regions (i.e., brain connectivity) and functions in each region can be an effective approach to extracting differences between individuals with ASD and typically developing (TD) individuals. Brain connectivity is a multi-faceted concept. In the human brain, neurons and neural populations do not function individually. They interact with other elements in a coordinated manner through their afferent and efferent connections (8). In this context, anatomical relations through bundles of axons are designated as structural connectivity, which can be measured using structural brain imaging such as MRI and diffusion tensor imaging (DTI). Structural connectivity describes the architecture of interregional connections, but it provides less information related to how neurophysiological functions are supported by this architecture. In contrast, functional connectivity is based on statistical dependencies between time series of cerebral activity in different brain regions. The connectivity can be measured using fMRI, SPECT, EEG or magnetoencephalography (MEG) (9). As such, functional connectivity is thought to form a physiological basis of information processing (10). It can therefore be of more interest. These two types of connectivity are fundamentally different. Results from earlier studies are somewhat inconsistent, but many reports of the literature describing connectivity in ASD yield a promising hypothesis: ASD is a disorder of long-range under-connectivity combined with local over-connectivity (11). However, in light of the brain's inherent complexity, any hypothesis based on such a simple measure (i.e., mean of the strength of connectivity) might be an oversimplification. To meet this challenge and to describe the properties of complex networks on a large scale, the field of neuroscience has provided graph theory (12).

Within the graph theory framework, a complex system is described as a set of relations among discrete objects. A key concept of graph theory is reduction of a complex system to a "graph": a set of nodes (i.e., objects) and edges (i.e., relations). Using graph theory, one can describe properties of such graphs using the same parameters, irrespective of their constituent elements (10, 13). In this context, a brain network is definable as a graph in which the nodes represent brain regions and the edges linking pairs of nodes represent functional connectivity between pairs of corresponding brain regions. Based on such a graph, graph metrics represent the characteristics of the entire brain network as single numerical values. It is noteworthy that graph metrics differ from traditional measures of connectivity (e.g., means of connectivity) in two meaningful ways. First, graph theoretical analysis is applied to "graphs," for which spatial arrangements of nodes were not considered. Particularly, edges are not weighted by the length of connections. Angles between edges are not specified. For that reason, graph metrics theoretically preserve very little or no spatial information. The results therefore might not be reconciled with earlier findings obtained for the connection-length-dependent over-connectivity and under-connectivity. Second, using graph theory, one can describe a certain property of the entire brain network in a single measure. In this sense, one need not address the difficulty posed by multiple comparisons. In contrast, for example, comparing the means of functional connectivities for each pair of brain regions can be expected to result in multiple comparisons. Erroneous inferences become more likely. With the help of graph theory, properties of a given graph can be described using various measures. Well-established and widely used measures include the mean clustering coefficient (CC), average shortest path length (cPL), and small-worldness (SW). Because CC represents the degree to which connected nodes are clustered, it is thought to represent the tendencies of the brain to process information locally (i.e., local functional segregation) (14). Characteristic path length (cPL) represents the average number of edges in shortest paths (i.e., sequence of edges connecting one node to another), where the average is taken over all possible pairs of nodes. For that reason, cPL is thought to indicate integration of information from remote brain regions (i.e., global functional integration) (14). Networks with high CC and low cPL are well-connected both locally and globally, and are therefore designated as small-world networks. Such networks are thought to represent an optimal balance between functional local segregation and global integration (15, 16). To describe how much a given network possesses small-world properties, small-worldness (SW) is defined as the ratio of normalized CC and cPL. SW is a particularly interesting property in that the healthy human brain is a small-world network (10, 17), but brain networks reportedly deviate from small-world networks in some neurological conditions such as Alzheimer's disease (17), depression (18), and schizophrenia (19).

Several studies have applied graph theory to compare the brain networks of typically developing individuals to those of patients with ASD in terms of CC, cPL, or SW. Two studies particularly examined graphs of structural connectivity (i.e., DTI). Others have emphasized functional connectivity. Among those latter studies, two used resting-state fMRI. All others have been EEG/MEG studies. Unsurprisingly considering methodological differences such as imaging modalities, participant characteristics, and graph theoretical measures, the results obtained from DTI-derived or resting-state fMRI-derived networks are inconsistent. The first report of structural networks was a study by Rudie et al. (20). They investigated structural networks generated based on DTI-derived fiber tracts in adolescents with and without ASD. Using six graph theoretical measures (i.e., CC, cPL, normalized CC, normalized cPL, SW, and modularity), the authors reported that the ASD

group showed significantly lower modularity, but no significant differences were found in the other five measures. In a study conducted later by Qin et al. (21), children with ASD (2.89 ± 0.97 years old) and TD children (3.15 ± 1.12 years old) were recruited. Among seven measures (i.e., CC, cPL, normalized CC, normalized cPL, SW, global and local efficiency), their DTI-derived structural network showed significantly lower cPL and higher global/local efficiency in children with ASD. Combining those results, the structural brain network of ASD would show lower cPL and higher global/local efficiency in early childhood, after which those characteristics become less evident in later developmental stages. Adolescents with ASD would then show lower modularity than typically developing individuals. Among studies assessing functional connectivity, two used resting-state fMRI (20, 22). For one of those studies (20), Rudie et al. also investigated functional networks generated from resting-state fMRI. Results showed significantly lower CC, cPL, and modularity in the adolescent ASD group. It is noteworthy that Kaku et al. reported contradictory results: children with severe ASD were found to have significantly higher normalized CC and small-worldness than children with mild or moderate ASD (22). It remains unclear whether the relation between autistic symptoms and CC derived from resting-state fMRI is somewhat non-linear (i.e., individuals with ASD show lower CC than TD individuals, but those who have severe ASD shows paradoxically higher CC) or the relation is age-dependent (i.e., higher CC in childhood, but lower CC in adolescents corresponds to lower social communication).

All other reported graph theoretical studies of functional connectivity have used MEG or EEG. One must be cautious when comparing results of these studies because of the different imaging modalities (EEG vs. MEG), participant characteristics, and graph theoretical measures. Moreover, in MEG/EEG studies, synchronization measures differ among studies. Within the framework of those limitations, however, a consensus seems to hold that brain networks of adults with ASD constructed based on resting-state MEG/EEG derived functional connectivity show lower CC and higher cPL than those of healthy controls. However, the results are inconsistent for the younger population. The first report was of a study conducted by Pollonini et al. (23). They recruited young adults with and without ASD and investigated the functional networks generated from resting-state MEG recordings. Based on their findings, they reported significantly lower CC and higher cPL (in the broadband signal) in the ASD group than in healthy controls. From a later study, adults with ASD were also reported as having significantly lower CC (in the theta combined with the alpha band, and beta band) and higher cPL (in the beta band) than healthy controls had (24). Furthermore, Han et al. reported that children (6–11 years old) with ASD showed lower CC and lower SW in widely various frequencies, but the difference was less evident in younger children (3–6 years old) (25). It is noteworthy that the graph theoretical measures were correlated with ASD symptom severity in the alpha band. Regrettably, however, the results obtained from this study should be compared with caution because they did not exclude effects of medication. All the reports described above indicate lower CC in ASD patients than in healthy control participants. One notable exception is a study conducted by Ye et al. (26). They reported higher CC and lower cPL in the theta band for adolescents (12–15 years old) with ASD compared to healthy controls. It remains unclear whether the properties of resting state MEG/EEG-derived functional brain networks are specifically different in adolescents with ASD from those in adults or children with ASD, in that lower CC and lower SW in childhood ASD reported by Han et al. might arise as an effect of medication.

Results from studies that used non-resting state EEG/MEG are inconsistent. On the one hand, Boersma et al. investigated non-resting state EEG data (i.e., children passively viewed pictures of cars and faces) obtained from children with and without ASD (2–5 years old). Based on their findings, they reported that children with ASD had lower CC, lower SW (in theta and alpha bands), and higher cPL (in broad band) than those found for healthy control participants (27). On the other hand, Takahashi et al. investigated MEG data obtained when children actively watched animated video programs. They reported that children with ASD (4–7 years old) showed significantly higher SW in the gamma band and lower SW in the delta band, but differences in CC or cPL were not significant (28). It is noteworthy that among the three graph theoretical studies of children with ASD (25, 27, 28), lower SW has been almost consistently reported. For the other graph metrics, however, the findings are inconsistent. Considering the recording conditions [resting-state (25) vs. during visual stimulation (27, 28)], the difference might arise from atypical functional connectivity during visual information processing in ASD (29, 30), but the possible effect of medication in the study by Han et al. makes it difficult to compare the results directly. Furthermore, no earlier studies have investigated the relation between the graph metrics and ASD symptom severity after controlling for medication effects. In this context, resting-state MEG/EEG studies of children with and without ASD, excluding medication effects, might have a great merit, yet no such studies have been conducted. For such a study, it would be desirable to investigate relations between graph theoretical measures and autistic symptoms.

Therefore, for this study, we examined the resting-state MEG-derived functional network in children with and without ASD using graph theory. Furthermore, we examined the relation between graph theoretical measures and social communication. Based on results of earlier studies, we hypothesized that children with ASD show lower SW in resting-state MEG. Particularly, our hypotheses were the following: (1) Children with ASD show lower SW than TD children do. (2) Lower SW corresponds to severe ASD symptoms.

MATERIALS AND METHODS

Experimental Design

For child participants with or without ASD, we assessed autism symptom severity using the Social Responsiveness Scale (SRS) (31). Intelligence was assessed using the Kaufman Assessment Battery for Children (K-ABC, Japanese version) (32). We recorded resting state MEG data. Signal sources are mapped onto the Desikan–Killiany atlas of 68 brain regions. Then

MEG-derived functional brain networks were constructed in terms of the phase lag index (PLI). Applying graph theory, we calculated SW from the graphs of functional networks. Furthermore, as an exploratory analysis, we calculated CC and cPL for completeness. We then compared the graph metrics between ASD and TD. If a significant group effect was found in any graph metric, we investigated the relation between autism symptom severity and the graph metric.

Ideally, to calculate the necessary sample size to test our hypothesis, we had to know the effect size of having ASD on SW in exactly the same setting (e.g., using resting-state MEG and graphs of PLI-derived functional networks for children with and without ASD). However, no such earlier study has been described, as explained in the *Introduction.* We therefore expanded the search scope to include studies in which children with and without ASD were compared in terms of SW obtained from functional connectivity graphs (25, 27, 28). Unfortunately, we were unable to extract or calculate the standard effect size from those studies because of a lack of information. Consequently, we chose to assume the effect size as large because the three studies found significant effects of ASD on SW in small sample sizes: Boersma et al. compared 12 children with ASD and 19 TD children (27); Han et al. compared 20 children with ASD and 40 TD children (25); and Takahashi et al. compared 24 children with ASD and 24 TD children (28). To assess differences between two independent means in two groups, we set the effect size as 0.8, set the alpha value as 0.05, and set the (1—beta) value as 0.8. The statistical power was calculated for the one-tailed not two-tailed *t*-test because we hypothesized that children with ASD show lower SW than TD children do. The required sample size was therefore calculated as 21 for each group. For the sample size calculation, we used software (G∗Power ver. 3.121.6; Heinrich-Heine-Universität Düsseldorf).

Participants

The clinical group included 21 children with ASD recruited from Kanazawa University and affiliated hospitals. The control group included 25 TD children with no reported behavioral or language difficulty. The ASD diagnosis was made according to the Diagnostic and Statistical Manual of Mental Disorders (4th edition, DSM-IV) (33), using the Diagnostic Interview for Social and Communication Disorders (DISCO) (34), and the Autism Diagnostic Observation Schedule-2 (ADOS-2) (35, 36). We excluded children with (1) blindness, (2) deafness, (3) any other neuropsychiatric disorder, or (4) ongoing medication regimen. Written informed consent was obtained from parents before the children participated. The Ethics Committee of Kanazawa University Hospital approved the methods and procedures, which were conducted in accordance with the Declaration of Helsinki.

In case some were unable to complete the MEG recording, we recruited a few more participants than indicated as necessary by the sample size calculation. Unfortunately, however, one girl with ASD was excluded from analyses during MEG data preprocessing (see *Preprocessing* below). In consequence, we analyzed 20 children with ASD (14 boys, 6 girls, 60–89 months old) and 25 TD children (15 boys, 10 girls, 60–91 months old), which were fewer than the number indicated by the sample size calculation.

Assessment of Social Autism Symptom Severity

Participant's autism symptom severity was assessed in the SRS: a 65-item rating scale that measures social communication and autistic mannerisms. A parent of each participant filled out the SRS. We used gender-normed T scores (SRS-T) and its five subscales: social awareness (SRS-AWA, ability to recognize social cues), social cognition (SRS-COG, interpreting social behavior), social communication (SRS-COM, reciprocal communication in social situation), social motivation (SRS-MOT, motivation to participate in social interactions), and autistic mannerism (SRS-MAN, circumscribed interests and stereotypy). Higher scores represent greater autism symptom severity.

The SRS can be completed by a parent or another adult informant. By virtue of this feature, it involves ratings of children in their natural social contexts and reflects what has been observed consistently over weeks or months of time, rather than merely reflecting results of a single clinical or laboratory observation (31). Nevertheless, one must be cautious when interpreting the SRS results because all such parent rating scales have important shortcomings, such as parent bias and limited reliability, compared to direct observation by expert clinicians.

Assessment of Intelligence

Intelligence of the participants was assessed using the K-ABC. In K-ABC, skills for problem-solving abilities are interpreted as intelligence and are measured on the Mental Processing Scale (MPS) (37). Knowledge of facts, defined as achievement, is measured on the Achievement Scale (ACH). In this sense, K-ABC was developed to distinguish intelligence from knowledge (32, 37). Those scores are provided as age-adjusted standardized scores, normalized to have a mean of 100 and standard deviation of 15.

MEG Recordings

MEG data were recorded using a 151-channel Superconducting Quantum Interference Device (SQUID) whole-head coaxial gradiometer MEG system for children (PQ 1151R; Yokogawa/KIT, Kanazawa, Japan) in a magnetically shielded room (Daido Steel Co., Ltd., Nagoya, Japan) installed at the MEG Center (Ricoh Co., Ltd., Kanazawa, Japan). We used a custom-made child-sized MEG system to measure brain responses in children because some difficulties arise when using conventional adult-sized MEG systems for young children. Using the child-sized MEG system ensures that sensors are positioned easily and effectively for the child's brain. Moreover, it ensures that head movements are constrained (38).

We undertook great effort to keep each child motionless during the recording. We instructed each child not to move the head or body to avoid motion artifacts. Then, one staff member escorted the child into the shielded room. The room was decorated with colorful pictures of cartoon characters, generally of a signature vehicle in a popular animation series. To encourage the child further to maintain a steady head position, the staff

member stayed in the room. In this way, we were able to entertain most of the children. Additionally, they were monitored carefully using a video monitoring system. If the head position of the subject had obviously moved from its starting position, those related MEG data were excluded from further analyses.

Low pass filtered MEG data (500 Hz) were collected at a 2,000 Hz sampling rate. The MEG recordings were made in a resting state: the participant lay supine on a bed and gazed at a fixation cross mark projected onto a screen during the MEG recording. Then MEG data were recorded for 130 s for each participant. The time of MEG recording was between 11 A.M. and 3 P.M. No child showed a clear sign of drowsiness in terms of MEG waveforms. Ideally, longer recording durations are desirable. For children, especially children with ASD, however, it was difficult to keep them sitting still for long durations. The recording period had to be determined with compromise. Given that limitation, we adopted 50 s as the minimum, as we did for an earlier study (28) in which we analyzed artifact-free segments of length minimum of 50 s and found significantly different SW between children with and without ASD. We set the recording time as 130 s, slightly longer than 50 s, to secure a minimum of 50 s and to spare some time.

MRI Recordings

A 1.5 T MRI scanner (SIGNA Explorer; GE Healthcare, USA) was used to obtain structural brain images from all participants and to compute individual head models for source analysis. The T1-weighted gradient echo and Silenz pulse sequence (TR = 435.68 ms, TE = 0.024 ms, flip angle = 7°, FOV = 220 mm, matrix size = 256 × 256 pixels, slice thickness = 1.7 mm, a total of 130 transaxial images) images were used for anatomical reference. All participant's MRI images were recorded.

Co-registration of MEG on MRI Image

We co-registered the MEG and MRI images according to the marker locations. Four markers were recorded by the MEG and the MRI: midline frontal, vertex, and each bilateral mastoid process. For MEG, we used four coils generating a magnetic field. For MRI, we used four pieces of lipid capsule as markers because those are observed as high-intensity regions. Additionally, we showed points on mastoid processes, nasion, and the skull surface visually in MRI. About 15–25 points were shown for each participant.

MEG Data Analysis

The MEG analyses were performed using Brainstorm (39), which is documented and freely available under the GNU general public license for download online.

Preprocessing

The MEG data were preprocessed according to recommendations from the Organization for Human Brain Mapping (40). First, we downsampled the MEG data to 500 Hz. Second, we excluded three sensors from analyses because their signal quality was poor. Third, after applying notch filters (60, 120, and 180 Hz) to remove power-supply noise, we applied a band-pass filter (0.5–200 Hz). Fourth, we used the independent component analysis (ICA) to remove blink and cardiac artifacts. Finally, segments containing apparent motion noise or radio frequency interference were excluded from analyses after they were visually identified by an MEG expert who was blinded to the identities of participants. One girl's motion noise was excessive. For that reason, we excluded data obtained from this child from subsequent analyses. Data were segmented for continuous segments of 5 s. A minimum of 10 segments (50 s recording period) was accepted for each subject. Each epoch was band-pass filtered for commonly used frequency bands: delta (2–4 Hz), theta (4–8 Hz), alpha (8–13 Hz), beta (13–30 Hz), and gamma (30–60 Hz). This preprocessing procedure is identical to that used for our earlier study (28).

Atlas-Guided Source Reconstruction and Segmenting

We performed signal source estimation using the participant's original anatomy. An anatomically constrained MEG approach that places an anatomical constraint on the estimated sources was used to estimate the brain signal sources (41). When the sources are estimated, each participant's recorded brain activity is assumed to lie in the cortical mantle. We coregistered MEG on participant's MRI images. A head model was computed using the overlapping spheres algorithm (42) with the default source space (a lower-resolution cortical surface representation, with 15,000 vertices). We used weighted minimum-norm estimation to estimate source orientation constraints (43). An identity matrix was used as noise covariance because no noise recording is available. Signal sources were grouped together into 68 regions represented in the Desikan–Killiany atlases (44). When we grouped sources, we used principal component analysis.

We chose Desikan–Killiany atlases considering the limit of spatial resolution of MEG as well as a balance between interpretability of the results and fineness of estimation. Graph theoretical analysis of the functional brain network fundamentally depends on the definition of nodes (i.e., brain regions). A parcellation scheme must be chosen that reasonably samples the brain regions. Results from fewer regions of interest (ROI) are expected to offer increased interpretability, but functionally and anatomically distinct regions can be regarded as a single ROI. Conversely, results from many ROIs finely represent functional connectivity patterns, but their interpretability might be difficult (45). Between these two extremes, Hallquist et al. reported in their recent literature review that researchers should divide the brain into at least 200 functional regions for fMRI studies (46). In MEG studies, however, more compromises must be made because of its low spatial resolution. In this context, Farahibozorg et al. investigated the optimal number of parcels while simultaneously minimizing the leakage between them. They concluded that the number was approximately 70 parcels, which is expected to reflect the limit of spatial resolution of MEG (47). Based on these considerations, we adopted the Desikan–Killiany brain atlas as suitable for this study.

Phase Lag Index

To estimate functional connectivity between signal sources, we used the phase lag index (PLI). Although functional interactions

can be measured by quantifying the phase relation between their time series (48), one must consider that reconstructed sources might contain spurious and artificial interactions because of field spread. In such cases, artificial synchrony might be observed between nearby signal sources (49). This kind of artificial synchrony can be removed by suppressing zero-lag synchrony and by detecting exclusively lagged interactions. One mixing-insensitive interaction metric, PLI, attenuates artificial interactions (50). Briefly, the instantaneous phase at each time point of the filtered waveform was calculated for each epoch using the Hilbert transform. Then, phase difference $\Delta\varphi(tk)(k = 1,2,3, \ldots, N$, where N is the number of time points in an epoch) was calculated for each time point. The value of PLI between two signal sources in an epoch was obtained using the following definition (50).

$$PLI = \left| \frac{1}{N} \sum_{k=1}^{N} sign\left[\Delta\varphi\left(t_k\right)\right] \right| \quad (1)$$

We used PLI to estimate phase synchrony between source pairs for each frequency band. The value of PLI is in the range of zero to one, inclusive. Two more synchronized sources have PLI that is closer to one. It is noteworthy that PLI does not indicate which of the two signals is leading in phase.

Graph Construction and Graph Metrics

To describe brain characteristics, we used graph theory. A graph is a basic topographical representation of a network consisting of "nodes" and "edges." The network used for this study comprised 68 nodes (brain regions defined by Desikan–Killiany) connected by weighted edges (calculated as PLI values). Therefore, an undirected weighted functional connectivity matrix (68 × 68) was constructed for each frequency band (i.e., delta, theta, alpha, beta, gamma) and for each epoch. We averaged the matrices of all epochs for each participant. Binary graph approaches were applied to simplify characteristics of a graph and to remove spurious connections. Because no formal consensus exists for a robust method for threshold selection, we set proportional threshold κ, the proportion of total connections retained, as 0.2 according to results reported for earlier studies (28, 50, 51) (A κ of 0.2 indicates that the strongest 20% of the connections were selected.). Furthermore, considering κ-dependency of graph metrics, we also investigated a set of κ for 0.1–0.3 with 0.02 increments. For these binary matrices, we calculated the most commonly used graph metrics: The clustering coefficient (CC), the characteristic path length (cPL), and small-worldness (SW) (15). Consequently, the graph metrics were obtained from each frequency band (i.e., delta, theta, alpha, beta, and gamma) for each set of proportional thresholds κ. To calculate them, we used the Brain Connectivity Toolbox (http://www.brain-connectivity-toolbox.net/, ver. 2019-03-03). Mathematical definitions of those metrics have been reported elsewhere in the literature (10, 52).

The number of connections between the nearest neighbors of a node as a proportion of the maximum number of possible connections, expressed as CC, represents how clustered a graph's nodes are. The presence of clusters in functional networks suggests organization of segregated neural processing (10). In addition, cPL represents the average length of the shortest path that must be traversed to go from one node to another. That value represents how rapidly a graph conveys information from one region to another and suggests the degree of integration of a graph (10). In rare cases, two nodes are disconnected; thereby, PL becomes infinite. To avoid this difficulty, we calculate only from connected nodes according to a method used for our earlier study (28). Additionally, SW was determined by the ratio of normalized CC and normalized cPL. When a graph has high CC and low cPL, the graph is more clustered but it conveys information more rapidly. Such a property is designated as SW. The property is thought to reflect an optimal balance of functional integration and segregation (52). To evaluate the SW of a graph, CC and cPL are adjusted because these metrics clearly depend on the numbers of nodes and edges of the graph. SW is therefore defined as the ratio of normalized CC and cPL. In this way, a graph of high SW is a network that is markedly more clustered than random networks (i.e., randomly generated networks for which the numbers of nodes and edges are the same), yet they have approximately the same characteristic path length (16). The SW measure captures this property in a single statistic (52). Normalized CC and cPL were obtained from a random network that is randomized by rewiring all edges five times. We produced 1000 random networks and their CC and cPL (hereinafter, CCrand and cPLrand) for each graph. Then, SW was found using the ratio of normalized CC and cPL (i.e., CC/CCrand and cPL/cPLrand). For each subject, CC, cPL, and SW were calculated on each frequency band.

Statistical Analysis

Statistical analyses were conducted using software (Stata ver. 14.2; Stata Corp., College Station, TX, USA). We tested differences in age and scores in K-ABC and SRS between ASD and TD using Student *t*-tests (two-tailed). Sex difference was tested using chi-square tests.

The differences between ASD and TD on SW were tested using Student's *t*-test (one-tailed) for each frequency band (delta, theta, alpha, beta, and gamma). Then, to elucidate differences between ASD and TD on graph metrics further, we matched the two groups in terms of MPS in K-ABC while considering the possible effects of intelligence on functional connectivity (53). To improve the balance, we used coarsened exact matching (CEM) (54). Subsequently, we applied adjusted regression analysis. Particularly, we predict graph metrics based on the condition (ASD or TD) with CEM-weight for weighting. For the CEM algorithm, we temporarily coarsen (or categorize) each variable based on its distribution or on natural or intuitive divisions. Each participant is then assigned to one of a specified set of strata in which the participant characteristics are matched exactly on a set of coarsened variables. A weighting variable (CEM-weight) is generated to equalize the number of treated and control cases in one stratum. It is used for subsequent regression analyses (54). We used Sturge's rule as a binning algorithm (54). This report describes the degree of imbalance before and after matching by measurement of the multivariate L1 distance. The L1 distance represents how two groups are balanced in terms of matched variables (in our case, K-ABC). The L1 distance is

a value between zero and one: a smaller value represents better balance. Our primary emphasis was examination of differences of SW for five frequency bands: delta, theta, alpha, beta, and gamma. Significance was inferred for $P < 0.01$ after Bonferroni correction for five comparisons was applied. We also analyzed cPL and CC for completeness, but we formulated no particular hypothesis related to those measures. Effect sizes were provided as R^2. Although we primarily emphasized the graphs of the proportional threshold 0.2 for consistency with earlier studies (28, 38, 51), this procedure was applied for a set of κ over the range of 0.1–0.3 with 0.02 increments.

To investigate the relation between SW and autism symptom severity, we specifically examined the metric obtained from the graphs of threshold 0.2 as a representative for consistency with earlier studies (28, 38, 51). If a significant group effect was found for SW in any frequency band, then we applied a linear regression models to predict the SW based on the SRS-T score. In doing so, we assessed the relation between autism symptom severity and SW in such frequency bands. We analyzed effects of SRS on the SW only in children with ASD because we observed that SRS-T scores were much lower and homogeneous in TD children, thereby indicating the presence of the floor effect. Significance was inferred for $P < 0.05$, but we used appropriate correction for multiple comparisons if a significant group effect was found for more than one frequency band.

Furthermore, we investigated the relation between SW and SRS sub-scales to discern which sub-scale drives the effect. For sub-scale analysis, significance was inferred for $P < 0.01$ after Bonferroni correction was applied for five multiple comparisons: *social communication, social awareness, social cognition, social motivation*, and *autistic mannerisms* sub-scales.

In addition, considering the possibly different results derived from informant-based (i.e., SRS) and laboratory-based (ADOS-2) measures, we analyzed effects of ADOS-social interaction and communication scores on SW. Particularly, we applied a linear regression model to predict SW based on ADOS-social interaction and communication scores. Effect sizes were provided as R^2.

Before applying any linear regression model, we verified that our data meet the assumptions for regression analysis before application of linear regression. Specifically, we used standard methods to verify linearity, normality, homogeneity of variance, model specifications, and influence. As a result, the assumption of homogeneity was violated for some regression models. Therefore, we used heteroscedasticity-robust standard errors (55).

RESULTS

One girl with ASD was unable to complete K-ABC because of severe psychomotor agitation. We found no significant differences in sex, age, or epoch number. Significant differences were found in the SRS total score, SRS sub-scale, Mental Processing Scale, and Achievement Scale. **Table 1** presents the related results. Among the 20 children with ASD, module 1 was applied to one child, module 2 was applied to 17 children, and module 3 was applied to two children. **Supplementary Table 1** presents the subject's sub-scores in ADOS-2.

TABLE 1 | Characteristics of participants.

	ASD	TD	χ^2 or *t*	*P*-value
N	20	25		
Sex (% Male)†	70	60	0.49	0.486
Age in months‡	73.5	69.2	−1.73	0.091
Epoch number‡	19.7	21.2	1.25	0.217
SRS total score‡	68.8	46.5	−7.57	< 0.001*
K-ABC scores				
MPS‡	99.2	114.5	3.15	0.003*
Achievement scale‡	95.3	106.9	2.41	0.020*

†*Chi-square test.*
‡*Student's t-test.*
**Statistical significance.*
ASD, autism spectrum disorder; TD, typically developing children; K-ABC, Kaufman Assessment Battery for Children; SRS, Social Responsiveness scale; MPS, Mental Processing scale.

Group Differences in SW: One-Tailed *T*-tests

Our primary emphasis was to investigate differences in SW between the brain network of children with and without ASD. We first investigated the SW in each frequency band setting κ at 0.2 for consistency with earlier studies (15, 26, 35). Student's *t*-test showed that children with ASD had significantly lower SW in the beta band than TD children did [$t(43) = 2.67$, $p = 0.005$ for a one-tailed *t*-test and $p = 0.011$ for a two-tailed *t*-test]. The differences were not significant for any other frequency band.

Similar patterns were observed for the other κ. Children with ASD showed lower SW in the beta band, the differences of which were most marked when κ was set as 0.14–0.22. **Figure 1**, **Supplementary Figures 1–4**, **Supplementary Table 2** present the relevant results.

Group Differences in Graph Metrics in Matched Participants – CEM

To investigate differences between ASD and TD on graph metrics further, we matched the two groups in terms of MPS in K-ABC considering possible effects of intelligence on functional connectivity. We first investigated the graph metrics setting κ at 0.2. After improving balance using the CEM algorithm, 15 ASD children and 25 TD children comprised the matched participants. The L1 distance improved from 0.300 to 0.115. After matching, we used linear regression with CEM weights to predict the graph metrics based on the condition (i.e., ASD or TD). Only for the model predicting SW in the beta band was the main effect of the condition ($t(40) = -2.83$, $p = 0.007$) found to be significant. **Table 2** presents results obtained from the graphs with κ of 0.2. Similar patterns are observed for the neighboring κ. The differences were marked when the proportional threshold was set as 0.16–0.22. Significant difference in SW was found in the theta band when κ was set as 0.10, but the difference was not significant when κ was set as 0.12 or higher. Therefore, we discarded

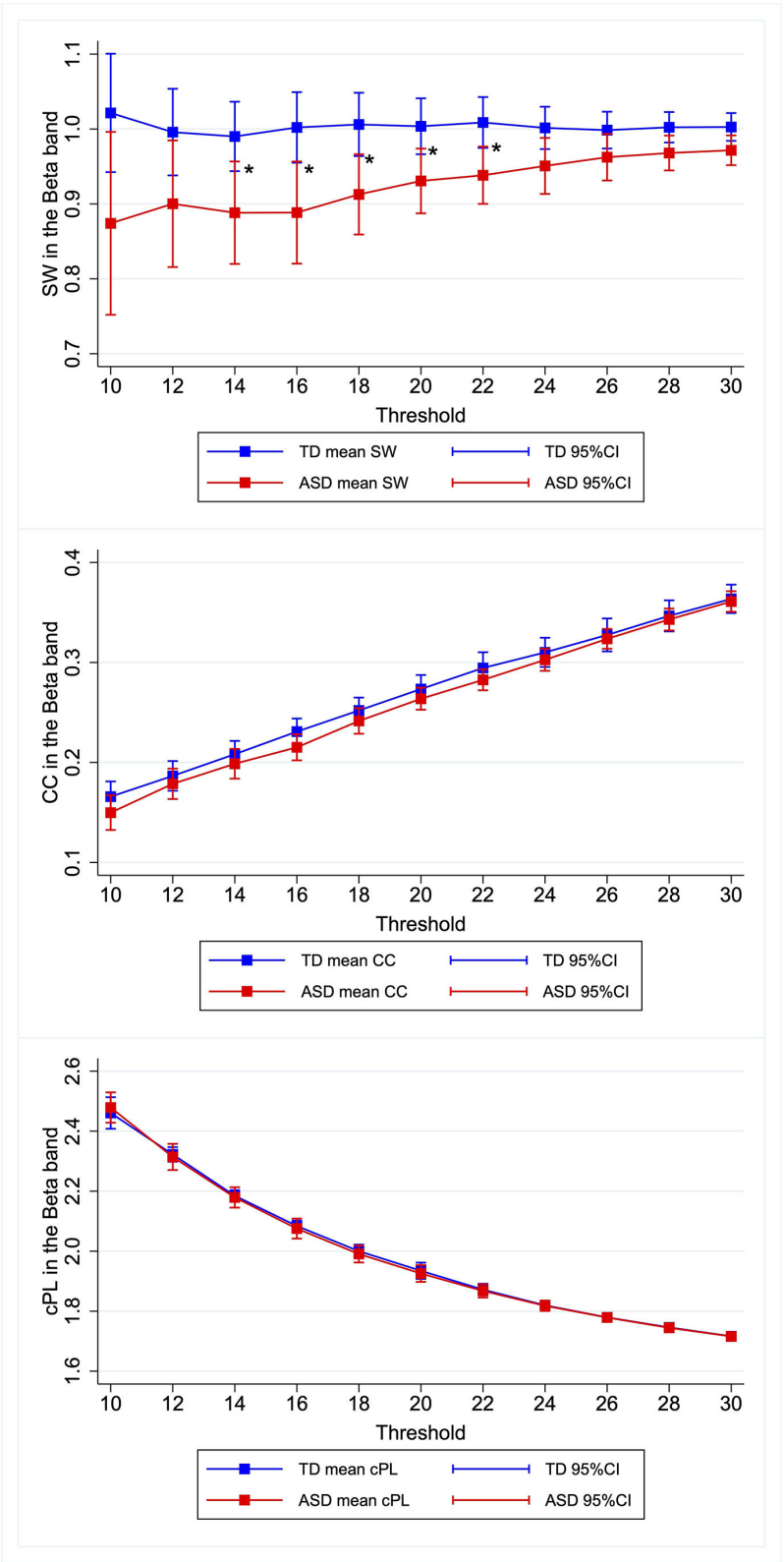

FIGURE 1 | Group differences in graph metrics for different proportional thresholds in the beta band. Means of the respective graph metrics are presented with 95% confidence intervals for the respective proportional thresholds. Children with ASD show lower SW in the beta band for widely various proportional thresholds. ASD, children with autism spectrum disorder; TD, typically developing children; SW, small-worldness CC, clustering coefficient; cPL, characteristic path lengths. *Indicate statistical significance.

TABLE 2 | Difference between ASD and TD in graph metrics in matched participants with κ of 0.2.

Frequency band	Graph metrics	Coeff.	S.E.	*t*	*p*	95% CI			R^2
Delta	SW	0.001	0.017	0.05	0.957	−0.034	–	0.036	<0.001
	CC	−0.002	0.006	−0.31	0.758	−0.014	–	0.010	0.003
	cPL	0.005	0.005	1.05	0.301	−0.005	–	0.016	0.028
Theta	SW	−0.016	0.021	−0.75	0.456	−0.060	–	0.027	0.015
	CC	0.006	0.009	0.73	0.473	−0.011	–	0.024	0.014
	cPL	0.014	0.009	1.62	0.113	−0.003	–	0.031	0.065
Alpha	SW	−0.023	0.025	−0.90	0.375	−0.073	–	0.028	0.021
	CC	−0.022	0.019	−1.19	0.243	−0.061	–	0.016	0.036
	cPL	−0.005	0.023	−0.21	0.833	−0.052	–	0.042	0.001
Beta	SW	−0.083	0.293	−2.83	0.007*	−0.142	–	−0.024	0.174
	CC	−0.005	0.010	−0.54	0.592	−0.025	–	0.015	0.008
	cPL	0.008	0.018	0.44	0.661	−0.028	–	0.043	0.005
Gamma	SW	−0.009	0.032	−0.29	0.776	−0.075	–	0.056	0.002
	CC	−0.001	0.011	−0.06	0.952	−0.022	–	0.021	<0.001
	cPL	−0.006	0.012	−0.52	0.608	−0.031	–	0.018	0.007

**Statistical significance.*

ASD, autism spectrum disorder; TD, typically developing children; SW, small-worldness; CC, clustering coefficient; cPL, characteristic path length.

TABLE 3 | Effect of SRS score on SW in the beta band in ASD participants with κ of 0.2.

vs. SW	Coeff.	Robust S.E.	95% CI			*t*	*p*	*F*	R^2
SRS-T	−0.003	0.001	−0.006	–	0.000	−2.14	0.047*	4.57	0.196
SRS-AWA	−0.004	0.002	−0.008	–	−0.001	−2.69	0.015	7.23	0.258
SRS-COG	−0.004	0.001	−0.007	–	−0.001	−3.00	0.008*	9.01	0.281
SRS-COM	−0.003	0.002	−0.007	–	0.000	−1.81	0.088	3.27	0.154
SRS-MOT	−0.001	0.002	−0.005	–	0.003	−0.69	0.500	0.47	0.037
SRS-MAN	−0.002	0.002	−0.006	–	0.001	−1.27	0.219	1.62	0.112

**Statistical significance.*

ASD, autism spectrum disorder; TD, typically developing children; SW, small-worldness; SRS-T, Social Responsiveness Scale Total score; SRS-AWA, Social Awareness sub-scale; SRS-COG, Social Cognition sub-scale; SRS-COM, Social Communication sub-scale; SRS-MOT, Social Motivation sub-scale; SRS-MAN, Social Mannerism sub-scale.

this result as noise. **Supplementary Table 3** presents the results. Although our primary emphasis is on SW, we investigated group differences for other graph metrics (i.e., CC and cPL) for each frequency band and each κ. Significant differences were found for CC in the delta band when κ was set as 0.10 and were found for cPL in the theta band when κ was set as 0.30, but the differences were non-significant for the other κ. Hence we discarded these results as noise. We found no significant effect of group in any of the models. **Supplementary Table 3** presents the results.

Relation Between SW and Autism Symptom Severity

To elucidate the relation between SW and autism symptom severity, we specifically examined the SW in the beta band obtained from the graphs of $\kappa = 0.2$ as a representative for consistency with earlier studies (28, 38, 51). We applied a linear regression model to predict the SW in the beta band based on SRS-T score. The regression model revealed the main effect of SRS-T score as significant ($t(18) = -2.14$, $p = 0.047$). For sub-scale analysis, a significant main effect was found only for the model predicting SW in the beta band based on the SRS-cognition sub-scale ($t(18) = -3.00$, $p = 0.008$). The higher SRS-awareness sub-scale tended to correlate with lower SW in the beta band, but the effect was non-significant after Bonferroni correction ($t(18) = -2.69$, $p = 0.015$). Those results indicate that a higher SRS-T score was associated with lower SW in the beta band in ASD children, in which SRS-cognition and SRS-awareness drove this effect. **Table 3** presents the results. A graph showing the relation between social sub-scale scores and small-worldness is presented in **Figure 2**.

As an exploratory analysis, we applied linear regression to predict SW in the beta band based on ADOS-social interaction and communication scores. Among the 20 children with ASD, one subject was applied module 1, 17 subjects were applied module 2, and two subjects were applied module 3. Observations were therefore insufficient for module 1 and module 3. Consequently, we analyzed the effects of ADOS-social interaction and communication scores on the SW only for 17 individuals who were applied to module 2. We did not find a significant effect of ADOS-social interaction and communication scores ($t(15) = 0.22$, $p = 0.831$). This non-significant result contrasts against the significant relation found between the SRS scores and SW in the beta band. **Supplementary Table 4** presents the results.

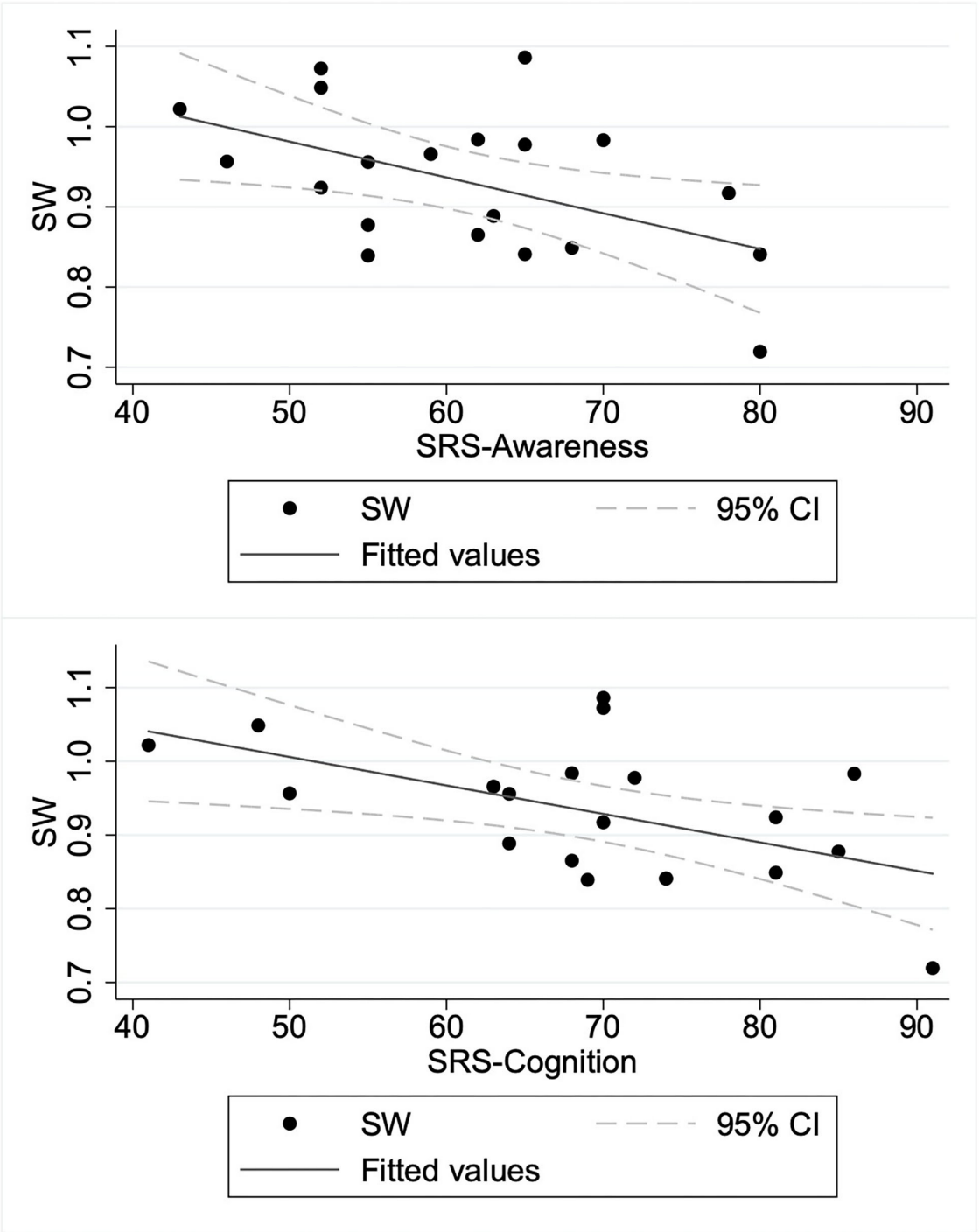

FIGURE 2 | Relation between social sub-scale scores and small-worldness in children with autism spectrum disorder. ASD, children with autism spectrum disorder; SRS-Awareness, Awareness sub-scale of Social Responsiveness Scale; SRS-Cognition, Cognition sub-scale of Social Responsiveness Scale; SW, small-worldness.

DISCUSSION

For TD children and children with ASD (5–8 years old), we recorded resting-state MEG data. No participant was taking medication. We constructed functional brain networks in terms of PLI and analyzed the properties of those networks to explore differences between the two groups. Children with ASD were found to have significantly lower SW in the beta band than TD children did, but not in the other frequency bands. Furthermore, in children with ASD, lower SW in the beta band corresponded

TABLE 4 | Earlier EEG/MEG studies for ASD using graph theory.

Authors	Year	*N* (ASD vs.TD)	Ages	Device	Band	Autistic traits
Boersma et al. (27)	2013	12 vs. 19	2–5	EEG (with Pictures)	Broad	cPL↑
					Alpha, Theta	CC↓,SW↓
Takahashi et al. (28)	2017	24 vs. 24	4–7	MEG (with Animation)	Gamma	SW↑
					Delta	SW↓
Han et al. (25)	2017	60 vs. 76	3–6	EEG	Broad	None
		20 vs. 40	6–11			CC↓, SW↓
Ye et al. (26)	2014	16 vs. 15	12–15	MEG	Theta	CC↑, cPL↓
Pollonini et al. (23)	2010	8 vs. 8	around 19*	MEG	Broad	CC↓, cPL↑
Barttfeld et al. (24)	2011	10 vs. 10	16–38	EEG	Beta	CC↓, cPL↑

ASD, autism spectrum disorder; TD, typically developing children; EEG, electroencephalography; MEG, magnetoencephalography; SW, small-worldness; CC, clustering coefficient; cPL, characteristic path length.

↑ or ↓ indicate significant increase or decrease.

**Authors did not describe the age range of participants. 18.7 ± 0.7 for ASD group, 19.0 ± 1.2 for TD group.*

to severe autistic symptoms in terms of SRS-T scores. This association was driven by the association between the SW in the beta band and SRS-cognition sub-scale. However, the relation between SW in the beta band and ADOS-social interaction and communication sub-scale was found to be non-significant.

For the beta band, we found significantly lower SW in the ASD group than in TD children. This result accords with results reported by Han et al. (25). After using resting-state EEG to investigate 6–11-year-old children, they reported that children with ASD showed lower CC and lower SW for widely various frequencies including the beta band. Nevertheless, they did not exclude effects of medication. In this context, the results obtained from the present study confirm the reduced SW in the functional brain network of children with ASD such that the difference cannot be explained by medication effects. Ye et al. similarly compared ASD and healthy control subjects, but of a slightly older age (12–15 years old) (26). In contrast to the non-significant results obtained for CC and cPL in the current study, they reported higher CC and lower cPL in the ASD group. Although comparing these findings directly is difficult because they neither explicitly exclude the effects of medication nor calculate SW, the present results can extend their results, indicating that the altered CC and cPL in the brain network of ASD would be less evident in a younger population. Boersma et al. and Takahashi et al. investigated children with and without ASD, similarly to the current study, but they used non-resting state EEG/MEG (27, 28). Particularly, Boersma et al. investigated children (aged 2–5 years) with and without ASD using EEG data obtained while children passively viewed images of cars and faces. The ASD group was found to show lower CC and higher cPL, as well as lower SW. Takahashi et al. investigated a similar age range (aged 4–7 years) using MEG data obtained while children watched animated video programs. They found that the ASD group showed higher SW in the gamma band and lower SW in the delta band, but the differences in CC or cPL were not significant. Considering atypical functional connectivity during visual information processing in ASD (29, 30), a difference between those results and the current analysis might arise from different recording conditions (i.e., resting state vs. visual stimulation). Overall, the present results provide additional evidence of age-dependent change in the resting-state functional brain networks of ASD by demonstrating that children with ASD show lower SW than those of healthy controls. Given the results from earlier studies, individuals with ASD are expected to show higher CC and lower cPL in their later developmental stage. They would then show lower CC and higher cPL during adulthood. Summarized results from earlier studies are presented in **Table 4**.

To date, only a report by Han et al. has described a study investigating the association between graph theoretical measures and autistic symptoms. However, they did not exclude medication effects (25). For that study, ASD symptom severity as measured by the autism behavior checklist (56) was negatively correlated with CC and positively correlated with cPL in the alpha band. This report is therefore the first describing that ASD symptom severity measured by SRS is related to a graph metric (i.e., SW in the beta band) of resting-state MEG-derived functional brain networks in childhood ASD after controlling for medication effects. This association was driven by association between the SW and SRS-cognition sub-scale. Against our expectations, however, the relation between ADOS-social interaction and communication scores and the SW was not found to be significant. This inconsistency might arise from the different results derived from parent ratings (i.e., SRS) and clinical observations (ADOS-2). Those different results might be explained by contextual factors and different perspectives. Parents might have more opportunities to observe their child's everyday behaviors. Such behaviors might not be apparent during brief one-to-one test situations (i.e., the controlled test setting for ADOS-2). However, parents are not necessarily trained to differentiate and capture autistic behaviors, whereas clinicians are trained extensively to be able to capture autistic behaviors accurately. Clinicians also have vast amounts of knowledge about typical and atypical development of children. For these reasons, by combining results from two regression analyses (SW vs. SRS scores and SW vs. ADOS-social interaction and communication score), it might be found that lower SW in children with ASD corresponds to fewer social behaviors appearing only in

situations outside of an examination room. However, the results should be interpreted with caution because of major limitations: parent ratings entail parent bias and provide lower reliability than direct observations made by expert clinicians.

Some limitations must be described. First, most of the children with ASD examined for this study were high-functioning children who were able to remain stationary during MEG measurements. Therefore, the findings might not be applicable to children with lower verbal or intellectual abilities, or who have difficulty remaining stationary. Second, we computed PLI for each of >10 epochs of 5 s. This shorter epoch length might affect the PLI values and PLI-based graph metrics. For that reason, one must be cautious when comparing the present results with those from other studies using different epoch lengths. For example, Fraschini et al. analyzed effects of epoch length on PLI and PLI-derived graph metrics using six epochs for each epoch length (i.e., 1, 2, 4, 6, 8, 10, 12, 14, and 16 s) (57). They reported that, in the source space, PLI values and PLI-based graph metrics (weighted CC and weighted cPL) show a decrease with increasing epoch length, where the results stabilize for epochs with lengths of longer than 10 s. Furthermore, at the network level, shorter epochs showed less clear patterns of PLI than those obtained from longer epochs, possibly reflecting inter-epoch variation in neuronal activity. It is noteworthy, however, that their study found no significant relation between epoch length and the standard error of the mean PLI and PLI-based graph metrics with better behavior (in terms of stability) was observed for measures extracted from source level analyses compared with results obtained from sensor level analyses. Although it is difficult to compare those results directly because of methodological differences (e.g., EEG vs. MEG, frequency bands, source estimation methods), the evidence suggests that the results presented herein might be valuable in terms of test–retest reliability, but one must be cautious when comparing results from different studies using data obtained using different epoch lengths. Third, we exerted great effort to keep the participants motionless. Despite that effort, it is still possible that motion artifacts resulted from subtle movement during the acquisition. In addition, the head motion possibly differed between the two groups. Unfortunately, we did not have access to head motion data from MEG scans to ascertain whether this was true. Further study using a quantification algorithm for head movement can be expected to help clarify how motion artifacts affect the graph metrics. Fourth, comparison of the results obtained from this study with those from other graph theoretical studies using different quantities of ROIs (i.e., number of nodes) and different proportional thresholds should be done only with due caution. An important difficulty arises from the fact that graph metrics depend on the number of graph nodes and edges (58). Especially, the dependence cannot be neglected when the nodes are fewer than 200 (58). No satisfactory method for correcting for such effects has been reported in the relevant literature. Fifth, the sample was smaller than the sample size calculation indicated. A study with low statistical power has a reduced likelihood that a significant result reflects a true effect. In fact, it might overestimate the effect size (59). For that reason, to estimate the effect sizes of group difference (i.e., ASD vs. healthy controls) accurately in graph metrics, studies examining a larger sample must be conducted. Sixth, one must be cautious when interpreting the results of parent-report measures such as SRS because all such scales entail important shortcomings, such as parent bias and limited reliability, compared to direct observation by expert clinicians.

For this study, we specifically examined young TD children and children with ASD because early diagnosis of ASD is important for supporting developmental follow-up in children with ASD. Our study provides important information that can be expected to improve our understanding of neurophysiological mechanisms underlying the earlier development of social abilities and brain networks in children with ASD. As a highly non-invasive method, MEG can provide a potential biomarker for ASD in young children by application of the observed behavioral and neurophysiological alterations in patients with ASD.

DATA AVAILABILITY STATEMENT

The raw data supporting the conclusions of this article will be made available by the authors, without undue reservation.

ETHICS STATEMENT

Written informed consent was obtained from the minor(s)' legal guardian/next of kin for the publication of any potentially identifiable images or data included in this article.

AUTHOR CONTRIBUTIONS

DS, TH, CH, K-mA, and MK: contributed to conception and design of the study. CH, K-mA, YY, SI, ST, and KY: acquired the data. DS and SN: wrote source code for analysis. DS, TH, and MK: analyzed the data. DS: wrote the first draft of the manuscript. TH and MK: wrote sections of the manuscript. All authors contributed to manuscript revision, read, and approved the submitted version.

FUNDING

This study was supported by the Center of Innovation Program of the Japan Science and Technology Agency, JST, JSPS KAKENHI Grant Numbers: 20H03599 and 20K16623.

SUPPLEMENTARY MATERIAL

The Supplementary Material for this article can be found online at: https://www.frontiersin.org/articles/10.3389/fpsyt.2021.790234/full#supplementary-material

REFERENCES

1. American Psychiatric Association. *Diagnostic and Statistical Manual of Mental Disorders (DSM-5®)*. American Psychiatric Pub (2013). Available online at: https://play.google.com/store/books/details?id=-JivBAAAQBAJ
2. Maglione MA, Gans D, Das L, Timbie J, Kasari C. Technical Expert Panel, HRSA Autism Intervention Research—Behavioral (AIR-B) Network. Nonmedical interventions for children with ASD: recommended guidelines and further research needs. *Pediatrics.* (2012) 2(Suppl. 130):S169–78. doi: 10.1542/peds.2012-0900O
3. Hyman SL, Levy SE, Myers SM. Council on Children with Disabilities, Section on Developmental and Behavioral Pediatrics. Identification, evaluation, and management of children with autism spectrum disorder. *Pediatrics.* (2020) 145:e20193447. doi: 10.1542/peds.2019-3447
4. Pardo CA, Eberhart CG. The neurobiology of autism. *Brain Pathol.* (2007) 17:434–47. doi: 10.1111/j.1750-3639.2007.00102.x
5. Donovan APA, Basson MA. The neuroanatomy of autism – a developmental perspective. *J Anat.* (2017) 230:4–15. doi: 10.1111/joa.12542
6. Hull JV, Dokovna LB, Jacokes ZJ, Torgerson CM, Irimia A, Van Horn JD. Resting-state functional connectivity in autism spectrum disorders: a review. *Front Psychiatry.* (2016) 7:205. doi: 10.3389/fpsyt.2016.00205
7. Ishii R, Canuet L.MEG revealed new functional hub of atypical brain network in autism spectrum disorders. *Clin Neurophysiol.* (2018) 129:2022–3. doi: 10.1016/j.clinph.2018.06.008
8. Horwitz B. The elusive concept of brain connectivity. *Neuroimage.* (2003) 19:466–70. doi: 10.1016/S1053-8119(03)00112-5
9. Friston KJ. Functional and effective connectivity in neuroimaging: a synthesis. *Hum Brain Mapp.* (1994) 2:56–78. doi: 10.1002/hbm.460020107
10. Bullmore E, Sporns O. Complex brain networks: graph theoretical analysis of structural and functional systems. *Nat Rev Neurosci.* (2009) 10:186–98. doi: 10.1038/nrn2575
11. O'Reilly C, Lewis JD, Elsabbagh M. Is functional brain connectivity atypical in autism? A systematic review of EEG and MEG studies. *PLoS ONE.* (2017) 12:e0175870. doi: 10.1371/journal.pone.0175870
12. De Vico Fallani F, Richiardi J, Chavez M, Achard S. Graph analysis of functional brain networks: practical issues in translational neuroscience. *Philos Trans R Soc Lond B Biol Sci.* (2014) 369:20130521 doi: 10.1098/rstb.2013.0521
13. Strogatz SH. Exploring complex networks. *Nature.* (2001) 410:268–76. doi: 10.1038/35065725
14. Rubinov M, Sporns O. Complex network measures of brain connectivity: uses and interpretations. *Neuroimage.* (2010) 52:1059–69. doi: 10.1016/j.neuroimage.2009.10.003
15. Bassett DS, Bullmore ET. Small-world brain networks revisited. *Neuroscientist.* (2017) 23:499–516. doi: 10.1177/1073858416667720
16. Sporns O, Zwi JD. The small world of the cerebral cortex. *Neuroinformatics.* (2004) 2:145–62. doi: 10.1385/NI:2:2:145
17. Stam CJ, de Haan W, Daffertshofer A, Jones BF, Manshanden I, van Cappellen van Walsum AM, et al. Graph theoretical analysis of magnetoencephalographic functional connectivity in Alzheimer's disease. *Brain.* (2009) 132:213–24. doi: 10.1093/brain/awn262
18. Zhang J, Wang J, Wu Q, Kuang W, Huang X, He Y, et al. Disrupted brain connectivity networks in drug-naive, first-episode major depressive disorder. *Biol Psychiatry.* (2011) 70:334–42. doi: 10.1016/j.biopsych.2011.05.018
19. Micheloyannis S, Pachou E, Stam CJ, Breakspear M, Bitsios P, Vourkas M, et al. Small-world networks and disturbed functional connectivity in schizophrenia. *Schizophr Res.* (2006) 87:60–6. doi: 10.1016/j.schres.2006.06.028
20. Rudie JD, Brown JA, Beck-Pancer D, Hernandez LM, Dennis EL, Thompson PM, et al. Altered functional and structural brain network organization in autism. *Neuroimage Clin.* (2012) 2:79–94. doi: 10.1016/j.nicl.2012.11.006
21. Qin B, Wang L, Zhang Y, Cai J, Chen J, Li T. Enhanced topological network efficiency in preschool autism spectrum disorder: a diffusion tensor imaging study. *Front Psychiatry.* (2018) 9:278. doi: 10.3389/fpsyt.2018.00278
22. Kaku SM, Jayashankar A, Girimaji SC, Bansal S, Gohel S, Bharath RD, et al. Early childhood network alterations in severe autism. *Asian J Psychiatr.* (2019) 39:114–9. doi: 10.1016/j.ajp.2018.12.009
23. Pollonini L, Patidar U, Situ N, Rezaie R, Papanicolaou AC, Zouridakis G. Functional connectivity networks in the autistic and healthy brain assessed using granger causality. *Conf Proc IEEE Eng Med Biol Soc.* (2010) 2010:1730–3. doi: 10.1109/IEMBS.2010.5626702
24. Barttfeld P, Wicker B, Cukier S, Navarta S, Lew S, Sigman M, et al. big-world network in ASD: dynamical connectivity analysis reflects a deficit in long-range connections and an excess of short-range connections. *Neuropsychologia.* (2011) 49:254–63. doi: 10.1016/j.neuropsychologia.2010.11.024
25. Han J, Zeng K, Kang J, Tong Z, Cai E, Chen H, et al. Development of brain network in children with autism from early childhood to late childhood. *Neuroscience.* (2017) 367:134–46. doi: 10.1016/j.neuroscience.2017.10.015
26. Ye AX, Leung RC, Schäfer CB, Taylor MJ, Doesburg SM. Atypical resting synchrony in autism spectrum disorder. *Hum Brain Mapp.* (2014) 35:6049–66. doi: 10.1002/hbm.22604
27. Boersma M, Kemner C, de Reus MA, Collin G, Snijders TM, Hofman D, et al. Disrupted functional brain networks in autistic toddlers. *Brain Connect.* (2013) 3:41–9. doi: 10.1089/brain.2012.0127
28. Takahashi T, Yamanishi T, Nobukawa S, Kasakawa S, Yoshimura Y, Hiraishi H, et al. Band-specific atypical functional connectivity pattern in childhood autism spectrum disorder. *Clin Neurophysiol.* (2017) 128:1457–65. doi: 10.1016/j.clinph.2017.05.010
29. Leung RC, Ye AX, Wong SM, Taylor MJ, Doesburg SM. Reduced beta connectivity during emotional face processing in adolescents with autism. *Mol Autism.* (2014) 5:51. doi: 10.1186/2040-2392-5-51
30. Bangel KA, Batty M, Ye AX, Meaux E, Taylor MJ, Doesburg SM. Reduced beta band connectivity during number estimation in autism. *Neuroimage Clin.* (2014) 6:202–13. doi: 10.1016/j.nicl.2014.08.020
31. Constantino JN. *Gruber CP. Social responsive scale (SRS) Manual*. Los Angeles, CA: Western Psychological Services (2005)
32. Kaufman AS. *K-ABC: Kaufman Assessment Battery for Children: Administration and Scoring Manual*. American Guidance Service (1983). Available online at: https://play.google.com/store/books/details?id=8FoQAQAAMAAJ. doi: 10.1037/t27677-000
33. Bell CC, DSM-IV. Diagnostic and statistical manual of mental disorders. *JAMA.* (1994) 272:828–9. doi: 10.1001/jama.1994.03520100096046
34. Wing L, Leekam SR, Libby SJ, Gould J, Larcombe M. The diagnostic interview for social and communication disorders: background, inter-rater reliability and clinical use. *J Child Psychol Psychiatry.* (2002) 43:307–25. doi: 10.1111/1469-7610.00023
35. Lord C, Risi S, Lambrecht L, Cook EH, Leventhal BL, DiLavore PC, et al. The autism diagnostic observation schedule-generic: a standard measure of social and communication deficits associated with the spectrum of autism. *J Autism Dev Disord.* (2000) 30:205–23. Available at: https://www.ncbi.nlm.nih.gov/pubmed/11055457 doi: 10.1023/A:1005592401947
36. McCrimmon A, Rostad K. Test review: Autism diagnostic observation schedule, second edition (ADOS-2) manual (part II): toddler module. *J Psychoeduc Assess.* (2014) 32:88–92. doi: 10.1177/0734282913490916
37. Kaufman AS, O'Neal MR, Avant AH, Long SW. Introduction to the Kaufman assessment battery for children (K-ABC) for pediatric neuroclinicians. *J Child Neurol.* (1987) 2:3–16. doi: 10.1177/088307388700200102
38. Kikuchi M, Shitamichi K, Yoshimura Y, Ueno S, Remijn GB, Hirosawa T, et al. Lateralized theta wave connectivity and language performance in 2- to 5-year-old children. *J Neurosci.* (2011) 31:14984–8. doi: 10.1523/JNEUROSCI.2785-11.2011
39. Tadel F, Baillet S, Mosher JC, Pantazis D, Leahy RM. Brainstorm: a user-friendly application for MEG/EEG analysis. *Comput Intell Neurosci.* (2011) 2011:879716. doi: 10.1155/2011/879716
40. Pernet C, Garrido MI, Gramfort A, Maurits N, Michel CM, Pang E, et al. Issues and recommendations from the OHBM COBIDAS MEEG committee for reproducible EEG and MEG research. *Nat Neurosci.* (2020) 23:1473–83. doi: 10.1038/s41593-020-00709-0
41. Dale AM, Liu AK, Fischl BR, Buckner RL, Belliveau JW, Lewine JD, et al. Dynamic statistical parametric mapping: combining fMRI and MEG for high-resolution imaging of cortical activity. *Neuron.* (2000) 26:55–67. doi: 10.1016/S0896-6273(00)81138-1
42. Huang MX, Mosher JC, Leahy RM. A sensor-weighted overlapping-sphere head model and exhaustive head model comparison for MEG. *Phys Med Biol.* (1999) 44:423–40. doi: 10.1088/0031-9155/44/2/010

43. Baillet S, Mosher JC, Leahy RM. Electromagnetic brain mapping. *IEEE Signal Process Mag.* (2001) 18:14–30. doi: 10.1109/79.962275
44. Desikan RS, Ségonne F, Fischl B, Quinn BT, Dickerson BC, Blacker D, et al. An automated labeling system for subdividing the human cerebral cortex on MRI scans into gyral based regions of interest. *Neuroimage.* (2006) 31:968–80. doi: 10.1016/j.neuroimage.2006.01.021
45. Craddock RC, James GA, Holtzheimer PE, Hu XP, Mayberg HS. A whole brain fMRI atlas generated via spatially constrained spectral clustering. *Hum Brain Mapp*. (2012) 33:1914–28. doi: 10.1002/hbm.21333
46. Hallquist MN, Hillary FG. Graph theory approaches to functional network organization in brain disorders: a critique for a brave new small-world. *Netw Neurosci.* (2019) 3:1–26. doi: 10.1162/netn_a_00054
47. Farahibozorg S-R, Henson RN, Hauk O. Adaptive cortical parcellations for source reconstructed EEG/MEG connectomes. *Neuroimage.* (2018) 169:23–45. doi: 10.1016/j.neuroimage.2017.09.009
48. Pereda E, Quiroga RQ, Bhattacharya J. Nonlinear multivariate analysis of neurophysiological signals. *Prog Neurobiol.* (2005) 77:1–37. doi: 10.1016/j.pneurobio.2005.10.003
49. Palva S, Palva JM. Discovering oscillatory interaction networks with M/EEG: challenges and breakthroughs. *Trends Cogn Sci.* (2012) 16:219–30. doi: 10.1016/j.tics.2012.02.004
50. Stam CJ, Nolte G, Daffertshofer A. Phase lag index: assessment of functional connectivity from multi channel EEG and MEG with diminished bias from common sources. *Hum Brain Mapp.* (2007) 28:1178–93. doi: 10.1002/hbm.20346
51. Alaerts K, Geerlings F, Herremans L, Swinnen SP, Verhoeven J, Sunaert S, et al. Functional organization of the action observation network in autism: a graph theory approach. *PLoS ONE.* (2015) 10:e0137020. doi: 10.1371/journal.pone.0137020
52. Bassett DS, Bullmore E. Small-world brain networks. *Neuroscientist.* (2006) 12:512–23. doi: 10.1177/1073858406293182
53. Langer N, Pedroni A, Gianotti LRR, Hänggi J, Knoch D, Jäncke L. Functional brain network efficiency predicts intelligence. *Hum Brain Mapp.* (2012) 33:1393–406. doi: 10.1002/hbm.21297
54. Blackwell M, Iacus S, King G, Porro G. Cem: Coarsened exact matching in Stata. *Stata J.* (2009) 9:524–46. doi: 10.1177/1536867X0900900402
55. White H, A. Heteroskedasticity-consistent covariance matrix estimator and a direct test for heteroskedasticity. *Econometrica.* (1980) 48:817–38. doi: 10.2307/1912934
56. Volkmar FR, Cicchetti DV, Dykens E, Sparrow SS, Leckman JF, Cohen DJ. An evaluation of the autism behavior checklist. *J Autism Dev Disord.* (1988) 18:81–97. doi: 10.1007/BF02211820
57. Fraschini M, Demuru M, Crobe A, Marrosu F, Stam CJ, Hillebrand A. The effect of epoch length on estimated EEG functional connectivity and brain network organisation. *J Neural Eng.* (2016) 13:036015. doi: 10.1088/1741-2560/13/3/036015
58. van Wijk BCM, Stam CJ, Daffertshofer A. Comparing brain networks of different size and connectivity density using graph theory. *PLoS ONE.* (2010) 5:e13701. doi: 10.1371/journal.pone.0013701
59. Button KS, Ioannidis JPA, Mokrysz C, Nosek BA, Flint J, Robinson ESJ, et al. Power failure: why small sample size undermines the reliability of neuroscience. *Nat Rev Neurosci.* (2013) 14:365–76. doi: 10.1038/nrn3475

Conflict of Interest: The authors declare that the research was conducted in the absence of any commercial or financial relationships that could be construed as a potential conflict of interest.

frontiers in Psychiatry

ORIGINAL RESEARCH
published: 17 December 2021
doi: 10.3389/fpsyt.2021.775156

Abnormalities in Electroencephalographic Microstates Among Adolescents With First Episode Major Depressive Disorder

Yuqiong He[1], *Qianting Yu*[1], *Tingyu Yang*[1], *Yaru Zhang*[1], *Kun Zhang*[1], *Xingyue Jin*[1], *Shuxian Wu*[1], *Xueping Gao*[1,2], *Chunxiang Huang*[1,2], *Xilong Cui*[1,2*] *and Xuerong Luo*[1,2*]

[1] National Clinical Research Center for Mental Disorders, Department of Psychiatry, The Second Xiangya Hospital of Central South University, Changsha, China, [2] Autism Center of the Second Xiangya Hospital, Central South University, Changsha, China

OPEN ACCESS

Edited by:
Junpeng Zhang,
Sichuan University, China

Reviewed by:
Tianzhen Chen,
Shanghai Jiao Tong University, China
Zhifen Liu,
First Hospital of Shanxi Medical University, China

***Correspondence:**
Xilong Cui
cuixilong@csu.edu.cn
Xuerong Luo
luoxuerong@csu.edu.cn

Specialty section:
This article was submitted to Neuroimaging and Stimulation, a section of the journal Frontiers in Psychiatry

Received: 13 September 2021
Accepted: 24 November 2021
Published: 17 December 2021

Citation:
He Y, Yu Q, Yang T, Zhang Y, Zhang K, Jin X, Wu S, Gao X, Huang C, Cui X and Luo X (2021) Abnormalities in Electroencephalographic Microstates Among Adolescents With First Episode Major Depressive Disorder. Front. Psychiatry 12:775156. doi: 10.3389/fpsyt.2021.775156

Background: Recent studies have reported changes in the electroencephalograms (EEG) of patients with major depressive disorder (MDD). However, little research has explored EEG differences between adolescents with MDD and healthy controls, particularly EEG microstates differences. The aim of the current study was to characterize EEG microstate activity in adolescents with MDD and healthy controls (HCs).

Methods: A total of 35 adolescents with MDD and 35 HCs were recruited in this study. The depressive symptoms were assessed by Hamilton Depression Scale (HAMD) and Children's Depression Inventory (CDI), and the anxiety symptoms were assessed by Chinese version of DSM-5 Level 2-Anxiety-Child scale. A 64-channel EEG was recorded for 5 min (eye closed, resting-state) and analyzed using microstate analysis. Microstate properties were compared between groups and correlated with patients' depression scores.

Results: We found increased occurrence and contribution of microstate B in MDD patients compared to HCs, and decreased occurrence and contribution of microstate D in MDD patients compared to HCs. While no significant correlation between depression severity (HAMD score) and the microstate metrics (occurrence and contribution of microstate B and D) differing between MDD adolescents and HCs was found.

Conclusions: Adolescents with MDD showed microstate B and microstate D changes. The obtained results may deepen our understanding of dynamic EEG changes among adolescents with MDD and provide some evidence of changes in brain development in adolescents with MDD.

Keywords: adolescents, major depressive disorder, EEG resting state, EEG microstate, first-episode depression

INTRODUCTION

Major depressive disorder (MDD), characterized by low mood, loss of interest, possible symptoms of physical discomfort, suicidal behaviors, and cognitive dysfunction, is one of the most common mental disorders (1), and has been the second leading cause of disability worldwide because of its significant impact on the quality of life (2). In recent years, the prevalence of MDD has increased in adolescents and young adults (3), and up to 20% of adolescents are affected by MDD, which severely affected their lives and increased the risk of suicide (4). Early diagnosis and treatment contribute to decreasing MDD severity and improving the well-being and prognosis of MDD patients. Due to lack of effective and specific indicators, the diagnosis of MDD is based on patients' clinical symptoms, which is more tricky for adolescents as the manifestation of MDD among them is less typical than among adults (5, 6). Therefore, identifying potential biomarkers of depression is very important for the diagnosis and treatment of MDD, and studies on MDD among adolescent population are necessary and urgent.

A large number of functional magnetic resonance imaging (fMRI) studies have reported changes in brain structure and function among MDD patients (7, 8), including reduced hippocampal volume (9), thinner cortex in parahippocampal-limbic and insular-limbic areas (10), reduced connectivity within the frontoparietal control system (11) and disrupted network connectivity in the default mode network (DMN) (12, 13). Although many fMRI studies have explored differences between MDD patients and healthy subjects in depth, these studies cannot dynamically assess changes of brain with time. The electroencephalograms (EEG) can compensate for this defect of fMRI because of its good time resolution and can capture rapid changes in the dynamics of neuronal network (14). Because of its low cost, non-invasive, and easy to complete, EEG has been widely used in the neurocognitive disciplines in recent years. Previous studies among patients with MDD have found higher theta power in the frontal cortex and rostral anterior cingulate compared to healthy subjects (15). Higher power of the gamma band was also found among adult MDD patients with suicide ideation (16). Researches among adolescents with MDD showed lower theta band and decreased resting-state connectivity in the frontal cortex (17). Lower left-sided alpha power was also found in adolescents with MDD, and left-sided alpha power was related to depression scores (18). Currently, all of these EEG analyses are mainly based on traditional approaches, such as powder spectral analysis (18) and resting-state connectivity (17).

Resting EEG involves a limited number of potential topographic maps, as each topographic map remains stable for a certain period of time (60–120 ms) before quickly switching to another topographic map. All these topographic map are called "EEG microstates," and they dynamically change with time in an organized manner (19). The change in the EEG microstate indicates a change in the overall coordination of neuronal activity in the participant over time (20). Although different numbers of cluster maps have been reported in previous study (21, 22), four cluster maps, which are termed A, B, C, and D, are consistently identified in majority researches (23, 24). Studies based on EEG-fMRI technical have revealed the hemodynamic correlation of EEG microstate: microstate A may be associated with auditory network, while microstate B may be associated with the visual network, microstate C may reflect activity in the default mode network and the activity of the dorsal attention network may be related to microstate D (20, 25). Based on the dynamic changes of the four EEG microstate maps, the spontaneous brain activity can be represented by the duration, occurrence, contribution and transition possibility sequence of each EEG microstate maps (20). Capturing the temporal difference of dynamic changes of EEG microstates could be a promising method to study the spontaneous brain activity of adolescents with MDD.

In recent years, EEG microstate analysis has been used in patients with mental disorder, such as bipolar disorder (26), methamphetamine use disorder (27), schizophrenia (28), and depression (21, 22). Different psychopathological conditions showed different EEG microstate feature changes. Microstate B features were found to be related to depression scores among bipolar disorder patients (26). Studies among adults with MDD found that higher occurrence of microstate A was associated with depressive symptoms (21), and the contribution and duration of microstate D were reduced among depressed patients compared to healthy subjects and related to depression severity (22). Existing studies also found that EEG microstate feature may change with medication or the use of repetitive transcranial magnetic stimulation (rTMS). The duration, occurrence and contribution of microstate B decreased among the MDD patients after 2 weeks medication (29). These findings indicate that in-depth study of EEG microstates may provide new evidence for the diagnosis and treatment of adolescents with MDD. While to date, there has been no research on EEG microstate among MDD adolescents.

Here, we used EEG microstate as a new approach to explore the difference of spontaneous resting EEG between adolescents with MDD and HCs. The aims of the present study were to test whether there are differences in the temporal characteristics of EEG microstates between adolescents with MDD and HCs and whether there is a correlation between clinical symptoms and microstates.

MATERIALS AND METHODS

Participants

The MDD patients were recruited in the outpatient clinic of the Second Xiangya Hospital, Central South University. The diagnostic process was performed by a child and adolescent psychiatrist with an intermediate professional title or above. The kid version of the Mini International Neuropsychiatric interview (Mini-kid) was used to confirm the diagnosis and to eliminate other mental disorders. The inclusion criteria for patients were: (1) 12–17 years old; (2) a diagnosis of MDD according to the Diagnostic and Statistical Manual of Mental Disorder-Fifth Edition criteria (DSM-5); (3) first episode; (4) no history of psychiatric drug treatment before completing the examination; (5) the Children's Depression Inventory (CDI)

TABLE 1 | Demographic and clinical data of the participants.

Characteristic	MDD $N = 35$	HC $N = 35$	t/χ^2	p
Age, *M* (SD)	14.58 ± 1.46	15.05 ± 1.67	−1.241	0.219
Gender, male/female (*n*)	10/25	15/20	1.556	0.212
Education years, *M* (SD)	8.69 ± 1.47	8.69 ± 1.71	0.251	1
Duration of illness (months)	15.20 ± 11.07	NA	NA	NA
CDI score, *M* (SD)	38.34 ± 7.85	9.57 ± 4.65	18.662	<0.001
Anxiety score, *M* (SD)	40.26 ± 7.85	NA	NA	NA
HAMD score, *M* (SD)	21.97 ± 2.73	NA	NA	NA
GEV (%)	74.08 ± 1.92	73.77 ± 2.74	0.558	0.579

M, mean; SD, standard deviation; MDD, major depressive disorder; HC, healthy control; GEV, global explained variance.

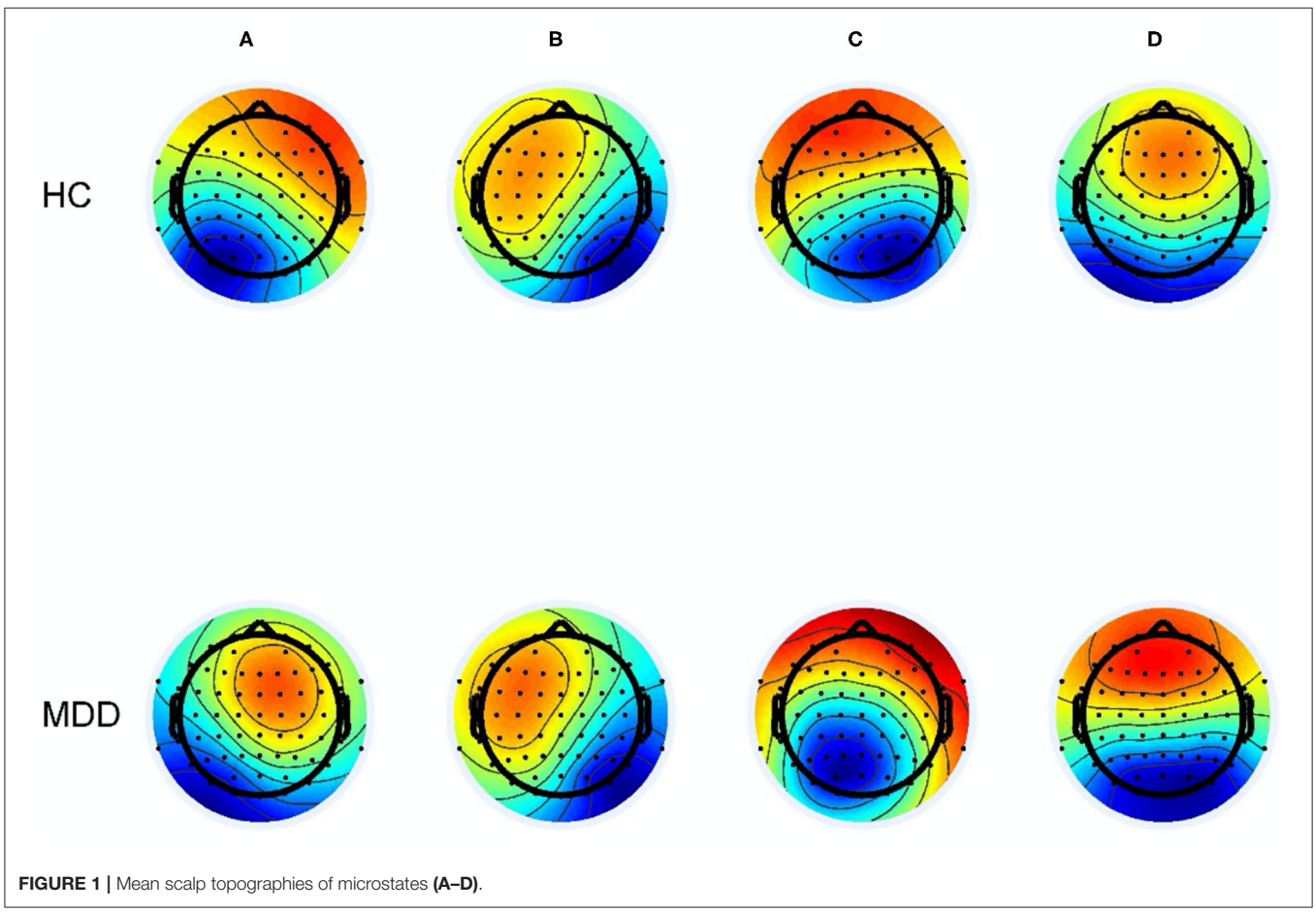

FIGURE 1 | Mean scalp topographies of microstates **(A–D)**.

score ≥19 (30) and Hamilton Rating Scale for Depression (HAMD-17) score ≥17. The Mini-kid and the assessment for the depression symptoms (HAMD-17) were completed by two professional psychiatrists, who received consistent training before the beginning of the experiment. The HCs were recruited through advertising in a junior school in Changsha, Hunan Province and in online social media platforms (WeChat Moments). The inclusion criteria for the HCs were: (1) 12–17 years old; (2) no history of psychiatric illness by the Mini-kid interview; (3) no first-degree relatives with psychiatric disorders; (4) no history of psychiatric medication use. All the subjects were interviewed by two professional psychiatrists and met the inclusion criteria. Those subjects (1) meeting the diagnostic criteria for mental disorders other than depression (only for MDD patients); (2) suffering from other nervous system diseases (brain trauma, epilepsy, intracranial tumors, etc.) or serious physical diseases; or (3) unable to complete the examination for other reasons were excluded. Finally, 35 adolescents with MDD

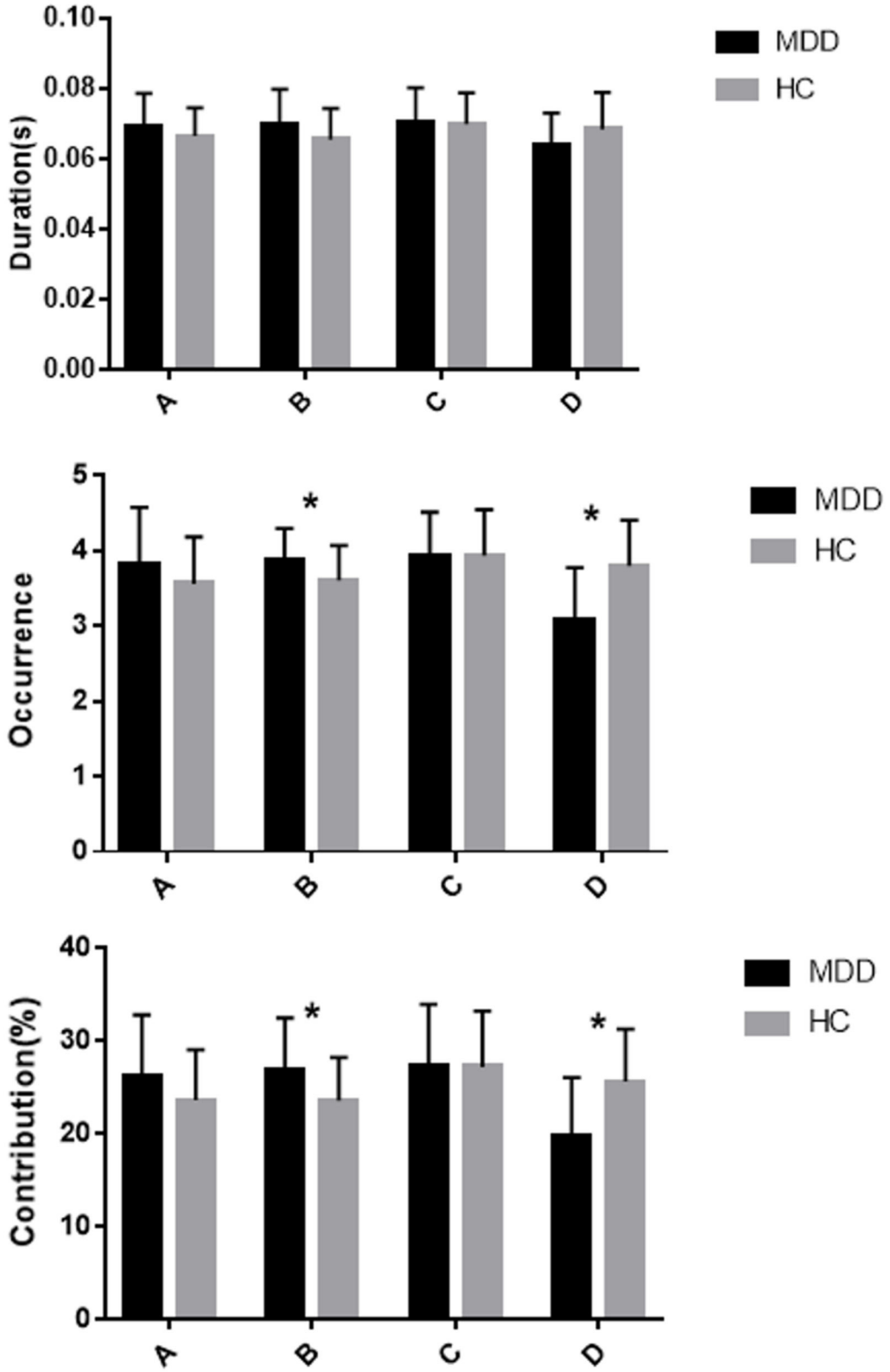

FIGURE 2 | Mean and standard error of microstate metrics (duration, occurrence, and contribution) of MDD (black) and HC (gray) groups * significant difference between MDD and HC groups, as assessed by the unpaired *t*-test with Bonferroni correction.

and 35 HCs participated this study. The general information such as gender, age and education years were collected among both groups, and the duration of illness were collected among the patient group.

This study was approved by the National Clinical Center Medical Ethics Committee of the Second Xiangya Hospital, Central South University. Written informed consent was provided by both the participants and their guardians.

Symptom Ratings

Depression symptoms were assessed using the Children's Depression Inventory (CDI) (31) and Hamilton Rating Scale for Depression (HAMD-17). CDI is the most widely used self-assessment scale for children and adolescents with MDD. The CDI consists of 27 items scored using 0–2 points. The total score is obtained by totaling all items: the higher the score, the higher the degree of depression. Cronbach's α for the CDI was found to be 0.8504 in a study of Chinese children and adolescents (32). The HAMD-17 was conducted as an interview with the subjects to assess the severity of depressive symptoms. HAMD-17 consists of 17 items scored on a 5-point scale, with 0 indicating no symptoms and 4 indicating extremely severe symptoms. Anxiety symptoms were assessed using the Chinese version of the DSM-5 Level 2-Anxiety-Child scale. It consists of 13 items scored on a scale of 1–5: the higher the score, the higher the anxiety symptoms. Cronbach's α for this test was 0.90 in a study of Chinese children and adolescents (33).

EEG Recordings and Pre-processing

A standard clinical EEG protocol of 5 min (resting-state and eyes closed) was recorded using 64 scalp electrodes with the International 10–20 system. Participants were asked to seat in a quiet room comfortably. The electrooculogram was recorded by one facial electrode located 1 cm below the middle of the right eye. EEG data were recorded at a sampling rate of 5,000 Hz. The data were referenced to the FCz electrode. Before the experiment, we reduced the electrode impedance below 5K Ω.

Pre-processing was performed using MATLAB 2013b and EEG tools. First, the sampling rate was lowered to 500. The data were band-pass filtered with cutoffs of 0.1–45 Hz and segmented into 2 s per epoch. When there were artifacts in a channel, the spherical interpolation method was used for interpolation (34), and <6 channels for each subject were replaced. When the signal quality of a segment was poor (the voltages of more than 10 channels exceed 80 mV), it would be excluded. After that, each subject retained at least 3 min EEG signals. Eye artifact correction was performed using independent component analysis (35).

Microstate Analysis

The Microstate Analysis plug-in (Version 0.3) for EEGLAB (34) developed by Thomas Koenig was used for the microstate analysis. Artifact-free EEGs were band-pass filtered between 2 and 20 Hz then the data were re-referenced for the whole brain (36). The global field power (GFP) is calculated, and topographic maps selected for clustering are those at GFP peak (37). The polarity of the clusters was ignored. The number of clusters was selected as four based on previous researches which four clusters have been widely used and differences were found between HCs and patients with mental disorders (24). The microstate map of each participant was calculated by the original instantaneous diagram using atomic aggregation hierarchical clustering (AAHC) (38). The grand-mean model diagrams of each group (HC group, MDD group) were calculated and labeled as "A," "B," "C," and "D." The first and last segments were ignored by the microstate toolbox. The following parameters were extracted from the microstate data: duration (average duration of the four different microstate categories), occurrence (how many times per second the four microstate categories appear on average), contribution (percentage of time covered by the four microstate categories), and transition possibility (probability of conversion between the four microstate categories). The global explained variance (GEV) is calculated to assess to what extent the microstate topographic can explain the original EEG data.

Data Analysis

Data were analyzed using SPSS version 21 (IBM). Categorical variables are reported as the count (n) and percentage (%). Continuous variables are expressed as the mean (M) ± standard deviation (SD). The independent sample t-test was used to compare general demographic information between the two groups. We used 4 (microstate classes) × 2 (groups) repeated measures analysis of variance (ANOVA) to evaluate the interaction effects of each microstate parameter. Greenhouse–Geisser correction for ANOVA was applied. The two tailed unpaired t-test was performed for each microstate separately as *post-hoc* analysis to assess the difference between MDD patients and HCs, if the interaction microstate * group was significant. Bonferroni correction was used for the *post-hoc* comparisons, and $p < 0.013$ (i.e., 0.05/4, there were 4 different types of microstates) was considered statistically significant for microstate features. Pearson correlation analysis was used to analyze the relationships between HAMD scores and the microstate metrics differing between MDD adolescents and HCs. The statistical tests were two-sided and the level of statistical significance was set as $\alpha = 0.05$. Bonferroni correction was applied for multiple correlation analyses.

RESULTS

Participant Characteristics

The demographic characteristics of the two groups and symptom ratings in the MDD group are shown in **Table 1**. There were no significant differences in age, education years, or gender between the two groups (all $p > 0.05$). For patients with MDD, the mean duration of illness was 15.20 ± 11.07 months. The CDI score of the MDD group was 38.34 ± 7.85, higher than that in HCs (9.57 ± 4.65), and the difference was significant ($p < 0.001$). The anxiety score was 40.26 ± 7.85, and the HAMD score was 21.97 ± 2.73 among the MDD group. Four microstates (classes A to D) in the two groups were identified by AAHC. The average global explained variance was 74.08 ± 1.92% and 73.77 ± 2.74% for MDD group and HCs, respectively, and the difference was not significant ($p = 0.579$). The four microstate topographic

TABLE 2 | Comparison of microstates between the MDD group and HC group.

		MDD		HC			
		M	SD	*M*	SD	*t*	*p*
Duration	A	0.0694	0.0094	0.0667	0.0080	1.266	0.210
	B	0.0700	0.0100	0.0656	0.0089	1.921	0.059
	C	0.0705	0.0100	0.0700	0.0089	0.180	0.858
	D	0.0643	0.0089	0.0685	0.0106	−1.800	0.076
Occurrence	A	3.8142	0.7684	3.5605	0.6258	1.512	0.135
	B	3.8897	0.4083	3.6105	0.4615	2.681	0.009
	C	3.9352	0.5801	3.9337	0.6130	0.011	0.992
	D	3.0691	0.7062	3.7987	0.6058	−4.639	<0.001
Contribution	A	0.2617	0.0663	0.2366	0.0540	1.807	0.075
	B	0.2686	0.0561	0.2359	0.0462	2.657	0.010
	C	0.2721	0.0673	0.2722	0.0604	−0.001	0.999
	D	0.1976	0.0632	0.2564	0.0564	−4.107	<0.001

M, mean; SD, standard deviation; MDD, major depressive disorder; HC, healthy control. Bonferroni correction for the post-hoc comparisons: $p < 0.013$.

TABLE 3 | Comparison and means for all transition probabilities in the MDD and HC groups.

	MDD		HC				
	Mean	SD	Mean	SD	*t*	*p*	Direction
A-B	0.0910	0.0246	0.0721	0.0179	3.662	<0.001	MDD > HC
A-C	0.0953	0.0265	0.0786	0.0209	2.936	0.005	MDD > HC
A-D	0.0619	0.0181	0.0779	0.0153	−3.999	<0.001	MDD < HC
B-A	0.0920	0.0227	0.0721	0.0187	3.994	<0.001	MDD > HC
B-C	0.0942	0.0209	0.0841	0.0181	2.157	0.035	MDD > HC
B-D	0.0689	0.0277	0.0768	0.0225	−1.311	0.194	
C-A	0.0940	0.0263	0.0812	0.0205	2.270	0.026	MDD > HC
C-B	0.0946	0.0197	0.0831	0.0166	2.626	0.011	MDD > HC
C-D	0.0688	0.0204	0.0902	0.0237	−4.055	<0.001	MDD < HC
D-A	0.0622	0.0168	0.0751	0.0164	−3.267	0.002	MDD < HC
D-B	0.0697	0.0278	0.0778	0.0224	−1.337	0.186	
D-C	0.0678	0.0216	0.0918	0.0252	−4.284	<0.001	MDD < HC

M, mean; SD, standard deviation; MDD, major depressive disorder; HC, healthy control. Bonferroni correction for the post-hoc comparisons: $p < 0.013$.

maps resemble those in the previous literature in both groups (**Figure 1**).

Microstate Metrics

Repeated measures ANOVA was conducted to compare the microstate duration, occurrence, contribution and transition possibility between the two groups. EEG microstate (A, B, C, D) were regarded as a within-subject factor and group (MDD or HC) as a between-subject factor. The results for microstate duration showed that the Microstate * Group interaction effect was significant (F =4.559; $p = 0.006$), while the within-subject factor effect (F =1.657; $p = 0.185$) and group effect ($F = 0.373$; $p = 0.543$) were not significant. *Post-hoc* comparisons showed no significant difference in microstates (A, B, C, D) between the two groups (all $p > 0.013$; **Figure 2**; **Table 2**).

The results for microstate occurrence showed there were significant main effect of microstate ($F = 9.827$; $p < 0.001$) and Microstate * Group interaction effect ($F = 9.606$; $p < 0.001$), but no significant main effect of Group ($F = 0.479$; $p = 0.491$). *Post-hoc* analysis showed that the MDD group had a higher frequency of microstate B and a lower frequency of microstate D compared to the HC group, and these differences were statistically significant (both $p < 0.013$). The occurrence of microstates A and C did not differ significantly between the MDD group and HC group ($p = 0.135$ and $p = 0.992$, respectively; **Figure 2**; **Table 2**).

For the contribution of microstates, the main effect of microstate ($F = 5.260$; $p = 0.003$) and Microstate * Group interaction effect ($F = 7.889$, $p < 0.001$) were significant, but the main effect of Group ($F = 0$; $p = 1$) was not significant. *Post-hoc* analysis showed more microstate B contribution and less

TABLE 4 | Correlation for microstate metrics and HAMD score.

	r	*p*
Occurrence B	0.253	0.143
Occurrence D	0.017	0.923
Contribution B	0.341	0.045
Contribution D	0.089	0.611

Bonferroni correction for multiple correlations: $p < 0.013$.

microstate D contribution in the MDD group compared to the HC group, and the differences were statistically significant (both $p < 0.013$). There were no statistically significant differences in other microstate contributions between the HC and MDD groups (both $p > 0.013$; **Figure 2**; **Table 2**).

For the transition probabilities, there were significant main effect of the microstate ($F = 3.878$; $p < 0.001$) and significant Microstate * Group interaction effect ($F = 5.174$, $p < 0.001$), while the main effect of Group ($F = 0.582$; $p = 0.448$) was not significant. *Post-hoc* analysis showed that the MDD group had a lower possibility of transition from "A to D," "C to D," "D to A," and "D to C" than the HC group, and the differences were significant (all $p < 0.013$). Furthermore, the MDD group showed a higher possibility of transition from "A to B," "A to C," "B to A," and "C to B" than the HC group, and the differences were significant (all $p < 0.013$; **Table 3**).

Relationship Between Microstate Metrics and Depression Score

Finally, we examined the relationship between depression severity (HAMD score) and the microstate metrics (occurrence and contribution of microstate B and D) differing between MDD adolescents and HCs. We found that contribution of microstate B is correlated with HAMD score ($r = 0.341$, $p = 0.045$, uncorrected). After Bonferroni correction was applied, the significance was gone ($p > 0.013$, **Table 4**).

DISCUSSION

To the best of our knowledge, this is the first study to explore the dynamic activity of resting-state large-scale brain networks among adolescents with MDD. Our results indicate that adolescents with MDD show alterations in sub second of the whole brain. Compared to HCs, adolescents with MDD showed abnormally increased occurrence of microstate B and decreased occurrence of microstate D. The increase in microstate B may be caused by more transitions from microstate C to microstate B. Adolescents with MDD had less transitions from "A to D" and more transition from "D to C," which were the reasons for the decrease in microstate D among MDD subjects compared with the HCs.

Limited research has examined EEG microstate duration and/or occurrence in depressed patients. Our results showed the difference in microstate duration between adolescents with MDD and HCs was not obvious, which is inconsistent with other studies in adult MDD patients (22, 39). For example, Murphy et al.'s (22) research showed that the duration of microstate D was reduced among the adults MDD patients compared to the healthy subjects. However, our results are in line with the Damborská's results which found no difference in duration between the adults MDD patients and HCs (21). Although there was no change in the duration, the occurrence and contribution changed in adolescents with MDD. Our results showed that adolescents with MDD patients had higher contribution, occurrence of microstate B. This finding is in line with a previous research which found that the duration, occurrence, and contribution of microstate B were decreased as depressive symptoms improved among MDD adults (29). The head surface signal source displays microstate B was closely associated with right posterior alpha activity by accurate low resolution electromagnetic tomography (eloreta) (40). The adolescents with MDD showed reduced posterior alpha compared to HCs, and posterior alpha activity was related to depression symptoms, anhedonia symptoms, rumination (41). Microstate class B was significantly correlated with blood oxygenation level dependent (BOLD) changes in the striatum, extra-striatal cortex, and bilateral occipital cortex, which is related to the visual network (20, 42, 43). Microstate B was also found to be correlated to posterior temporal gyrus (44). Previous fMRI research of depressed subjects has found lower functional anterior cingulate cortex and posterior superior temporal gyrus connectivity compared to HCs (45). These regions play vital roles in integrating, collecting and processing information from the external environment and the internal body (46), and understanding emotions or feeling of other people (47). The increase of microstate B among MDD patients in the current study is in line with that MDD patients have deficits in cognitive function and depression symptoms, anhedonia symptoms. The higher occurrence of microstate B was mainly caused by the increased transition from "C to B" among MDD patients. Microstate C reflects part of the DMN, which is a task negative network (20). Among patients with MDD, overactivation of the DMN may be related to negative rumination (12). Other researchers have suggested that abnormalities in DMN connectivity are associated with deficits in emotion regulation among MDD patients (48). Therefore, the more frequent transition from "C to B" may reflect that adolescents with MDD have more frequent spontaneous rumination and emotion regulation.

Our results agree with previous studies reporting a decrease in microstate D (contribution and occurrence) among the adults MDD patients (22). Microstate D was found to be closely associated to the dorsal attention network (25). The decrease in microstate D is consistent with a large number of previous fMRI studies which showed decreased connectivity of the dorsal attention network among patients with MDD (11). The dorsal attention network is involved in internally- or externally-oriented attention. Decreases in connectivity of the dorsal attention network may predict deficits in attention among MDD patients (49). In addition, connectivity between the frontoparietal network and dorsal attention network is weaker among adults MDD patients than HCs (11). Decreased connectivity of the frontoparietal

network and dorsal attention network is reported to be associated with higher levels of maladaptive rumination (50). Imbalances in these different network connections could lead to not only cognitive and executive dysfunction, but also emotional regulation dysfunction, which are characteristics of MDD (51).

The current study was the first study to explore the EEG microstate changes among adolescents with first episode MDD and HCs under resting-state. Although the participants in our study was adolescents, the results were partially consistent with previous studies among adults (22, 29). Both the adolescents and adults with MDD showed an increased (decreased) occurrence and contribution of microstate B (D). There are also some different findings among adults MDD patients. For example, Murphy et al. (22) found decreased duration of microstate D while we didn't. The differences may be explained by different methodologies, such as different clustering methods and different numbers of selected topographic maps (21, 22). Moreover, all subjects in this study are teenagers and their brains are in a stage of continuous development. It has been found in previous study that the duration of microstates increases continuously with increases in age (52). One thing that cannot be ignored is that depression itself may have effect on the brain development (53), resulting in divergence at different stages. One advantage of this study is that we assessed differences between the adolescents with first episode MDD and HC groups in the general resting condition, i.e., there is no cognitive task or emotional processing, so some task-related confounders can be eliminated (54). In addition, research conducted among adolescents may have a certain predictive ability for their mental health in adulthood.

LIMITATIONS

There are several limitations of this study that should be noted. First, the EEG microstate depends on source modeling technology. However, the source modeling is based on the poor spatial resolution of EEG. Secondly, the patients with MDD included in the present study are adolescents. As the first depressive episode in early adolescence may be a manifestation of a later diagnosis of bipolar disorder, some of the patients in this study may be diagnosed with bipolar disorder in later life. Thirdly, the present study only included 35 patients and 35 HCs. A larger number of subjects should be included in future studies. Lastly, although there was no gender difference between the two groups, it should be pointed out that the gender of subjects was not completely matched between groups. There are differences in EEG microstates between males and females in terms of the duration and occurrence of specific microstates (52). Therefore, future research should include more subjects to study potential gender effects.

CONCLUSIONS

The results of this study supported changes in microstate B and D of adolescents with MDD compared to HCs. It provided new insights into dynamic changes in resting-state EEGs of MDD adolescents, and provides some evidence for further exploration of biomarkers and early diagnosis of MDD among adolescents.

DATA AVAILABILITY STATEMENT

The datasets used and/or analyzed during the current study are available from the corresponding author upon reasonable request.

ETHICS STATEMENT

The studies involving human participants were reviewed and approved by National Clinical Center Medical Ethics Committee of the Second Xiangya Hospital, Central South University. Written informed consent to participate in this study was provided by the participants' legal guardian/next of kin.

AUTHOR CONTRIBUTIONS

YQH, QTY, TYY, YRZ, XPG, CXH, and XRL contributed to conception and design of the study. YQH, QTY, TYY, YRZ, KZ, XYJ, and SXW participated in data collection and investigation and evaluation of the study. YQH, QTY, and XLC performed the statistical analysis. YQH and XLC wrote the first draft of the manuscript. XLC and XRL contributed to critical revision. All authors contributed to manuscript revision, read, and approved the submitted version.

FUNDING

This study was supported by the National Key Research and Development Program of China (No. 2017YFC1309904), Hunan Provincial Innovation Foundation for Post-graduates (No. CX2019159).

ACKNOWLEDGMENTS

The authors would like to acknowledge all respondents who participated in the study and the research assistants who had contributed to the recruitment process and data collection.

REFERENCES

1. Malhi GS, Mann JJ. Depression. *Lancet (London, England)*. (2018) 392:2299–312. doi: 10.1016/S0140-6736(18)31948-2
2. Lam RW, McIntosh D, Wang J, Enns MW, Kolivakis T, Michalak EE, et al. Canadian network for mood and anxiety treatments (CANMAT) 2016 clinical guidelines for the management of adults with major depressive disorder: section 1. Disease burden and principles of care. *Can J Psychiatry Revue Can Psychiatr*. (2016) 61:510–23. doi: 10.1177/0706743716659061
3. Mojtabai R, Olfson M, Han B. National trends in the prevalence and treatment of depression in adolescents and young adults. *Pediatrics*. (2016) 138:e2016878. doi: 10.1542/peds.2016-1878

4. Mendelson T, Tandon SD. Prevention of depression in childhood and adolescence. *Child Adolesc Psychiatr Clin North Am*. (2016) 25:201–18. doi: 10.1016/j.chc.2015.11.005
5. Diagnosis of depression in children and adolescents. Clinical pointers to a difficult diagnosis. *Presc Int*. (2010) 19:81–3.
6. Zwolińska W, Dmitrzak-Weglarz M, Słopień A. Biomarkers in child and adolescent depression. *Child Psychiatry Hum Dev*. (2021). doi: 10.1007/s10578-021-01246-y. [Epub ahead of print].
7. Zhang FF, Peng W, Sweeney JA, Jia ZY, Gong QY. Brain structure alterations in depression: psychoradiological evidence. *CNS Neurosci Therap*. (2018) 24:994. doi: 10.1111/cns.12835
8. O'Callaghan G, Stringaris A. Reward processing in adolescent depression across neuroimaging modalities. *Zeitschrift fur Kinder Jugendpsychiatrie Psychother*. (2019) 47:535–41. doi: 10.1024/1422-4917/a000663
9. Barch DM, Tillman R, Kelly D, Whalen D, Gilbert K, Luby JL. Hippocampal volume and depression among young children. *Psychiatry Res Neuroimaging*. (2019) 288:21–8. doi: 10.1016/j.pscychresns.2019.04.012
10. Neufeld NH, Kaczkurkin AN, Sotiras A, Mulsant BH, Dickie EW, Flint AJ, et al. Structural brain networks in remitted psychotic depression. *Neuropsychopharmacology*. (2020) 45:1223–31. doi: 10.1038/s41386-020-0646-7
11. Kaiser RH, Andrews-Hanna JR, Wager TD, Pizzagalli DA. Large-scale network dysfunction in major depressive disorder: a meta-analysis of resting-state functional connectivity. *JAMA psychiatry*. (2015) 72:603–11. doi: 10.1001/jamapsychiatry.2015.0071
12. Zhou HX, Chen X, Shen YQ, Li L, Chen NX, Zhu ZC, et al. Rumination and the default mode network: meta-analysis of brain imaging studies and implications for depression. *Neuroimage*. (2020) 206:116287. doi: 10.1016/j.neuroimage.2019.116287
13. Yan CG, Chen X, Li L, Castellanos FX, Bai TJ, Bo QJ, et al. Reduced default mode network functional connectivity in patients with recurrent major depressive disorder. *Proc Natl Acad Sci USA*. (2019) 116:9078–83. doi: 10.1073/pnas.1900390116
14. Baumgartner C, Koren JP. Seizure detection using scalp-EEEG. *Pilepsia*. (2018) 59(Suppl. 1):14–22. doi: 10.1111/epi.14052
15. Arns M, Etkin A, Hegerl U, Williams LM, DeBattista C, Palmer DM, et al. Frontal and rostral anterior cingulate (rACC) theta EEG in depression: implications for treatment outcome? *Eur Neuropsychopharmacol*. (2015) 25:1190–200. doi: 10.1016/j.euroneuro.2015.03.007
16. Arikan MK, Gunver MG, Tarhan N, Metin B. High-Gamma: a biological marker for suicide attempt in patients with depression. *J Affect Disord*. (2019) 254:1–6. doi: 10.1016/j.jad.2019.05.007
17. McVoy M, Aebi ME, Loparo K, Lytle S, Morris A, Woods N, et al. Resting-state quantitative electroencephalography demonstrates differential connectivity in adolescents with major depressive disorder. *J Child Adolesc Psychopharmacol*. (2019) 29:370–7. doi: 10.1089/cap.2018.0166
18. Grünewald BD, Greimel E, Trinkl M, Bartling J, Großheinrich N, Schulte-Körne G. Resting frontal EEG asymmetry patterns in adolescents with and without major depression. *Biol Psychol*. (2018) 132:212–6. doi: 10.1016/j.biopsycho.2018.01.003
19. Lehmann D, Ozaki H, Pal I, EEG. alpha map series: brain micro-states by space-oriented adaptive segmentation. *Electroencephalogr Clin Neurophysiol*. (1987) 67:271–88. doi: 10.1016/0013-4694(87)90025-3
20. Michel CM, Koenig T. EEG microstates as a tool for studying the temporal dynamics of whole-brain neuronal networks: a review. *NeuroImage*. (2018) 180:577–93. doi: 10.1016/j.neuroimage.2017.11.062
21. Damborská A, Tomescu MI, Honzírková E, Barteček R, Horínková J, Fedorová S, et al. EEG Resting-State Large-Scale Brain Network Dynamics Are Related to Depressive Symptoms. *Front Psychiatry*. (2019) 10:548. doi: 10.3389/fpsyt.2019.00548
22. Murphy M, Whitton AE, Deccy S, Ironside ML, Rutherford A, Beltzer M, et al. Abnormalities in electroencephalographic microstates are state and trait markers of major depressive disorder. *Neuropsychopharmacology*. (2020) 45:2030–7. doi: 10.1038/s41386-020-0749-1
23. Santarnecchi E, Khanna AR, Musaeus CS, Benwell CSY, Davila P, Farzan F, et al. EEG Microstate Correlates of Fluid Intelligence and Response to Cognitive Training. *Brain Topogr*. (2017) 30:502–20. doi: 10.1007/s10548-017-0565-z
24. de Bock R, Mackintosh AJ, Maier F, Borgwardt S, Riecher-Rössler A, Andreou C, et al. microstates as biomarker for psychosis in ultra-high-risk patients. *Transl Psychiatry*. (2020) 10:300. doi: 10.1038/s41398-020-00963-7
25. Britz J, Van De Ville D, Michel CM, BOLD. correlates of EEG topography reveal rapid resting-state network dynamics. *Neuroimage*. (2010) 52:1162–70. doi: 10.1016/j.neuroimage.2010.02.052
26. Vellante F, Ferri F, Baroni G, Croce P, Migliorati D, Pettoruso M, et al. Euthymic bipolar disorder patients and EEG microstates: a neural signature of their abnormal self experience? *J Affect Disord*. (2020) 272:326–34. doi: 10.1016/j.jad.2020.03.175
27. Chen T, Su H, Zhong N, Tan H, Li X, Meng Y, et al. Disrupted brain network dynamics and cognitive functions in methamphetamine use disorder: insights from EEG microstates. *BMC Psychiatry*. (2020) 20:334. doi: 10.1186/s12888-020-02743-5
28. da Cruz JR, Favrod O, Roinishvili M, Chkonia E, Brand A, Mohr C, et al. (2020) *EEG microstates are a candidate endophenotype for schizophrenia Nature communications, 11(1)*. (3089). doi: 10.1038/s41467-020-16914-1
29. Yan D, Liu J, Liao M, Liu B, Wu S, Li X, et al. Prediction of Clinical Outcomes With EEG Microstate in Patients With Major Depressive Disorder. *Front Psychiatry*. (2021) 12:695272. doi: 10.3389/fpsyt.2021.695272
30. Timbremont B, Braet C, Dreessen L. Assessing depression in youth: relation between the Children's Depression Inventory and a structured interview. *J Clin Child Adolesc Psychol*. (2004) 33:149–57. doi: 10.1207/S15374424JCCP3301_14
31. Samm A, Värnik A, Tooding LM, Sisask M, Kölves K, von Knorring AL. Children's Depression Inventory in Estonia. *Single items and factor structure by age and gender European child & adolescent psychiatry*. (2008) 17:162–70. doi: 10.1007/s00787-007-0650-z
32. Yu DV Li X. Preliminary use of the children's depression inventory in China(in Chinese version). *Chinese Mental Health Journal*. (2000) 14:227–45.
33. Zhang Y, Zhang X, Zhong J, Wang JJCMHJ. (2018) Preliminary revision of the Chinese version of DSM-5 Level 2-Anxiety-Child Age 11-17 in a Chinese adolescent sample(in Chinese version). *Chinese Mental Health Journal, 32(7)*(7), 552-7.
34. Delorme A, Makeig S, EEGLAB. an open source toolbox for analysis of single-trial EEG dynamics including independent component analysis. *J Neurosci Methods*. (2004) 134:9–21. doi: 10.1016/j.jneumeth.2003.10.009
35. Jung TP, Makeig S, Westerfield M, Townsend J, Courchesne E, Sejnowski TJ. Removal of eye activity artifacts from visual event-related potentials in normal and clinical subjects. *Clin Neurophysiol*. (2000) 111:1745–58. doi: 10.1016/S1388-2457(00)00386-2
36. Van de Ville D, Britz J, Michel CM, EEG. microstate sequences in healthy humans at rest reveal scale-free dynamics. *Proc Natl Acad Sci U S A*. (2010) 107:18179–84. doi: 10.1073/pnas.1007841107
37. von Wegner F, Knaut P, Laufs H, EEG. Microstate Sequences From Different Clustering Algorithms Are Information-Theoretically Invariant. *Front Comput Neurosci*. (2018) 12:70. doi: 10.3389/fncom.2018.00070
38. Murray MM, Brunet D, Michel CM. Topographic ERP analyses: a step-by-step tutorial review. *Brain Topogr*. (2008) 20:249–64. doi: 10.1007/s10548-008-0054-5
39. Strik WK, Dierks T, Becker T, Lehmann D. Larger topographical variance and decreased duration of brain electric microstates in depression. *J. Neural Trans Gen Section*. (1995) 99:213–22. doi: 10.1007/BF01271480
40. Milz P, Pascual-Marqui RD, Achermann P, Kochi K, Faber PL. The EEG microstate topography is predominantly determined by intracortical sources in the alpha band. *Neuroimage*. (2017) 162:353–61. doi: 10.1016/j.neuroimage.2017.08.058
41. Umemoto A, Panier LYX, Cole SL, Kayser J, Pizzagalli DA, Auerbach RP. Resting posterior alpha power and adolescent major depressive disorder. *J Psychiatr Res*. (2021) 141:233–40. doi: 10.1016/j.jpsychires.2021.07.003
42. Custo A, Van De Ville D, Wells WM, Tomescu MI, Brunet D, Michel CM. Electroencephalographic resting-state networks: source localization of microstates. *Brain Connect*. (2017) 7:671–82. doi: 10.1089/brain.2016.0476
43. Yuan H, Zotev V, Phillips R, Drevets WC, Bodurka J. Spatiotemporal dynamics of the brain at rest–exploring EEG microstates as electrophysiological signatures of BOLD resting state networks. *Neuroimage*. (2012) 60:2062–72. doi: 10.1016/j.neuroimage.2012.02.031

44. Xu J, Pan Y, Zhou S, Zou G, Liu J, Su Z, et al. EEG microstates are correlated with brain functional networks during slow-wave sleep. *Neuroimage.* (2020) 215:116786. doi: 10.1016/j.neuroimage.2020.116786
45. Harada K, Ikuta T, Nakashima M, Watanuki T, Hirotsu M, Matsubara T, et al. Altered connectivity of the anterior cingulate and the posterior superior temporal gyrus in a longitudinal study of later-life depression. *Front Aging Neurosci.* (2018) 10:31. doi: 10.3389/fnagi.2018.00031
46. Abu-Akel A, Shamay-Tsoory S. Neuroanatomical and neurochemical bases of theory of mind. *Neuropsychologia.* (2011) 49:2971–84. doi: 10.1016/j.neuropsychologia.2011.07.012
47. Corradi-Dell'Acqua C, Hofstetter C, Vuilleumier P. Cognitive and affective theory of mind share the same local patterns of activity in posterior temporal but not medial prefrontal cortex. *Soc Cogn Affect Neurosci.* (2014) 9:1175–84. doi: 10.1093/scan/nst097
48. Sheline YI, Barch DM, Price JL, Rundle MM, Vaishnavi SN, Snyder AZ, et al. The default mode network and self-referential processes in depression. *Proc Natl Acad Sci USA.* (2009) 106:1942–7. doi: 10.1073/pnas.0812686106
49. Snyder HR. Major depressive disorder is associated with broad impairments on neuropsychological measures of executive function: a meta-analysis and review. *Psychol Bull.* (2013) 139:81–132. doi: 10.1037/a0028727
50. Hamilton JP, Furman DJ, Chang C, Thomason ME, Dennis E, Gotlib IH. Default-mode and task-positive network activity in major depressive disorder: implications for adaptive and maladaptive rumination. *Biol Psychiatry.* (2011) 70:327–33. doi: 10.1016/j.biopsych.2011.02.003
51. Rive MM, van Rooijen G, Veltman DJ, Phillips ML, Schene AH, Ruhé HG. Neural correlates of dysfunctional emotion regulation in major depressive disorder. A systematic review of neuroimaging studies. *Neurosci Biobehav Rev.* (2013) 37:2529–53. doi: 10.1016/j.neubiorev.2013.07.018
52. Tomescu MI, Rihs TA, Rochas V, Hardmeier M, Britz J, Allali G, et al. From swing to cane: sex differences of EEG resting-state temporal patterns during maturation and aging. *Dev Cogn Neurosci.* (2018) 31:58–66. doi: 10.1016/j.dcn.2018.04.011
53. Ho TC, Connolly CG, Henje Blom E, LeWinn KZ, Strigo IA, Paulus MP, et al. Emotion-dependent functional connectivity of the default mode network in adolescent depression. *Biol Psychiatry.* (2015) 78:635–46. doi: 10.1016/j.biopsych.2014.09.002
54. Gusnard DA, Raichle ME, Raichle ME. Searching for a baseline: functional imaging and the resting human brain. *Nat Rev Neurosci.* (2001) 2:685–94. doi: 10.1038/35094500

Conflict of Interest: The authors declare that the research was conducted in the absence of any commercial or financial relationships that could be construed as a potential conflict of interest.

Publisher's Note: All claims expressed in this article are solely those of the authors and do not necessarily represent those of their affiliated organizations, or those of the publisher, the editors and the reviewers. Any product that may be evaluated in this article, or claim that may be made by its manufacturer, is not guaranteed or endorsed by the publisher.

frontiers in Psychiatry

ORIGINAL RESEARCH
published: 14 January 2022
doi: 10.3389/fpsyt.2021.779201

Repetitive Transcranial Magnetic Stimulation Modulates Frontal and Temporal Time-Varying EEG Network in Generalized Anxiety Disorder: A Pilot Study

Penghui Song[1,2,3,4†], *Han Tong*[5,6†], *Luyan Zhang*[7], *Hua Lin*[1], *Ningning Hu*[1], *Xin Zhao*[1], *Wensi Hao*[1], *Peng Xu*[7*] and *Yuping Wang*[1,4,8*]

[1] Department of Neurology, Xuanwu Hospital, Capital Medical University, Beijing, China, [2] Central Laboratory, Xuanwu Hospital, Capital Medical University, Beijing, China, [3] Beijing Geriatric Medical Research Center, Beijing, China, [4] Beijing Key Laboratory of Neuromodulation, Beijing, China, [5] Neuroscience Graduate Program, University of Cincinnati College of Medicine, Cincinnati, OH, United States, [6] Division of Behavioral Medicine and Clinical Psychology, Cincinnati Children's Hospital Medical Center, Cincinnati, OH, United States, [7] Center for Information in Medicine, University of Electronic Science and Technology of China, Chengdu, China, [8] Beijing Institute for Brain Disorders, Collaborative Innovation Center for Brain Disorders, Capital Medical University, Beijing, China

OPEN ACCESS

Edited by:
Junpeng Zhang,
Sichuan University, China

Reviewed by:
Kyung Mook Choi,
Daejeon Korean Medicine Hospital of Daejeon University, South Korea
Takefumi Ueno,
Hizen Psychiatric Center (NHO), Japan

***Correspondence:**
Peng Xu
xupeng@uestc.edu.cn
Yuping Wang
doctorwangyuping@163.com

[†] *These authors have contributed equally to this work*

Specialty section:
This article was submitted to Neuroimaging and Stimulation, a section of the journal Frontiers in Psychiatry

Received: *18 September 2021*
Accepted: *06 December 2021*
Published: *14 January 2022*

Citation:
Song P, Tong H, Zhang L, Lin H, Hu N, Zhao X, Hao W, Xu P and Wang Y (2022) Repetitive Transcranial Magnetic Stimulation Modulates Frontal and Temporal Time-Varying EEG Network in Generalized Anxiety Disorder: A Pilot Study. Front. Psychiatry 12:779201. doi: 10.3389/fpsyt.2021.779201

Generalized Anxiety Disorder (GAD) is a highly prevalent yet poorly understood chronic mental disorder. Previous studies have associated GAD with excessive activation of the right dorsolateral prefrontal cortex (DLPFC). This study aimed to investigate the effect of low-frequency repetitive transcranial magnetic stimulation (repetitive TMS, rTMS) targeting the right DLPFC on clinical symptoms and TMS-evoked time-varying brain network connectivity in patients with GAD. Eleven patients with GAD received 1 Hz rTMS treatment targeting the right DLPFC for 10 days. The severity of the clinical symptoms was evaluated using the Hamilton Anxiety Scale (HAMA) and the Hamilton Depression Scale (HAMD) at baseline, right after treatment, and at the one-month follow-up. Co-registration of single-pulse TMS (targeting the right DLPFC) and electroencephalography (TMS-EEG) was performed pre- and post-treatment in these patients and 11 healthy controls. Time-varying brain network connectivity was analyzed using the adaptive directed transfer function. The scores of HAMA and HAMD significantly decreased after low-frequency rTMS treatment, and these improvements in ratings remained at the one-month follow-up. Analyses of the time-varying EEG network in the healthy controls showed a continuous weakened connection information outflow in the left frontal and mid-temporal regions. Compared with the healthy controls, the patients with GAD showed weakened connection information outflow in the left frontal pole and the posterior temporal pole at baseline. After 10-day rTMS treatment, the network patterns showed weakened connection information outflow in the left frontal and temporal regions. The time-varying EEG network changes induced by TMS perturbation targeting right DLPFC in patients with GAD were characterized by insufficient information outflow in the left frontal and temporal regions. Low-frequency rTMS targeting the right DLPFC reversed these abnormalities and improved the clinical symptoms of GAD.

Keywords: generalized anxiety disorder, rTMS, DLPFC, TMS-EEG, time-varying EEG networks

INTRODUCTION

Generalized anxiety disorder (GAD) is a common and debilitating mental disorder; its prevalence rate was found to be 5.7% in an epidemiological survey (1, 2). Patients with GAD mainly present with difficulty in mood regulation and have unrealistic, excessive, and uncontrollable worries about daily affairs (for no reason and for at least 6 months) GAD may be accompanied by dysfunction, such as fatigue, difficulty concentrating, irritability, muscle tension, sleep disturbances, etc (3, 4). The treatment of GAD is still based on drug therapy, supplemented by psychological counseling (5–7); however, the side effects, for instance, delayed movement or dizziness, often lead to treatment cessation (8). Despite the many drug options available, almost 40% of patients with GAD do not respond to pharmacologic treatment (9). Therefore, new treatments for GAD are urgently needed.

Transcranial magnetic stimulation (TMS) is a non-invasive, effective brain stimulation technique that can activate cortical neurons; and its principle is based on Faraday's electromagnetic induction theory (10, 11). Repetitive TMS (rTMS) can reduce or increase cortical excitability depending on the stimulation frequency (12): low-frequency rTMS ($\leq$1HZ) can reduce the excitability of the motor cortex while high-frequency rTMS ($\geq$5HZ) can excite the adjacent cerebral cortex (13). rTMS has been successfully applied in the treatment of anxiety, depression, epilepsy, stroke, and other neurological and psychotic disorders (14–20).

Co-registration of TMS and electroencephalography (TMS-EEG) is a multimodal imaging technique for the direct and non-invasive exploration of cortical reactivity (21, 22). The technique can assess a variety of neurophysiological processes, including cortical responses, local excitation and inhibition, oscillatory activity, effective connectivity, and neuroplasticity, as well as provide important information about the transmission of activity throughout the brain (23). One of the main advantages of TMS-EEG is that it can be used to simultaneously assess the different neurophysiological characteristics of the cortical areas through a time-varying EEG network (24–26).

Recent evidence from neuroimaging studies strongly suggests that mood regulation in patients with GAD is associated with abnormalities in neural circuits of the frontal limbic region, including the dorsolateral prefrontal cortex (DLPFC) (27). The DLPFC plays a central role in emotional regulation by connecting the cortical and subcortical regions (for example, the dorsal anterior cingulate cortex, inferior frontal gyrus, ventral anterior cingulate cortex, and ventral anterior cingulate cortex) (28). Patients with GAD showed greater connectivity between the limbic and prefrontal regions than healthy controls (29).

This study aimed to investigate the effect of low-frequency rTMS targeting the right DLPFC on clinical symptoms and TMS-evoked time-varying brain network connectivity in patients with GAD.

SUBJECTS AND METHODS

Subjects

Eleven patients with GAD (6 men, mean age = 42.1 $\pm$ 9.0 years) were recruited between July 2015 and January 2016 from the Department of Neurology, Xuanwu Hospital, Capital Medical University. The inclusion criteria for the patients with GAD were as follows: (1) meeting the diagnostic criteria for generalized anxiety disorder in the DSM-V; (2) aged between 18 and 55 years; (3) having a Hamilton anxiety scale (HAMA) score >14; (4) patients who had taken anti-anxiety drugs did not need to stop taking them, but the medication frequency and dose needed to remain unchanged in the 1 month preceding the experiment; (5) having no abnormalities on physical examination of the nervous system; (6) being right-handed. The exclusion criteria for the GAD group were as follows: (1) having other types of anxiety diagnosed based on the DSM-V; (2) scoring >20 on the Hamilton depression scale (HAMD); (3) having secondary anxiety due to other organic diseases; (4) having a history of brain surgery and epilepsy; (5) having metallic foreign bodies, such as cardiac pacemakers and stents; (6) being a pregnant or lactating patient. Furthermore, 11 healthy subjects (6 men, mean age = 34.5 $\pm$ 9.6 years) matched with the GAD group in terms of gender and age were recruited into the control group. This study was approved by the Ethics Committee of Xuanwu Hospital, Capital Medical University. All subjects provided informed consent to participate in this study.

Neuropsychological Assessment

Each patient with GAD was assessed before and right after rTMS treatment and at the follow-up visit (1 month) using the Hamilton Anxiety Scale (HAM-A) (30) and the Hamilton Depression Rating Scale (HAM-D, 17 items) (31).

Measurement of the Resting Motor Threshold

Single-pulse TMS was applied with a figure-of-eight coil (70 mm diameter) connected to a monophasic Magstim stimulator (Magstim Company Ltd., London, UK) to measure the resting motor threshold (rMT), which was defined as the lowest stimulation intensity that could produce at least five motor-evoked potentials with wave amplitudes >50 μV among 10 trials in the right first dorsal interosseous muscle. The surface electromyography was recorded using disc-shaped Ag-Cl electrodes that were placed in a tendon-belly arrangement. The stimulating coil was positioned tangentially to the skull with the coil handle pointing backward and laterally at 45° from the anteroposterior axis.

TMS-EEG Data Acquisition

Twenty-minute TMS-EEG data were acquired using a magnetic field-compatible EEG amplifier (Yunshen Ltd, Beijing, China) digitized with a sampling rate of 1,024 Hz and an electrode cap with 32 TMS-compatible electrodes positioned according to the 10–20 system (Greentek Ltd, Wuhan, China). The electrode impedances were maintained below 5 kΩ. The AFz was used

as the grounding electrode, and the nasal tip electrode served as the reference. One hundred and twenty single-pulse TMS stimuli were applied to the right DLPFC (corresponding to F4 points on the subject's scalp, according to the international 10–20 system) at 90% RMT. Each stimulus was applied at an interval of 4 s. The subjects were asked to stay still and have their eyes closed throughout data acquisition. They were also provided with earplugs to block out ambient and coil discharge noises.

rTMS Treatment

rTMS treatment was administered to all patients with GAD using Magstim Rapid 2 stimulator (Magstim Company Ltd., London, UK). The stimulation site was the right DLPFC (corresponding to F4 points on the subject's scalp, according to the international 10–20 system). The coil plane was tangential and was kept parallel to the scalp, with the coil handle facing the occipital side. The following stimulus parameters were used: frequency, 1 Hz; intensity, 90% RMT; number of stimuli, 1,500 per day for 10 consecutive days.

TMS-EEG Data Preprocessing

MATLAB (R2015b, The Mathworks, USA) was used for EEG data preprocessing and time-varying network analysis. First, EEG data was imported and the filtering bandwidth was adjusted to 3–30 Hz, with the data sampling rate reduced by 8 times to 128 Hz. EEG data from 1,000 ms before to 2,000 ms after each stimulus point were intercepted as data segments, and about 80–100 data segments were retained for each subject's EEG data.

Time-Varying EEG Network Analysis

Adaptive Directed Transfer Function and the Multivariable Adaptive Autoregressive Model

The adaptive directed transfer function (ADTF) was based on the multivariable adaptive autoregressive model (base on the preprocessed TMS-EEG data) (32):

$$X(t) = \sum_{i=1}^{P} \Lambda(i,t)X(t-i) + E(t) \tag{1}$$

Type: $X(t)$ was the vector data that varied over time, $\Lambda(i, t)$ was the time-varying model coefficient matrix that can be determined by the Kalman filter method (33), $E(t)$ was multivariate independent white noise, and P was the optimal order of the model that can be determined by the Schwarz Bayesian criterion. We then took the Fourier transform of (1):

$$\begin{aligned} &\Lambda(f)X(f) = E(f) \\ &\mathrm{X}(f) = \Lambda^{-1}(f)E(f) = H(f)E(f) \end{aligned} \tag{2}$$

In the formula: $\Lambda(f) = \sum_{k=0}^{p} \Lambda_k e^{-j2\pi f \Delta tk} (\Lambda_{k=0} = I)$, $H(f)$ was the transfer coefficient matrix, corresponding to the time-varying model coefficient matrix $\Lambda(i, t)$, and we could get the time-varying transfer coefficient matrix $H(f, t)$. The element $H_{ij}(f, t)$ represented the connection relationship between the element J and the element I at frequency f and time t. The ADTF value could be expressed as follows:

$$ADTF_{ij}(f,t) = \left|H_{ij}(f,t)\right|^2 \tag{3}$$

Standardized as:

$$\gamma_{ij}^2(f,t) = -\frac{\left|H_{ij}(f,t)\right|^2}{\sum_{m=1}^{n}\left|H_{im}(f,t)\right|^2} \tag{4}$$

The above equation described the directional causal relationship between elements J and I at time T; it was an effective relationship. In order to calculate all the information flowing from one node to another in a particular frequency band, it was usually possible to combine all ${\gamma_{ij}}^2$ in that frequency band:

$$\Theta_{ij}^2(t) = \frac{\sum_{k=f_1}^{f-2}\gamma_{ij}^2(k,t)}{f_2 - f_1}, \quad \Theta_{ij}^2 \in [0,1] \tag{5}$$

Time-Varying EEG Network Patterns

MATLAB (R2015b) was utilized to identify the dynamic EEG network patterns in healthy subjects and pre- or post- the rTMS treatment.

(1) Calculate 40 time-varying adtf matrices from 360ms before the stimulation point to 40ms before the stimulation point of each data segment in the 3–30 Hz, average all data segments to obtain the baseline time-varying ADTF matrix of each subject, and then average 40 time points in this period to obtain the average baseline ADTF matrix of each subject.

(2) Calculate 246 time-varying ADTF matrices from 60 to 2,000 ms after the stimulation point of each data segment in the 3–30 Hz, and average all data segments to obtain the time-varying ADTF matrix of each subject.

(3) Subtract the average baseline ADTF matrix from the time-varying ADTF matrix of each subject to obtain the time-varying ADTF matrix after baseline correction.

(4) Take the baseline corrected ADTF value of the first 10% of the minimum negative value at each sampling time point of 60–2,000ms, and draw the time-varying brain network diagram of weakened connection used Brain_graphic (24).

Statistical Analysis

Demographic and clinical variables were compared using between-group two-sample, two-tailed t-tests or chi-squares. The HAMA and HAMD scores of GAD patients at three time points (before treatment, at the end of treatment, and 1 month after the end of treatment) were analyzed using repeated-measures ANOVA. The effects were considered significant if $p < 0.05$.

RESULTS

Neuropsychological Characteristics

We enrolled a total of 22 subjects into the study: 11 patients with GAD (6 men, mean age = 42.1 ± 9.0 years) and 11

TABLE 1 | Neuropsychological characteristics of GAD.

Variables	Before treatment	After treatment	1 month after treatment
HAMA	21.45 ± 4.13	11.27 ± 4.36*	11.36 ± 3.72#
HAMD	13.45 ± 4.66	8.73 ± 3.72*	8.27 ± 3.29#

*Data are presented as mean ± SD. *P < 0.05 vs. before treatment in the same group, #P < 0.05 vs. before treatment in the same group. GAD, Generalized anxiety disorder; HAMA, Hamilton Anxiety Scale; HAMD, Hamilton Depression Scale.*

healthy subjects (6 men, mean age = 34.5 ± 9.6 years). The healthy subjects were matched with the patients with GAD in terms of gender and age. All the subjects completed the entire study without adverse events. The HAMA and HAMD scores significantly decreased after rTMS treatment and 1 month after treatment (**Table 1**).

Time-Varying EEG Network Patterns

From the above time-varying network analysis, **Figure 1** shows the EEG network patterns of the patients with GAD before and after treatment as well as those of the healthy controls. In the healthy controls, the time-varying EEG network after single-pulse TMS of the right DLPFC showed the hub node on the left frontal (119 and 212 ms) and left mid-temporal (212 ms and 415 ms) weakened connection patterns. Compared with that of the healthy controls, the time-varying EEG network after single-pulse TMS targeting the right DLPFC of the patients with GAD before therapy showed the hub node on the left frontal pole (119 ms) and left posterior temporal pole (212 and 415 ms) weakened connection patterns. Compared with the patterns before treatment, the time-varying EEG network after single-pulse TMS targeting the right DLPFC of the patients with GAD after rTMS treatment showed the hub node on the left frontal (119 and 212 ms) and left temporal (212 and 415 ms) weakened connection patterns. The results show that the time-varying network pattern after treatment is very similar to the healthy subject, indicating that rTMS treatment promotes the restoration of brain network connections.

DISCUSSION

Summary of Key Findings

To the best of our knowledge, this study was the first to use time-varying EEG networks to investigate the underlying neural connection mechanisms of GAD. In the present study, we found that low-frequency rTMS stimulating the right DLPFC was effective at improving the symptoms of GAD, and the abnormal time-varying EEG networks in GAD showed a trend toward normalization after rTMS treatment. Furthermore, this effect was sustained: at 1 month follow-up visit, GAD continued to report fewer anxiety symptoms as the HAMA and HAMD scores continued to significantly decline from those reported at the end of treatment. This study demonstrates that rTMS does have potential as an effective augmentative treatment in GAD.

Comparison With Previous Studies

The prefrontal lobe is an important part of the neural loop of emotional processing. It plays an important regulatory role through its round-trip connection with the temporal lobe and limbic system, in which the DLPFC is the pivotal brain region. Using fMRI, Bystritsky et al. found that the right DLPFC of patients with GAD was abnormally activated, and they recruited 10 patients with GAD to undergo low-frequency rTMS therapy for a total of 6 times for 3 weeks (1 Hz, 90% rMT, 900 stimuli per time), with the stimulation targeting the right DLPFC; the HAMA score significantly reduced at the end of the treatment (34). Gretchen et al. (35) stimulated the right DLPFC with rTMS (1 Hz, 90% RMT) and observed that after active rTMS treatment, the activity of the right DLPFC significantly improved and there were improvements in self-reported emotion regulation difficulties at posttreatment and at the 3-month follow-up in the active group only. In the present study, patients with GAD were treated with low-frequency rTMS (1 Hz, 90% RMT), targeting the right DLPFC for 10 days. The results showed that the clinical symptoms of 11 patients with GAD improved after treatment, and the scores of HAMA and HAMD significantly decreased compared to those before treatment. The curative effect lasted at least 1 month.

Interpretation of Findings

The left and right hemispheres of the human brain are functionally asymmetrical. According to the theory of the titer model of brain emotions, the right hemisphere plays a leading role in the processing of negative emotions, while the left hemisphere is mainly responsible for processing positive emotions (36). A study using fMRI found that showing subjects pictures with obvious emotional colors led to increased blood flow in the bilateral anterior cingulate gyri, DLPFC, amygdala, and anterior temporal brain (37). Negative images more significantly activated the relevant brain regions of the right hemisphere, and positive meanings significantly activated the relevant brain regions in the left hemisphere (38). Although our study has shown that rTMS can improve GAD symptoms through the regulation of the DLPFC, the exact neurobiological mechanisms remain unclear. We consider that GAD is a disease of abnormal brain function in which the different cortex areas have abnormal connections.

Abnormal functional connectivity of GAD has been reported widely in fMRI studies. Compared with healthy controls, the function connectivity of the right medial prefrontal gyrus of the default mode network and the superior temporal gyrus of the salience network increased significantly in the GAD patients (39). We used the adaptive directed transfer function to analyze TMS-EEG signals, as well as to prove the existence of network abnormality in GAD. Compared with the healthy controls in patients with GAD, the time-varying EEG network showed that the right DLPFC has insufficient inhibition of information outflow from the left frontal and temporal regions, and that the abnormal activation of the left temporal lobe leads to overreaction to external stimulus processing. Therefore, low-frequency rTMS is administered to the right DLPFC to inhibit its

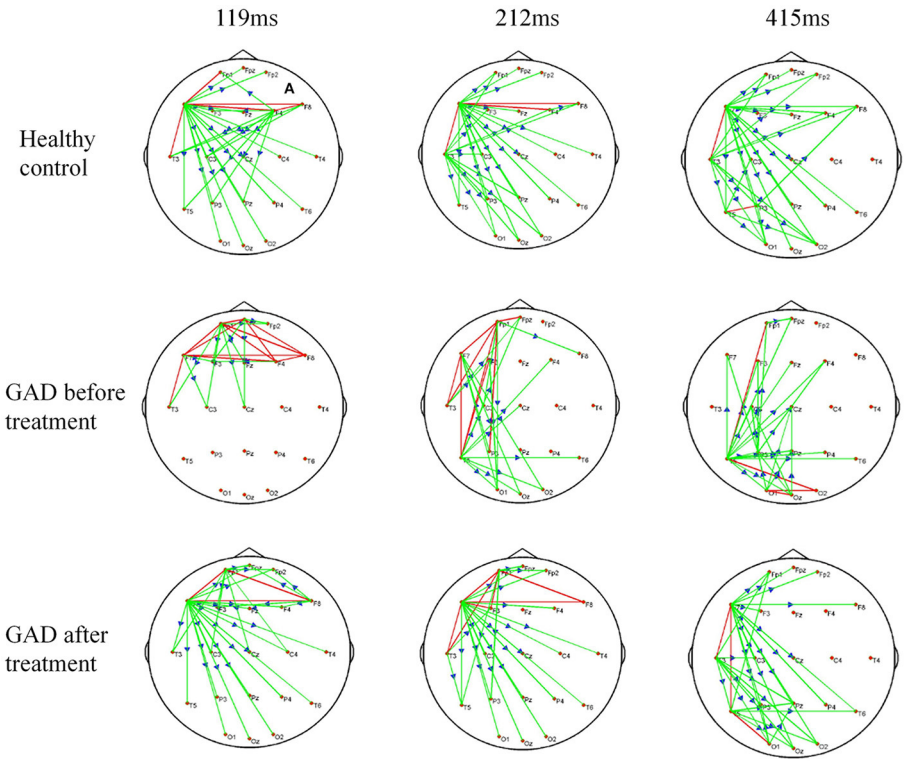

FIGURE 1 | The time-varying EEG network connections after single-pulse TMS stimulation compared to before stimulation. Time, after single TMS. Green lines, decreased infor mation; blue arrows, the direction of information flow; Red lines, two-way decreased information; GAD, Generalized anxiety disorder.

activity and promote the restoration of the information outflow trend toward the normal.

Excessive and uncontrollable worry is the core symptom of GAD, the pathological worry pattern might be linked with alterations of fronto-limbic regions, such as the DLPFC and amygdala, to handle the external threat through the heightened arousal and distress state (40). RTMS strengthened the GAD processing advantage of positive emotions by activating information outflow from the left frontal lobe. As a result, the symptoms of anxiety and depression significantly improved. This observation may support the hypothesis that GAD may be a disorder of brain functional connectivity, and rTMS treatment could reverse this abnormity.

Strengths and Limitations

This study had several limitations. First, the sample size was relatively small; a larger sample size is needed in further investigations. Second, we should add a sham stimulation group as a control. Third, further studies need to use the neuro-navigated system to locate DLPFC to improve the accuracy of stimulation. Last but not least, we only used HAMA to measure anxiety in patients with GAD; in the subsequent studies, we will add the State-Trait Anxiety Inventory (STAI), a more sensitive inventory in case of GAD because it measures both state and trait anxiety.

CONCLUSION

The present study was designed to determine the effectiveness of low-frequency rTMS treatment for GAD. We found that the curative effect lasted at least 1 month. Our study revealed that the right DLPFC in GAD has insufficient inhibition of information outflow in the left frontal and temporal regions. Low-frequency rTMS treatment targeting the right DLPFC may reverse these abnormal changes and improve the symptoms of anxiety.

DATA AVAILABILITY STATEMENT

The raw data supporting the conclusions of this article will be made available by the authors, without undue reservation.

ETHICS STATEMENT

The studies involving human participants were reviewed and approved by Ethics Committee of Xuanwu Hospital, Capital Medical University. The patients/participants provided their written informed consent to participate in this study.

AUTHOR CONTRIBUTIONS

PX and YW contributed to the conception of the study. HT, NH, and XZ performed the experiments. LZ and HT performed the data analyses. PS and WH wrote the manuscript. HT, HL, and YW helped to perform the analysis with constructive

discussions. All authors contributed to the article and approved the submitted version.

FUNDING

The study was supported by National Key R&D Program of China (Grant Numbers: 2021YFC2501404, 2019YFC0121200, 2019YFC0121202, 2019YFC0121203, 2018YFC1314500, 2018YFA0108503, and 2016YFC1306302), National Natural Science Foundation of China (Grant Numbers: 82001388, 81771398, and 81801285), and Beijing Municipal Administration of Hospital Clinical Medicine Development of Special Funding Support (Grant Number: ZYLX201706).

REFERENCES

1. Kessler RC, Berglund P, Demler O, Jin R, Merikangas KR, Walters EE. Lifetime prevalence and age-of-onset distributions of DSM-IV disorders in the National Comorbidity Survey Replication. *Arch Gen Psychiatry.* (2005) 62:593–602. doi: 10.1001/archpsyc.62.6.593
2. Ströhle A, Gensichen J, Domschke K. The diagnosis and treatment of anxiety disorders. *Dtsch Arztebl Int.* (2018) 155:611–20. doi: 10.3238/arztebl.2018.0611
3. DeMartini J, Patel G, Fancher TL. Generalized anxiety disorder. *Ann Intern Med.* (2019) 170:ITC49–64. doi: 10.7326/AITC201904020
4. Kampman O, Viikki M, Leinonen E. Anxiety disorders and temperament-an update review. *Curr Psychiatry Rep.* (2017) 19:27. doi: 10.1007/s11920-017-0779-5
5. Bandelow B, Zohar J, Hollander E, Kasper S, Möller HJ, Zohar J. World Federation of Societies of Biological Psychiatry (WFSBP) guidelines for the pharmacological treatment of anxiety, obsessive-compulsive and post-traumatic stress disorders—first revision. *World J Biol Psychiatry.* (2008) 9:248–312. doi: 10.1080/15622970802465807
6. Daitch C. Cognitive behavioral therapy, mindfulness, and hypnosis as treatment methods for generalized anxiety disorder. *Am J Clin Hypn.* (2018) 61:57–69. doi: 10.1080/00029157.2018.1458594
7. Slee A, Nazareth I, Bondaronek P, Liu Y, Cheng Z, Freemantle N. Pharmacological treatments for generalised anxiety disorder: a systematic review and network meta-analysis. *Lancet.* (2019) 393:768–77. doi: 10.1016/S0140-6736(18)31793-8
8. Buoli M, Caldiroli A, Caletti E, Paoli RA, Altamura AC. New approaches to the pharmacological management of generalized anxiety disorder. *Expert Opin Pharmacother.* (2013) 14:175–84. doi: 10.1517/14656566.2013.759559
9. Baldwin DS, Waldman S, Allgulander C. Evidence-based pharmacological treatment of generalized anxiety disorder. *Int J Neuropsychopharmacol.* (2011) 14:697–710. doi: 10.1017/S1461145710001434
10. Cirillo P, Gold AK, Nardi AE, Ornelas AC, Nierenberg AA, Camprodon J, et al. (2019). Transcranial magnetic stimulation in anxiety and trauma-related disorders: a systematic review and meta-analysis. *Brain Behav.* 9, e01284. doi: 10.1002/brb3.1284
11. Taylor R, Galvez V, Loo C. Transcranial magnetic stimulation (TMS) safety: a practical guide for psychiatrists. *Australas Psychiatry.* (2018) 26:189–92. doi: 10.1177/1039856217748249
12. Pernia AM, Zorzo C, Prieto MJ, Martinez JA, Higarza SG, Mendez M. Equipment for repetitive transcranial magnetic stimulation. *IEEE Trans Biomed Circuits Syst.* (2020) 14:525–34. doi: 10.1109/TBCAS.2020.2981012
13. Tracy DK, de Sousa DAM, Nalesnik N, Mao L, Lage C, Shergill SS. Neuroimaging effects of 1 Hz right temporoparietal rTMS on normal auditory processing: implications for clinical hallucination treatment paradigms. *J Clin Neurophysiol.* (2014) 31:541–6. doi: 10.1097/WNP.0000000000000098
14. Choi KM, Jang K, Jang KI, Um YH, Kim M, Kim D, et al. The effects of 3 weeks of rTMS treatment on P200 amplitude in patients with depression. *Neurosci Lett.* (2014) 577:22–7. doi: 10.1016/j.neulet.2014.06.003
15. Choi KM, Choi S, Lee SM, Jang K, Chae J. Three weeks of rTMS treatment maintains clinical improvement but not electrophysiological changes in patients with depression: a 6-week follow-up pilot study. *Front Psychiatry.* (2019) 10:351. doi: 10.3389/fpsyt.2019.00351
16. Dionísio A, Duarte IC, Patrício M, Castelo-Branco M. The use of repetitive transcranial magnetic stimulation for stroke rehabilitation: a systematic review. *J Stroke Cerebrovasc Dis.* (2018) 27:1–31. doi: 10.1016/j.jstrokecerebrovasdis.2017.09.008
17. Kiebs M, Hurlemann R, Mutz J. Repetitive transcranial magnetic stimulation in non-treatment-resistant depression. *Br J Psychiatry.* (2019) 215:445–6. doi: 10.1192/bjp.2019.75
18. Rachid F. Repetitive transcranial magnetic stimulation in the treatment of eating disorders: a review of safety and efficacy. *Psychiatry Res.* (2018) 269:145–56. doi: 10.1016/j.psychres.2018.08.013
19. Tsuboyama M, Kaye HL, Rotenberg A. Review of transcranial magnetic stimulation in epilepsy. *Clin Ther.* (2020) 42:1155–68. doi: 10.1016/j.clinthera.2020.05.016
20. Yang LL, Zhao D, Kong LL, Sun YQ, Wang ZY, Gao YY. High-frequency repetitive transcranial magnetic stimulation (rTMS) improves neurocognitive function in bipolar disorder. *J Affect Disord.* (2019) 246:851–6. doi: 10.1016/j.jad.2018.12.102
21. Tremblay S, Rogasch NC, Premoli I, Blumberger DM, Casarotto S, Chen R. Clinical utility and prospective of TMS-EEG. *Clin Neurophysiol.* (2019) 130:802–44. doi: 10.1016/j.clinph.2019.01.001
22. Kimiskidis K. Transcranial magnetic stimulation (TMS) coupled with electroencephalography (EEG): biomarker of the future. *Rev Neurol.* (2016) 172:123–6. doi: 10.1016/j.neurol.2015.11.004
23. Koch G. The new era of TMS-EEG: Moving towards the clinical practice. *Clin Neurophysiol.* (2019) 130:791–2. doi: 10.1016/j.clinph.2019.02.004
24. Song P, Lin H, Li S, Wang L, Liu J, Li N, et al. Repetitive transcranial magnetic stimulation (rTMS) modulates time-varying electroencephalography (EEG) network in primary insomnia patients: a TMS-EEG study. *Sleep Med.* (2019) 56:157–63. doi: 10.1016/j.sleep.2019.01.007
25. Song P, Lin H, Liu C, Jiang Y, Lin Y, Xue Q, et al. Transcranial magnetic stimulation to the middle frontal gyrus during attention modes induced dynamic module reconfiguration in brain networks. *Front Neuroinform.* (2019) 13:22. doi: 10.3389/fninf.2019.00022
26. Song P, Li S, Wang S, Wei H, Lin H, Wang Y. Repetitive transcranial magnetic stimulation of the cerebellum improves ataxia and cerebello-fronto plasticity in multiple system atrophy: a randomized, double-blind, sham-controlled and TMS-EEG study. *Aging.* (2020) 12:20611–22. doi: 10.18632/aging.103946
27. Ochsner KN, Silvers JA, Buhle JT. Functional imaging studies of emotion regulation: a synthetic review and evolving model of the cognitive control of emotion. *Ann N Y Acad Sci.* (2012) 1251:E1–24. doi: 10.1111/j.1749-6632.2012.06751.x
28. Diekhof EK, Geier K, Falkai P, Gruber O. Fear is only as deep as the mind allows: a coordinate-based meta-analysis of neuroimaging studies on the regulation of negative affect. *Neuroimage.* (2011) 58:275–85. doi: 10.1016/j.neuroimage.2011.05.073
29. Andreescu C, Sheu LK, Tudorascu D, Gross JJ, Walker S, Banihashemi L, et al. Emotion reactivity and regulation in late-life generalized anxiety disorder: functional connectivity at baseline and post-treatment. *Am J Geriatr Psychiatry.* (2015) 23:200–14. doi: 10.1016/j.jagp.2014.05.003
30. Hamilton M. The assessment of anxiety states by rating. *Br J Med Psychol.* (1959) 32:50–5. doi: 10.1111/j.2044-8341.1959.tb00467.x
31. Hamilton M. A rating scale for depression. *J Neurol Neurosurg Psychiatry.* (1960) 23:56–62. doi: 10.1136/jnnp.23.1.56
32. Zhang L, Liang Y, Li F, Sun H, Peng W, Du P, et al. Time-varying networks of inter-ictal discharging reveal epileptogenic zone. *Front Comput Neurosci.* (2017) 11. doi: 10.3389/fncom.2017.00077

33. Arnold M, Milner XHR, Witte H, Bauer R, Braun C. Adaptive AR modeling of nonstationary time series by means of Kalman filtering. *IEEE Transac Biomed Eng.* (1998) 45:553–62. doi: 10.1109/10.668741
34. Bystritsky A, Kaplan JT, Feusner JD, Kerwin LE, Wadekar M, Burock M, et al. A preliminary study of fMRI-guided rTMS in the treatment of generalized anxiety disorder. *J Clin Psychiatry.* (2008) 69:1092–8. doi: 10.4088/JCP.v69n0708
35. Diefenbach GJ, Bragdon LB, Zertuche L, Hyatt CJ, Hallion LS, Tolin DF. Repetitive transcranial magnetic stimulation for generalised anxiety disorder: a pilot randomised, double-blind, sham-controlled trial. *Br J Psychiatry.* (2016) 209:222–8. doi: 10.1192/bjp.bp.115.168203
36. Heller W, Nitschke JB, Etienne MA, Miller GA. Patterns of regional brain activity differentiate types of anxiety. *J Abnorm Psychol.* (1997) 106:376–85. doi: 10.1037/0021-843X.106.3.376
37. Lai CH. Task MRI-based functional brain network of anxiety. *Adv Exp Med Biol.* (2020) 1191:3–20. doi: 10.1007/978-981-32-9705-0_1
38. Alfano KM, Cimino CR. Alteration of expected hemispheric asymmetries: valence and arousal effects in neuropsychological models of emotion. *Brain Cogn.* (2008) 66:213–20. doi: 10.1016/j.bandc.2007.08.002
39. Xiong H, Guo RJ, Shi HW. Altered default mode network and salience network functional connectivity in patients with generalized anxiety disorders: an ICA-based resting-state fMRI study. *Evid Based Complement Alternat Med.* (2020) 2020:4048916. doi: 10.1155/2020/4048916
40. Meeten F, Davey GC, Makovac E, Watson DR, Garfinkel SN, Critchley HD. Goal directed worry rules are associated with distinct patterns of amygdala functional connectivity and vagal modulation during perseverative cognition. *Front Hum Neurosci.* (2016) 10:553. doi: 10.3389/fnhum.2016.00553

Conflict of Interest: The authors declare that the research was conducted in the absence of any commercial or financial relationships that could be construed as a potential conflict of interest.

frontiers in Psychiatry

ORIGINAL RESEARCH
published: 17 February 2022
doi: 10.3389/fpsyt.2021.813460

From Sound Perception to Automatic Detection of Schizophrenia: An EEG-Based Deep Learning Approach

Carla Barros[1], *Brian Roach*[2,3], *Judith M. Ford*[2,3], *Ana P. Pinheiro*[1,4*†] *and Carlos A. Silva*[5,6†]

[1] *Psychological Neurosciences Lab, Psychology Research Center (CIPsi), School of Psychology, University of Minho, Braga, Portugal,* [2] *Psychiatry Service, San Francisco Veteran Affairs Medical Center (VAMC), San Francisco, CA, United States,* [3] *Department of Psychiatry, University of California, San Francisco, San Francisco, CA, United States,* [4] *Research Center for Psychological Science (CICPSI), Faculdade de Psicologia, Universidade de Lisboa, Lisbon, Portugal,* [5] *Center for MicroElectromechanical Systems (CMEMS-UMinho), University of Minho, Guimarães, Portugal,* [6] *LABBELS - Associate Laboratory, Guimarães, Portugal*

Deep learning techniques have been applied to electroencephalogram (EEG) signals, with promising applications in the field of psychiatry. Schizophrenia is one of the most disabling neuropsychiatric disorders, often characterized by the presence of auditory hallucinations. Auditory processing impairments have been studied using EEG-derived event-related potentials and have been associated with clinical symptoms and cognitive dysfunction in schizophrenia. Due to consistent changes in the amplitude of ERP components, such as the auditory N100, some have been proposed as biomarkers of schizophrenia. In this paper, we examine altered patterns in electrical brain activity during auditory processing and their potential to discriminate schizophrenia and healthy subjects. Using deep convolutional neural networks, we propose an architecture to perform the classification based on multi-channels auditory-related EEG single-trials, recorded during a passive listening task. We analyzed the effect of the number of electrodes used, as well as the laterality and distribution of the electrical activity over the scalp. Results show that the proposed model is able to classify schizophrenia and healthy subjects with an average accuracy of 78% using only 5 midline channels (Fz, FCz, Cz, CPz, and Pz). The present study shows the potential of deep learning methods in the study of impaired auditory processing in schizophrenia with implications for diagnosis. The proposed design can provide a base model for future developments in schizophrenia research.

Keywords: auditory processing, convolutional neural network, deep learning, EEG, schizophrenia

OPEN ACCESS

Edited by:
Jing Xiang,
Cincinnati Children's Hospital Medical Center, United States

Reviewed by:
Yoji Hirano,
Kyushu University, Japan
Armida Mucci,
University of Campania Luigi Vanvitelli, Italy

***Correspondence:**
Ana P. Pinheiro
appinheiro@psicologia.ulisboa.pt

† These authors have contributed equally to this work

Specialty section:
This article was submitted to Neuroimaging and Stimulation, a section of the journal Frontiers in Psychiatry

Received: *11 November 2021*
Accepted: *31 December 2021*
Published: *17 February 2022*

Citation:
Barros C, Roach B, Ford JM, Pinheiro AP and Silva CA (2022) From Sound Perception to Automatic Detection of Schizophrenia: An EEG-Based Deep Learning Approach. Front. Psychiatry 12:813460. doi: 10.3389/fpsyt.2021.813460

1. INTRODUCTION

Schizophrenia (SZ) is a chronic and complex brain disorder that affects social and cognitive functioning (1). SZ is characterized by the presence of positive (e.g., hallucinations and delusions) and negative symptoms (e.g., blunted affect), as well as cognitive deficits (2). About 75% of patients experience hallucinations in the auditory modality, most frequently as voices (3). Deficits in auditory processing have frequently been reported in SZ, which may reflect auditory cortex pathology (4). Some studies have documented larger deficits in patients with (vs. without) auditory hallucinations (5).

Several studies aimed to probe the neural mechanisms underpinning auditory processing abnormalities in SZ, using different techniques such as electroencephalography (EEG). Event-related potentials (ERP) of the EEG represent the averaged electrical activity elicited in response to an event (e.g., stimulus, motor response). They provide a suitable method to specify the time course of brain activity in response to auditory stimulation, for example (6). Alterations in ERP components have been consistently documented in SZ and proposed as potential biomarkers of this disorder (7). For example, the mismatch negativity (MMN) and P300 amplitudes are robustly attenuated in SZ (8, 9). In turn, sensory gating studies have shown reduced P50 suppression in SZ patients in auditory paired-stimulus paradigms (10–13). Other studies have focused on the N100 ERP component, specifically showing generalized amplitude reductions in response to sounds in SZ. This reduction seems to be more pronounced in patients who experience auditory hallucinations (14, 15).

Deep learning applied to EEG data could represent a promising contribution to a more accurate prediction of psychosis conversion in at-risk states of or treatment response in diagnosed patients, as well as of disease trajectories (16). EEG-based deep learning algorithms have also seen growing interest among neuroscientists, especially in the context of brain-signal decoding. However, deep learning is still a poorly explored method in the development of EEG-based models applied to SZ diagnosis and prediction. Convolutional networks have been implemented with the goal of recognizing and classifying patterns from multivariate time series, such as the EEG signal (17–19). The success of this type of neural network applied to EEG data for decoding purposes has prompted us to investigate the use of convolutional neural networks (CNN) for SZ classification.

1.1. Related Work

SZ classification on the basis of early auditory EEG-derived ERP components has already been attempted with classical machine learning models (20–22). Components such as the P300, MMN, or N100 were mainly elicited with auditory oddball and passive listening paradigms and used as input features in SZ recognition with random forest (RF), support vector machine (SVM), or linear discriminant analysis (LDA) classifiers. The results of these studies underscore the potential of auditory ERP components recurrently proposed as SZ biomarkers when their characteristics are used as features to discriminate patients from healthy subjects. A limitation of these approaches relates to the process underlying feature extraction and selection, which requires domain expertise. The few studies that probed the potential of deep learning in EEG-based classification of SZ (23–27) achieved the best performances with CNN-based models applied to resting-state EEG data, which is independent of cognitive or sensory processing. Despite their capacity to discriminate healthy from SZ subjects, these models do not inform about auditory processing, which is affected in SZ (4). Very recently, Aristizabal et al. (28) explored both machine and deep learning techniques to identify children at risk of SZ on the basis of EEG data collected during a passive auditory oddball task. In the classical machine learning approach, the mean amplitude was extracted in the 80–220 ms and 160–290 ms latency intervals, when ERP components indexing of sensory processing (N100 and P200, respectively) are expected to emerge. The mean values were extracted for 5 midline electrodes: Fz, FCz, Cz, CPz, and Pz. Using common classifiers, such as decision trees, k-nearest neighbors, and SVM, the discrimination between healthy and at-risk children based on those features was unsuccessful. As for the deep learning approach, a 2D-CNN-LSTM was proposed, composed of one 2D convolutional layer, followed by normalization and fully-connected layers. The information from the previous block was processed with a stack of two LSTM (long-short term memory) networks, whose output was transformed with sigmoid non-linearity for classification purposes. This model based on EEG single-trials achieved the best performance in at-risk children identification. For each trial, a spatio-temporal 2D signal was created using a 300 ms post-stimulus window focusing on the 5 midline electrodes. The machine learning attempt illustrates the difficulty in specifying stimulus-related signal features that allow a precise identification of SZ risk. The results of both approaches may reflect the developmental phase of the population under study, namely ongoing developmental brain maturation processes. Notwithstanding, this study demonstrates the potential of deep learning methods in subjects' discrimination as a function of psychosis risk.

Evidence for altered auditory processing in SZ has fostered the investigation of the dynamics of electrical brain activity targeting the differentiation between patients and healthy subjects. Amplitude reduction of auditory evoked potentials such as the N100 have been consistently reported in the literature (14, 29). Those alterations have driven the use of machine learning methods for automatic SZ recognition. Beyond the time-consuming feature extraction, both machine learning models and ERP analysis exhibit a major limitation: the non-uniformity of the time windows and electrodes used for feature selection across studies. By contrast, deep learning methods profit from automatic pattern learning, with minimal human intervention. Although deep learning architectures based on EEG signals have been proposed for SZ classification, the learning of patterns from the electrical brain response to auditory stimuli is a scarcely investigated topic. A recent review provided a critical analysis of deep learning and classical machine learning methods to detect SZ based on EEG signals (30), highlighting the potentialities of these methods in clinical research. Notwithstanding, from this review it is also clear that more studies are necessary and that surpass the limitations of the existing ones. The current work intends to assess the potential of deep models to learn discriminatory EEG patterns in the early stages of auditory processing, which may inform about the significance of sensory changes to SZ diagnosis and prognosis. We followed good practices for the development and implementation of machine learning methods proposed in Barros et al. (30).

1.2. Contributions

This paper presents a multi-channel deep convolutional neural network for SZ and healthy control (HC) single-trial EEG

classification across subjects. The CNN-based architecture is proposed for trial-wise decoding of EEG signals elicited in response to externally generated auditory stimulation. The main contributions of this work are:

- The application of deep learning methods to SZ classification using stimulus-related EEG single-trials recorded during auditory processing of pure tones. Unlike previous deep learning research using resting-state EEG data for the same purpose, our model is based on sensory processing measures. Since auditory impairments have been documented in SZ, we hypothesize that the signal's dynamic during sound processing is altered in this disorder.
- The recording of EEG data during a passive listening task to provide discriminatory information. The proposed task is of short duration, easily implemented in a clinical environment, and does not require an overt response from the subject.
- The specification of which number of electrodes and which scalp localization should be used to most accurately predict whether the signal belongs to a SZ subject or not. This study sheds light on which electrode location is most relevant for identifying changes in brain activity during auditory processing since most studies in this field use a different number and combination of electrodes.
- The comparison of classical machine learning with deep learning architectures to classify SZ based on auditory EEG responses. Given the advantages of deep learning over machine learning methods, we hypothesize that deep neural networks will be able to learn different patterns based on auditory EEG signals, allowing a more accurate classification of SZ subjects.
- The use of ensemble methods to reduce the variance of predictions of the developed deep learning model.

This paper is organized as follows. The methodology used for data acquisition and the deep learning model's architecture are detailed in Section 2. Section 3 describes the dataset, the evaluation procedure, and the experimental setup. In Section 4, the results are described and discussed. Finally, Section 5 presents the main conclusions.

2. METHODOLOGY

In this section, we describe the methodology used for EEG data acquisition. With a simple listening task, we aimed to elicit auditory evoked potentials that shed light on the time course of auditory processing. The signal dynamics elicited by auditory stimuli is also explained, showing the expected pattern in both control and SZ subjects. Afterward, the proposed deep learning architecture is presented in detail, which aims to extract information from the time course of the EEG signal and its topographical distribution. The main objective is to obtain a model capable of recognizing patterns in the electrical brain activity underlying auditory processing in SZ. Lastly, the traditional machine learning approaches commonly found in other proposals are introduced. The implementation of these algorithms provides a strong base model for a proper analysis of the specific advantages of deep learning (over machine learning) methods in predicting whether an individual suffers from SZ or not, on the basis of auditory processing alterations.

2.1. EEG Data Acquisition

EEG data were recorded using 64 electrodes according to the 10-10 international system configuration, while subjects performed an auditory task (see **Figure 1A**). After EEG signal acquisition, offline pre-processing was performed: the signal was filtered, segmented, and carefully inspected to remove potential artifacts.

2.1.1. EEG Task

The task involved the presentation of 100 tones, with a variable inter-stimulus interval (ISI—temporal interval from the offset of one stimulus to the onset of another) ranging between 1,000 and 2,000 ms (**Figure 1B**). The presentation of each sound is called a trial. During data acquisition, the EEG signals were obtained over electrodes placed on the scalp of the participant, who were asked to listen passively to the sounds. This task allows examining the response of the auditory system to externally generated sounds.

2.1.2. Auditory ERP Components

The N100 and the P200 components are typically elicited in response to sound onset. The N100 can be elicited by any discernible auditory stimulus irrespective of task demands (14). This negative potential typically occurs between 80 and 120 ms after sound onset, with maximal amplitude over fronto-central and central electrodes (6, 31). The P200 is a positive deflection that occurs approximately 200 ms after sound onset (6). This component is distributed over centro-parietal electrodes. Its amplitude is generally maximal over the vertex (6, 32). Both N100 and P200 auditory components measured during passive listening tasks can reflect early automatic attention allocation and stimulus categorization, respectively (33). Considering the consistently reported alterations in the N100 and P200 amplitudes in psychosis (14, 32), an approach focused on the time window of these early auditory processing indices has the potential to accurately discriminate HC and SZ subjects.

The ERP analysis consists of averaging all segments related to a given condition from a subject and subsequently computing the grand averages, which represent the average of EEG activity across subjects. When conducting this traditional analysis, the background activity (unrelated to the stimulus) is faded away and the N100 and P200 components emerge. The typical grand averages waveforms obtained from the ERP analysis are illustrated in **Figure 2**, showing a reduction in the amplitude of the N100 and P200 in SZ. Although the main assumption of signal averaging is that the EEG signal in each trial has stable characteristics, such as morphology, the truth is that ERP averaging hides the intertrial variability in latency and amplitude of the underlying components (34). Therefore, the averaged ERP signals may only represent an approximate picture of the neural processes elicited by an auditory stimulus. Thus, we adopted a single-trial approach, considering the above-mentioned trial-to-trial variability.

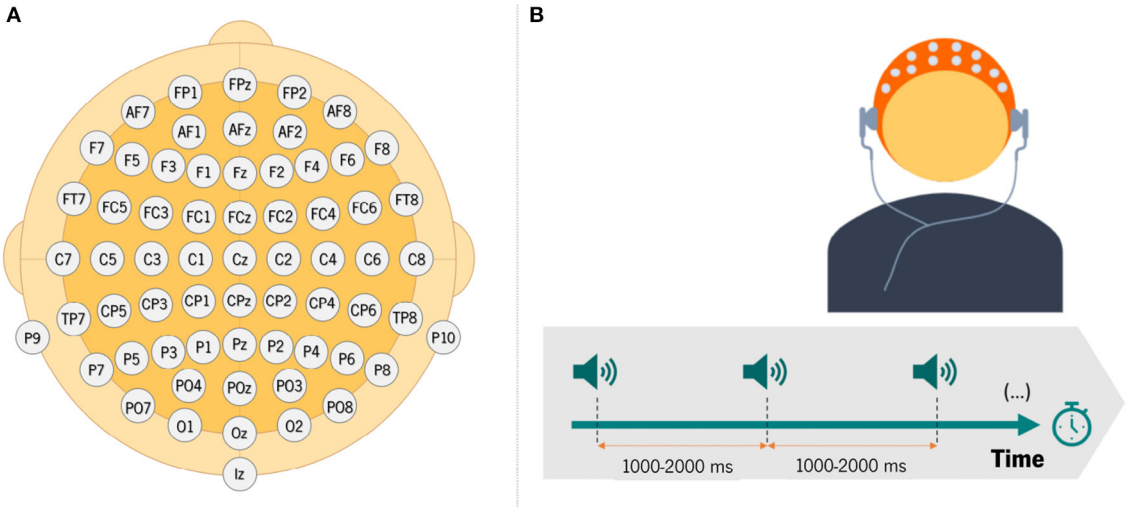

FIGURE 1 | (A) Illustration of electrodes placement over the scalp for EEG data recording; **(B)** schematic illustration of the auditory-only condition of the experimental paradigm.

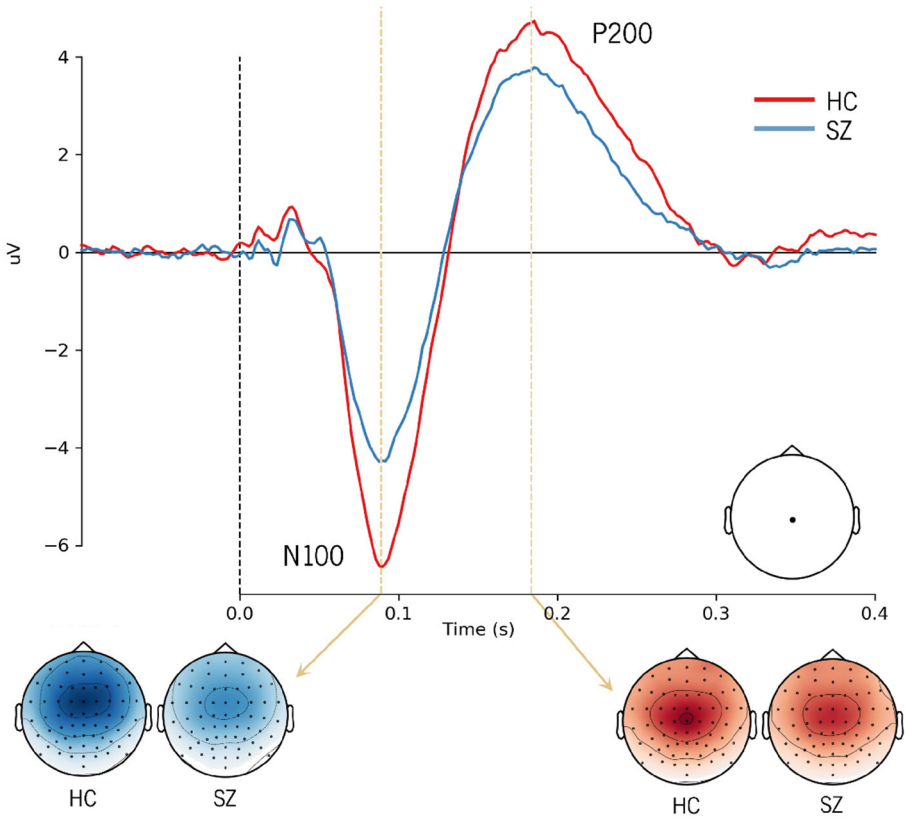

FIGURE 2 | Grand average ERP waveforms showing the N100 and P200 responses to external sounds over Cz electrode in healthy subjects and SZ patients. The topographic distribution of the N100 and P200 components is also shown in both groups.

2.2. Deep Learning Architecture

In the current work, we propose a CNN-based deep learning architecture for SZ classification. The model takes the EEG single-trial recordings as input and provides the probability that a given segment comes from a SZ or HC subject. The acronym SzNet will be used hereinafter to refer to the proposed model.

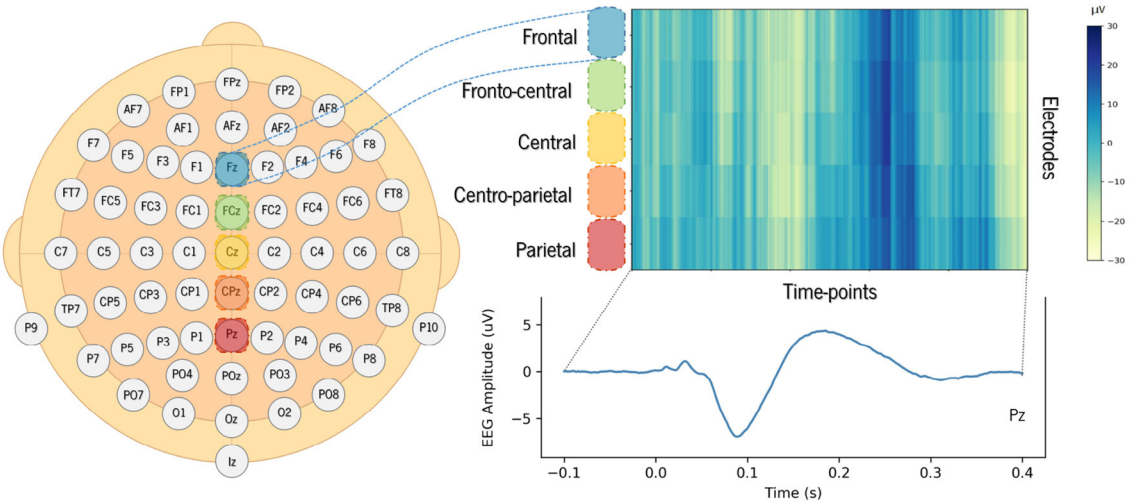

FIGURE 3 | Example of an EEG compounded 2D signal created from one single trial using a set of 5 electrodes. The color scale shows amplitude, in microvolts, over the time points recorded for each of the selected electrodes.

CNNs are able to find patterns by convolving a filter, or kernel, over the data. Depending on the data structure, the convolutional process can occur in different dimensions. A 1D convolution layer creates a kernel that slides over a single dimension. This can be relevant to find correlations between points in the temporal course or topographical distribution of the EEG data. On the other hand, the use of 2D convolutions allows correlating temporal and spatial information, ensuring that patterns are learned from both dimensions. The maximum signal amplitudes can change in their topographical distribution over time. This is illustrated in **Figure 2** by differences in the scalp distribution of the auditory N100 (blue) and P200 (red) peaks reported in the literature, with dark colors corresponding to their maximal activity (N100 - fronto-central distribution; P200 - central distribution).

Therefore, a 2D convolutions strategy allows extracting information about amplitude variation over time and, simultaneously, across electrodes. In order to take advantage of bidimensional convolutions, we created a 2D structure for each trial by stacking 1D signals captured from midline electrodes over frontal (Fz), fronto-central (FCz), central (Cz), centro-parietal (CPz), and parietal (Pz) regions of the scalp. We obtained spatio-temporal 2D signals for the EEG segments in which the rows correspond to the selected electrodes, and the columns to the time points of the segment window considered, as illustrated in **Figure 3**. The value of each coordinate corresponds to the amplitude of the signal. The electrodes (rows) were stacked from the frontal to the parietal regions in the images created, so that the network could extract features with functional meaning.

A schematic representation of the main blocks of the proposed method is presented in **Figure 4**. The first block corresponds to EEG data acquisition and preprocessing, and the second one corresponds to the detailed architecture of the SzNet model. The SzNet architecture is composed of three main types of layers: convolutional, pooling, and fully-connected (FC) layers. Those layers are stacked to increase the network depth, enhancing the selectivity and the sensitivity to slightly relevant variations (35). The learning process of the network is divided into two phases. The first (blue-shaded area in **Figure 4**) involves learning patterns from the time course of each EEG segment for each electrode. The second (orange-shaded area in **Figure 4**) aims to correlate those patterns between different electrodes of interest, extracting spatial information. This approach intended to mimic the traditional analysis of this type of data.

The proposed model consists of a stack of 14 layers of neural network connections. Layers 1, 2, 4, 5, 7, and 8 perform 9-point 1D convolutions (9x1 shaped kernels) over the time dimension. This small-size kernel allows capturing more detailed information about the signal's temporal course. After each convolutional layer, the batch normalization is conducted. In deep learning methods, the output of one layer is the input of the next, and so forth. If the parameters of one layer change, the distribution of the input values of the next layer also changes. This shift in inputs distributions, or covariance shift, can be problematic in deep learning methods with many layers (36). Batch normalization mitigates the covariate shift ensuring the normalization of the activations of each layer (36). The batch normalization is followed by the application of the ReLU function. Layers 3, 6, and 9 are subsampling max-pooling layers (MaxPool2D), which also aim to reduce the number of network parameters. As the network expands, the number of channels used is increased to improve network capacity. Sixteen channels are initially set for the first set of convolutional layers, being duplicated after each max-pooling layer from there onwards up to the 9th layer.

From this point onwards, the learning process is slightly different, with special attention to the scalp distribution of the EEG amplitude. The 10th layer, with 32 channels, performs 3-point 1D convolutions over the spatial dimension (1x3 kernel), searching patterns in the distribution across the different

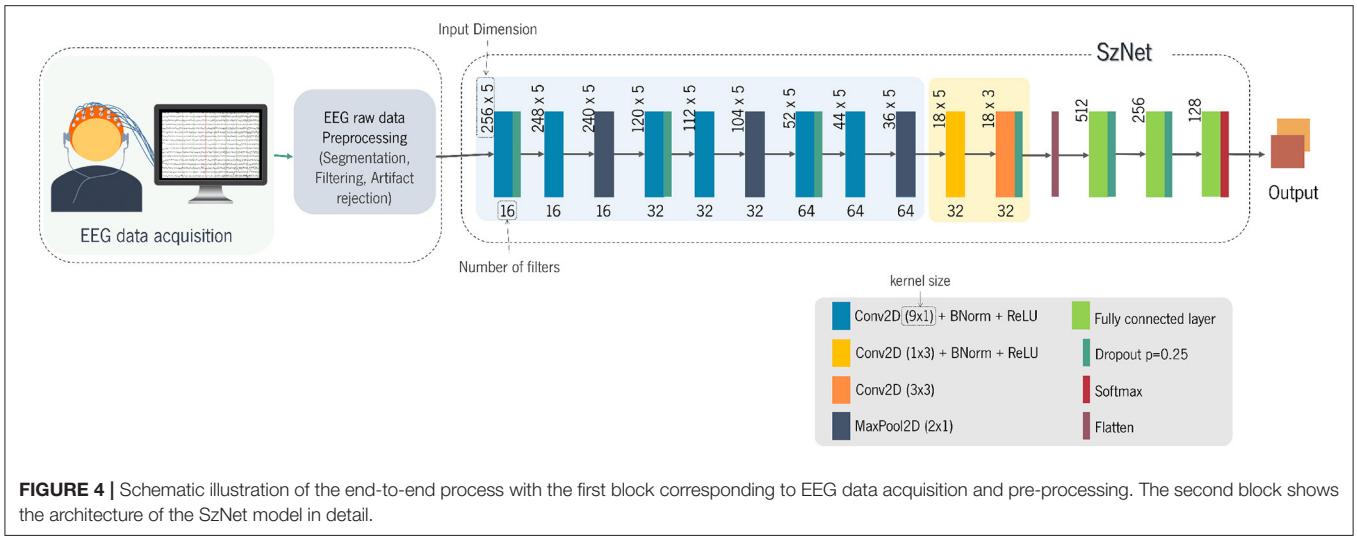

FIGURE 4 | Schematic illustration of the end-to-end process with the first block corresponding to EEG data acquisition and pre-processing. The second block shows the architecture of the SzNet model in detail.

electrodes. Afterward, 2D convolutions with 3x3 kernels are applied to find correlations between temporal and spatial information. This layer also has 32 channels, and its output is flattened, becoming a 1D structure with 512 points. This transformation is followed by 3 FC layers, which aim to aggregate information from high-level features extracted in preceding layers and determine which features are more strongly correlated with a particular class. The fully connected layers are implemented through linear functions. The last layer is fully connected to all its inputs (128) and the 2 outputs nodes (one for SZ and other for HC). The first two FC layers are followed by the ReLU function. After the last FC layer, the softmax function is applied to determine the probability distribution of the two outputs.

2.3. Traditional Machine Learning

There are few publicly available databases of EEG signals from subjects with a diagnosis of SZ. This hampers the comparison of the distinct classical machine learning or deep learning models proposed in the literature. To assess whether our deep network architecture brings advantages over traditional machine learning methods, we tested different algorithms.

Given the versatility of RFs, these algorithms were applied to perform the SZ classification using features extracted from auditory ERP data. In fact, RF is a robust classification algorithm. This model consists of a large number of small decision trees, known as estimators. RF combines predictions of the estimators to produce a more accurate prediction. This method performs well with heterogeneous and high-dimensionality features, and its ensemble design allows to compensate for the overfitting of standard decision trees (37).

2.4. Ensemble Strategy

The ensemble technique consists of combining multiple models, known as base learners, in order to reduce the generalization error and variance (38). Rather than having a single learner as the best predictor, different models are trained separately and then averaged to produce one optimal predictive model (38). This is the strategy behind RF, which is considered a strong classifier. RF uses bagging (Bootstrap Aggregation) to increase the diversity in training of the ensemble (39) and decision trees as base learners (37). A large set of trees are ensembled, and then averaged (40). Since trees are remarkably noisy and weaker classifiers, they strongly benefit from averaging (40).

In an attempt to improve the generalization ability of the proposed deep learning model, we also adopted an ensemble strategy.

3. EXPERIMENTAL SETUP

In this section, we detail the EEG dataset used, describing the preprocessing and the transformations applied to prepare data to be used as the model's input. Lastly, we describe the setup of our deep learning and traditional machine learning classifiers.

3.1. Data

The experimental EEG recordings used in this study were obtained from a publicly available Kaggle dataset (41), hereinafter referred to as *dataset A*. The use of a small pool of training data may result in an increased risk of model overfitting, and, consequently, of poor generalization to new data. Although some methods can be implemented, such as the *k*-fold cross-validation technique, the increase in data quantity can help to minimize overfitting. For this reason, *dataset A* was extended with EEG data collected by our research team, using a similar sensory task, hereinafter referred to as *dataset B*. The entire dataset used in this study encompasses EEG recordings from 63 HC and 65 SZ subjects [*dataset A*: 32 HC and 49 SZ (17 early illness, 32 chronic); *dataset B*: 31 HC and 16 SZ (all first-episode)]. Each subject dataset comprises EEG segments (one segment per trial). Both databases were merged after statistical analyses showed that differences between the two were not significant (see **Supplementary Material**).

3.1.1. Data Acquisition and Preprocessing

EEG data were recorded using a 64-channel Active Two Biosemi system (Biosemi, Amsterdam, The Netherlands) during the passive listening task, involving the presentation of 100 sounds: 1,000 Hz, 80 dB sound pressure level (SPL), 50 ms duration tones for *dataset A*, and 680 Hz, 70 dB SPL, 50 ms duration tones for *dataset B*. Individual segments (trials - one per tone presented) were created from continuous recordings with a 3,000 ms duration, time-locked to tone onset with 1,500 ms pre-stimulus and 1,500 ms post-stimulus. For the EEG data collection, subjects performed a basic auditory-motor task composed of three different conditions: auditory-motor condition; auditory-only condition; and motor condition, as described in Ford et al. (42) and Pinheiro et al. (43). For the purposes of the current study, only data from the auditory-only condition were considered. *Dataset A* were acquired in a continuous mode at a digitization rate of 1,024 Hz and referenced off-line to averaged earlobe electrodes. *Dataset B* were collected also in a continuous mode but at a sampling rate of 512 Hz and re-referenced to the averaged mastoid electrodes. Both datasets were preprocessed off-line using EEGLab, a MatLab Toolbox (44). Before preprocessing, *dataset A* was downsampled to 512 Hz so that all data had the same sampling frequency. The EEG data were digitally filtered with a 0.1 Hz high-pass filter, and the outlier channels were interpolated. The trials were normalized with a baseline correction by subtracting the mean amplitude of the −100 to 0 ms pre-stimulus interval to the whole segment. Trials were subjected to the FASTER toolbox for artifact rejection and rejection of outlier single trials (45). This preprocessing procedure is explained in more detail in Ford et al. (42).

3.2. Deep Learning Algorithm

3.2.1. Temporal Window

Since the focus of this study was on auditory processing, we selected a shorter time window instead of using the signal from the entire segment. The time window considered as input for the proposed model was shortened to 500 ms of duration, corresponding to a total of 256 time points. EEG segments were extracted from −100 to 400 ms time-locked to sound onset, comprising the expected latencies of the auditory N100 and P200 peaks. **Figure 3** provides an example of the 2D structure generated for one trial showing the amplitude for the selected ROI (set of electrodes).

3.2.2. Data Normalization

The amplitude range of EEG recordings varies substantially across subjects, or even within a subject. The normalization of the neural network inputs allows not only comparable measures but also the gradient descent to converge faster. Consequently, the EEG data structures created were transformed before the training phase. The min-max normalization was applied in order to rescale the data. The absolute minimum and maximum values were determined for each training segment and for each electrode. The rescaling was then performed, with the segments' amplitudes varying between the average value of the minima and the average value of the maxima determined for each electrode. A Z-score standardization was then applied allowing data of the entire sample to have zero mean and unit variance. This standardization forces data from both groups of subjects to have the same distribution.

3.2.3. Data Partitioning

Each subject's dataset was composed of a variable number of segments after the removal of segments with artifacts (mean of segments/subject: 94,86 ± 2,27). In total, 5,756 trials from 63 HC subjects and 5,853 trials from 65 SZ subjects were used. A stratified 10-fold cross-validation was performed. The dataset splitting was performed by subject rather than by segment. This procedure ensured that segments of a subject contained in a fold did not leak into other folds. The subjects' datasets were shuffled and split into 10-folds, while ensuring that each fold had the same proportion of SZ and HC subjects' data. In each of the ten iterations, the model was trained using 9-folds, while the remaining fold was used for the test. From the subjects contained in the 9 training folds of each iteration, approximately 90% of them were effectively used for training, while the remaining were used as a validation set. Also, in this split we ensured that the selected subjects contained all their EEG segments (see **Supplementary Material** for more information on dataset splitting). The validation dataset was used to tune hyperparameters and provide an unbiased evaluation of the model. This division was also stratified according to SZ and HC classes, after shuffling the subjects. As in the folds split, the procedure also ensured that segments of a subject did not leak into other folds, so that segments belonging to a training subject were used neither for validation nor for testing. In each iteration, all data segments contained in the training and validation sets were randomized.

3.2.4. Model Training and Hyperparameters

The training process was performed on 300 epochs. The EEG images of all subjects that belonged to the training set were randomly shuffled. The network was trained with ADAM optimizer ($lr = 1 \times 10^{-4}$) and a mini-batch of size 4. Regularization techniques are implemented to prevent overfitting. The learning algorithm is modified in order to reduce its generalization error, but not the training error (38). For regularization, a spatial dropout of 0.25 at some convolutions was used, as illustrated in **Figure 4**. To limit the model's capacity, the L^2 regularization was also implemented by adding a parameter norm penalty of 1×10^{-4} to the cost function. The Xavier Glorot uniform (46) was used as initializer of the model's parameters, ensuring the zero-mean and keeping the variance of activations the same across every layer. The cross-entropy of the outputs was calculated concerning the true labels, generating a loss. The negative loss likelihood (NLL) function was used to determine the loss (47). As described before, the model output is a probability of an image label being assigned to the SZ or HC groups. For validation purposes, a probability threshold of 50% was considered to classify the segment as SZ or HC. The accuracy of the model was determined by all EEG images included in the analysis using cross-validation. During the optimization by backpropagation, we saved the optimal model evaluated with the validation

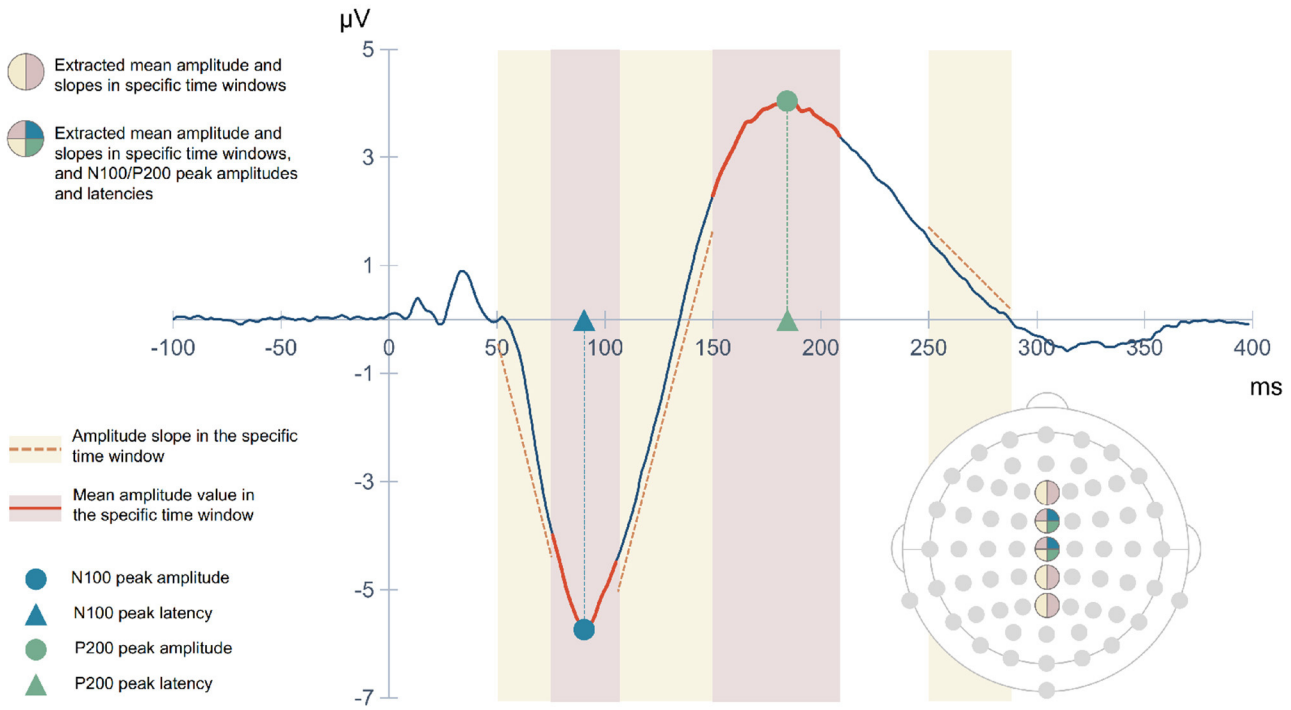

FIGURE 5 | Schematic representation of the features extracted from each subject's ERP waveform.

data set. The typical duration of model training is about 15 h (90 min/fold).

3.3. Traditional Machine Learning Algorithms

3.3.1. Feature Extraction

EEG feature extraction was performed based on ERP waveforms, which were obtained for each subject after averaging across all trials. **Figure 5** provides a schematic illustration of the extracted features. The ERP mean amplitude was determined from 75 to 105 ms latency window (post-stimulus onset), corresponding to the window in which the N100 ERP component typically emerges, and from 150 to 210 ms latency window capturing the P200 component. Both time windows are shown with red shading in **Figure 5**. We also included three slopes as features: the beginning of N100 deflection, the transition from N100 to P200, and the final descending section of the P200 component. Yellow shaded areas in **Figure 5** mark the latency intervals considered for calculating these slopes. All these five features were extracted from the signals captured by the electrodes Fz, FCz, Cz, CPz, and Pz. In addition, the amplitudes (circular symbol) and latencies (triangular symbol) of the N100 and P200 peaks (blue and green marks, respectively, in **Figure 5**) over FCz and Cz electrodes were also extracted. A matrix of features was created, with rows corresponding to the subjects and the columns corresponding to the 33 features extracted for each one.

3.3.2. Data Partitioning and Normalization

A stratified 10-fold cross-validation method was applied to test machine learning models. Subjects (features matrix rows) were shuffled and split into 10-folds, ensuring that each fold had the same proportion of SZ and HC subjects data and that no subject was repeated in any fold. As implemented in the deep learning model, in each of the 10 iterations, the model was trained using 9-folds, while the remaining fold was used for the test. From the subjects contained in the 9 training folds of each iteration, approximately 10% of them were used in the validation set.

3.3.3. Models Training and Hyperparameters

The SZ classification was firstly performed with the RF algorithm using features extracted from the 5 electrodes. Several tests were performed to evaluate the effect of the different extracted features. The hyperparameter tuning was conducted for each one, focused on the number of estimators, maximum number of features, maximum depth of the tree, and split criterion using the validation set. Initially, only the mean amplitudes in the N100 and P200 windows were used, with ten features included per subject. RF configured with 100 estimators, a maximum number of features of 5, and a maximum depth of 2, achieved the best performance. Afterward, the N100 and P200 peak amplitudes and latencies were added to the previous data set, totaling 18 features per subject. The best model was configured with 50 estimators, a maximum number of 10, and a maximum depth of 2. Finally, slopes were also considered (Section 4.4.1 will provide the rationale for including slopes as features). The best model performance using the 33 features per subject was achieved with

TABLE 1 | Metrics used to assess the model's performance, their formulas, and descriptions.

Metric	Formula	Description
Accuracy	$\frac{TP+TN}{TP+TN+FP+FN}$	Proportion of correctly predicted subjects labels
Recall	$\frac{TP}{TP+FN}$	Proportion of correctly predicted SZ subjects
Specificity	$\frac{TN}{TN+FP}$	Proportion of correctly predicted HC subjects
Precision	$\frac{TP}{TP+FP}$	How consistent predictions are when tests are repeated
AUC-ROC	Area under the curve: *Recall* vs. $\frac{FP}{FP+TN}$	How much the model is capable of distinguishing between classes

TN, True Negative; TP, True Positive; FN, False Negative; FP, False Positive.

100 estimators, using a maximum of 2 features in each split and a maximum depth of 15 in each tree. In both cases, the criterion used to find the optimum split in the validation set was the *Gini* impurity measure.

3.4. Ensemble Method

We used the SzNet as base learner and the hard voting algorithm as the ensemble method. We combined 5 fits of the SzNet model trained with different randomly selected seeds in model's weights initialization. This approach is justified by the fact that different initializations lead the neural networks to converge to distinct solutions (48). The hard voting of predictions from separately trained models is one of the simplest ensemble methods and it predicts the class with the largest sum of votes from the models.

3.5. Evaluation Metrics

In order to test the models' performance, all input samples of each subject were fed into the model. The probability of each sample belonging to a SZ subject was computed. Unlike validation, a subject-based approach was considered to test the model. Thus, the average of each subject's input samples probabilities was determined and the same probability threshold (50%) was used to assign a label to the subject. This label can be positive (SZ) or negative (HC). To describe the prediction quality, five metrics were derived from the confusion matrix (**Table 1**).

3.6. Implementation Details

Both deep and traditional machine learning models were implemented on a workstation with an Intel® Core™ CPU (i7-4770k, 3.5 GHz) and an NVIDIA® GPU (GeForce® GTX 1070). Deep learning models were implemented using the open-source framework Pytorch, based on Torch library. RF algorithms were also written in python using *Scikit Learn* (49) and *NumPy* (50) packages.

4. RESULTS AND DISCUSSION

In this section, we start by motivating the choice of kernel for time-domain convolutions. Thereafter, we present and discuss the ablative study, which assesses the relevance of the amount and location of EEG spatial-temporal information used. In this ablative study, we evaluate the number of electrodes used as well as their location over the scalp. After, we compare our proposal with related work, and we present its limitations.

4.1. Kernel Size for Temporal Convolution

The kernel size determines the receptive field of a convolution and provides information about the number of input datapoints the network can look at (51). This is a factor to take into account when considering a network's ability to encode the features, and it is associated with the learning parameters.

In this study, the kernel size used for time-domain convolution defines what information is extracted from the EEG signal. The decomposition of EEG signals can reveal oscillatory activity in specific frequency bands (52). Activity in each band has been associated with different functions. The faster rhythms of the EEG signal, corresponding to the gamma band (above 30 Hz), are linked to complex auditory information processing. Desynchronization of these oscillations during auditory processing has been reported in SZ (52, 53). Thus, we search for the best kernel size using cross-validation. After testing various sizes, the 9x1 kernel was the one that reflected the best results.

4.2. Ablation Study

4.2.1. Relevance of the Number and Location of Electrodes

Different regions of interest (ROI) were analyzed in order to understand whether and which spatial information is relevant for SZ discrimination. The effects of the number of electrodes and their location were tested. The choice of specific electrodes considered the topographical distribution found both for N100 and P200 ERP components (**Figure 2**). Since the largest amplitudes of these components are widely spread over the frontal, central, and parietal areas, the first approach used all the 35 electrodes covering these regions. Then, the number of electrodes was reduced, keeping the coverage of the same scalp areas, but varying its location from the left hemisphere to the right. Three combinations of electrodes were considered (5, 15, and 35 electrodes over the frontal, fronto-central, central, centro-parietal, and parietal regions). The three models are hereinafter referred to as SzNet-5, SzNet-15, and SzNet-35 corresponding to the three sets used: 5, 15, and 35-electrodes sets, respectively. To assess the use of 15 and 35 electrodes, the SzNet architecture was slightly changed: an extra convolutional layer (with 32 filters) was incremented after layer 9, followed by a ReLU function (additional details on the architectures of these models are provided in the **Supplementary Material**). The electrodes in 2D structures were also aligned from the frontal to the parietal region, and from the left to the right hemisphere, as exemplified in **Figure 6**. *N* corresponds to the number of electrodes from each scalp region tested, which was set to 3 for SzNet-15 and to 7 for SzNet-35. The kernel size used in the extra convolutional layer is dependent on *N*. This layer aimed to gather information from each region (frontal, fronto-central, central, centro-parietal, and parietal). Convolutions with stride equal to *N* in the spatial dimension allowed obtaining one feature per region, as illustrated in **Figure 6**. The remaining network was unaltered.

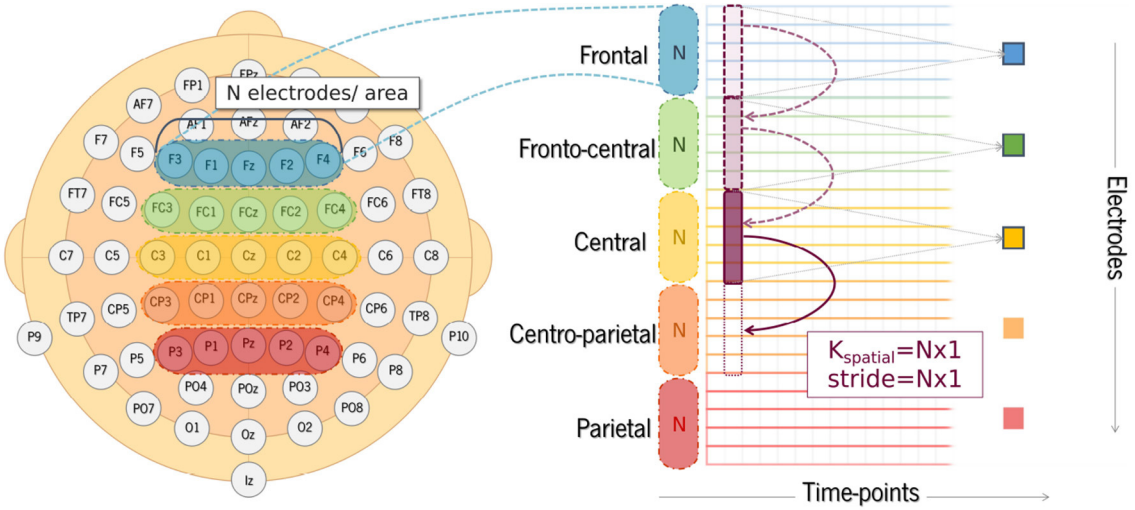

FIGURE 6 | Illustration of the electrode alignment in the 2D structure created for each EEG segment, and schematization of the convolutional process of the extra layer added to the SzNet-15 and SzNet-35 networks. $K_{spatial}$ represents the kernel used in the convolutional layer. *N* corresponds to the number of electrodes of each area tested.

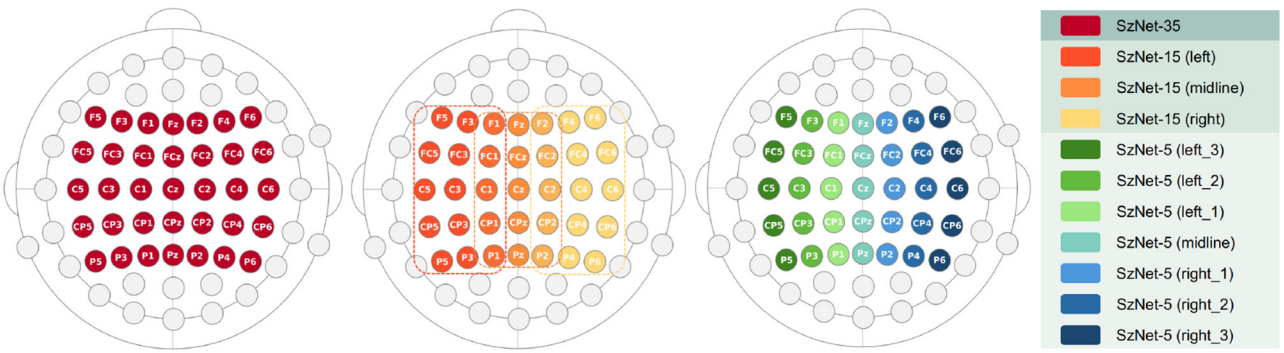

FIGURE 7 | Schematic representation of the different ROIs showing the topographical distribution of electrodes considered to test the three models SzNet-35, SzNet-15, and SzNet-5.

Figure 7 schematically presents the ROI, which varies in number of electrodes and hemispheric location, used to evaluate the performance of the three models developed. The 10-fold cross-validation metrics, computed for each subset of electrodes, are presented in **Table 2**. The results of SzNet-5 and SzNet-15 using different spatial subsets show differences in accuracy as a function of electrode location in the training and data sets. The training and testing with midline and right ROI data showed improved performances. Both accuracy and AUC-ROC metrics show that SzNet-5 with midline and right-1 data, and SzNet-15-midline achieved the best performances. The lower result achieved by the SzNet-5 left-1 subset can account for the slightly lower performance obtained by SzNet-15-midline.

Although no asymmetries in auditory processing alterations have been reported in SZ patients (54), these results suggest that changes in amplitude of right hemisphere EEG signals are contributing more to the discrimination of SZ and HC subjects. Nonetheless, the use of midline electrodes seems more beneficial and is corroborated by most of N100 studies in SZ, which often report a medial to midline N100 amplitude decrease (14). The results suggest that the use of small subsets of electrodes can improve SZ classification.

Our results suggest that the model using 5 midline electrodes (SzNet-5-midline) more accurately predicts whether the EEG signals come from a SZ or a HC subject. Although with minor differences, this model achieved the best performance, on average, for every metric. Subtle differences in accuracy values can represent important practical improvements since a variation of only 0.8% is necessary to indicate or detect the increase or decrease of a unit in the number of correctly identified subjects.

4.2.2. Benefiting From Electrode Alignment

We propose the alignment of electrodes in the 2D data structures created to feed the deep learning model. Instead of randomly

TABLE 2 | Performance of the models tested (SzNet-5, SzNet-15 and SzNet-35) using different spatial ROI evaluated with five metrics: accuracy; AUC-ROC; precision; recall; and specificity.

Model	ROI	Accuracy	AUC-ROC	Precision	Recall	Specificity
SzNet-35	-	0.71 ± 0.07	0.71 ± 0.08	0.70 ± 0.7	0.77 ± 0.09	0.65 ± 0.11
SzNet-15	Left	0.67 ± 0.09	0.67 ± 0.09	0.67 ± 0.14	0.79 ± 0.15	0.55 ± 0.26
SzNet-15	Midline	0.76 ± 0.07	0.76 ± 0.07	0.79 ± 0.13	0.77 ± 0.17	0.74 ± 0.19
SzNet-15	Right	0.73 ± 0.10	0.72 ± 0.10	0.69 ± 0.10	**0.88 ± 0.15**	0.56 ± 0.19
SzNet-5	Left3	0.71 ± 0.10	0.70 ± 0.10	0.70 ± 0.08	0.77 ± 0.19	0.63 ± 0.17
SzNet-5	Left2	0.72 ± 0.05	0.71 ± 0.04	0.75 ± 0.11	0.72 ± 0.20	0.71 ± 0.17
SzNet-5	Left1	0.67 ± 0.08	0.67 ± 0.08	0.71 ± 0.13	0.70 ± 0.20	0.65 ± 0.24
SzNet-5	Midline	**0.78 ± 0.08**	**0.78 ± 0.08**	**0.82 ± 0.13**	0.77 ± 0.15	**0.79 ± 0.17**
SzNet-5	Right1	0.77 ± 0.08	0.77 ± 0.09	0.81 ± 0.21	0.72 ± 0.21	0.77 ± 0.09
SzNet-5	Right2	0.72 ± 0.11	0.72 ± 0.11	0.70 ± 0.10	0.78 ± 0.19	0.65 ± 0.14
SzNet-5	Right3	0.67 ± 0.07	0.67 ± 0.07	0.70 ± 0.14	0.72 ± 0.23	0.61 ± 0.26
SzNet-5	Midline**	0.77 ± 0.09	0.77 ± 0.09	0.86 ± 0.16	0.68 ± 0.15	0.85 ± 0.16

*The highest values achieved for each metric are highlighted in a different color. Similarly, the model and ROI that achieved the best results are marked. **randomly aligned ROI.*

stacking the EEG signal segments, we hypothesized that the alignment according to the topographical arrangement of the electrodes could represent a more realistic way to extract spatial information from the data structures. To confirm that network performance benefits from this strategy, a comparison between random and organized arrangements of segments was conducted for the proposed model, SzNet-5, using the midline ROI. The 10-fold cross-validation metrics are presented in **Table 2**, with the randomly aligned ROI marked with asterisks at the bottom of the table. With the organized alignment, the accuracy, AUC-ROC, and recall metrics were improved. The most notorious difference is in the recall value, which is higher when the signal segments are not randomly stacked. The increase in this metric means that the ratio of diagnosed patients incorrectly identified as healthy subjects decreased, which would be a positive result in clinical diagnosis. This may suggest that the spatial dynamics of brain activity over time may be relevant in characterizing auditory processing in SZ.

4.3. Relevance of SzNet

SZ classification based on classical machine learning methods applied to EEG data recorded during auditory tasks has been performed using features extracted from ERP components. Besides requiring expertise, there is a great variability in the extracted features. By contrast, the use of deep learning allowed the SzNet model to automatically learn patterns from EEG single-trials. Despite the heterogeneity of the disorder, the model managed to distinguish whether the signal belongs to SZ or HC considering a short time window focused on early auditory processing stages. Although it may simultaneously be considered a limitation, the fact that the SZ sample is not subdivided according to the different disease subgroups or stages (e.g., first-episode or chronic patients), mimics the heterogeneity that will always exist in a real clinical situation. Another advantage of our approach is the reduced number of trials and the task used for EEG data acquisition. The elicitation of some ERP components such as the MMN, whose features are recurrently used for classification purposes, requires a large number of stimuli and, consequently, is time-consuming. On the contrary, the passive listening task used in our study is simple and manageable in a clinical environment, where diagnosis is expected to be rapidly made. Besides binary classification, another aim of the current study was to understand if auditory processing impairments may contribute to the characterization of SZ, in particular considering alterations in ERP components that have been proposed as SZ biomarkers. Only the study conducted by Aristizabal et al. (28) documented the application of deep learning methods to auditory EEG signals. Their aim was to identify subjects at risk of developing SZ using the time course of EEG signals in response to auditory stimuli. With a shallower architecture combining convolutional and recurrent networks and with less learnable parameters, an accuracy of 72.54% was achieved. The problem addressed as well as the database used differ from ours, therefore the studies are not directly comparable. Still, it should be noted that Ahmedt-Aristizabal and collaborators used the same 5 electrodes (Fz, FCz, Cz, CPz, Pz) for which our ablative study showed an improved performance. The SzNet results indicate that changes in the auditory processing are key features in SZ diagnosis. This shows the need to look at sensory changes that are often neglected in clinical assessment, and supports the addition of a new domain to the Research Domain Criteria (RDoC) framework, focused on sensory impairments in psychiatric disorders (55).

4.4. Machine Learning vs. Deep Learning

The application of classical machine learning algorithms allowed us to obtain a base-model to compare with the proposed deep learning model.

4.4.1. Features Selection

The selection of relevant features plays an essential role in machine learning classification. The auditory N100 and P200 components shed light on the sensory processing of sounds, and their latency and amplitude are affected by the level of

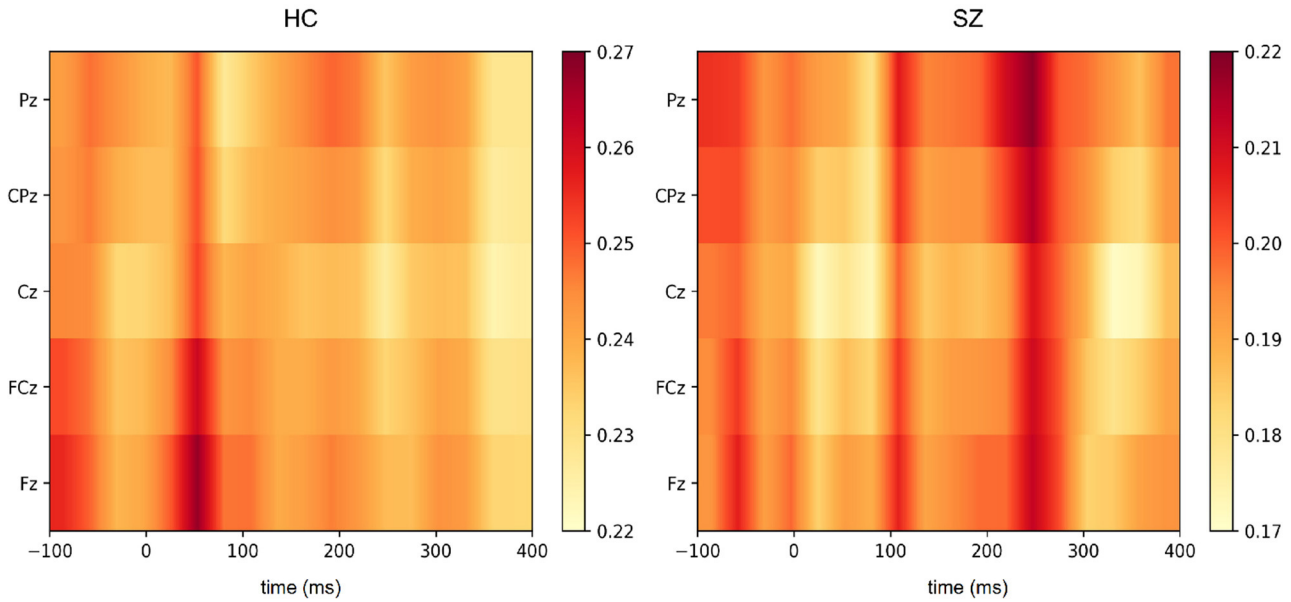

FIGURE 8 | Heatmaps (yellow to red colormap) obtained using Grad-CAM for the segments most likely to belong to HC and SZ subjects.

subject's arousal, alertness, and attention (56). Abnormalities in these components have been consistently reported in SZ patients, which include reduced amplitude of the N100 as well as reduced amplitude and shorter peak latencies of the P200 (57). Moreover, both auditory ERP components have been used to examine sensory and information processing impairments in SZ (58). In light of this, our focus turned to these components, in particular their amplitude and latency. Time windows for the extraction of the N100 and P200 mean amplitudes were based on visual inspection of the grand average waveforms and on previous studies (6). Since the N100 and P200 peak amplitudes are topographically distributed over frontocentral and central regions, as seen in **Figure 2**, the FCz and Cz signals were considered for the analysis of both peak amplitude and latency.

While auditory processing abnormalities in SZ have been investigated by means of ERP analyses, our deep learning approach extracts features from the signal that may be directly correlated to those components and that are relevant to the discrimination of SZ and healthy subjects. Therefore, the interpretation of the feature extraction in the implemented SzNet model provides more information about their relationship with specific ERP components. The Grad-CAM (Gradient-weighted Class Activation Mapping) algorithm was used to produce a saliency map of the critical regions in the input EEG segments for the classification (59). The importance of the features extracted by the SzNet model (considering the last convolutional layer features) is represented by heatmaps obtained by Grad-CAM implementation in **Figure 8**. The color scale shows the variation of features relevance, with dark tones representing highly discriminative features in the signal morphology.

For this purpose, we considered the EEG segments correctly identified with a greater degree of certainty (probabilities above 0.80). An averaged heatmap of the selected samples was computed for SZ and HC (**Figure 8**). An average of the EEG segments was also computed to inform on the features' location and correspondence in the spatio-temporal images.

Figure 9 illustrates HC and SZ heatmaps over Cz and averaged temporal segments (see **Supplementary Material** for the other electrodes representations). Group differences around 250 ms post-stimulus onset appear to have been the most critical temporal feature for the classification of SZ segments. Interestingly, the transition of more pronounced negative to positive deflections around 110 ms post-stimulus onset, i.e., from the N100 to the P200 deflection, may have been pivotal for SZ identification. This transition is more abrupt in HC as a result of increased N100 and P200 amplitudes. Both salient features seem to have a more significant effect across the five electrodes (**Figure 8**). The feature extracted from HC segments seem to be more prominent (higher heatmap values) for the classification by inspecting both heatmaps. It should be noted that the most important features to identify HC are located around 50 ms post-stimulus onset. Subtle differences in this time interval may correspond to the transition from a P50-like deflection, whose latency seems to vary between groups, to a N100 deflection. The transitions from P50 to N100, N100 to P200, and the P200 end seem to have relevance for the discrimination of the two groups. In order to interpret these findings, we also extracted the slopes in the time intervals corresponding to those three transitions as input features for machine learning models.

RF can provide a measure of the importance of each feature, according to its contribution to the overall classification performance. Benefiting from the increased system interpretability, the features' weights may provide important information on the critical EEG electrodes and

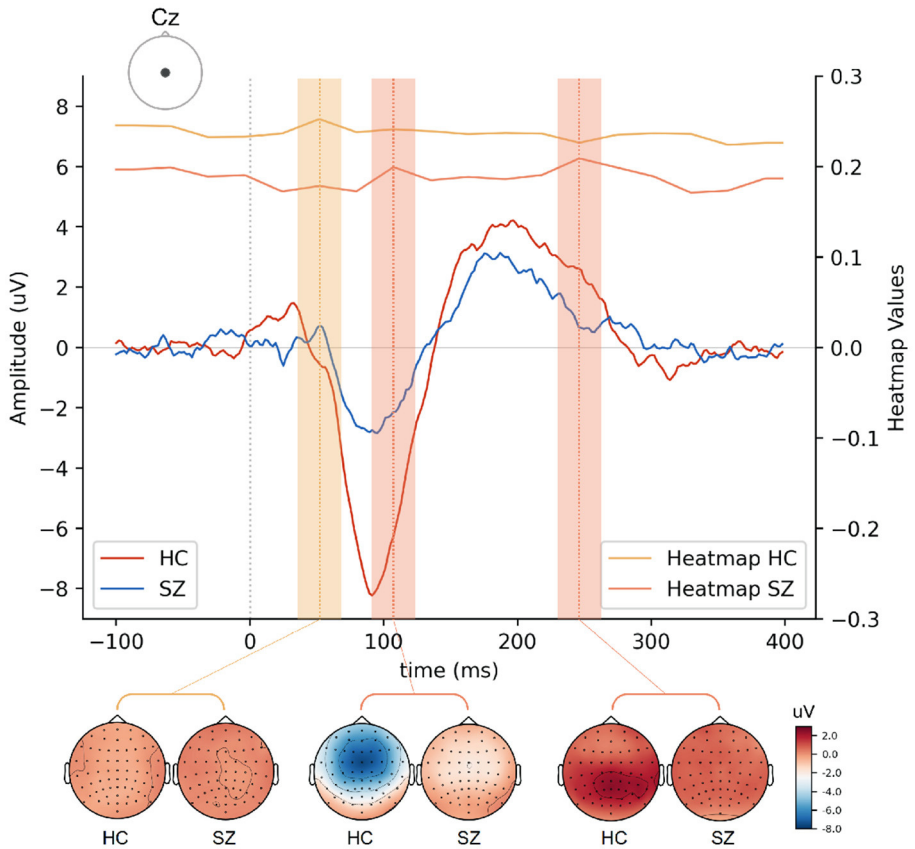

FIGURE 9 | Grad-CAM heatmaps cross-section and averaged EEG signals over Cz electrode drawn for HC and SZ groups. The time intervals associated with the most relevant features are shaded with the color corresponding to the heatmap of each group. Topographical distribution maps of EEG signal amplitudes at those time intervals are also presented for each group.

features for discriminating SZ. **Figure 10** shows the weight of each feature for the RF result considering 33 features. N100 features from frontal, fronto-central, and central scalp regions were the most important features for classification, which is consistent with the literature (14). However, the slopes extracted from the transitions between ERP components appear to have been significant. This result suggests that the temporal dynamics of early auditory processing is altered in SZ. Hence, all these features were considered to obtain the best performance as they seem to have an impact on the differentiation of subjects with SZ.

4.4.2. Models Performance

Table 3 presents the RF models' performance using ERP features for SZ classification. The inclusion of amplitude and latency of the N100 and P200 peaks over FCz and Cz electrodes (RF-18) improved the classification achieved by the RF, which only include the N100 and P200 mean amplitudes over all the 5 midline electrodes (RF-10). The best result was obtained when adding all 33 features (RF-33), which included the slopes in the three transition time intervals between ERP components suggested by the GRAD-CAM implementation. The best model distinguished HC and SZ subjects with an accuracy of 73%. Adding the slopes values as features increased the specificity, which suggests that these features may have a more significant influence on the identification of HC subjects.

The performance of the deep learning method surpasses that of the traditional machine learning models, and demonstrates the potential of the model we propose here for SZ classification. Unlike standard techniques in which features are extracted manually and provided to the model for classification, the deep learning model performs both feature extraction and classification. CNNs are able to detect highly specific features of the training dataset under the constraints of the specific prediction, such as the data labels (38). The end-to-end training forces feature extraction by minimizing the loss for SZ classification. Through this optimization technique, CNNs provide improved models and, thus, more accurate results (38).

4.5. Ensemble Learning

The result of the ensemble of SzNet models' predictions are presented in **Table 3**. An improved performance is observed using 5 models, surpassing the single SzNet result (see **Supplementary Material**). As expected, the voting ensemble offered a lower variance in predictions made over base learners, which improved the generalization ability.

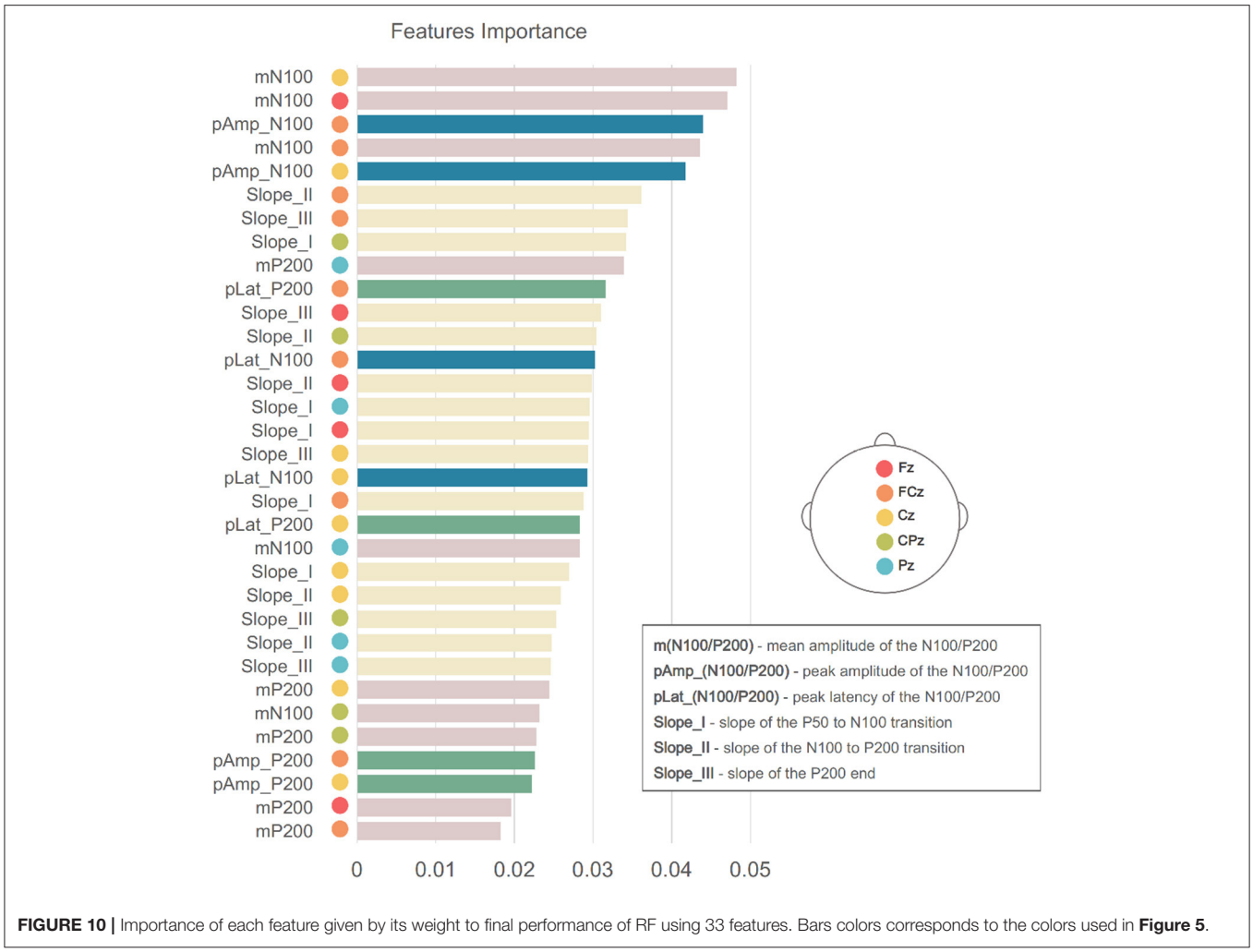

FIGURE 10 | Importance of each feature given by its weight to final performance of RF using 33 features. Bars colors corresponds to the colors used in **Figure 5**.

TABLE 3 | Results of the classification performed by the RF, the proposed deep learning model, and the ensemble learning method.

Model	Features	Accuracy	Precision	Recall	Specificity	AUC-ROC
RF	10	0.69 ± 0.10	0.70 ± 0.15	0.70 ± 0.17	0.69 ± 0.14	0.70 ± 0.10
RF	18	0.70 ± 0.11	0.71 ± 0.14	0.70 ± 0.17	0.71 ± 0.15	0.70 ± 0.11
RF	33	0.73 ± 0.13	0.73 ± 0.15	0.70 ± 0.17	0.76 ± 0.13	0.73 ± 0.13
Proposed		0.78 ± 0.08	0.82 ± 0.13	0.77 ± 0.15	0.79 ± 0.17	0.78 ± 0.08
Ensemble		0.80 ± 0.08	0.82 ± 0.14	0.82 ± 0.14	0.78 ± 0.18	0.80 ± 0.08

4.6. Limitations and Future Directions

The single-trial EEG recordings contain task-related activity. However, this activity is overlaid with task-unrelated brain processes, which results in a low signal-to-noise ratio (SNR). Variations in SNR across trials and subjects, which may also arise from differences in EEG data acquisition parameters, may affect signal quality. Moreover, fluctuations in the latency and magnitude of the EEG responses to stimuli, combined with the high dimensionality of EEG signals, increase both intra- and intersubject variability. The best performances from raw EEG data may be achieved with larger training data sets, which also prevents overfitting: more subjects and more trials per subject to overcome inter and intrasubject variability, respectively. Data augmentation techniques may increase the diversity of the data available for training the model, and thus prevent overfitting. Notwithstanding, we note that our attempts at data augmentation did not lead to improved SzNet model performance.

As mentioned before, SZ subgroups or stages (e.g., first episode vs. chronic) were not considered in this study. Future studies should address whether SzNet performance is affected by illness stage and symptom severity. However, some requirements should be taken into account: adaptation

of the SzNet model for multi-class classification; inclusion of a larger amount of data from each SZ subgroup. Following the adaptation of the model to multiple classes, an important approach might be to include data from subjects at risk of developing SZ or in prodromal stages. This line of development may allow prediction of disease onset and a better understanding of the course of the underlying auditory processing alterations.

SzNet can provide a baseline model for future developments and analyses. A well-characterized public SZ EEG database is highly recommended for the direct comparison and objective evaluation of the performances of different algorithms.

5. CONCLUSION

This paper presents the application of a deep convolutional neural network to the analysis of EEG signals recorded in a passive listening task in healthy and SZ adults. Using only 5 midline electrodes (Fz, FCz, Cz, CPz, and Pz), the proposed model achieved an average accuracy of 78% in the discrimination between SZ and HC subjects. By ensembling predictions of 5 fits of this model, trained with different weights initialization, SZ classification achieved an accuracy of 80%. The deep network allowed the automatic learning of patterns from the time course and spatial distribution of EEG single-trials, capable of detecting alterations in brain indices of auditory processing in SZ, despite the great heterogeneity of the disorder. SzNet provides a base model for future developments in SZ research and, specifically, (differential) diagnosis and prediction.

DATA AVAILABILITY STATEMENT

A publicly available dataset was used in data analysis. *Dataset B* can be found here: https://www.kaggle.com/broach/button-tone-sz.

ETHICS STATEMENT

The studies involving human participants were reviewed and approved by University of California at San Francisco's Human Research Protection Program (HRPP), USA, and by the Ethics Committees of Faculdade de Psicologia da Universidade de Lisboa, Universidade do Minho, and Hospital de Santa Maria, Portugal. The patients/participants provided their written informed consent to participate in this study.

AUTHOR CONTRIBUTIONS

CB, AP, and CS: conception and design of study. BR, JF, and AP: acquisition of data. CB: implementation of machine and deep learning models, analysis and interpretation of data, and drafting the manuscript. CS, AP, BR, and JF: revising the manuscript critically for important intellectual content. All authors contributed to the article and approved the submitted version.

FUNDING

This research work was supported by Grant SFRH/BD/111083/2015, funded by Fundação para a Ciência e Tecnologia (FCT) under the Programa Operacional Capital Humano (POCH) co-funded by Portugal 2020 and European Social Fund, by Grant PTDC/MHC-PCN/0101/2014 funded by FCT, and by project UID/EEA/04436/2019 funded by FCT through national funds (PID-DAC). It was also funded by an NIMH grant (R01-S MH058262) and a Department of Veterans Affairs (USA) Senior Research Career Award to JF.

ACKNOWLEDGMENTS

The authors would like to thank Ana P. Lopes, Adriano Pinto, and Sérgio Pereira for sharing knowledge, for their precious suggestions and pertinent discussions, which helped to improve the quality of this work.

SUPPLEMENTARY MATERIAL

The Supplementary Material for this article can be found online at: https://www.frontiersin.org/articles/10.3389/fpsyt.2021.813460/full#supplementary-material

REFERENCES

1. Kahn RS. On the origins of schizophrenia. *Am J Psychiatry*. (2020) 177:291–7. doi: 10.1176/appi.ajp.2020.20020147
2. Green MF, Horan WP, Lee J. Social cognition in schizophrenia. *Nat Rev Neurosci*. (2015) 16:620–31. doi: 10.1038/nrn4005
3. Waters F, Fernyhough C. Hallucinations: a systematic review of points of similarity and difference across diagnostic classes. *Schizophren Bull*. (2016) 11;43:32–43. doi: 10.1093/schbul/sbw132
4. Javitt DC, Sweet RA. Auditory dysfunction in schizophrenia: integrating clinical and basic features. *Nat Rev Neurosci*. (2015) 16:535. doi: 10.1038/nrn4002
5. McKay CM, Headlam DM, Copolov DL. Central auditory processing in patients with auditory hallucinations. *Am J Psychiatry*. (2000) 157:759–66. doi: 10.1176/appi.ajp.157.5.759
6. Luck SJ. Event-related potentials. *APA Handb Res Methods Psychol*. (2012) 1:523–46. doi: 10.1037/13619-028
7. Bodatsch M, Brockhaus-Dumke A, Klosterkötter J, Ruhrmann S. Forecasting psychosis by event-related potentials-systematic review and specific meta-analysis. *Biol Psychiatry*. (2015) 77:951–8. doi: 10.1016/j.biopsych.2014.09.025
8. Light GA, Swerdlow NR, Thomas ML, Calkins ME, Green MF, Greenwood TA, et al. Validation of mismatch negativity and P3a for use in multi-site studies of schizophrenia: characterization of demographic, clinical, cognitive, and functional correlates in COGS-2. *Schizophren Res*. (2015) 163:63–72. doi: 10.1016/j.schres.2014.09.042
9. Javitt DC, Spencer KM, Thaker GK, Winterer G, Hajós M. Neurophysiological biomarkers for drug development in schizophrenia. *Nat Rev Drug Discov*. (2008) 7:68. doi: 10.1038/nrd2463
10. Edgar J, Huang M, Weisend M, Sherwood A, Miller G, Adler L, et al. Interpreting abnormality: an EEG and MEG study of P50 and

the auditory paired-stimulus paradigm. *Biol Psychol*. (2003) 65:1–20. doi: 10.1016/S0301-0511(03)00094-2
11. Hamilton HK, Williams TJ, Ventura J, Jasperse LJ, Owens EM, Miller GA, et al. Clinical and cognitive significance of auditory sensory processing deficits in schizophrenia. *Am J Psychiatry*. (2018) 175:275–83. doi: 10.1176/appi.ajp.2017.16111203
12. Shen CL, Chou TL, Lai WS, Hsieh MH, Liu CC, Liu CM, et al. P50, N100, and P200 auditory sensory gating deficits in schizophrenia patients. *Front Psychiatry*. (2020) 11:868. doi: 10.3389/fpsyt.2020.00868
13. Freedman R, Olsen-Dufour AM, Olincy A, the Consortium on the Genetics of Schizophrenia. P50 inhibitory sensory gating in schizophrenia: analysis of recent studies. *Schizophren Res*. (2020) 218:93–8. doi: 10.1016/j.schres.2020.02.003
14. Rosburg T, Boutros NN, Ford JM. Reduced auditory evoked potential component N100 in schizophrenia–A critical review. *Psychiatry Res*. (2008) 161:259–74. doi: 10.1016/j.psychres.2008.03.017
15. Van Lutterveld R, Sommer IE, Ford JM. The neurophysiology of auditory hallucinations-a historical and contemporary review. *Front Psychiatry*. (2011) 2:28. doi: 10.3389/fpsyt.2011.00028
16. Bzdok D, Meyer-Lindenberg A. Machine learning for precision psychiatry: opportunities and challenges. *Biol Psychiatry Cogn Neurosci Neuroimaging*. (2018) 3:223–30. doi: 10.1016/j.bpsc.2017.11.007
17. Salama ES, El-Khoribi RA, Shoman ME, Shalaby MAW. EEG-based emotion recognition using 3D convolutional neural networks. *Int J Adv Comput Sci Appl*. (2018) 9:329–37. doi: 10.14569/IJACSA.2018.090843
18. Fawaz HI, Forestier G, Weber J, Idoumghar L, Muller PA. Deep learning for time series classification: a review. *Data Mining Knowledge Discov*. (2019) 33:917–63. doi: 10.1007/s10618-019-00619-1
19. Schirrmeister RT, Springenberg JT, Fiederer LDJ, Glasstetter M, Eggensperger K, Tangermann M, et al. Deep learning with convolutional neural networks for EEG decoding and visualization. *Hum Brain Mapp*. (2017) 38:5391–420. doi: 10.1002/hbm.23730
20. Taylor JA, Matthews N, Michie PT, Rosa MJ, Garrido MI. Auditory prediction errors as individual biomarkers of schizophrenia. *Neuroimage Clin*. (2017) 15:264–73. doi: 10.1016/j.nicl.2017.04.027
21. Boostani R, Sabeti M. Optimising brain map for the diagnosis of schizophrenia. *Int J Biomed Eng Technol*. (2018) 28:105–19. doi: 10.1504/IJBET.2018.094728
22. Hsieh TH, Wu KY, Liang SF. Identification of schizophrenic patients and healthy controls based on musical perception using AEP analysis. *Int J Clin Skills*. (2018) 8:1419–32. doi: 10.4172/Neuropsychiatry.1000473
23. Chu L, Qiu R, Liu H, Ling Z, Zhang T, Wang J. Individual recognition in schizophrenia using deep learning methods with random forest and voting classifiers: Insights from resting state EEG streams. *arXiv [Preprint]. arXiv:170703467*. (2017).
24. Phang CR, Ting CM, Noman F, Ombao H. Classification of EEG-based brain connectivity networks in schizophrenia using a multi-domain connectome convolutional neural network. *arXiv [Preprint]. arXiv:190308858*. (2019). doi: 10.1109/NER.2019.8717087
25. Naira CAT, Alamo CJLD. Classification of people who suffer schizophrenia and healthy people by EEG signals using deep learning. *Int J Adv Comput Sci Appl*. (2019) 10. doi: 10.14569/IJACSA.2019.0101067
26. Oh SL, Vicnesh J, Ciaccio EJ, Yuvaraj R, Acharya UR. Deep convolutional neural network model for automated diagnosis of schizophrenia using EEG signals. *Appl Sci*. (2019) 9:2870. doi: 10.3390/app9142870
27. Calhas D, Romero E, Henriques R. On the use of pairwise distance learning for brain signal classification with limited observations. *Artif Intell Med*. (2020) 2020:101852. doi: 10.1016/j.artmed.2020.101852
28. Aristizabal DA, Fernando T, Denman S, Robinson JE, Sridharan S, Johnston PJ, et al. Identification of children at risk of schizophrenia via deep learning and EEG responses. *IEEE J Biomed Health Inform*. (2020) 25:69–76. doi: 10.1109/JBHI.2020.2984238
29. Foxe JJ, Yeap S, Snyder AC, Kelly SP, Thakore JH, Molholm S. The N1 auditory evoked potential component as an endophenotype for schizophrenia: high-density electrical mapping in clinically unaffected first-degree relatives, first-episode, and chronic schizophrenia patients. *Eur Arch Psychiatry Clin Neurosci*. (2011) 261:331–9. doi: 10.1007/s00406-010-0176-0
30. Barros C, Silva CA, Pinheiro AP. Advanced EEG-based learning approaches to predict schizophrenia: promises and pitfalls. *Artif Intell Med*. (2021) 2021:102039. doi: 10.1016/j.artmed.2021.102039
31. Hyde M. The N1 response and its applications. *Audiol Neurotol*. (1997) 2:281–307. doi: 10.1159/000259253
32. Ferreira-Santos F, Silveira C, Almeida P, Palha A, Barbosa F, Marques-Teixeira J. The auditory P200 is both increased and reduced in schizophrenia? A meta-analytic dissociation of the effect for standard and target stimuli in the oddball task. *Clin Neurophysiol*. (2012) 123:1300–8. doi: 10.1016/j.clinph.2011.11.036
33. Lijffijt M, Lane SD, Meier SL, Boutros NN, Burroughs S, Steinberg JL, et al. P50, N100, and P200 sensory gating: relationships with behavioral inhibition, attention, and working memory. *Psychophysiology*. (2009) 46:1059–68. doi: 10.1111/j.1469-8986.2009.00845.x
34. Spencer KM. Averaging, detection, and classification of single-trial ERPs. In: Todd C. Handy, editor. *Event Related Potentials: A Methods Handbook*. Cambridge, MA: MIT Press (2005). p. 209.
35. LeCun Y, Bengio Y, Hinton G. Deep learning. *Nature*. (2015) 521:436. doi: 10.1038/nature14539
36. Ioffe S, Szegedy C. Batch normalization: Accelerating deep network training by reducing internal covariate shift. In: Bach F, Blei D, editors. *Proceedings of the 32nd International Conference on Machine Learning*. Lille: PMLR (2015). p. 448–56. Available online at: http://proceedings.mlr.press/v37/ioffe15.pdf
37. Breiman L. Random forests. *Mach Learn*. (2001) 45:5–32. doi: 10.1023/A:1010933404324
38. Goodfellow I, Bengio Y, Courville A. *Deep Learning*. Cambridge, MA: MIT Press (2016).
39. Bian Y, Chen H. When does diversity help generalization in classification ensembles? *IEEE Trans Cybernet*. (2021). 1–17. doi: 10.1109/TCYB.2021.3053165
40. Hastie T, Tibshirani R, Friedman J. *The Elements of Statistical Learning: Data Mining, Inference, and Prediction*. New York, NY: Springer Science & Business Media (2009). doi: 10.1007/978-0-387-84858-7
41. Roach B. *EEG Data From Basic Sensory Task in Schizophrenia: Button Press and Auditory Tone Event Related Potentials from 81 Human Subjects*. (2017). Available online at: https://www.kaggle.com/broach/button-tone-sz
42. Ford JM, Palzes VA, Roach BJ, Mathalon DH. Did I do that? Abnormal predictive processes in schizophrenia when button pressing to deliver a tone. *Schizophren Bull*. (2013) 40:804–12. doi: 10.1093/schbul/sbt072
43. Pinheiro AP, Schwartze M, Amorim M, Coentre R, Levy P, Kotz SA. Changes in motor preparation affect the sensory consequences of voice production in voice hearers. *Neuropsychologia*. (2020) 146:107531. doi: 10.1016/j.neuropsychologia.2020.107531
44. Delorme A, Makeig S. EEGLAB: an open source toolbox for analysis of single-trial EEG dynamics including independent component analysis. *J Neurosci Methods*. (2004) 134:9–21. doi: 10.1016/j.jneumeth.2003.10.009
45. Nolan H, Whelan R, Reilly RB. FASTER: fully automated statistical thresholding for EEG artifact rejection. *J Neuroscience Methods*. (2010) 192:152–62. doi: 10.1016/j.jneumeth.2010.07.015
46. Glorot X, Bengio Y. Understanding the difficulty of training deep feedforward neural networks. In: *Proceedings of the Thirteenth International Conference on Artificial Intelligence and Statistics*. (2010). p. 249–56.
47. Murphy KP. *Machine Learning: a Probabilistic Perspective*. Cambridge, MA: MIT Press (2012).
48. Fort S, Jastrzebski S. Large scale structure of neural network loss landscapes. *arXiv [Preprint]. arXiv:190604724*. (2019).
49. Pedregosa F, Varoquaux G, Gramfort A, Michel V, Thirion B, Grisel O, et al. Scikit-learn: machine learning in Python. *J Mach Learn Res*. (2011) 12:2825–30. doi: 10.5555/1953048.2078195
50. Harris CR, Millman KJ, van der Walt SJ, Gommers R, Virtanen P, Cournapeau D, et al. Array programming with NumPy. *Nature*. (2020) 585:357–62. doi: 10.1038/s41586-020-2649-2

51. Le H, Borji A. What are the receptive, effective receptive, and projective fields of neurons in convolutional neural networks? *arXiv [Preprint]. arXiv:170507049*. (2017).
52. Roach BJ, Mathalon DH. Event-related EEG time-frequency analysis: an overview of measures and an analysis of early gamma band phase locking in schizophrenia. *Schizophren Bull*. (2008) 34:907–26. doi: 10.1093/schbul/sbn093
53. Leicht G, Kirsch V, Giegling I, Karch S, Hantschk I, Möller HJ, et al. Reduced early auditory evoked gamma-band response in patients with schizophrenia. *Biol Psychiatry*. (2010) 67:224–31. doi: 10.1016/j.biopsych.2009.07.033
54. Force RB, Venables NC, Sponheim SR. An auditory processing abnormality specific to liability for schizophrenia. *Schizophren Res*. (2008) 103:298–310. doi: 10.1016/j.schres.2008.04.038
55. Harrison LA, Kats A, Williams ME, Aziz-Zadeh L. The importance of sensory processing in mental health: a proposed addition to the Research Domain Criteria (RDoC) and suggestions for RDoC 2.0. *Front Psychol*. (2019) 10:103. doi: 10.3389/fpsyg.2019.00103
56. Lightfoot G. Summary of the N1-P2 cortical auditory evoked potential to estimate the auditory threshold in adults. In: *Seminars in Hearing*. New York, NY: Thieme Medical Publishers (2016). p. 1. doi: 10.1055/s-0035-1570334
57. Salisbury DF, Collins K, McCarley RW. Reductions in the N1 and P2 auditory event-related potentials in first-hospitalized and chronic schizophrenia. *Schizophren Bull*. (2010) 36:991–1000. doi: 10.1093/schbul/sbp003
58. Mazer P, Macedo I, Paiva TO, Ferreira-Santos F, Pasion R, Barbosa F, et al. Abnormal habituation of the auditory event-related potential P2 component in patients with schizophrenia. *Front Psychiatry*. (2021) 12:297. doi: 10.3389/fpsyt.2021.630406
59. Selvaraju RR, Cogswell M, Das A, Vedantam R, Parikh D, Batra D. Grad-cam: visual explanations from deep networks via gradient-based localization. In: *Proceedings of the IEEE International Conference on Computer Vision*. (Venice). (2017). p. 618–26. doi: 10.1109/ICCV.2017.74

Conflict of Interest: The authors declare that the research was conducted in the absence of any commercial or financial relationships that could be construed as a potential conflict of interest.

Publisher's Note: All claims expressed in this article are solely those of the authors and do not necessarily represent those of their affiliated organizations, or those of the publisher, the editors and the reviewers. Any product that may be evaluated in this article, or claim that may be made by its manufacturer, is not guaranteed or endorsed by the publisher.

frontiers | Frontiers in Psychiatry

ORIGINAL RESEARCH
published: 05 April 2022
doi: 10.3389/fpsyt.2022.810362

Detection of Schizophrenia Cases From Healthy Controls With Combination of Neurocognitive and Electrophysiological Features

Qing Tian[1,2,3], Ning-Bo Yang[4], Yu Fan[2,3], Fang Dong[3], Qi-Jing Bo[3], Fu-Chun Zhou[3], Ji-Cong Zhang[5], Liang Li[6], Guang-Zhong Yin[2], Chuan-Yue Wang[3,7]* and Ming Fan[1,8]**

[1] Laboratory of Brain Disorders, Collaborative Innovation Center for Brain Disorders, Beijing Institute of Brain Disorders, Capital Medical University, Ministry of Science and Technology, Beijing, China, [2] Suzhou Guangji Hospital, The Affiliated Guangji Hospital of Soochow University, The Institute of Mental Health, Suzhou, China, [3] Beijing Key Laboratory of Mental Disorders, The National Clinical Research Center for Mental Disorders, Beijing Anding Hospital, Beijing Institute for Brain Disorders Center of Schizophrenia, Capital Medical University, Beijing, China, [4] Department of Psychiatry, First Affiliated Hospital of Henan University of Science and Technology, Luoyang, China, [5] Beijing Advanced Innovation Centre for Biomedical Engineering, Beijing Advanced Innovation Center for Big Data-Based Precision Medicine, The School of Biological Science and Medical Engineering, Beihang University, Beijing, China, [6] Department of Psychology, Peking University, Beijing, China, [7] Advanced Innovation Center for Human Brain Protection, Capital Medical University, Beijing, China, [8] Institute of Military Cognition and Brain Sciences, Academy of Military Medical Sciences, Beijing, China*

OPEN ACCESS

Edited by:
Junpeng Zhang, Sichuan University, China

Reviewed by:
Takefumi Ueno, Hizen Psychiatric Center (NHO), Japan
Mary V. Seeman, University of Toronto, Canada

***Correspondence:**
Guang-Zhong Yin
yingzgjyy@163.com
Chuan-Yue Wang
wang_cy@ccmu.edu.cn
Ming Fan
fanmingchina@126.com

Specialty section:
This article was submitted to Neuroimaging and Stimulation, a section of the journal Frontiers in Psychiatry

Received: *06 November 2021*
Accepted: *21 February 2022*
Published: *05 April 2022*

Citation:
Tian Q, Yang N-B, Fan Y, Dong F, Bo Q-J, Zhou F-C, Zhang J-C, Li L, Yin G-Z, Wang C-Y and Fan M (2022) Detection of Schizophrenia Cases From Healthy Controls With Combination of Neurocognitive and Electrophysiological Features. Front. Psychiatry 13:810362. doi: 10.3389/fpsyt.2022.810362

Background: The search for a method that utilizes biomarkers to identify patients with schizophrenia from healthy individuals has occupied researchers for decades. However, no single indicator can be employed to achieve the good in clinical practice. We aim to develop a comprehensive machine learning pipeline based on neurocognitive and electrophysiological combined features for distinguishing schizophrenia patients from healthy people.

Methods: In the present study, 69 patients with schizophrenia and 50 healthy controls participated. Neurocognitive (contains seven specific domains of cognition) and electrophysiological [prepulse inhibition, electroencephalography (EEG) power spectrum, detrended fluctuation analysis, and fractal dimension (FD)] features were collected, all these features were taken together to generate the identification models of schizophrenia by applying logistics, random forest, and extreme gradient boosting algorithm. The classification capabilities of these models were also evaluated.

Results: Both the neurocognitive and electrophysiological feature sets showed a good classification effect with the highest accuracy greater than 85% and AUC greater than 90%. Specifically, the performances of the combined neurocognitive and electrophysiological feature sets achieved the highest accuracy of 93.28% and AUC of 97.91%. The extreme gradient boosting algorithm as a whole presented more stably and precisely in classification efficiency.

Conclusion: The highest classification accuracy of 93.28% by combination of neurocognitive and electrophysiological features shows that both measurements are appropriate indicators to be used in discriminating schizophrenia patients and healthy individuals. Also, among three algorithms, extreme gradient boosting had better classified performances than logistics and random forest algorithms.

Keywords: schizophrenia, neurocognition, electrophysiology, electroencephalography, prepulse inhibition (PPI), biomarker, machine learning, classification

INTRODUCTION

Schizophrenia is one of the most severe mental disorders, affecting 20 million people worldwide (1). Extensive studies show that cognitive deficits are one of the core features of significant neurological dysfunction associated with schizophrenia and are typically associated with a poor prognosis (2, 3). In addition, cognitive deficits are no less predictive of schizophrenia and its level than positive and negative symptoms, if not better (4, 5). Several specific areas of cognition can be assessed by a neurocognitive measure battery, which usually involves the speed of processing, attention, working memory, and verbal learning (6).

In addition, pre-pulse inhibition (PPI) is considered an indicator that reflects information processing deficits in patients with schizophrenia, which is based on electrophysiological measures (7, 8). Most previous studies show that PPI is reduced in schizophrenic patients and their unaffected first-degree relatives (9). However, in comparison to neurocognitive measurements, PPI presents only a moderate effect size (Cohen's $d < 0.8$) (10). Yang et al. (11) reports a novel PPI paradigm involving attentional enhancement effects of PPI while providing a more significant effect size (Cohen's $d > 1.2$). Additionally, electroencephalography (EEG) is a non-invasive electrophysiological measure widely applied to assess the neural response of the brain to external stimulation. The EEG power spectrum describes the distribution of power into each frequency band and is commonly used in schizophrenia research (12, 13). Extensive research shows that patients with chronic schizophrenia have abnormal EEG frequencies at rest compared with healthy individuals (12, 14–16). Meanwhile, more advanced EEG analytical methods have been studied in recent years, such as detrended fluctuation analysis (DFA), a fractal analytical method to quantify long-range temporal correlations (LRTCs) in power-law form. A previous study reports strongly reduced LRTCs in both alpha and beta frequency bands in patients with schizophrenia (17).

The current gold standard for schizophrenia diagnosis is built on the International Classification of Diseases, 11th Revision (ICD-11) or the Diagnostic and Statistical Manual of Mental Disorders, 5th Edition (DSM-5). These diagnostic methods rely on descriptive psychopathology, which, to some extent, reflects the subjective judgment of psychiatrists. Therefore, there is an urgent need for clinicians to have an objective measure of characteristics. Nevertheless, frustratingly, due to the heterogeneity of the etiology and clinical variability, excellent biomarkers for the diagnosis of schizophrenia are still lacking. In fact, there is no single indicator that can be adopted in clinical practice. In recent years, the role of machine learning in auxiliary diagnosis has received increasing attention throughout the field of schizophrenia research. In translational medicine and clinical practices, these methods are widely involved in exploration for presymptomatic screening, prognostic prediction, and supporting treatment decisions (18). However, to date, there is a paucity of literature about building machine learning models on neurocognitive and electrophysiological biomarkers.

This study developed a comprehensive machine learning pipeline based on neurocognitive (contains seven specific areas of cognition) and electrophysiological [PPI, EEG power spectrum, detrended fluctuation analysis, and fractal dimension (FD)] features by using logistics, random forest, and extreme gradient boosting (XGBoost) algorithms and evaluated their classification capabilities separately.

MATERIALS AND METHODS

Experimental Subjects

This study enrolled 69 patients with schizophrenia and 50 healthy controls. The diagnosis was established by the researchers from interviews using the Structured Clinical Interview for DSM-IV (SCID) and supplemented by clinical notes. All subjects were right-handed, and their audiometric assessments (pure tone audiometry, 1,000 Hz) were normal. The inclusion criteria for the enrollment of patients with schizophrenia are as follows: 1) all clinically stable subjects had no history of neurological disorders or head trauma, 2) no history of electroconvulsive therapy within the past 6 months, and 3) no history of alcohol/drug dependence or abuse (except tobacco). Patients were excluded because of unstable medical conditions or IQ below 70. During this study, all patients received antipsychotic treatments as usual. The healthy control group (CON) consisted of subjects matched to the schizophrenia group (SCZ) in terms of gender, age, years of education, and smoking history. The exclusion criteria for the CON include substance abuse, suicidal risk, major head trauma, and neuropsychiatric disorders. Before signing the informed consent, each subject received a detailed description of the aims and procedures for participation in the study. The independent ethics committee of Beijing Anding Hospital approved the study. The psychopathological status of the patients was also assessed by the Positive and Negative Syndrome Scale (PANSS). The demographic and clinical characteristics of SCZ and CON are summarized in **Table 1**.

Neurocognitive Assessments

The neurocognitive function of the subjects was assessed using the Repeatable Battery for the Assessment of Neuropsychological Status (RBANS; Chinese version) (19). The RBANS assesses five separate cognitive domains: immediate memory (IMM), delayed memory (DEM), visuospatial and constructional (VC), attention (ATT), and language functioning (LAN). Besides RBANS, the Stroop Color-Word Test (Chinese version) (20) was also administered. Each subject was asked to complete two interference tasks, and color (INT-C) and word (INT-W) interference times were recorded. In this part of the experiment, five RBANS features (IMM, DEM, VC, ATT, LAN) and two Stroop features (INT-C, INT-W) were extracted.

Electrophysiological Assessments

Prepulse Inhibition Measures

Subjects were comfortably seated in a reclining chair with their arms fully relaxed in a natural position. Acoustic startle measured through electromyogram (EMG) signal was recorded from the right orbiculate oculi muscle. Electrode impedances were maintained at <5 kΩ. The eye-blink component of auditory startle reflexes was quantified by the human EMG startle reflexes system (EMG XEYE human startle reflex, Tian Ming Hong Yuan Instruments Company, Beijing, China). In addition, the EMG was bandpass filtered to 100–1,000 Hz and amplified 10,000 times. Acoustic startle stimuli were presented binaurally through two headphones. Acoustic signals were characterized by a sound-level meter (AUDit and System 824, Larson Davis, United States).

PPI was tested according to the same paradigm used in previous research (11, 21). In short, the precedence effect was utilized to generate two different perceived spatial relations between the prepulse and background sound: perceptual separation and perceptual colocation. A more detailed description of the PPI paradigm and related theories are available in previous studies (11, 21). Finally, two features were extracted from this test (perceived spatial colocation PPI, PSC-PPI; perceived spatial separation PPI, PSS-PPI).

Electroencephalography Recording and Processing

Electroencephalography Data Preprocessing

Subjects were comfortably seated in a reclining chair. Then, they closed their eyes and remained relaxed and quiet for 5 min. Continuous EEG was digitized at 1,000 Hz using the EGI EEG system (EGI, Electrical Geodesics, Inc., America) with 128-electrode HydroCelnet referenced to the vertex (Cz). Off-line preprocessing of EEG data was conducted by using EEGLAB (v2019.1) (22) and FieldTrip (23) toolboxes in MATLAB (MATLAB Release 2017b, MathWorks, Inc.). EEG raw data was first resampled to a 500-Hz sampling rate and bandpass filtered to 0.5–45 Hz. For each subject, artifact removal was administered using both continuous raw data and independent component analysis (ICA, algorithm: runica) within EEGLAB. ICA components were classified using an EEGLAB plugin *ICLabel* tool (24). Eye movement, blink, heartbeat, muscular activity, or other artifacts were distinguished from the ICA data. The EEG data were then manually inspected to verify artifact removal. The bad electrodes were replaced with interpolated data from the remaining electrodes. Finally, all electrodes were rereferenced to an average reference.

TABLE 1 | Demographic and clinical characteristics of healthy control and schizophrenia group.

Factor	CON (N = 50)	SCZ (n = 69)	χ^2/t	P
Gender (male/female)	38/12	49/20	0.37	0.545[a]
Age (year)	42.2 ± 8.8	44.8 ± 7.0	−1.80	0.074[b]
Education (years of schooling)	10.9 ± 3.1	10.8 ± 2.5	0.15	0.882[b]
Smoking (yes/no)	24/26	35/34	0.09	0.769[a]
Duration of illness (year)		19.7 ± 8.3		
Age at onset (year)		24.5 ± 6.6		
CPZe (mg/day)		292.7 ± 265.3		
PANSS score		63.3 ± 13.1		
Positive Symptoms		12.8 ± 4.5		
Negative Symptoms		20.0 ± 6.4		
General Psychopathology		30.5 ± 5.6		

Mean ± SD are reported for age, education, duration of illness, age at onset, CPZe, and all PANSS scores.
CON, Health Control Group; SCZ, Schizophrenia Group; CPZe, Chlorpromazine Equivalent Doses; PANSS, Positive and Negative Syndrome Scale.
[a]*Indicates P-value for chi-square test.*
[b]*Indicates P-value for independent sample t-test.*

Power Spectrum Features

The power spectral density (PSD) of each electrode was evaluated using the Fast Fourier Transform (FFT, Welch method, 2s sliding window, 50% overlap, 0.5-Hz frequency step), yielding an EEG spectrum ranging from 0.5 to 45 Hz. The frequency bands were selected as follows: delta (1.0–4.0 Hz), theta (4.0–8.0 Hz), alpha (8.0–14.0 Hz), beta (14.0–30.0 Hz). D, T, A, and B denote delta, theta, alpha, and beta frequency bands, respectively. AL and AR were computed by averaging the power in the alpha band for the left (Fp1, F3, C3, P3, O1, F7, T3, T5) and right hemispheres (Fp2, F4, C4, P4, O2, F8, T4, T6). (D + T)L and (D + T)R were averaged by summing the power of delta and theta in the left and right hemispheres. AFp and AO were calculated by averaging the alpha band power for the Fp channels (Fp1, Fp2) and the O channels (O1, O2). The absolute power (Abs) and relative power (Rel) in each frequency band were computed for each electrode. A/T ratio, A/B ratio, (D + T)/(A + B) ratio, (D + T)/(A + B) ratio, (D + T)L/(D + T)R ratio, AFp/AO ratio were calculated for Abs as well as Rel. In PSD, 20 features were extracted. For detailed features information, see **Table 2**.

Detrended Fluctuation Analysis Features

Detrended fluctuation analysis is an analytical method based on scale-free theory for estimating long-range temporal correlations (LRTCs) in power-law form (25). That is, if a time series data has a non-random temporal structure with slowly decaying autocorrelations, DFA can quantify the rate of decay of these correlations as indexed by the DFA power-law exponent. Some evidence suggests that the DFA reflects brain maturation and may prove useful as a potential biomarker for the pathophysiology of neurodevelopmental disorders (26). DFA calculation was

TABLE 2 | Statistical comparison of neurocognitive and electrophysiological features.

Features	CON (N = 50)	SCZ (n = 69)	t	P [a]
IMM ***	89.24 ± 19.73	54.70 ± 15.30	10.75	0.000
VC **	89.92 ± 20.65	78.81 ± 15.47	3.36	0.003
LAN ***	91.88 ± 16.30	77.68 ± 12.51	5.38	0.000
ATT ***	104.34 ± 15.94	91.09 ± 12.26	5.13	0.000
DEM ***	90.66 ± 19.16	64.39 ± 18.32	7.57	0.000
INT-C **	4.21 ± 3.88	7.39 ± 5.95	−3.30	0.003
INT-W **	16.78 ± 9.27	24.69 ± 12.85	−3.71	0.001
PSC-PPI (%) **	31.70 ± 26.15	11.26 ± 29.07	3.95	0.001
PSS-PPI (%) ***	50.65 ± 25.92	14.70 ± 25.30	7.57	0.000
Abs-D (μV^2)	10.43 ± 12.57	11.01 ± 13.61	−0.23	0.824
Abs-T (μV^2) *	3.30 ± 3.60	6.67 ± 7.96	−2.79	0.014
Abs-A (μV^2)	7.19 ± 8.18	9.78 ± 10.56	−1.45	0.264
Abs-B (μV^2)	0.80 ± 0.73	0.99 ± 1.07	−1.09	0.376
Abs-A/T	2.79 ± 3.25	2.25 ± 2.41	1.03	0.393
Abs-A/B	9.17 ± 7.99	10.77 ± 9.32	−0.98	0.397
Abs-(D + T)/(A + B)	3.67 ± 6.58	2.27 ± 2.55	1.61	0.202
Abs-(D + T)L/(D + T)R	1.00 ± 0.26	1.05 ± 0.33	−1.01	0.393
Abs-AL/AR	0.98 ± 0.33	0.97 ± 0.28	0.22	0.824
Abs-AFp/AO **	1.49 ± 1.75	0.69 ± 0.61	3.51	0.002
Rel-D *	3.64 ± 1.54	2.98 ± 1.31	2.53	0.028
Rel-T *	1.37 ± 0.65	1.85 ± 1.01	−2.94	0.010
Rel-A	2.32 ± 1.16	2.55 ± 0.89	−1.22	0.376
Rel-B	0.36 ± 0.15	0.34 ± 0.18	0.72	0.550
Rel-A/T	2.46 ± 2.45	2.01 ± 1.82	1.14	0.376
Rel-A/B	8.35 ± 6.62	9.71 ± 6.61	−1.11	0.376
Rel-(D + T)/(A + B)	2.69 ± 2.53	2.18 ± 2.36	1.13	0.376
Rel-(D + T)L/(D + T)R	1.02 ± 0.13	1.05 ± 0.14	−1.10	0.376
Rel-AL/AR	0.98 ± 0.13	0.98 ± 0.12	0.37	0.754
Rel-AFp/AO	0.76 ± 0.42	0.80 ± 0.24	−0.61	0.592
DFA-D	0.73 ± 0.04	0.75 ± 0.07	−2.06	0.082
DFA-T *	0.68 ± 0.05	0.70 ± 0.06	−2.38	0.039
DFA-A **	0.77 ± 0.09	0.71 ± 0.09	3.42	0.003
DFA-B ***	0.66 ± 0.07	0.61 ± 0.06	4.21	0.000
FD	1.60 ± 0.04	1.61 ± 0.04	−0.70	0.550

Mean ± SD are reported for all features.

[a]*Indicates P-value for independent sample t-test, and false discovery rate (FDR) was used to adjust P-value.*

CON, Health Control Group; SCZ, Schizophrenia Group; IMM, immediate memory score; VC, visuospatial/constructional score; LAN, language score; ATT, attention score; DEM, delayed memory score; INT-C, color interference time; INT-W, word interference time; PPI, prepulse inhibition; PSC-PPI, perceived spatial co-location PPI; PSS-PPI, perceived spatial separation PPI; Abs, absolute power spectra; Rel, relative power spectra; D, T, A, B denote delta, theta, alpha, and beta frequency band, respectively; L, left; R, right; Fp, frontal pole; O, occipital; DFA, detrended fluctuation analysis; FD, fractal dimension.

*$P < 0.05$; **$P < 0.01$; ***$P < 0.001$.*

performed using the Neurophysiological Biomarker Toolbox (NBT).[1] First, all electrodes were filtered in delta, theta, alpha, and beta oscillations, respectively. Then, the amplitude envelope was generated from each frequency band. Finally, the DFA value for each electrode was estimated per participant and stored for each frequency band separately. DFA-D, DFA-T, DFA-A, DFA-B were computed by averaging all electrodes in delta, theta, alpha, and beta frequency bands.

Fractal Dimension Features

Brain complexity can be described as the highly structured temporal structure observed in the EEG signal between pure randomness (e.g., white noise) and the absence of variability (constancy or pure periodicity). The EEGLAB plugin *myFractal*[2] was used to calculate FD for each electrode. Finally, the FD feature was extracted by averaging the FD value of all electrodes.

Statistical Analyses

Statistics were performed in RStudio (Version 1.2.5033, RStudio, Inc., Boston, United States) with R software (Version 3.6.3). The demographic and primary clinical data include gender, age, years of education, smoking history, duration of illness, age of illness onset, chlorpromazine equivalent doses, PANSS total score, PANSS positive score, PANSS negative score, and PANSS general psychopathology score. All demographic and clinical variables except gender and smoking history were expressed as means and SDs. The independent t-test and the chi-square test were conducted to evaluate potential differences in demographic, clinical variables neurocognitive, and electrophysiological between CON and SCZ. The false discovery rate (FDR) was computed to adjust P-values for multiple testing based on the Benjamini-Hochberg method (27). $P < 0.05$ (two-tailed) was considered as indicative of statistical significance. PASS version 11.0 (NCSS, LLC., Kaysville, UT, United States) was used for statistical power calculation.

Classification

All analyses were carried out using R 3.6.3 software. To choose the optimal features for SCZ and CON classification, the classification ability of each feature was first evaluated. A self-compiled function was used to compute Cohen's d-values of each feature. Receiver operating characteristic curve (ROC) analysis of each feature was created using the package of pROC in R. ROC values of every feature containing accuracy, sensitivity, specificity, and area under ROC curve (AUC) was used for analyses.

All features were then divided into two different categories: neurocognitive and electrophysiological sets. The *rfe* function (R caret package) was used for feature selection by the multivariate recursive feature elimination method (28). The main idea of multivariate recursive feature elimination is to build the model repeatedly and then select the best (or worst) features, put the selected features aside, and then repeat the process over the remaining features until all the features have been traversed. In this process, the order to be eliminated is the order of the features. The *rfe* was first fitted to all features using the bagged tree algorithm. Each feature was ranked according to its importance to the model. In each iteration of feature selection, the ranked features were retained, the model was refitted, and performance was assessed. The final selection of features in each set was based on 10-fold cross-validation.

[1]https://github.com/NBT-Analytics/NBTpublic

[2]https://github.com/rami-codes/myFractal

Then, two optimal subsets (neurocognitive and electrophysiological selected feature sets) and one combination feature set (containing two subsets) were obtained. After feature selection, the logistics algorithm (R stats package), the random forest algorithm (29) (R randomForest package), and the Extreme Gradient Boosting XGBoost algorithm (30) (R xgboost package) were utilized to estimate the classification models from the three features sets. When dealing with medium-sized structured data or table data, it is generally considered that the algorithm based on decision tree is the best. Random forest is an ensemble method to build decision trees. Intuitively speaking, each decision tree is a classifier, and then, for an input sample, N trees have N classification results. The random forest integrates all the classified voting results and specifies the classification with the most votes as the final output. The classification results of several weak classifiers are voted to form a strong classifier, which is the idea of the random forest. XGBoost is another ensemble machine learning algorithm that uses a decision tree as a weak classifier and then integrates these weak classifiers into a strong classifier. In the process of integration, different weights are usually given according to classification accuracy of weak classifiers. Moreover, after adding weak classifiers, the data is usually reweighed to strengthen the classification. Shortly after the XGBoost was put forward, 17 of the 29 champions in Kaggle Data Challenge 2015 used the XGBoost method, which defeated the neural network method.

Finally, the performance of these models is validated using the 10-fold cross-validation method. The results of the validation were then averaged. The classification performance was evaluated by accuracy, sensitivity, and specificity. Besides this, the performance of each model was also evaluated using ROC curves.

RESULTS

Demographics and Clinical Characteristics

SCZ (N = 69) and CON (N = 50) were well matched for gender, age, years of education, and smoking history. There were no significant differences between SCZ and CON in the distribution of these characteristics (**Table 1**).

Statistical Comparisons of All Extracted Features Between Schizophrenia Group and Control Group

The statistical analysis results of all features are presented in **Table 2**. The means and standard deviations of all features are shown. In total, all neurocognitive features were statistically different between SCZ and CON. It can also be observed that all PPI features differed significantly between the two groups. Among the EEG power spectrum features, only absolute theta power (Abs-T), absolute power AFp/AO ratio (Abs-AFp/AO), relative delta power (Rel-D), and relative power theta (Rel-T) showed statistically significant differences. In addition, the DFA of CON is lower than that of SCZ (DFA-T) in the theta band as well as both alpha and beta bands of CON being significantly higher than that of SCZ (DFA-A, DFA-B). None of the FDs differed significantly between SCZ and CON. Among all features, the P-values for IMM, LAN, ATT, DEM, PSS-PPI, and DFA-B were less than 0.001.

Cohen's d and Classification Performance of Single Feature

To choose optimal features to distinguish SCZ from CON, the Cohen's d and the ROC values were first evaluated for each feature. The ROC values included accuracy (%), sensitivity (%),

TABLE 3 | Cohen's d and the classification performance of single feature.

Features	Cohen's d	Accuracy (%)	Sensitivity (%)	Specificity (%)	AUC (%)
IMM	1.42	84.03	73.91	98.00	91.87
VC	0.60	69.75	95.65	34.00	64.65
LAN	0.90	76.47	75.36	78.00	75.74
ATT	0.86	77.31	85.51	66.00	77.84
DEM	1.16	83.19	82.61	84.00	86.58
INT-C	0.59	64.71	53.62	80.00	66.00
INT-W	0.65	67.23	53.62	86.00	71.26
PSC-PPI	0.69	70.59	76.81	62.00	70.61
PSS-PPI	1.16	80.67	79.71	82.00	84.32
Abs-D	0.04	53.78	49.28	60.00	50.00
Abs-T	0.50	67.23	62.32	74.00	67.13
Abs-A	0.27	68.07	86.96	42.00	61.71
Abs-B	0.20	60.5	72.46	44.00	57.88
Abs-A/T	0.19	37.82	7.25	80.00	48.7
Abs-A/B	0.18	67.23	91.3	34.00	58.43
Abs-(D + T)/(A + B)	0.30	63.87	81.16	40.00	56.96
Abs-(D + T)L/(D + T)R	0.19	53.78	23.19	96.00	54.26
Abs-AL/AR	0.04	42.86	43.48	42.00	51.54
Abs-AFp/AO	0.62	68.07	76.81	56.00	67.68
Rel-D	0.46	66.39	82.61	44.00	63.1
Rel-T	0.53	63.03	62.32	64.00	64.35
Rel-A	0.23	63.87	78.26	44.00	56.23
Rel-B	0.13	53.78	36.23	78.00	56.12
Rel-A/T	0.21	56.3	52.17	62.00	52.87
Rel-A/B	0.21	65.55	89.86	32.00	58.35
Rel-(D + T)/(A + B)	0.21	63.03	79.71	40.00	55.59
Rel-(D + T)L/(D + T)R	0.20	58.82	56.52	62.00	56.61
Rel-AL/AR	0.07	47.06	46.38	48.00	47.8
Rel-AFp/AO	0.11	60.5	66.67	52.00	59.13
DFA-D	0.38	57.14	30.43	94.00	58.52
DFA-T	0.43	61.34	62.32	60.00	61.57
DFA-A	0.61	68.07	63.77	74.00	70.1
DFA-B	0.73	71.43	75.36	66.00	71.94
FD	0.13	54.62	46.38	66.00	53.46

AUC, area under receiver operating characteristic curve; IMM, immediate memory score; VC, visuospatial/constructional score; LAN, language score; ATT, attention score; DEM, delayed memory score; INT-C, color interference time; INT-W, word interference time; PPI, prepulse inhibition; PSC-PPI, perceived spatial co-location PPI; PSS-PPI, perceived spatial separation PPI; Abs, absolute power spectra; Rel, relative power spectra; D, T, A, B denote delta, theta, alpha, and beta frequency band, respectively; L, left; R, right; Fp, frontal pole; O, occipital; DFA, detrended fluctuation analysis; FD, fractal dimension.

specificity (%), and AUC (%). **Table 3** shows these indexes from the neurocognitive and electrophysiological features. As can be seen in **Table 3**, a total of 14 features had d-values that exceeded the range of medium effect sizes (Cohen's d = 0.5) (31), which is generally consistent with the statistical result. These include IMM, VC, LAN, ATT, DEM, INT-C, INT-W, PSC-PPI, PSS-PPI, Abs-T, Abs-AFp/AO, Rel-T, DFA-A, and DFA-B. Among them, the Cohen's d-values of LAN, ATT, DEM, and PSS-PPI were all greater than 0.8, indicating a large effect size, whereas the Cohen's d-value of IMM reached 1.42, suggesting a minimal effect size. In **Table 3**, it is evident that the neurocognitive features performed better than the electrophysiological features in terms of ROC values. IMM was the most suitable neurocognitive feature for classification with an accuracy of 84.03%, and its AUC reached 91.87%. Five neurocognitive features (IMM, LAN, ATT, DEM, and INT-W) had AUC values greater than 70%, demonstrating functional discrimination capacities of features (32). The PSS-PPI was the best potential electrophysiological feature with an accuracy of 80.67% and an AUC of 84.32%. All four electrophysiological features (PSC-PPI, PSS-PPI, DFA-A, and DFA-B) had AUCs greater than 70%.

TABLE 4 | Classification performances of combined features.

Feature set	Accuracy (%)	Sensitivity (%)	Specificity (%)	AUC (%)
NSF subset models				
Logistics algorithm	82.35	88.41	74.00	89.88
Random forest algorithm	88.24	82.61	96.00	96.59
XGBoost algorithm	89.08	89.86	88.00	93.99
ESF subset models				
Logistics algorithm	82.35	86.96	76.00	90.84
Random Forest algorithm	84.87	91.30	76.00	91.88
XGBoost algorithm	88.24	89.86	86.00	90.52
ASF set models				
Logistics algorithm	87.39	92.75	80.00	92.54
Random forest algorithm	93.28	94.20	92.00	97.36
XGBoost algorithm	93.28	91.30	96.00	97.91

NSF subset, Neurocognitive Selected Features subset include IMM, LAN, ATT, DEM, INT-C, INT-W features; ESF subset, Electrophysiological Selected Features subset include PSC-PPI, PSS-PPI, Abs-T, Abs-A, Abs-AFp/AO, Abs-(D + T)/(A + B), Rel-D, Rel-T, Rel-A/B, DFA-A, DFA-B; ASF set, All Selected Features set include NSF subset and ESF subset.

Classification Performances of Combined Features

As mentioned in the methods, the REF method was used to select the neurocognitive and electrophysiological feature sets that could optimally distinguish between CON and SCZ. In addition, 10-fold cross-validation was used for feature selection to prevent overfitting. Finally, the neurocognitive selected features (NSF) subset contained immediate memory, delayed memory, attention, language functioning, color interference time, and word interference time. The electrophysiological selected features (ESF) subset contained PSC-PPI, PSS-PPI, Abs-T, Abs-A, Abs-AFp/AO, Abs-(D + T)/(A + B), Rel-D, Rel-T, Rel-A/B, DFA-A, and DFA-B. All selected features (ASF) included two subsets as described above. Then, the logistics, random forest and XGBoost algorithms were implemented to build classification models from the NSF subset, ESF subset, and ASF set. On this basis, these models were evaluated using a 10-fold cross-validation method.

Finally, the fitted values for the probability of people with schizophrenia ranged from 0 to 1. Accuracy, sensitivity, and specificity were calculated by setting cutoff points at 0.5 of the fitted values, and then the ROC curves were evaluated and AUCs were calculated based on the fitted values. These model evaluation indicators (accuracy, sensitivity, specificity, and AUC) are shown in **Table 4**. **Figure 1** shows the ROC curves for each model to represent the differences of ROC curves more clearly. As can be seen from **Table 4** and **Figure 1**, the model containing all selected feature sets exhibits the best classification performance regardless of the algorithm used (logistics accuracy of 87.39%, random forest and XGBoost accuracy of 93.28%). The NSF subset models and the ESF subset models showed roughly comparable levels of classification accuracy, but the NSF subset models performed better than the ESF subset in terms of AUC values. Besides this, the XGBoost algorithms performed more consistently and accurately in both accuracy and AUC among all the compared algorithms. The ASF set model with the XGBoost algorithm achieved the highest accuracy of 93.28% and an AUC of 97.91%. Statistical power was calculated by tests for one ROC curve procedure in PASS software. The power analysis showed that 50 patients and 69 healthy subjects were sufficient to have more than 90% statistical power at a two-sided alpha of 0.05 for significance level (**Supplementary Table 1**).

To better present the differences in the classification ability of these three algorithms, scatterplots were drawn with the fitted values of the NSF subset as the horizontal coordinates and the fitted values of the ESF subset as the vertical coordinates (**Figure 2**). It is apparent that the fitted values of the random forest and XGBoost algorithm are more densely distributed in this plot compared to the logistics algorithm, which also suggests that the random forest and XGBoost algorithms provide better performance in distinguishing schizophrenia patients from healthy individuals.

DISCUSSION

Classification Performance of Neurocognition in Schizophrenia

First, this study sought to determine which feature set was more beneficial in distinguishing between schizophrenic patients and healthy control subjects to construct the model. The second aim of the project was to identify which machine learning algorithm performed better in terms of classification ability and robustness.

The highest classification accuracy was 84.03% based on a single neurocognitive feature, achieved by immediate memory. A high level of immediate memory is considered as a predictor of improved cognitive impairments in schizophrenic patients (33). This also implies a potential opportunity for evaluating the prognostic or medical effect by using an immediate memory score. Other neurocognitive indicators performed well. For

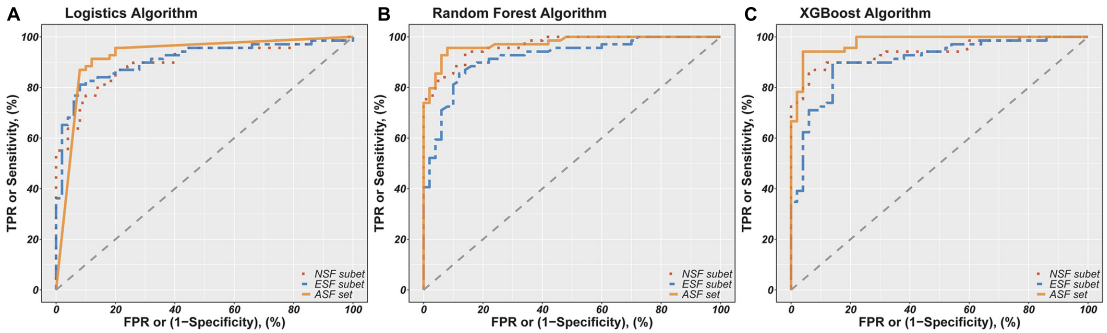

FIGURE 1 | Receiver Operator Characteristics (ROC) curves for classification of schizophrenia patients and controls based on different combinations of features using logistics **(A)**, random forest **(B)**, and XGBoost algorithm **(C)**. NSF subset, Neurocognitive Selected Features subset include IMM, LAN, ATT, DEM, INT-C, INT-W features; ESF subset, Electrophysiological Selected Features subset include PSC-PPI, PSS-PPI, Abs-T, Abs-A, Abs-AFp/AO, Abs-(D+T)/(A+B), Rel-D, Rel-T, Rel-A/B, DFA-A, DFA-B. ASF set, All Selected Features set include NSF subset and ESF subset. The red, green and blue lines show the ROC curves for the NSF subset, ESF subset and ASF set, respectively. The AUC of logistics models based on NSF subset, ESF subset, ASF set was 89.88%, 90.84%, 92.54%. The AUC of random forest models based on NSF subset, ESF subset, ASF set was 96.59 91.88%, 97.36%. The AUC of XGBoost models based on NSF subset, ESF subset, ASF set was 93.99%, 90.52%, 97.91%.

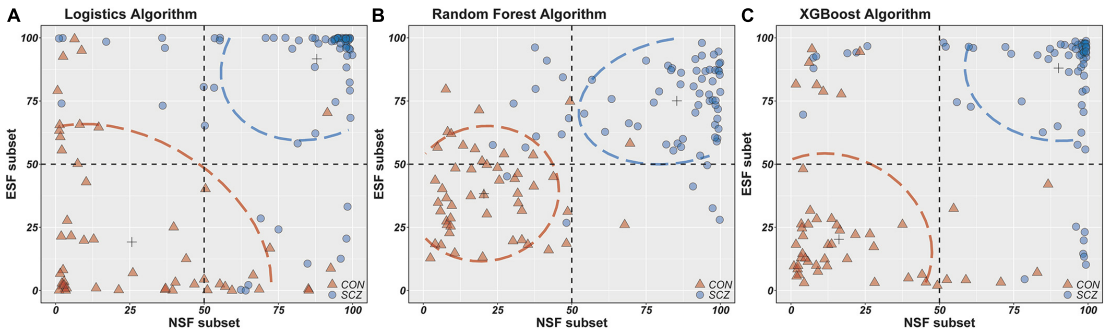

FIGURE 2 | The horizontal/longitudinal coordinate axis represents the probability of people with schizophrenia (%). NSF subset, Neurocognitive Selected Features subset include IMM, LAN, ATT, DEM, INT-C, INT-W features; ESF subset, Electrophysiological Selected Features subset include PSC-PPI, PSS-PPI, Abs-T, Abs-A, Abs-AFp/AO, Abs-(D + T)/(A + B), Rel-D, Rel-T, Rel-A/B, DFA-A, DFA-B; ASF set, All Selected Features set include NSF subset and ESF subset. **(A–C)** Scatter plots from two features set (NSF subset and ESF subset) using logistics, random forest and XGBoost models.

instance, the delayed memory score also received an excellent classified effect (accuracy of 83.19% and AUC of 86.58%). The classification accuracy of the combined neurocognitive feature set was slightly higher than that of any single feature classifier (accuracy of 89.08% and AUC of 93.99%).

Previous studies demonstrate the importance of neurocognitive-based machine learning techniques for diagnosing schizophrenia. Vacca et al. (34) employed several machine learning techniques (logistics regression, decision tree, random forest, k-nearest neighbor, neural network, support vector machine) to distinguish between 86 schizophrenic patients and 115 healthy subjects. The best methods turned out to be support vector machine and neural network with accuracies of 87 and 84.8%. Antonucci et al. (35) investigated the discriminatory performance of genetic, environmental, and neurocognitive classifiers by using support vector classification and repeated nested cross-validation. The cognitive classifier showed an accuracy of 88.7%, followed by environmental (65.1%) and genetic (55.5%) classifiers. The findings of the two studies are in line with the current study, revealing that neurocognition is a robust indicator in differentiating schizophrenia from healthy people.

Classification Performance of Electrophysiology in Schizophrenia

PPI deficits are involved in the biological bases of schizophrenia and proposed as a potential biomarker for genetic studies with more than 50% of PPI variance attributed to genetic factors (36). Mackeprang et al. (37) argue that PPI was not affected by antipsychotic treatment and, instead, was a stable vulnerability index for schizophrenia. Mena et al. (38) used longitudinal data to examine whether PPI deficits exhibit a temporary effect in the acute phase of schizophrenia. The result suggests that the PPI remained reduced at the 3 months post-discharge assessment, implying that the PPI was a biomarker of schizophrenia. However, in practice, the PPI did not separate schizophrenic subjects from healthy controls (39). In comparison to neurocognitive and other electrophysiological measures, the PPI showed a medium Cohen's d-value of below 0.6 (40). The

previous study establishes a novel PPI paradigm by using a precedence effect–based perceived separation, which produced a Cohen's d-value of 1.27 and an AUC of 85.2% (11). The current study analyzes whether PSC-PPI and PSS-PPI single features could distinguish SCZ from CON. The accuracy of PSS-PPI was 80.67%, and the AUC was 84.32%.

In addition, other single markers were tested for their ability to identify schizophrenia based on the EEG power spectrum, detrended fluctuation analysis, and fractal dimension. DFA is a method to evaluate the large-scale functional neural dysconnectivity of schizophrenic patients at the temporal level. It was found that DFA was substantially attenuated in both alpha and beta frequency bands in patients. DFA-B presented the highest accuracy of 71.43% and AUC of 71.94% in a single EEG feature.

Compared with the best single electrophysiological feature (PSS-PPI), the combined electrophysiological feature increased the accuracy from 80.67 to 88.24% and the AUC from 84.42 to 91.88%. Devia et al. (41) report that the EEG signals from a free-viewing paradigm distinguished patients from healthy subjects with an overall accuracy of 71%. Thilakavathi et al. (42) analyzed the EEG power spectrum and found that the vector machine classifier produced an accuracy of 88% when features were combined together. Laton et al. (43) used a combination of oddball and mismatch event-related potentials and increased accuracy from 79.8 to 84.7% for a single feature. The above findings suggest that it is essential to select the appropriate EEG feature set to better distinguish between schizophrenic and healthy individuals.

Classification Performance of Combined Neurocognitive and Electrophysiological Features in Schizophrenia

The results show that both neurocognitive and electrophysiological feature sets had a good performance with accuracy values greater than 80% and AUC values greater than 85%. Specifically, the combined neurocognitive and electrophysiological features delivered the highest accuracy of 93.28% and AUC of 97.91%. In fact, the XGBoost algorithm as a whole presented a more stable and accurate classification efficiency in this study. As previous research indicates, XGBoost had several advantages in terms of speed and accuracy over other tree-based ensemble methods, such as Random Forests, AdaBoost, and the traditional gradient boosted trees (30).

Potential Limitations

There are several potential limitations to this study. First, this is a single-center study with limited sample size. Due to the relatively small number of subjects in the study, caution should be exercised when attempting to generalize these findings to clinical applications. Second, there is a lack of drug-naïve patient groups. Drugs may have potentially confounded the findings of the classification performances of these models and clinical status. Third, it is related to the duration of the disease. Nevertheless, no correlation was found between all features and CPZe as well as duration of illness (**Table 5**). The last one is model interpretability. Indeed, classic statistical regression models, such as linear regression, perform better in terms of interpretability than black-box machine learning models. Perhaps it is for this reason that the acceptance of machine learning among clinicians is lacking. However, schizophrenia is likely to be etiologically heterogeneous, resulting in poor prediction performance of a linear model. Linear regression

TABLE 5 | Correlation between all features and CPZs, duration of illness in patients.

Features	CPZe		Duration of illness	
	r	*P*	r	*P*
IMM	0.100	0.398	−0.050	0.671
VC	0.000	0.991	−0.020	0.861
LAN	−0.100	0.432	0.140	0.245
ATT	−0.090	0.478	0.070	0.563
DEM	0.080	0.518	0.020	0.849
INT-C	−0.010	0.955	−0.010	0.955
INT-W	−0.180	0.132	−0.010	0.926
PSC-PPI	−0.150	0.233	0.080	0.507
PSS-PPI	−0.200	0.101	0.190	0.115
Abs-D	0.050	0.677	0.040	0.768
Abs-T	−0.050	0.708	0.120	0.330
Abs-A	0.050	0.667	0.140	0.264
Abs-B	0.140	0.254	0.130	0.283
Abs-A/T	0.150	0.222	−0.010	0.912
Abs-A/B	−0.050	0.674	0.050	0.705
Abs-(D + T)/(A + B)	−0.090	0.456	−0.010	0.937
Abs-(D + T)L/(D + T)R	−0.010	0.952	0.120	0.321
Abs-AL/AR	−0.080	0.496	0.100	0.421
Abs-AFp/AO	0.030	0.799	−0.010	0.953
Rel-D	0.040	0.763	−0.060	0.610
Rel-T	−0.210	0.078	0.070	0.547
Rel-A	0.080	0.513	0.030	0.803
Rel-B	0.010	0.926	−0.020	0.879
Rel-A/T	0.150	0.211	−0.020	0.893
Rel-A/B	−0.040	0.740	0.070	0.544
Rel-(D + T)/(A + B)	−0.100	0.405	−0.020	0.880
Rel-(D + T)L/(D + T)R	0.130	0.280	0.050	0.677
Rel-AL/AR	−0.170	0.159	0.080	0.519
Rel-AFp/AO	−0.020	0.850	0.090	0.478
DFA-D	0.080	0.503	0.160	0.197
DFA-T	−0.010	0.947	0.080	0.496
DFA-A	−0.040	0.720	−0.040	0.752
DFA-B	0.040	0.740	0.180	0.137
FD	0.130	0.281	−0.080	0.519

P-value for spearman rank correlation analysis, and false discovery rate (FDR) was used to adjust P-value.

CPZe, Chlorpromazine Equivalent Doses; IMM, immediate memory score; VC, visuospatial/constructional score; LAN, language score; ATT, attention score; DEM, delayed memory score; INT-C, color interference time; INT-W, word interference time; PPI, prepulse inhibition; PSC-PPI, perceived spatial co-location PPI; PSS-PPI, perceived spatial separation PPI; Abs, absolute power spectra; Rel, relative power spectra; D, T, A, B denote delta, theta, alpha, and beta frequency band, respectively; L, left; R, right; Fp, frontal pole; O, occipital; DFA, detrended fluctuation analysis; FD, fractal dimension.

cannot model the inherent complexity of data sets (such as feature interaction). Therefore, when choosing an appropriate machine learning model, we usually need to weigh the accuracy and interpretability of the model.

In future research, to provide a simple, robust, and reliable model for detecting schizophrenia, first-episode, drug-naïve patients with schizophrenia will be recruited. Moreover, patients with depression and bipolar disorder will also be invited to participate in a future study to assess the specificity of the model and to determine whether the severity of these features varies across psychiatric disorders. Besides this, additional EEG features may be identified in the classification. Further research may also be conducted to evaluate the efficacy of interventions and prognosis.

CONCLUSION

In this study, a comprehensive machine learning pipeline was provided to detect patients with schizophrenia by applying logistics, random forest, and extreme gradient boosting (XGBoost) algorithm classifiers to neurocognition, electrophysiology, and their combination. The highest classification accuracy of 93.28% was achieved by combining neurocognitive and electrophysiological features, suggesting that these measurements are appropriate indicators for discriminating schizophrenia patients from healthy individuals. Also, among these three algorithms, XGBoost has better classification performances than the other two algorithms. These results suggest that neurocognitive and electrophysiological features can be used along with machine learning for potential clinical applications.

DATA AVAILABILITY STATEMENT

The original contributions presented in the study are included in the article/**Supplementary Material**, further inquiries can be directed to the corresponding authors.

ETHICS STATEMENT

The studies involving human participants were reviewed and approved by the Ethics Committee of Beijing Anding Hospital. The patients/participants provided their written informed consent to participate in this study.

AUTHOR CONTRIBUTIONS

G-ZY, C-YW, and MF designed the study. LL provided the PPI paradigm for the study. QT, N-BY, YF, FD, Q-JB, and F-CZ acquired and analyzed the data. J-CZ supplied the machine learning algorithm for the study. QT wrote the article, which all authors reviewed. All authors approved the final version to be published and can certify that no other individuals not listed as authors have made substantial contributions to the manuscript.

FUNDING

This study was funded by the National Natural Science Foundation of China (81971250), Jiangsu Province Key Research & Development Project (BE2018662 and BE2020764), Beijing Municipal Administration of Hospitals Clinical Medicine Development of Special Funding Support (ZYLX201807), Prevention and Control Program of Suzhou Major Diseases (Gwzx201801), the Project of Invigorating Health Care through Science, Technology and Education, Suzhou Medical Youth Talent (kjxw2018048), People's Livelihood Projects of Suzhou Science and Technology Bureau (SYSD2018168 and SYSD2018166), and Suzhou Clinical Medical Center for Mood Disorders (No. Szlcyxzx202109 to Xiao-Bin Zhang).

ACKNOWLEDGMENTS

We are grateful to Xiao-Bin Zhang for providing funding support and manuscript writing advice.

SUPPLEMENTARY MATERIAL

The Supplementary Material for this article can be found online at: https://www.frontiersin.org/articles/10.3389/fpsyt.2022.810362/full#supplementary-material

REFERENCES

1. Vos T, Abajobir AA, Abate KH, Abbafati C, Abbas KM, Abd-Allah F, et al. Global, regional, and national incidence, prevalence, and years lived with disability for 328 diseases and injuries for 195 countries, 1990–2016: a systematic analysis for the Global Burden of Disease Study 2016. *Lancet.* (2017) 390:1211–59.
2. Bowie CR, Reichenberg A, Patterson TL, Heaton RK, Harvey PD. Determinants of real-world functional performance in schizophrenia subjects: correlations with cognition, functional capacity, and symptoms. *Am J Psychiatry.* (2006) 163:418–25. doi: 10.1176/appi.ajp.163.3.418
3. Green MF, Kern RS, Braff DL, Mintz J. Neurocognitive deficits and functional outcome in schizophrenia: are we measuring the "right stuff"? *Schizophrenia Bull.* (2000) 26:119–36.
4. Galderisi S, Rossi A, Rocca P, Bertolino A, Mucci A, Bucci P, et al. The influence of illness—related variables, personal resources and context—related factors on real—life functioning of people with schizophrenia. *World Psychiatry.* (2014) 13:275–87.
5. Galderisi S, Rossi A, Rocca P, Bertolino A, Mucci A, Bucci P, et al. Pathways to functional outcome in subjects with schizophrenia living in the community and their unaffected first-degree relatives. *Schizophr Res.* (2016) 175:154–60.
6. Nuechterlein KH, Barch DM, Gold JM, Goldberg TE, Green MF, Heaton RK. Identification of separable cognitive factors in schizophrenia. *Schizophr Res.* (2004) 72:29–39.
7. Klamer D, Svensson L, Fejgin K, Palsson E. Prefrontal NMDA receptor antagonism reduces impairments in pre-attentive information processing. *Eur Neuropsychopharmacol.* (2011) 21:248–53. doi: 10.1016/j.euroneuro.2010.10.010

8. Swerdlow NR, Bhakta SG, Light GA. Room to move: plasticity in early auditory information processing and auditory learning in schizophrenia revealed by acute pharmacological challenge. *Schizophr Res.* (2018) 199:285–91. doi: 10.1016/j.schres.2018.03.037
9. Kumari V, Das M, Zachariah E, Ettinger U, Sharma T. Reduced prepulse inhibition in unaffected siblings of schizophrenia patients. *Psychophysiology.* (2005) 42:588–94. doi: 10.1111/j.1469-8986.2005.00346.x
10. Light GA, Swerdlow NR, Rissling AJ, Radant A, Sugar CA, Sprock J, et al. Characterization of neurophysiologic and neurocognitive biomarkers for use in genomic and clinical outcome studies of schizophrenia. *PLoS One.* (2012) 7:e39434. doi: 10.1371/journal.pone.0039434
11. Yang NB, Tian Q, Fan Y, Bo QJ, Zhang L, Li L, et al. Deficits of perceived spatial separation induced prepulse inhibition in patients with schizophrenia: relationships to symptoms and neurocognition. *BMC Psychiatry.* (2017) 17:135. doi: 10.1186/s12888-017-1276-4
12. Grin-Yatsenko VA, Ponomarev VA, Pronina MV, Poliakov YI, Plotnikova IV, Kropotov JD. Local and widely distributed EEG activity in schizophrenia with prevalence of negative symptoms. *Clin Eeg Neurosci.* (2017) 48:307–15.
13. Boutros NN, Arfken C, Galderisi S, Warrick J, Pratt G, Iacono W. The status of spectral EEG abnormality as a diagnostic test for schizophrenia. *Schizophr Res.* (2008) 99:225–37.
14. Koshiyama D, Miyakoshi M, Tanaka-Koshiyama K, Joshi YB, Molina JL, Sprock J, et al. Neurophysiologic characterization of resting state connectivity abnormalities in schizophrenia patients. *Front Psychiatry.* (2020) 11:608154. doi: 10.3389/fpsyt.2020.608154
15. Tanaka-Koshiyama K, Koshiyama D, Miyakoshi M, Joshi YB, Molina JL, Sprock J, et al. Abnormal spontaneous gamma power is associated with verbal learning and memory dysfunction in schizophrenia. *Front Psychiatry.* (2020) 11:832. doi: 10.3389/fpsyt.2020.00832
16. Yadav S, Haque NS, Das B, Das J, Tikka SK. Resting state quantitative electroencephalogram gamma power spectra in patients with first episode psychosis: an observational study. *Asian J Psychiatr.* (2021) 57:102550. doi: 10.1016/j.ajp.2021.102550
17. Nikulin VV, Jönsson EG, Brismar T. Attenuation of long-range temporal correlations in the amplitude dynamics of alpha and beta neuronal oscillations in patients with schizophrenia. *Neuroimage.* (2012) 61:162–9.
18. Li W, Yang Y, Liu ZH, Zhao YJ, Zhang Q, Zhang L, et al. Progression of mental health services during the COVID-19 outbreak in china. *Int J Biol Sci.* (2020) 16:1732–8. doi: 10.7150/ijbs.45120
19. Wang JH, Li CB, Cheng Y, Yi ZH, Long B, Wang JJ. Reliability and validity of repeatable battery for the assessment of neuropsychological status (RBANS) in schizophrenic patients: a preliminary study. *Shanghai Arch Psychiatry.* (2009) 21:265–8.
20. Xue W, Yanping R, Jiali H, Dongfeng Z. Evaluation of cognitive functions and its corelation with psychiatric symptoms in patients with schizophrenia. *J Capital Med Univ.* (2008) 4:423–7.
21. Li XB, Bo QJ, Tian Q, Yang NB, Mao Z, Zheng W, et al. Impact of childhood trauma on sensory gating in patients with first-episode schizophrenia. *BMC Psychiatry.* (2018) 18:258. doi: 10.1186/s12888-018-1807-7
22. Delorme A, Makeig S. EEGLAB: an open source toolbox for analysis of single-trial EEG dynamics including independent component analysis. *J Neurosci Methods.* (2004) 134:9–21. doi: 10.1016/j.jneumeth.2003.10.009
23. Oostenveld R, Fries P, Maris E, Schoffelen JM. FieldTrip: open source software for advanced analysis of MEG, EEG, and invasive electrophysiological data. *Comput Intell Neurosci.* (2011) 2011:156869. doi: 10.1155/2011/156869
24. Pion-Tonachini L, Kreutz-Delgado K, Makeig S. ICLabel: an automated electroencephalographic independent component classifier, dataset, and website. *Neuroimage.* (2019) 198:181–97. doi: 10.1016/j.neuroimage.2019.05.026
25. Hardstone R, Poil SS, Schiavone G, Jansen R, Nikulin VV, Mansvelder HD, et al. Detrended fluctuation analysis: a scale-free view on neuronal oscillations. *Front Physiol.* (2012) 3:450. doi: 10.3389/fphys.2012.00450
26. Smit DJ, de Geus EJ, van de Nieuwenhuijzen ME, van Beijsterveldt CE, van Baal GC, Mansvelder HD, et al. Scale-free modulation of resting-state neuronal oscillations reflects prolonged brain maturation in humans. *J Neurosci.* (2011) 31:13128–36. doi: 10.1523/JNEUROSCI.1678-11.2011
27. Benjamini Y, Hochberg Y. Controlling the false discovery rate: a practical and powerful approach to multiple testing. *J R Stat Soc B (Methodological).* (1995) 57:289–300.
28. Guan W, Zhou M, Hampton CY, Benigno BB, Walker LD, Gray A, et al. Ovarian cancer detection from metabolomic liquid chromatography/mass spectrometry data by support vector machines. *BMC Bioinformatics.* (2009) 10:259. doi: 10.1186/1471-2105-10-259
29. Liaw A, Wiener M. Classification and regression by randomForest. *R News.* (2002) 2:18–22.
30. Chen T, Guestrin C. Xgboost: a scalable tree boosting system. *Proceedings of the 22nd Acm Sigkdd International Conference on Knowledge Discovery and Data Mining*. New York, NY: ACM (2016).
31. Sawilowsky SS. New effect size rules of thumb. *J Modern Appl Stat Methods.* (2009) 8:26.
32. Elith J, Phillips SJ, Hastie T, Dudík M, Chee YE, Yates CJ. A statistical explanation of MaxEnt for ecologists. *Divers Distrib.* (2011) 17:43–57.
33. Xiu MH, Guan HY, Zhao JM, Wang KQ, Pan YF, Su XR, et al. Cognitive enhancing effect of high-frequency neuronavigated rTMS in chronic schizophrenia patients with predominant negative symptoms: a double-blind controlled 32-Week follow-up study. *Schizophr Bull.* (2020) 46:1219–30. doi: 10.1093/schbul/sbaa035
34. Vacca A, Longo R, Mencar C. Identification and evaluation of cognitive deficits in schizophrenia using "Machine learning". *Psychiatr Danub.* (2019) 31:261–4.
35. Antonucci LA, Pergola G, Pigoni A, Dwyer D, Kambeitz-Ilankovic L, Penzel N, et al. A pattern of cognitive deficits stratified for genetic and environmental risk reliably classifies patients with schizophrenia from healthy control subjects. *Biol Psychiatry.* (2020) 87:697–707. doi: 10.1016/j.biopsych.2019.11.007
36. Anokhin AP, Heath AC, Myers E, Ralano A, Wood S. Genetic influences on prepulse inhibition of startle reflex in humans. *Neurosci Lett.* (2003) 353:45–8. doi: 10.1016/j.neulet.2003.09.014
37. Mackeprang T, Kristiansen KT, Glenthoj BY. Effects of antipsychotics on prepulse inhibition of the startle response in drug-naive schizophrenic patients. *Biol Psychiatry.* (2002) 52:863–73. doi: 10.1016/s0006-3223(02)01409-9
38. Mena A, Ruiz-Salas JC, Puentes A, Dorado I, Ruiz-Veguilla M, De la Casa LG. Reduced prepulse inhibition as a biomarker of schizophrenia. *Front Behav Neurosci.* (2016) 10:202. doi: 10.3389/fnbeh.2016.00202
39. Massa N, Owens AV, Harmon W, Bhattacharya A, Ivleva EI, Keedy S, et al. Relationship of prolonged acoustic startle latency to diagnosis and biotype in the bipolar-schizophrenia network on intermediate phenotypes (B-SNIP) cohort. *Schizophr Res.* (2019) 216:357–66. doi: 10.1016/j.schres.2019.11.013
40. Light GA, Swerdlow NR. Future clinical uses of neurophysiological biomarkers to predict and monitor treatment response for schizophrenia. *Ann N Y Acad Sci.* (2015) 1344:105–19. doi: 10.1111/nyas.12730
41. Devia C, Mayol-Troncoso R, Parrini J, Orellana G, Ruiz A, Maldonado PE, et al. EEG classification during scene free-viewing for schizophrenia detection. *IEEE T Neur Sys Reh.* (2019) 27:1193–9.
42. Thilakavathi B, Devi SS, Malaiappan M, Bhanu K. EEG power spectrum analysis for schizophrenia during mental activity. *Australas Phys Eng S.* (2019) 42:887–97.
43. Laton J, Van Schependom J, Gielen J, Decoster J, Moons T, De Keyser J, et al. Single-subject classification of schizophrenia patients based on a combination of oddball and mismatch evoked potential paradigms. *J Neurol Sci.* (2014) 347:262–7.

Conflict of Interest: The authors declare that the research was conducted in the absence of any commercial or financial relationships that could be construed as a potential conflict of interest.

frontiers | Frontiers in Psychiatry

ORIGINAL RESEARCH
published: 23 May 2022
doi: 10.3389/fpsyt.2022.830819

Bibliometric Analysis of Quantitative Electroencephalogram Research in Neuropsychiatric Disorders From 2000 to 2021

Shun Yao[1,2†], Jieying Zhu[1†], Shuiyan Li[3], Ruibin Zhang[1], Jiubo Zhao[1,4], Xueling Yang[1,4] and You Wang[1,4*]*

[1] Department of Psychology, School of Public Health, Southern Medical University, Guangzhou, China, [2] Department of Neurosurgery, Huashan Hospital, Fudan University, Shanghai, China, [3] Department of Rehabilitation Medicine, School of Rehabilitation Medicine, Southern Medical University, Guangzhou, China, [4] Department of Psychiatry, Zhujiang Hospital, Southern Medical University, Guangzhou, China

OPEN ACCESS

Edited by:
Jing Xiang,
Cincinnati Children's Hospital Medical Center, United States

Reviewed by:
Yury (Juri) Kropotov,
N. P. Bechtereva Institute of the Human Brain (RAS), Russia
Deniz Doruk,
Mayo Clinic, United States

***Correspondence:**
Xueling Yang
yhtyxl2006@126.com
You Wang
wangyoupsy@foxmail.com

[†]These authors have contributed equally to this work and share first authorship

Specialty section:
This article was submitted to Neuroimaging and Stimulation, a section of the journal Frontiers in Psychiatry

Received: 07 December 2021
Accepted: 05 April 2022
Published: 23 May 2022

Citation:
Yao S, Zhu J, Li S, Zhang R, Zhao J, Yang X and Wang Y (2022) Bibliometric Analysis of Quantitative Electroencephalogram Research in Neuropsychiatric Disorders From 2000 to 2021. Front. Psychiatry 13:830819. doi: 10.3389/fpsyt.2022.830819

Background: With the development of quantitative electroencephalography (QEEG), an increasing number of studies have been published on the clinical use of QEEG in the past two decades, particularly in the diagnosis, treatment, and prognosis of neuropsychiatric disorders. However, to date, the current status and developing trends of this research field have not been systematically analyzed from a macroscopic perspective. The present study aimed to identify the hot spots, knowledge base, and frontiers of QEEG research in neuropsychiatric disorders from 2000 to 2021 through bibliometric analysis.

Methods: QEEG-related publications in the neuropsychiatric field from 2000 to 2021 were retrieved from the Web of Science Core Collection (WOSCC). CiteSpace and VOSviewer software programs, and the online literature analysis platform (bibliometric.com) were employed to perform bibliographic and visualized analysis.

Results: A total of 1,904 publications between 2000 and 2021 were retrieved. The number of QEEG-related publications in neuropsychiatric disorders increased steadily from 2000 to 2021, and research in psychiatric disorders requires more attention in comparison to research in neurological disorders. During the last two decades, QEEG has been mainly applied in neurodegenerative diseases, cerebrovascular diseases, and mental disorders to reveal the pathological mechanisms, assist clinical diagnosis, and promote the selection of effective treatments. The recent hot topics focused on QEEG utilization in neurodegenerative disorders like Alzheimer's and Parkinson's disease, traumatic brain injury and related cerebrovascular diseases, epilepsy and seizure, attention-deficit hyperactivity disorder, and other mental disorders like major depressive disorder and schizophrenia. In addition, studies to cross-validate QEEG biomarkers, develop new biomarkers (e.g., functional connectivity and complexity), and extract compound biomarkers by machine learning were the emerging trends.

Conclusion: The present study integrated bibliometric information on the current status, the knowledge base, and future directions of QEEG studies in neuropsychiatric disorders from a macroscopic perspective. It may provide valuable insights for researchers focusing on the utilization of QEEG in this field.

Keywords: bibliometrics, quantitative electroencephalogram, neuropsychiatric disorders, CiteSpace, VOSviewer

INTRODUCTION

Electroencephalography (EEG) is a tool for recording spontaneous electrical activity generated in the cerebral cortex using multiple electrodes placed on the scalp (1), providing real-time assessment of cerebral physiological functions (2). Since the German psychiatrist Hans Berger first tried to record human cerebral electrical activity from the scalp in 1928 (3), EEG technology has continued to develop, which is currently one of the most influential noninvasive tools available to clinicians for evaluating a patient's neurophysiological functions (4).

Quantitative EEG (QEEG) techniques separate complex EEG signals into components such as amplitude, frequency, and compress time, permitting the display of several hours of data on one image (5). QEEG empowers a neurologist or a psychiatrist's unprecedented ability to look at summarized EEG information, which was not previously possible with a visual examination of EEG traces. More importantly, QEEG can provide an objective, replicable measure of brain functions that is less dependent on subjective or behavioral reports that may vary across settings and informants (6). Therefore, QEEG can be used in more productive ways than non-QEEG to identify and categorize neuropsychiatric diseases, as well as to predict the outcome of therapeutic intervention (7).

To date, several studies have summarized the development of QEEG methodology (8–10) or systematically reviewed the research papers on the possible use of QEEG as a biomarker in adult or child psychiatric disorders (11, 12) and in Alzheimer's disease (13). However, to our knowledge, there is no existing study to analyze the developing status of the QEEG research field from a macroscopic perspective.

Bibliometrics, an important branch of intelligence science (14), uses the literature system and bibliometric characteristics as the research object and conducts quantitative and qualitative analyses of the literature (15). In recent years, bibliometric analysis has been applied to visualize the knowledge status, features, evolution, and emerging trends in various research fields (16). It can help scholars extract quantitative information on distribution by country/region, institution, author, journal, research hot spots, and frontiers in a particular field in a short time, providing in-depth reviews and insights about the research field (17). Therefore, the present study used bibliometric tools to analyze the QEEG studies in neuropsychiatric disorders from 2000 to 2021 to provide a comprehensive overview.

The specific research questions in the present study for QEEG research in neuropsychiatric disorders were as follows: 1) What are the overall publication trends, the geographic distributions, the most important journals, and who are the potential collaborators? 2) What is the knowledge framework in this field in terms of research hot spots and knowledge base? 3) What are the future directions of this field?

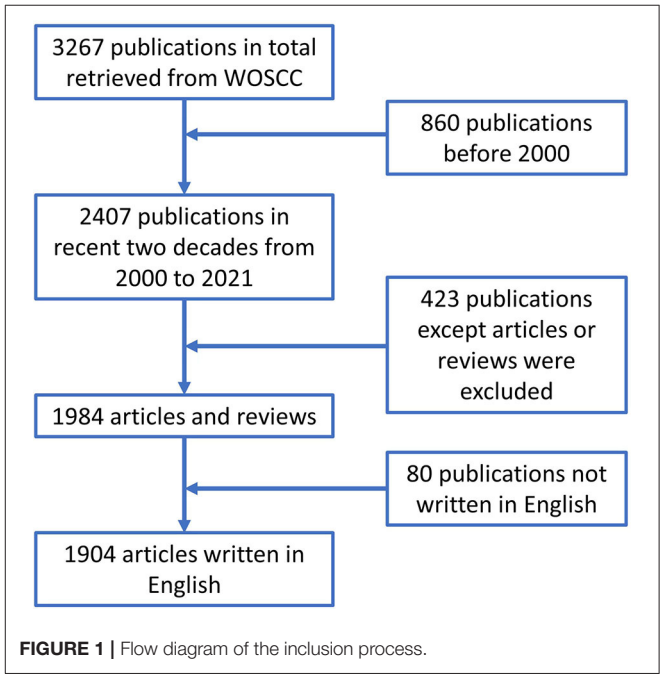

FIGURE 1 | Flow diagram of the inclusion process.

METHOD AND DATA SOURCE

Data Collection

Data for the present study were retrieved from the Web of Science Core Collection (WOSCC) database in January 2022. We used TS = [(quantitative electroencephalography) OR (QEEG) OR (quantitative EEG)] AND WC = [(neurology) OR (psychiatry) OR (neuropsychiatry)] as the search terms, where "TS" represents term subject and "WC" represents "Web of Science categories." The time limitation was between 1 January 2000 and 31 December 2021. Only literature published in English was included, and duplicated articles were deleted. To avoid bias due to daily database updates, we performed the literature retrieval from WOSCC on a single day, that is, 27 January 2022. A total of 1,904 publications were included and consisted of original articles and reviews. The search strategy is depicted in **Figure 1**.

Analysis Tools

All the collected data were converted into TXT format and exported for further visual analysis by bibliometric software,

including CiteSpaceV (5.8.R3) and VOSviewer (1.6.16), and the online literature analysis platform (*bibliometric.com*). Visualized information, such as yearly output, subject categories of WOS, and impact factor (IF), was analyzed based on the function of literature analysis on WOSCC. The number of countries, institutions, and international collaborations were analyzed by bibliometric.com. CiteSpaceV was used to perform collaboration network analysis (including authors, institutions, journals, co-cited journals, co-cited authors, and co-cited references) and related centrality. The specific parameters used in CiteSpaceV were set as follows. For the selection of time slices, a slice of 1 year was used for determining the connection strength, and cosine was used for this purpose. For the threshold, we selected the top 50 nodes in each time slice. Moreover, the pruning used a pathfinder and merged network. VOSviewer was used to analyze the keywords. The keyword co-occurrence map in VOSviewer only includes terms that appear at least 15 times under the binary count. The purpose of the algorithm is to ensure that the terms that occur more frequently have larger bubble images and the terms with high similarity are close to each other with a similar color. Finally, the keyword overlay map was used based on the occurrence of keywords to visualize the emerging topics from 2000 to 2021.

RESULTS

Annual Publications

A total of 1904 publications that met the retrieval criteria were included in further analysis. The total number of annual publications is shown in **Figure 2A**, which depicts an increasing trend from 2000 to 2021. As shown in **Figure 2B**, the trend of the annual publications in the neurology field showed steady growth. However, the yearly output of articles in the psychiatry area increased relatively slowly, indicating that the application of QEEG in psychiatric disorders requires more attention.

Analysis of Countries and Institutions

Publications of QEEG research were obtained from 71 countries. About 89.92% of the publications were from the top 10 countries (**Table 1**). The trends of annual output from the top 10 countries are shown in **Figure 3A**. Most publications were from the United States ($n = 657$, 34.5%). The centrality analysis in CiteSpaceV represented the influence of a node, and a node was of great significance when the centrality value is greater than 0.1. Countries with a centrality value greater than 0.1 were the United States ($n = 0.95$) and Germany ($n = 0.14$), suggesting that publications from these two countries had a greater influence on QEEG research. The international cooperation between countries is shown in **Figure 3C**. The most frequent collaboration was observed between the United States and Canada, followed by Australia.

A total of 2,433 institutions published QEEG-related articles. The trends of annual output from the top 10 institutions are shown in **Figure 3B**. The distribution of institutions is scattered. **Table 1** lists the top 10 productive institutions, and 343 papers have been published by these institutions, accounting for 18.01% of the total publications. About 60% of the top 10 institutions are from the United States, including the University of California, Los Angeles, Yale University, Massachusetts General Hospital, New York University, Harvard University, and Columbia University.

Analysis of Journals and Co-cited Journals

A total of 245 journals were involved, and the top 10 most active QEEG-related journals published 47.53% of the total publications ($n = 905$; **Figure 4A**). Among the top 10 journals in QEEG research, Clinical Neurophysiology ($n = 281$) was the most active journal, followed by Clinical EEG and Neuroscience ($n = 144$) and Journal of Clinical Neurophysiology ($n = 84$).

Co-cited journals were journals cited together by researchers, which usually reflected the foundation of a research field and were one of the most important indicators in bibliometric analysis. Half of the top 10 co-cited journals in QEEG research in neuropsychiatric disorders were published in Q1 according to JCR. Biological Psychiatry showed the highest impact factor (IF = 13.382). Clinical Neurophysiology ($n = 1{,}106$) ranked first in co-cited journals, followed by Electroencephalography and Clinical Neurophysiology ($n = 1{,}004$) and Neurology ($n = 880$), suggesting these journals were well recognized in QEEG research in the neuropsychiatric field (**Figure 4B**).

Analysis of Authors

A total of 8,003 authors contributed to QEEG research in neuropsychiatric disorders. As presented in **Table 2**, six authors published over 25 articles. The most productive authors were Cook IA and Leuchter AF who published 36 articles in this field. Their research direction is mainly focused on the abnormality of QEEG in major depression and its rehabilitation by pharmacological treatments.

Research Hot Topics Based on Keyword Analysis

To reveal the hot topics in the research field, we used VOSviewer to produce a keyword co-occurrence map (see **Figure 6**). The keyword co-occurrence map retrieved five major keyword clusters of QEEG research in neuropsychiatric disorders. As shown in **Figure 5**, each keyword cluster is depicted in a distinct color. That is, the blue cluster represents research in attention-deficit hyperactivity disorder (ADHD), the yellow cluster represents research in neurodegenerative disorders, such as Alzheimer's disease, the green cluster represents research in epilepsy, the purple cluster represents research in traumatic brain injury and related cerebrovascular diseases, and the red cluster represents research in psychiatric disorders, such as major depressive disorder and schizophrenia. These five research areas are currently hot topics in the research field.

Knowledge Base by Cluster Analysis of Co-cited References

Co-cited references are co-cited articles in the reference lists of other articles. The co-citation network by CiteSpaceV revealed 1,067 nodes, 3,989 co-citation links, and 22 clusters. These clusters represented the knowledge base and networks of

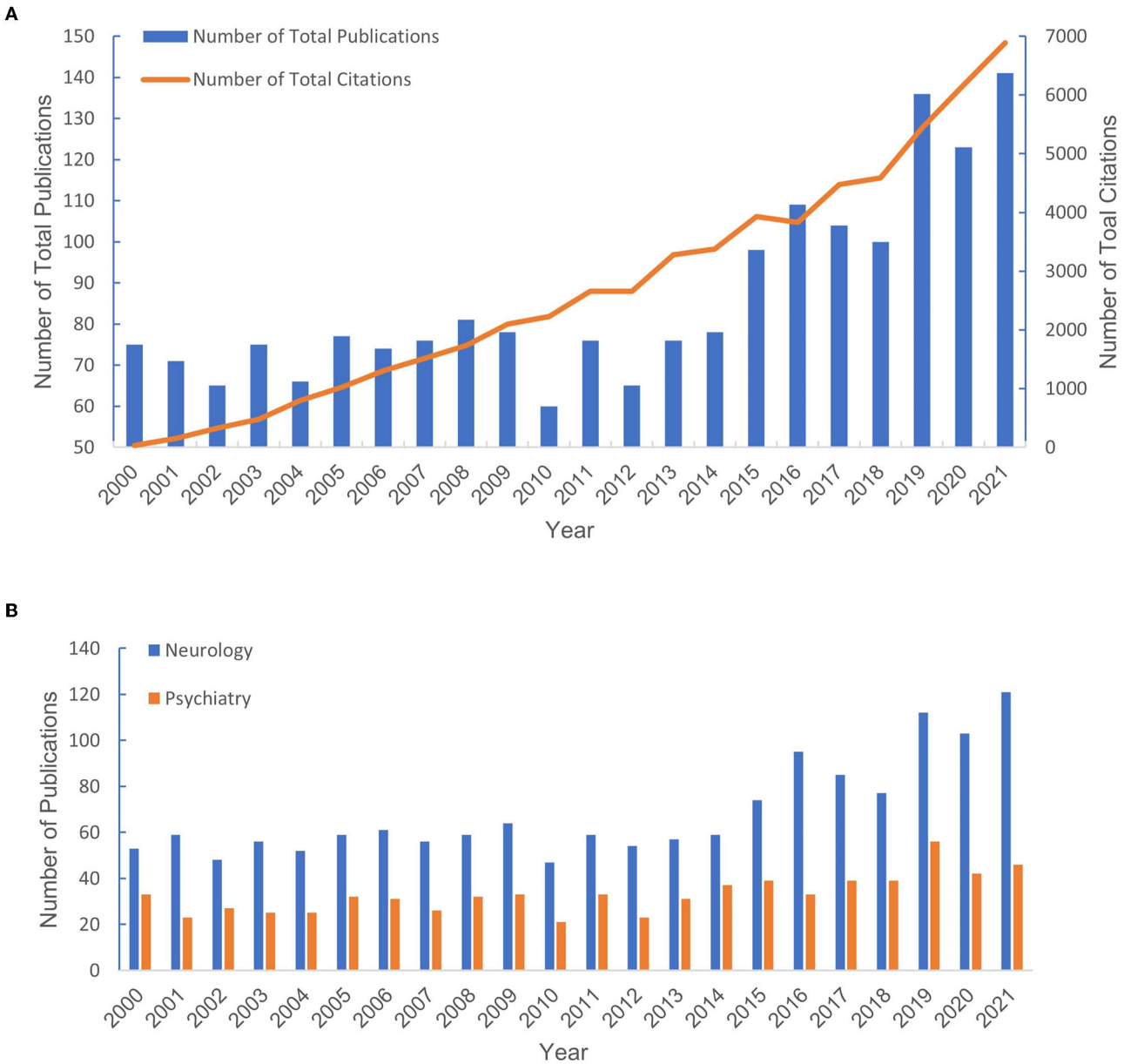

FIGURE 2 | The number of publications from 2000 to 2021. **(A)** The number of publications in neurology and psychiatry. **(B)** The total number of publications and the percentage of total publications.

QEEG studies in neuropsychiatric disorders. **Figure 6** shows all automatically extracted clusters. Each cluster is depicted with a unique color. The nodes in each cluster represent the co-cited documents, and the lines between the nodes represent the co-cited relationship. The labels of the clusters were extracted from the keywords of the citing publications, based on the latent semantic indexing (LSI) method. The general information about the co-citation clusters is summarized in **Table 3**, including the number of cited references, the average publication year of the cited references, and the silhouette value of each cluster. The silhouette value of a cluster ranges from 0 to 1, and a larger value indicated greater discrimination from other clusters (18). In addition, **Table 4** presented the research disease categories and domains retrieved from the co-cited reference clusters. **Supplementary Table S1** summarized highly co-cited references and the most relevant citing articles in each co-citation cluster.

Research Emerging Trends Based on Keyword Analysis

We also used VOSviewer to produce the overlay map to show the latest emerging topics (**Figure 7**). In VOSviewer, we set the threshold of occurrence frequency to 15, and 253 of the total 7,458 keywords met the criteria. Among

TABLE 1 | Top 10 countries and institutions with the highest number of publications from 2000 to 2021.

Rank	Country	Number of Publications	Centrality	Institution	Number of publications	Centrality
1	USA	657	0.95	Univ Calif Los Angeles (USA)	60	0.26
2	Germany	168	0.14	Sapienza University of Rome (Italy)	35	0.11
3	Italy	167	0.06	Univ Montreal (Canada)	34	0.09
4	Netherlands	118	0.02	Yale University (USA)	33	0.09
5	Canada	115	0.07	Massachusetts Gen Hospital (USA)	32	0.06
6	Australia	112	0.01	NYU(USA)	31	0.08
7	UK	107	0.09	University Sydney (Australia)	31	0.05
8	Switzerland	105	0.03	Harvard University (USA)	30	0.06
9	China	85	0.02	University Twente(Netherlands)	30	0.04
10	France	78	0.01	Columbia University (USA)	27	0.01

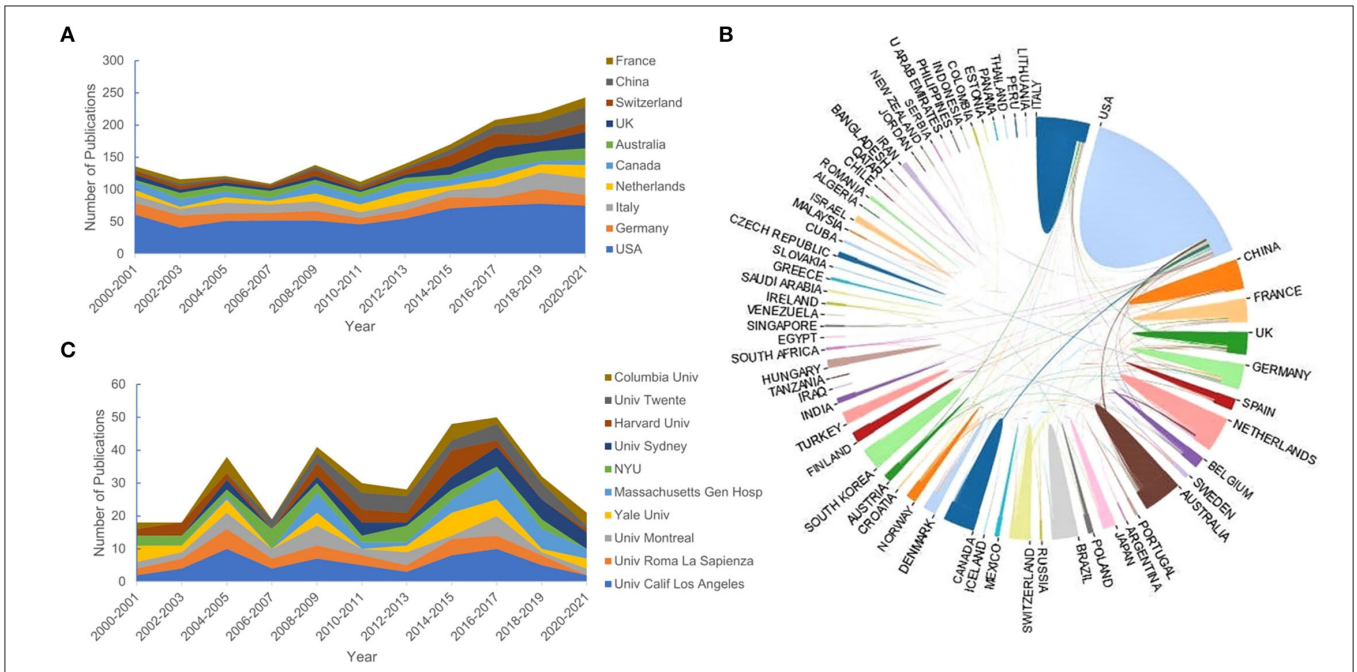

FIGURE 3 | The top 10 countries and institutions. **(A)** The number of publications of the top 10 countries. **(B)** The cooperative relationship between countries. **(C)** The number of publications of the top 10 institutions.

these keywords, "biomarker," "connectivity," and "machine learning" have emerged since 2018 and represented the future directions in QEEG studies in neuropsychiatric disorders. These emerging topics are depicted in yellow color in **Figure 7**.

DISCUSSION

General Information

The current study applied a visualized bibliometric method to analyze the research hot spots, the knowledge base, and

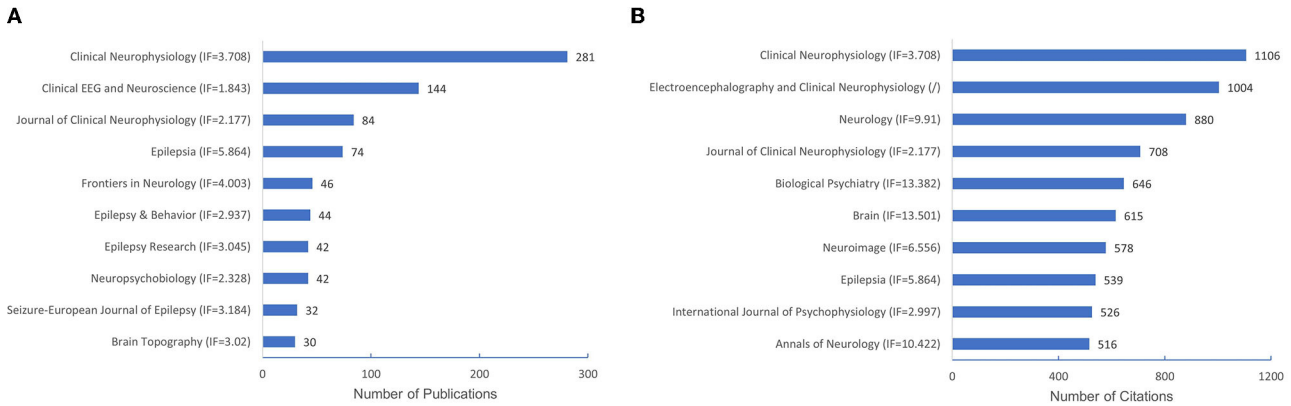

FIGURE 4 | The number of publications of the top 10 journals and co-cited journals. **(A)** The number of publications of the top 10 journals. **(B)** The number of citations of the top 10 co-cited journals.

TABLE 2 | Top 10 productive authors from 2000 to 2021.

Rank	Author	H-index	Country	Institution	Count	Citation count	Yearly average citation count
1	Cook IA	44	USA	University of California Los Angeles	36	1,464	67
2	Leuchter AF	43	USA	University of California Los Angeles	36	1,461	66
3	van Putten MJAM	16	Netherlands	University of Twente	29	1,067	49
4	Cagy M	2	-	Universidade Federal do Rio de Janeiro	26	199	9
5	Ribeiro P	-	-	-	26	208	9
6	Babiloni C	10	Italy	Sapienza University of Rome	25	905	41
7	Hunter AM	19	Scotland	University of Stirling	21	513	23
8	Piedade R	20	Brazil	Universidade Federal do Rio de Janeiro	21	183	8
9	Rossini PM	49	Italy	IRCCS San Raffaele Roma Rome	20	935	43
10	Del Percio C	41	Italy	Sapienza University of Rome	17	507	23

the emerging topics of the publications about QEEG in the neuropsychiatric research field. A total of 1,904 papers were collected based on 2000–2021 data from WoSCC. All papers were published by 2,433 institutions from 71 countries in 245 peer-reviewed journals with 57,237 co-cited references. The annual publication output and annual citation number revealed a steady growth in the research field. About 34.5% of the total publications were from the United States. Close cooperation between the United States, Canada, and Australia was found, suggesting their significant contribution to QEEG research in neuropsychiatric disorders. Among the 10 top institutions, 60% were from the United States, such as the University of California, Los Angeles, Yale University, Massachusetts General Hospital, New York University, Harvard University, and Columbia University. Among the top 10 authors, Cook IA and Leuchter AF published more studies and received higher co-citations, suggesting that their teams could be potential collaborators for researchers. Additionally, we found journals with high impact factors in our top 10 co-cited journals, such as Biological Psychiatry (IF = 13.382), Brain (IF = 13.501), and Annual of Neurology (IF = 10.422), which could be important sources of references.

Hot Topics of QEEG Research in the Neuropsychiatric Disorders

According to the keyword co-occurrence map by VOSviewer, five clusters were retrieved and represented five major categories of neuropsychiatric diseases in QEEG research. The blue cluster represented the psychiatric disorder "ADHD." ADHD is characterized by excessive restlessness and an extremely poor concentration span, resulting in impulsive and disruptive behavior. Bresnahan and Barry (19) suggested that QEEG might be used to differentiate ADHD adults from normal adults and adults who display the symptoms of ADHD without meeting the diagnostic criteria of ADHD. Elevated resting theta power and reduced alpha and beta power, together with elevated theta/alpha and theta/beta ratios, were found to be most reliably associated with ADHD (20, 21). Recently, novel measurements have emerged. For example, gamma power abnormalities might provide an opportunity to investigate the neurobiological mechanisms that underlie the clinical symptoms of ADHD (22–24).

The yellow cluster represented the neurodegeneration disorders, particularly Alzheimer's disease (AD) and Parkinson's disease (PD). Excessive slow wave activity has been shown in

TABLE 3 | Basic information of the co-cited reference clusters.

ID	Cluster name	Size	Avg (YR)	Silhouette
0	Mild cognitive impairment (mci)	108	2005	0.90
1	Attention deficit/hyperactivity disorder	79	2000	0.93
2	Cardiac arrest	78	2012	0.94
3	Theta/beta ratio	78	2011	0.92
4	Machine learning	65	2017	0.94
5	Nonconvulsive status epilepticus	57	2016	0.90
6	Depression	52	2008	0.97
7	Migraine	50	2006	1.00
8	schizophrenia	46	1997	0.93
9	Alzheimers disease	39	2000	0.98
10	Human immunodeficiency virus (hiv)	36	2011	0.98
11	Neurofeedback	34	2008	0.95
12	Cordance	32	1999	0.95
13	Seizure anticipation	32	1998	0.99
14	Biomarker	29	2015	0.99
15	Seizure detection	16	2015	1.00
16	Dysplasia focal cortical	12	1996	1.00
17	Stereo-eeg	11	2014	1.00
20	Methylphenidate	9	2014	0.99
21	Caffeine	8	1996	1.00
24	Obstructive sleep apnea	7	2017	1.00
29	Peri-/intraventricular hemorrhage (pivh)	5	2008	0.99

Size, number of publications in the cluster; Avg (YR), the average publication year of the references in the cluster.

TABLE 4 | Research disease categories and domains retrieved from the co-cited reference clusters.

General disease category	Disease	Pathology	Diagnosis	Treatment
Cerebrovascular diseases	Ischemic stroke		Cluster 2 cardiac arrest Cluster 7 migraine	Cluster2 cardiac arrest Cluster7 migraine
	Intracerebral hemorrhage		Cluster 29 peri-/intraventricular hemorrhage (pivh)	
Neurodegenerative diseases	Epilepsy	Cluster 17 stereo-eeg Cluster 16 dysplasia focal cortical Cluster 13 seizure anticipation	Cluster 5 nonconvulsive status epilepticus Cluster 15 seizure detection	Cluster 16 dysplasia focal cortical Cluster 15 seizure detection
	Alzheimer's disease	Cluster 8 schizophrenia Cluster 10 human immunodeficiency virus (hiv)	Cluster 0 mild cognitive impairment (mci) Cluster 9 alzheimer's disease	
	Parkinson's disease		Cluster 4 machine learning	Cluster 4 machine learning
Mental disorders	Attention-deficit/hyperactivity disorder	Cluster 1 attention deficit/hyperactivity disorder	Cluster 1 attention deficit/hyperactivity disorder Cluster 3theta/beta ratio	Cluster 11 neurofeedback Cluster 20 methylphenidate
	Depression			Cluster 6 depression Cluster 12 cordance Cluster 14 biomarker
Other	Substance abuse	Cluster 21 caffeine		
	Obstructive sleep apnea	Cluster 24 obstructive sleep apnea		

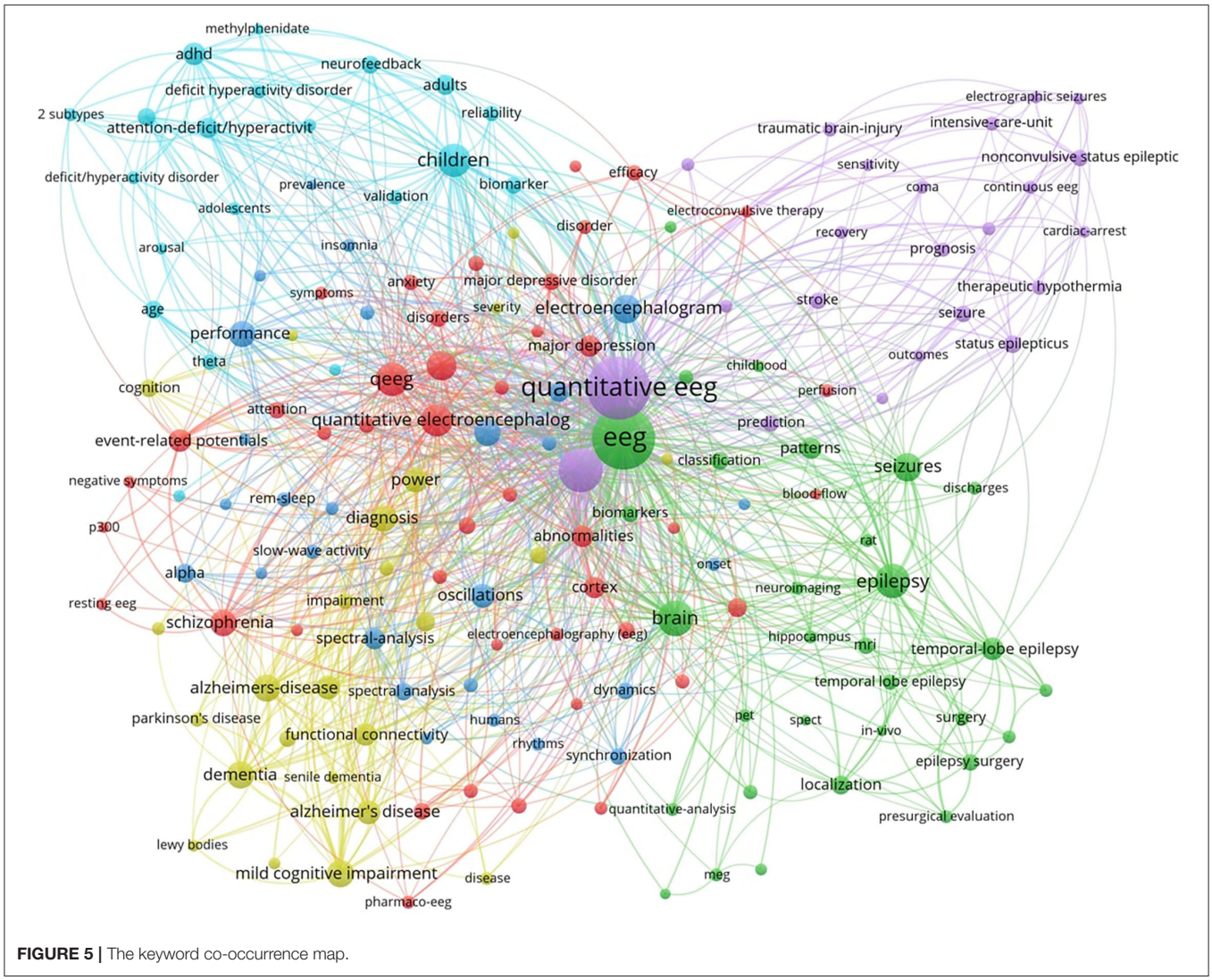

FIGURE 5 | The keyword co-occurrence map.

dementia of the Alzheimer's type that increases with disease progression (25). Compared to AD, the inter-hemispheric coherence values for the delta and theta bands in the fronto-temporo-central regions were higher in dementia with Lewy bodies (DLB). For patients with AD, the beta band was lower than DLB in almost all temporo-centro-parieto-occipital regions (26). Additionally, in patients with PD, abnormalities in QEEG, such as an increase in posterior theta power, were found with the occurrence of mild cognitive impairment or dementia (27). QEEG could also provide reliable biomarkers for objective monitoring of disease severity and progression in PD, as well as for promoting early diagnosis of nonmotor symptoms (28). For example, decreased dominant frequency and increased theta power, which reflect EEG slowing, were biomarkers of cognitive deterioration.

The green cluster represented "epilepsy" and "seizure," which included the temporal lobe epilepsy, electroconvulsive-induced epilepsy, and so on. Larsson and colleagues showed that peak alpha frequency (PAF) variability was compromised in patients with epilepsy (29). Park et al. suggested that the automatic quantitative ictal high-gamma oscillation analysis may be effective in delineating the epileptogenic zone (30). QEEG background activity may also provide useful information on seizure duration. A higher theta power ratio in the temporal region contralateral to the epileptic focus may suggest a longer epilepsy duration (31).

The purple cluster represented traumatic brain injury (TBI) and related cerebrovascular diseases, such as stroke and subarachnoid hemorrhage (SAH). QEEG might predict the prognosis after TBI. In particular, measures of alpha power and variability were indicative of relatively better functional outcomes within the first year after TBI. This was hypothesized to reflect intact thalamo-cortical loops and thus the potential for recovery of consciousness even in the apparent absence of current consciousness (32). QEEG can also be used to identify patients at risk of cerebral infarction. In patients with SAH, there was a moderate correlation between transcranial Doppler/color-coded duplex sonography (TCD/TCCS) frequencies and QEEG alpha

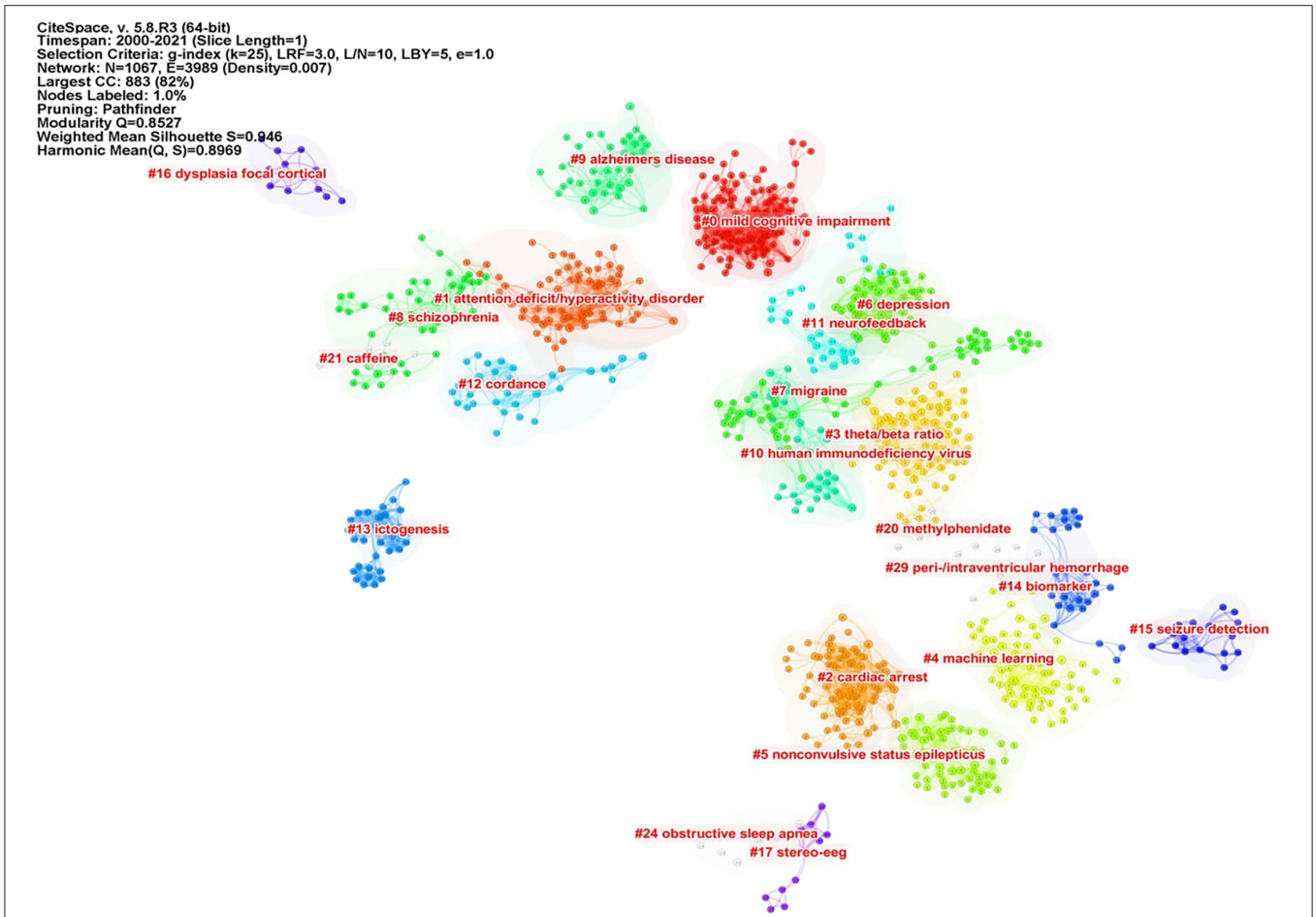

FIGURE 6 | Cluster analysis of co-cited references.

power reduction, but only QEEG could differentiate patients with and without cerebral infarction (33). Moreover, worsening alpha/delta ratio (ADR) on QEEG was a reliable predictor of delayed cerebral ischemia (DCI) in patients with aneurysmal SAH. Further studies are still needed to confirm the role of QEEG in the prediction of DCI (34).

The red cluster consisted of QEEG studies in several common psychiatric disorders, including major depressive disorder (MDD), anxiety, and schizophrenia (35, 36). Delta power values could be potentially used in the differential diagnosis between schizophrenia and depression. In patients with MDD, delta power over Fp1, Fp2, F4, and F8 regions was lower in comparison to schizophrenia patients (37). Impaired development of a resting-state brain network in adolescents with MDD may represent an intermediate phenotype that can be assessed with QEEG. Youth with MDD showed decreased resting connectivity in the alpha and theta frequency bands, particularly in the frontal cortex (38). In addition, Moon et. al found increased overall absolute delta power and relative gamma power as potential markers that could differentiate post-traumatic stress disorder (PTSD) from anxiety disorders (39).

Knowledge Base of QEEG Research in the Neuropsychiatric Field

To better clarify the knowledge base of QEEG research in the neuropsychiatric field, we analyzed the cited literature and the citing literature in each co-citation cluster (**Figure 6** and **Table 3**). A total of 22 clusters were extracted by CiteSpace through co-cited references analysis. These co-citation reference clusters could be classified into three disease categories: neurodegenerative diseases, cerebrovascular diseases, and mental disorders (**Table 4**). In these three disease categories, QEEG has been applied to investigate the pathological mechanisms, assist clinical diagnosis, and promote the selection of appropriate treatments. The most relevant co-cited articles and citing articles are listed in **Supplementary Table S1**.

In chronic neurodegenerative diseases, the majority of QEEG research is about Alzheimer's disease (AD) and Parkinson's disease (PD). In AD research, QEEG was mainly used to explore the pathology and diagnosis of AD. In the study of pathological mechanisms underlying AD, cluster 8 "schizophrenia" showed that there were similar QEEG characteristics between AD and schizophrenia (40–42) and

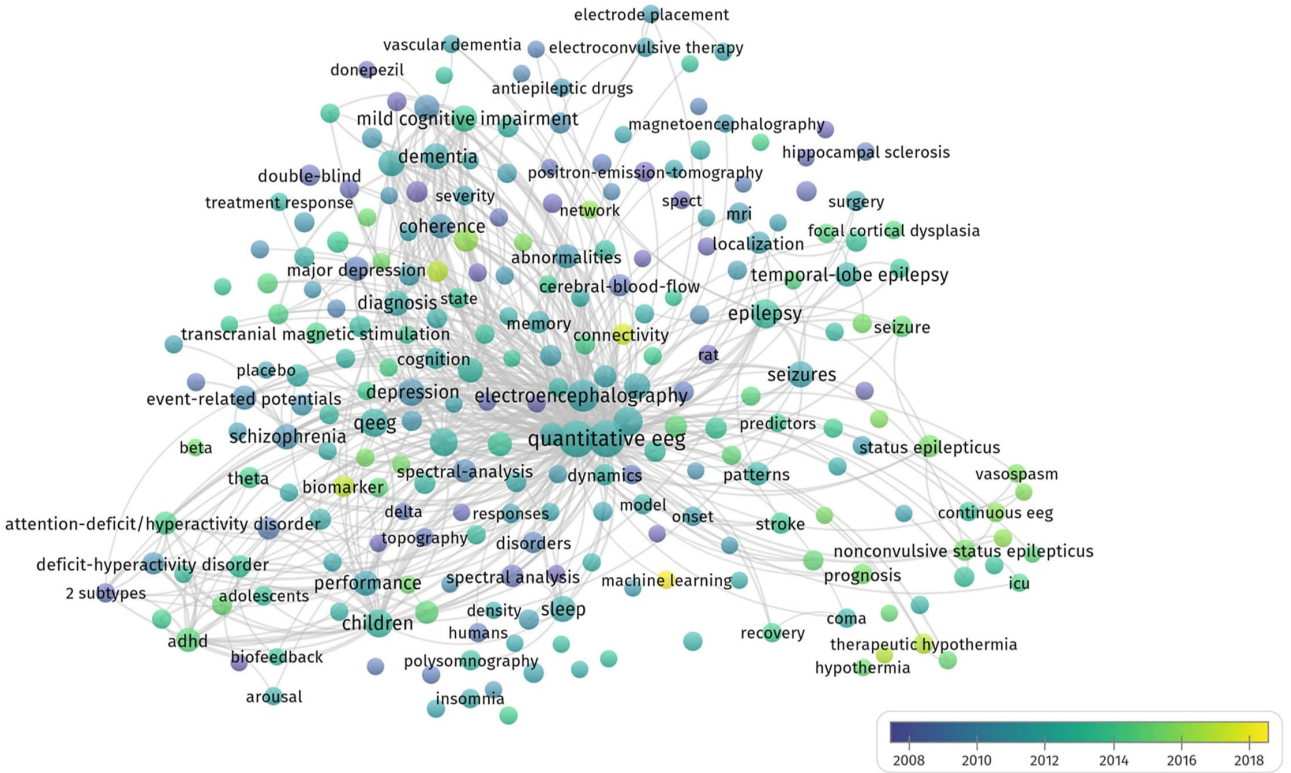

FIGURE 7 | The overlay map.

that schizophrenia was associated with an elevated risk of developing AD (43), which suggested that the pathological mechanisms of these two diseases may be related. The co-cited references of cluster 10 "human immunodeficiency virus (HIV)" indicated that cortical source mapping by low-resolution brain electromagnetic source tomography (LORETA) of resting state EEG rhythms could characterize neurodegenerative disorders-induced cognitive impairment, such as Parkinson's disease related dementia (PDD) and Alzheimer's disease (AD) (44, 45), while the citing documents in this cluster showed that HIV research also applied LORETA in evaluating the cognitive functions in patients with HIV (46, 47). In the study of AD diagnosis, cluster 9 "Alzheimer's disease" indicated that QEEG can accurately differentiate the stage of AD (48–51). Cluster 0 "mild cognitive impairment (MCI)" suggested that QEEG was a valuable tool for the early diagnosis of AD (52–56). For PD patients (co-cited references of cluster 4 "machine learning" indicated that QEEG could provide reliable biomarkers for nonmotor symptom severity and progression (28, 57). Besides, the citing articles in this cluster pointed out that preoperative QEEG biomarkers could predict cognitive deterioration of PD after subthalamic deep brain stimulation with high accuracy by using a machine learning pipeline (58, 59).

In the study of acute neurodegenerative diseases, QEEG was also an important method to study epilepsy pathology, epilepsy prediction, epilepsy detection, and epilepsy treatment. In the research of pathological mechanisms of epilepsy, co-cited references of cluster 17 "stereo eeg" demonstrated that QEEG could be used to explore the desynchronization and synchronous discharge of neurons in different stages of epilepsy (60, 61). The citing literature of this cluster showed that quantitative stereo EEG could be used to analyze the inhibitory and promoting factors of seizures in inter-ictal period (62, 63). Based on the hypersynchronization hypothesis of epileptic seizures, cluster 13 "seizure anticipation" found that the trend of abnormal synchronization of neurons can be detected by QEEG nonlinear analysis to predict epileptic seizures (64–66). In terms of epilepsy detection, the co-cited literature of cluster 5 "nonconvulsive status epilepticus" showed that the use of QEEG could accurately diagnose epilepsy (67–69), and the citing literature of this cluster showed that QEEG could also be used to monitor nonconvulsive status epilepticus (70). In addition, cluster 15 "seizure detection" showed that QEEG combined with quantitative electromyography (EMG) can identify the characteristics of different epileptic subtypes (71, 72). In terms of epilepsy treatment, citing articles of cluster 16 "dysplasia focal cortical" indicated that the QEEG index can provide a reliable basis for determining epileptic focus before the surgical treatment of focal epilepsy (73), and the co-cited documents in this cluster proved that QEEG index could accurately predict the surgical prognosis of epilepsy (74, 75). Cluster 15 also showed that QEEG could help to predict and prevent sudden unexpected death in epilepsy (SUDEP) (76, 77).

In cerebrovascular diseases, according to the co-cited literature of cluster 2 "cardiac arrest" (CA) and cluster 7 "migraine," EEG signals mainly come from the activities of pyramidal cells in the cerebral cortex, which are vulnerable to cerebral ischemia (78), so QEEG is suitable for detecting abnormal neural activities of ischemic stroke (IS) and evaluating the IS prognosis (79–81). The study of EEG characteristics of cerebral ischemia is also helpful to investigate other related diseases. Citing documents of cluster 2 suggested that cardiac arrest would cause secondary ischemic stroke. Therefore, even if cardiopulmonary resuscitation is successfully accepted, patients may have neurological sequelae. QEEG index can reflect brain activity in real time and assist doctors to judge the prognosis of patients with CA and take corresponding treatment in time (82, 83). The citing literature of cluster 7 showed that because migraine and ischemic stroke have similar EEG characteristics, it was speculated that the change in cerebral blood activity may be one of the manifestations of migraine (84, 85). In addition, according to cluster 29 "peri-/intraventricular hemorrhage (PIVH)," QEEG has also been used in the early diagnosis of intracerebral hemorrhage in premature infants in recent years (86–89). In brief, the knowledge base of QEEG in cerebrovascular diseases is mainly about monitoring and treating the abnormal brain functions related to cerebrovascular disease by using QEEG.

In the studies related to mental disorders, attention-deficit hyperactivity disorder (ADHD) and depression are two major application fields of QEEG. The cited and citing literature in cluster 1 "attention-deficit hyperactivity disorder" included various types of QEEG studies on ADHD, including the use of QEEG to study the etiology, diagnostic biomarkers, prognostic biomarkers, and add-on treatment of ADHD (20, 52, 86–93). First, the literature of cluster 1 indicated that QEEG could verify different etiological hypotheses of ADHD (90). Second, cluster 1 also denoted that QEEG could accurately judge the abnormal brain activities associated with ADHD (20, 93), and cluster 3 "theta/beta ratio" indicated that theta/beta ratio might be used as an index to identify ADHD subtypes (21, 94, 95). Third, the literature in cluster 20 "methylphenidate" mainly used the QEEG index to evaluate the efficacy of different drugs in the treatment of ADHD (96–98). Among them, methylphenidate has been proven to be a drug that can effectively alleviate the symptoms of ADHD (97, 98). Finally, it is particularly noteworthy that ADHD is the major application field of neurofeedback therapy. Cluster 11 "neurofeedback" showed that many studies have proved that neurofeedback therapy can effectively treat ADHD (54, 99–102), particularly when targeted, personalized neurofeedback treatment was applied (102). Moreover, the co-cited references of cluster 20 also showed the long-term efficacy of neurofeedback in the treatment of ADHD (103, 104). Therefore, the application of QEEG in the field of ADHD has a relatively good research foundation.

For the knowledge base of QEEG studies in other mental disorders, most studies on depression focused on evaluating the efficacy of antidepressants with QEEG indicators. The citing literature of cluster 6 "depression" (105, 106) and the co-cited literature in cluster 14 "biomarker" (107, 108) suggested that there may be methodological differences among studies and a lack of replications in this research area, so there is still no widely recognized QEEG index that can accurately predict the efficacy of antidepressants. Particularly, on the one hand, the co-cited literature in cluster 12 "cordance" suggested that cordance, a QEEG index that can comprehensively analyze relative EEG power and absolute EEG power and highlight the brain pathological activities (109), has not been able to predict the efficacy of antidepressants (110–112). On the other hand, the co-cited literature in cluster 6 (113–115) and the citing literature from cluster 12 (80, 116) showed that prefrontal theta cordance has the value of predicting the response of antidepressants, which indicated that the cordance index still has the potential for further research. Moreover, citing articles of cluster 14 argued that researchers can try using machine learning to explore QEEG biomarkers for evaluating the efficacy of antidepressants (117, 118).

Caffeine withdrawal response and sleep disorder are the remaining two clusters identified by CiteSpace, suggesting wide applications of QEEG in the neuropsychiatric field. The literature in cluster 21 "caffeine" showed that QEEG can be used to study the neural mechanism underlying the withdrawal response to drugs, such as caffeine and cocaine (119, 120). Cluster 24 "obstructive sleep apnea (OSA)" suggested that QEEG during sleep could help to reveal the pathological mechanism of OSA, while awake QEEG could evaluate the impact of OSA on cognitive functions (118, 121, 122).

Emerging Trends and Future Direction of QEEG Research in Neuropsychiatric Disorders

Overlay visualization presented the time of emergence of the keywords and reflected the latest and emerging research topics. From the overlay map shown in **Figure 7**, we can see that the recently searched keywords are shown by yellow nodes. The emerging keywords were "biomarker," "connectivity," and "machine learning."

As for QEEG biomarker research, recent studies started to cross-validate the prognostic value of previously suggested EEG biomarkers in larger independent datasets, since an increasing number of QEEG biomarkers in neuropsychiatric disorders were revealed in prior studies. For example, Ip and colleagues showed that alpha asymmetry seems to be the most promising EEG biomarker for the prediction of treatment response in women with MDD in comparison to alpha power, delta and theta activity at the anterior cingulate cortex (ACC) (123). Moreover, new QEEG biomarkers have also been investigated. Interictal high-frequency oscillation and modulation index have been found to improve the prediction accuracy of post-operative seizure outcomes (124).

QEEG-based functional connectivity has also been investigated in recent years as a diagnostic tool to predict the symptom severity of neuropsychiatric disorders. EEG functional connectivity has shown promising results as a diagnostic tool for AD. Similarly, in Down syndrome (DS) with Alzheimer's dementia, decreased alpha and increased delta coherence and

weighted phase lag index were observed when compared to DS (125). EEG functional connectivity and complexity were used to predict depression severity among depressive patients. A significant negative relationship was found between graph metrics (i.e., degree and clustering coefficient) and depression severity in the alpha band, while the EEG complexity measures in alpha and delta bands by the nonlinear analysis were positively associated with symptom severity (126).

Another breakthrough is QEEG-based machine learning studies. Through machine learning, a compound of automatically extracted EEG biomarkers differentiated good vs. poor cognitive function of PD patients with higher accuracy than a single spectral EEG feature (58). More QEEG biomarkers (e.g., coherence, spectral, and event-related potentials) should be investigated and combined with machine learning or deep learning methods to predict the occurrence, severity, and treatment response for neuropsychiatric disorders.

Strengths and Limitations

Our bibliometric study has several strengths. First of all, it is the first study to use the scientometric method to summarize the research history and development trends of QEEG studies in the neuropsychiatric field. It included the most comprehensive analysis, covering nearly all aspects of previous publications, and provided valuable information to QEEG researchers and helped them gain a better insight into the evolving research foci and trends. However, our study was also subjective to several limitations. First, the data come merely from WoSCC, and other databases, such as Embase or PubMed, were not searched, and hence this study may not completely represent all QEEG data. But notably, WoSCC is the most frequently used database for scientometric research. Second, the retrieved articles were restricted to those published in English, resulting in some linguistic bias.

CONCLUSION

The present study performed a bibliometric analysis of the overall scientific output of QEEG research in the neuropsychiatric field from 2000 to 2021. During the last two decades, QEEG has been applied to reveal the pathological mechanisms, assist clinical diagnosis, and promote the selection of effective treatments for a variety of neuropsychiatric diseases, including neurodegenerative diseases, cerebrovascular diseases, and mental diseases. Studies in these disease categories and domains added to the knowledge base of this research field. The hot topics of research included five major neuropsychiatric disorders, including ADHD, neurodegenerative disorders like Alzheimer's and Parkinson's disease, traumatic brain injury and related cerebrovascular diseases, epilepsy and seizure, and other psychiatric diseases, such as MDD and schizophrenia. Besides, future studies should focus on cross-validating promising QEEG biomarkers, developing new biomarkers (e.g, functional connectivity and complexity), and extracting biomarkers by machine learning.

AUTHOR CONTRIBUTIONS

SY and JZ contributed equally to the analysis of the data and wrote the manuscript. SL collected the bibliometric data and prepared the figures. RZ interpreted the data and revised the manuscript. JZ revised the manuscript. XY and YW designed the study, interpreted the data, and revised the manuscript. All authors contributed to the article and approved the submitted version.

FUNDING

This study was funded by the National Natural Science Foundation of China (grant nos: 31800928 and 72174082), Guangdong Provincial Philosophy and Social Sciences 13th Five-Year Plan Co-construction Project (grant no: GD18XXL04), and Guangzhou Philosophy and Social Sciences Development 13th Five-Year Plan Young Scholar Project of City of Rams (grant no: 2020GZQN42). Innovation and Entrepreneurship Training Program for College Students (project no: S202012121176).

ACKNOWLEDGMENTS

We would like to thank Yabin Tang from Southern Medical University for grammar revision.

SUPPLEMENTARY MATERIAL

The Supplementary Material for this article can be found online at: https://www.frontiersin.org/articles/10.3389/fpsyt.2022.830819/full#supplementary-material

REFERENCES

1. Paul K, Dittrichova J. The process of falling asleep in infancy [proceedings]. *Act Nerv Super (Praha)*. (1977) 19:272–3.
2. Huang X, Fan X, Ying J, Chen S. Emerging trends and research foci in gastrointestinal microbiome. *J Transl Med*. (2019) 17:67. doi: 10.1186/s12967-019-1810-x
3. Berger H. Über das Elektrenkephalog".ramm des Menschen. *Archiv für Psychiatrie und Nervenkrankheiten*. (1929) 87:527–70. doi: 10.1007/BF01797193
4. Mari-Acevedo J, Yelvington K, Tatum WO. Chapter 9 - Normal EEG variants. In: Levin KH, Chauvel P, editors. *Handb Clin Neurol. Vol 160*. Amsterdam: Elsevier (2019). p. 143–60. doi: 10.1016/B978-0-444-64032-1.00009-6
5. Okumura A. Chapter 8-electroencephalography in children with acute encephalitis/encephalopathy. In: Yamanouchi H, Moshé SL, Okumura A, editors. *Acute Encephalopathy and Encephalitis in Infancy and Its Related Disorders*. Missouri: Elsevier (2018). p. 63–70. doi: 10.1016/B978-0-323-53088-0.00008-7
6. Bailey T. Chapter thirteen-diagnosing and treating developmental disorders with qEEG and neurotherapy. In: Cantor DS, Evans JR, editors. *Clinical Neurotherapy*. Boston, MA: Academic Press (2014). p. 321–55.
7. Johnstone J, Lunt J. Chapter 1-use of quantitative EEG to Predict therapeutic outcome in neuropsychiatric disorders. In: Coben R, Evans JR, editors. *Neurofeedback and Neuromodulation Techniques and Applications*. San Diego, CA: Academic Press (2011). p. 3–23.
8. Nuwer M. Assessment of digital EEG, quantitative EEG, and EEG brain mapping: report of the American Academy of Neurology and the

American Clinical Neurophysiology Society. *Neurology.* (1997) 49:277–92. doi: 10.1212/WNL.49.1.277
9. Nuwer MR. Quantitative EEG: I. Techniques and problems of frequency analysis and topographic mapping. *J Clin Neurophysiol.* (1988) 5:1–43. doi: 10.1097/00004691-198801000-00001
10. Nuwer MR. Quantitative EEG: II. Frequency analysis and topographic mapping in clinical settings. *J Clin Neurophysiol.* (1988) 5:45–85. doi: 10.1097/00004691-198801000-00002
11. Livint Popa L, Dragos H, Pantelemon C, Verisezan Rosu O, Strilciuc S. The role of quantitative EEG in the diagnosis of neuropsychiatric disorders. *J Med Life.* (2020) 13:8–15. doi: 10.25122/jml-2019-0085
12. McVoy M, Lytle S, Fulchiero E, Aebi ME, Adeleye O, Sajatovic M. A systematic review of quantitative EEG as a possible biomarker in child psychiatric disorders. *Psychiatry Res.* (2019) 279:331–44. doi: 10.1016/j.psychres.2019.07.004
13. Smailovic U, Jelic V. Neurophysiological markers of Alzheimer's disease: quantitative EEG approach. *Neurol Ther.* (2019) 8(Suppl. 2):37–55. doi: 10.1007/s40120-019-00169-0
14. Wang X, Xu Z, Su S-F, Zhou W. A comprehensive bibliometric analysis of uncertain group decision making from 1980 to 2019. *Inf Sci.* (2021) 547:328–53. doi: 10.1016/j.ins.2020.08.036
15. Chen C, Lou Y, Li X-Y, Lv Z-T, Zhang L-Q, Mao W. Mapping current research and identifying hotspots on mesenchymal stem cells in cardiovascular disease. *Stem Cell Res Ther.* (2020) 11:498. doi: 10.1186/s13287-020-02009-7
16. Guo Y-M, Huang Z-L, Guo J, Guo X-R, Li H, Liu M-Y, et al. A bibliometric analysis and visualization of blockchain. *Future Generat Comput Syst.* (2021) 116:316–32. doi: 10.1016/j.future.2020.10.023
17. Bertoglio R, Corbo C, Renga F, Matteucci M. The digital agricultural revolution: a bibliometric analysis literature review. *IEEE Access.* (2021) 9:134762–82. doi: 10.1109/ACCESS.2021.3115258
18. Rousseeuw PJ. Silhouettes: a graphical aid to the interpretation and validation of cluster analysis. *J Comput Appl Math.* (1987) 20:53–65. doi: 10.1016/0377-0427(87)90125-7
19. Bresnahan SM, Barry RJ. Specificity of quantitative EEG analysis in adults with attention deficit hyperactivity disorder. *Psychiatry Res.* (2002) 112:133–44. doi: 10.1016/S0165-1781(02)00190-7
20. Barry RJ, Clarke AR, Johnstone SJ. A review of electrophysiology in attention-deficit/hyperactivity disorder: I. Qualitative and quantitative electroencephalography. *Clin Neurophysiol.* (2003) 114:171–83. doi: 10.1016/S1388-2457(02)00362-0
21. Ogrim G, Kropotov J, Hestad K. The quantitative EEG theta/beta ratio in attention deficit/hyperactivity disorder and normal controls: sensitivity, specificity, and behavioral correlates. *Psychiatry Res.* (2012) 198:482–8. doi: 10.1016/j.psychres.2011.12.041
22. Tombor L, Kakuszi B, Papp S, Réthelyi J, Bitter I, Czobor P. Decreased resting gamma activity in adult attention deficit/hyperactivity disorder. *World J Biol Psychiatry.* (2019) 20:691–702. doi: 10.1080/15622975.2018.1441547
23. Liao YC, Guo NW, Su BY, Chen SJ, Tsai HF, Lee KY. Frontal beta activity in the meta-intention of children with attention deficit hyperactivity disorder. *Clin EEG Neurosci.* (2021) 52:136–43. doi: 10.1177/1550059420933142
24. Müller A, Vetsch S, Pershin I, Candrian G, Baschera GM, Kropotov JD, et al. EEG/ERP-based biomarker/neuroalgorithms in adults with ADHD: development, reliability, and application in clinical practice. *World J Biol Psychiatry.* (2020) 21:172–82. doi: 10.1080/15622975.2019.1605198
25. Knott V, Mohr E, Mahoney C, Ilivitsky V. Quantitative electroencephalography in Alzheimer's disease: comparison with a control group, population norms and mental status. *J Psychiatry Neurosci.* (2001) 26:106–16.
26. Kai T, Asai Y, Sakuma K, Koeda T, Nakashima K. Quantitative electroencephalogram analysis in dementia with Lewy bodies and Alzheimer's disease. *J Neurol Sci.* (2005) 237:89–95. doi: 10.1016/j.jns.2005.05.017
27. Fonseca LC, Tedrus GM, Letro GH, Bossoni AS. Dementia, mild cognitive impairment and quantitative EEG in patients with Parkinson's disease. *Clin EEG Neurosci.* (2009) 40:168–72. doi: 10.1177/155005940904000309
28. Geraedts VJ, Boon LI, Marinus J, Gouw AA, van Hilten JJ, Stam CJ, et al. Clinical correlates of quantitative EEG in Parkinson disease: a systematic review. *Neurology.* (2018) 91:871–83. doi: 10.1212/WNL.0000000000006473
29. Larsson PG, Kostov H. Lower frequency variability in the alpha activity in EEG among patients with epilepsy. *Clin Neurophysiol.* (2005) 116:2701–6. doi: 10.1016/j.clinph.2005.07.019
30. Park SC, Lee SK, Che H, Chung CK. Ictal high-gamma oscillation (60-99 Hz) in intracranial electroencephalography and postoperative seizure outcome in neocortical epilepsy. *Clin Neurophysiol.* (2012) 123:1100–10. doi: 10.1016/j.clinph.2012.01.008
31. Fonseca E, Quintana M, Seijo-Raposo I, Ortiz de Zárate Z, Abraira L, Santamarina E, et al. Interictal brain activity changes in temporal lobe epilepsy: a quantitative electroencephalogram analysis. *Acta Neurol Scand.* (2022) 145:239–48. doi: 10.1111/ane.13543
32. Pauli R, O'Donnell A, Cruse D. Resting-State electroencephalography for prognosis in disorders of consciousness follocluster traumatic brain injury. *Front Neurol.* (2020) 11:586945. doi: 10.3389/fneur.2020.586945
33. Mueller TM, Gollwitzer S, Hopfengärtner R, Rampp S, Lang JD, Stritzelberger J, et al. Alpha power decrease in quantitative EEG detects development of cerebral infarction after subarachnoid hemorrhage early. *Clin Neurophysiol.* (2021) 132:1283–9. doi: 10.1016/j.clinph.2021.03.005
34. Yu Z, Wen D, Zheng J, Guo R, Li H, You C, et al. Predictive accuracy of alpha-delta ratio on quantitative electroencephalography for delayed cerebral ischemia in patients with aneurysmal subarachnoid hemorrhage: meta-analysis. *World Neurosurg.* (2019) 126:e510–6. doi: 10.1016/j.wneu.2019.02.082
35. Grin-Yatsenko VA, Ponomarev VA, Pronina MV, Poliakov YI, Plotnikova IV, Kropotov JD. Local and widely distributed EEG activity in schizophrenia with prevalence of negative symptoms. *Clin EEG Neurosci.* (2017) 48:307–15. doi: 10.1177/1550059416683283
36. Grin-Yatsenko VA, Baas I, Ponomarev VA, Kropotov JD. EEG power spectra at early stages of depressive disorders. *J Clin Neurophysiol.* (2009) 26:401–6. doi: 10.1097/WNP.0b013e3181c298fe
37. Begić D, Popović-Knapić V, Grubišin J, Kosanović-Rajačić B, Filipčić I, Telarović I, et al. Quantitative electroencephalography in schizophrenia and depression. *Psychiatr Danub.* (2011) 23:355–62.
38. McVoy M, Aebi ME, Loparo K, Lytle S, Morris A, Woods N, et al. Resting-state quantitative electroencephalography demonstrates differential connectivity in adolescents with major depressive disorder. *J Child Adolesc Psychopharmacol.* (2019) 29:370–7. doi: 10.1089/cap.2018.0166
39. Moon SY, Choi YB, Jung HK, Lee YI, Choi SH. Increased frontal gamma and posterior delta powers as potential neurophysiological correlates differentiating posttraumatic stress disorder from anxiety disorders. *Psychiatry Investig.* (2018) 15:1087–93. doi: 10.30773/pi.2018.09.30
40. Chiaramonti R, Muscas GC, Paganini M, Müller TJ, Fallgatter AJ, Versari A, et al. Correlations of topographical EEG features with clinical severity in mild and moderate dementia of Alzheimer type. *Neuropsychobiology.* (1997) 36:153–8. doi: 10.1159/000119375
41. Pascual-Marqui RD, Lehmann D, Koenig T, Kochi K, Merlo MC, Hell D, et al. Low resolution brain electromagnetic tomography (LORETA) functional imaging in acute, neuroleptic-naive, first-episode, productive schizophrenia. *Psychiatry Res.* (1999) 90:169–79. doi: 10.1016/S0925-4927(99)00013-X
42. Wienbruch C, Moratti S, Elbert T, Vogel U, Fehr T, Kissler J, et al. Source distribution of neuromagnetic slow wave activity in schizophrenic and depressive patients. *Clin Neurophysiol.* (2003) 114:2052–60. doi: 10.1016/S1388-2457(03)00210-4
43. Kochunov P, Zavaliangos-Petropulu A, Jahanshad N, Thompson PM, Ryan MC, Chiappelli J, et al. A white matter connection of schizophrenia and Alzheimer's disease. *Schizophr Bull.* (2021) 47:197–206. doi: 10.1093/schbul/sbaa078
44. Caviness JN, Hentz JG, Belden CM, Shill HA, Driver-Dunckley ED, Sabbagh MN, et al. Longitudinal EEG changes correlate with cognitive measure deterioration in Parkinson's disease. *J Parkinsons Dis.* (2015) 5:117–24. doi: 10.3233/JPD-140480
45. Babiloni C, De Pandis MF, Vecchio F, Buffo P, Sorpresi F, Frisoni GB, et al. Cortical sources of resting state electroencephalographic rhythms in Parkinson's disease related dementia and Alzheimer's disease. *Clin Neurophysiol.* (2011) 122:2355–64. doi: 10.1016/j.clinph.2011.03.029
46. Babiloni C, Pennica A, Del Percio C, Noce G, Cordone S, Muratori C, et al. Abnormal cortical sources of resting state electroencephalographic rhythms

in single treatment-naïve HIV individuals: a statistical z-score index. *Clin Neurophysiol.* (2016) 127:1803–12. doi: 10.1016/j.clinph.2015.12.007
47. Babiloni C, Buffo P, Vecchio F, Onorati P, Muratori C, Ferracuti S, et al. Cortical sources of resting-state EEG rhythms in "experienced" HIV subjects under antiretroviral therapy. *Clin Neurophysiol.* (2014) 125:1792–802. doi: 10.1016/j.clinph.2014.01.024
48. Wolf H, Jelic V, Gertz HJ, Nordberg A, Julin P, Wahlund LO. A critical discussion of the role of neuroimaging in mild cognitive impairment. *Acta Neurol Scand Suppl.* (2003) 179:52–76. doi: 10.1034/j.1600-0404.107.s179.10.x
49. Huang C, Wahlund L, Dierks T, Julin P, Winblad B, Jelic V. Discrimination of Alzheimer's disease and mild cognitive impairment by equivalent EEG sources: a cross-sectional and longitudinal study. *Clin Neurophysiol.* (2000) 111:1961–7. doi: 10.1016/S1388-2457(00)00454-5
50. Rodriguez G, Copello F, Vitali P, Perego G, Nobili F. EEG spectral profile to stage Alzheimer's disease. *Clin Neurophysiol.* (1999) 110:1831–7. doi: 10.1016/S1388-2457(99)00123-6
51. Jelic V, Johansson SE, Almkvist O, Shigeta M, Julin P, Nordberg A, et al. Quantitative electroencephalography in mild cognitive impairment: longitudinal changes and possible prediction of Alzheimer's disease. *Neurobiol Aging.* (2000) 21:533–40. doi: 10.1016/S0197-4580(00)00153-6
52. Jeong J. EEG dynamics in patients with Alzheimer's disease. *Clin Neurophysiol.* (2004) 115:1490–505. doi: 10.1016/j.clinph.2004.01.001
53. Jackson CE, Snyder PJ. Electroencephalography and event-related potentials as biomarkers of mild cognitive impairment and mild Alzheimer's disease. *Alzheimers Dement.* (2008) 4(1 Suppl. 1):S137–43. doi: 10.1016/j.jalz.2007.10.008
54. Jelic V, Kowalski J. Evidence-based evaluation of diagnostic accuracy of resting EEG in dementia and mild cognitive impairment. *Clin EEG Neurosci.* (2009) 40:129–42. doi: 10.1177/155005940904000211
55. Babiloni C, Binetti G, Cassetta E, Cerboneschi D, Dal Forno G, Del Percio C, et al. Mapping distributed sources of cortical rhythms in mild Alzheimer's disease. A multicentric EEG study. *Neuroimage.* (2004) 22:57–67. doi: 10.1016/j.neuroimage.2003.09.028
56. Babiloni C, Binetti G, Cassetta E, Dal Forno G, Del Percio C, Ferreri F, et al. Sources of cortical rhythms change as a function of cognitive impairment in pathological aging: a multicenter study. *Clin Neurophysiol.* (2006) 117:252–68. doi: 10.1016/j.clinph.2005.09.019
57. Engedal K, Snaedal J, Hoegh P, Jelic V, Bo Andersen B, Naik M, et al. Quantitative EEG applying the statistical recognition pattern method: a useful tool in dementia diagnostic workup. *Dement Geriatr Cogn Disord.* (2015) 40:1–12. doi: 10.1159/000381016
58. Geraedts VJ, Koch M, Contarino MF, Middelkoop HAM, Wang H, van Hilten JJ, et al. Machine learning for automated EEG-based biomarkers of cognitive impairment during deep brain stimulation screening in patients with Parkinson's disease. *Clin Neurophysiol.* (2021) 132:1041–48. doi: 10.1016/j.clinph.2021.01.021
59. Geraedts VJ, Koch M, Kuiper R, Kefalas M, Bäck THW, van Hilten JJ, et al. Preoperative electroencephalography-based machine learning predicts cognitive deterioration after subthalamic deep brain stimulation. *Mov Disord.* (2021) 36:2324–34. doi: 10.1002/mds.28661
60. Frauscher B, von Ellenrieder N, Ferrari-Marinho T, Avoli M, Dubeau F, Gotman J. Facilitation of epileptic activity during sleep is mediated by high amplitude slow waves. *Brain.* (2015) 138(Pt 6):1629–41. doi: 10.1093/brain/awv073
61. Jiruska P, de Curtis M, Jefferys JG, Schevon CA, Schiff SJ, Schindler K. Synchronization and desynchronization in epilepsy: controversies and hypotheses. *J Physiol.* (2013) 591:787–97. doi: 10.1113/jphysiol.2012.239590
62. Zubler F, Rubino A, Lo Russo G, Schindler K, Nobili L. Correlating interictal spikes with sigma and delta dynamics during non-rapid-eye-movement-sleep. *Front Neurol.* (2017) 8:288. doi: 10.3389/fneur.2017.00288
63. Campana C, Zubler F, Gibbs S, de Carli F, Proserpio P, Rubino A, et al. Suppression of interictal spikes during phasic rapid eye movement sleep: a quantitative stereo-electroencephalography study. *J Sleep Res.* (2017) 26:606–613. doi: 10.1111/jsr.12533
64. Martinerie J, Adam C, Le Van Quyen M, Baulac M, Clemenceau S, Renault B, et al. Epileptic seizures can be anticipated by non-linear analysis. *Nat Med.* (1998) 4:1173–6. doi: 10.1038/2667
65. Le Van Quyen M, Adam C, Martinerie J, Baulac M, Clémenceau S, Varela F. Spatio-temporal characterizations of non-linear changes in intracranial activities prior to human temporal lobe seizures. *Eur J Neurosci.* (2000) 12:2124–34. doi: 10.1046/j.1460-9568.2000.00088.x
66. van Drongelen W, Nayak S, Frim DM, Kohrman MH, Towle VL, Lee HC, et al. Seizure anticipation in pediatric epilepsy: use of Kolmogorov entropy. *Pediatr Neurol.* (2003) 29:207–13. doi: 10.1016/S0887-8994(03)00145-0
67. Swisher CB, White CR, Mace BE, Dombrowski KE, Husain AM, Kolls BJ, et al. Diagnostic accuracy of electrographic seizure detection by neurophysiologists and non-neurophysiologists in the adult ICU using a panel of quantitative EEG trends. *J Clin Neurophysiol.* (2015) 32:324–30. doi: 10.1097/WNP.0000000000000144
68. Finnigan S, Wong A, Read S. Defining abnormal slow EEG activity in acute ischaemic stroke: delta/alpha ratio as an optimal QEEG index. *Clin Neurophysiol.* (2016) 127:1452–59. doi: 10.1016/j.clinph.2015.07.014
69. Haider HA, Esteller R, Hahn CD, Westover MB, Halford JJ, Lee JW, et al. Sensitivity of quantitative EEG for seizure identification in the intensive care unit. *Neurology.* (2016) 87:935–44. doi: 10.1212/WNL.0000000000003034
70. Hernández-Hernández MA, Fernández-Torre JL. Color density spectral array of bilateral bispectral index system: electroencephalographic correlate in comatose patients with nonconvulsive status epilepticus. *Seizure.* (2016) 34:18–25. doi: 10.1016/j.seizure.2015.11.001
71. Beniczky S, Conradsen I, Pressler R, Wolf P. Quantitative analysis of surface electromyography: biomarkers for convulsive seizures. *Clin Neurophysiol.* (2016) 127:2900–7. doi: 10.1016/j.clinph.2016.04.017
72. Beniczky S, Conradsen I, Henning O, Fabricius M, Wolf P. Automated real-time detection of tonic-clonic seizures using a wearable EMG device. *Neurology.* (2018) 90:e428–34. doi: 10.1212/WNL.0000000000004893
73. Lemesle M, Berriolo-Riedinger A, Touzery C, Guy F, Toubeau M, Crevenat E, et al. Correlation between inter-ictal regional cerebral blood flow and sphenoidal electrodes–recorded inter-ictal spikes in mesial temporal lobe epilepsy. *Neurol Res.* (2000) 22:674–8. doi: 10.1080/01616412.2000.11740738
74. Cascino GD, Trenerry MR, So EL, Sharbrough FW, Shin C, Lagerlund TD, et al. Routine EEG and temporal lobe epilepsy: relation to long-term EEG monitoring, quantitative MRI, and operative outcome. *Epilepsia*. (1996) 37:651–6. doi: 10.1111/j.1528-1157.1996.tb00629.x
75. Lee BI, Lee JD, Kim JY, Ryu YH, Kim WJ, Lee JH, et al. Single photon emission computed tomography-EEG relations in temporal lobe epilepsy. *Neurology.* (1997) 49:981–91. doi: 10.1212/WNL.49.4.981
76. Alexandre V, Mercedes B, Valton L, Maillard L, Bartolomei F, Szurhaj W, et al. Risk factors of postictal generalized EEG suppression in generalized convulsive seizures. *Neurology.* (2015) 85:1598–603. doi: 10.1212/WNL.0000000000001949
77. Arbune AA, Conradsen I, Cardenas DP, Whitmire LE, Voyles SR, Wolf P, et al. Ictal quantitative surface electromyography correlates with postictal EEG suppression. *Neurology.* (2020) 94:e2567–76. doi: 10.1212/WNL.0000000000009492
78. Finnigan S, van Putten MJ. EEG in ischaemic stroke: quantitative EEG can uniquely inform (sub-)acute prognoses and clinical management. *Clin Neurophysiol.* (2013) 124:10–9. doi: 10.1016/j.clinph.2012.07.003
79. Finnigan SP, Walsh M, Rose SE, Chalk JB. Quantitative EEG indices of sub-acute ischaemic stroke correlate with clinical outcomes. *Clin Neurophysiol.* (2007) 118:2525–32. doi: 10.1016/j.clinph.2007.07.021
80. Hunter AM, Cook IA, Leuchter AF. The promise of the quantitative electroencephalogram as a predictor of antidepressant treatment outcomes in major depressive disorder. *Psychiatr Clin North Am.* (2007) 30:105–24. doi: 10.1016/j.psc.2006.12.002
81. Claassen J, Taccone FS, Horn P, Holtkamp M, Stocchetti N, Oddo M. Recommendations on the use of EEG monitoring in critically ill patients: consensus statement from the neurointensive care section of the ESICM. *Intensive Care Med.* (2013) 39:1337–51. doi: 10.1007/s00134-013-2938-4
82. Herman ST, Abend NS, Bleck TP, Chapman KE, Drislane FW, Emerson RG, et al. Consensus statement on continuous EEG in critically ill adults and children, part I: indications. *J Clin Neurophysiol.* (2015) 32:87–95. doi: 10.1097/WNP.0000000000000166
83. Feng G, Jiang G, Li Z, Wang X. Prognostic value of electroencephalography (EEG) for brain injury after cardiopulmonary resuscitation. *Neurol Sci.* (2016) 37:843–9. doi: 10.1007/s10072-016-2475-3

84. Bjørk MH, Stovner LJ, Engstrøm M, Stjern M, Hagen K, Sand T. Interictal quantitative EEG in migraine: a blinded controlled study. *J Headache Pain.* (2009) 10:331–9. doi: 10.1007/s10194-009-0140-4
85. Bjørk MH, Stovner LJ, Nilsen BM, Stjern M, Hagen K, Sand T. The occipital alpha rhythm related to the "migraine cycle" and headache burden: a blinded, controlled longitudinal study. *Clin Neurophysiol.* (2009) 120:464–71. doi: 10.1016/j.clinph.2008.11.018
86. Vecchierini MF, André M, d'Allest AM. Normal EEG of premature infants born between 24 and 30 weeks gestational age: terminology, definitions and maturation aspects. *Neurophysiol Clin.* (2007) 37:311–23. doi: 10.1016/j.neucli.2007.10.008
87. André M, Lamblin MD, d'Allest AM, Curzi-Dascalova L, Moussalli-Salefranque F, T SNT, et al. Electroencephalography in premature and full-term infants. Developmental features and glossary. *Neurophysiol Clin.* (2010) 40:59–124. doi: 10.1016/j.neucli.2010.02.002
88. Bowen JR, Paradisis M, Shah D. Decreased aEEG continuity and baseline variability in the first 48 hours of life associated with poor short-term outcome in neonates born before 29 weeks gestation. *Pediatr Res.* (2010) 67:538–44. doi: 10.1203/PDR.0b013e3181d4ecda
89. Soubasi V, Mitsakis K, Sarafidis K, Griva M, Nakas CT, Drossou V. Early abnormal amplitude-integrated electroencephalography (aEEG) is associated with adverse short-term outcome in premature infants. *Eur J Paediatr Neurol.* (2012) 16:625–30. doi: 10.1016/j.ejpn.2012.02.008
90. Clarke AR, Barry RJ, McCarthy R, Selikowitz M. Electroencephalogram differences in two subtypes of attention-deficit/hyperactivity disorder. *Psychophysiology.* (2001) 38:212–21. doi: 10.1111/1469-8986.3820212
91. Barry RJ, Clarke AR, McCarthy R, Selikowitz M. EEG coherence in attention-deficit/hyperactivity disorder: a comparative study of two DSM-IV types. *Clin Neurophysiol.* (2002) 113:579–85. doi: 10.1016/S1388-2457(02)00036-6
92. Hermens DF, Soei EX, Clarke SD, Kohn MR, Gordon E, Williams LM. Resting EEG theta activity predicts cognitive performance in attention-deficit hyperactivity disorder. *Pediatr Neurol.* (2005) 32:248–56. doi: 10.1016/j.pediatrneurol.2004.11.009
93. Monastra VJ, Lubar JF, Linden M, VanDeusen P, Green G, cluster W, et al. Assessing attention deficit hyperactivity disorder via quantitative electroencephalography: an initial validation study. *Neuropsychology.* (1999) 13:424–33. doi: 10.1037/0894-4105.13.3.424
94. Arns M, Conners CK, Kraemer HC. A decade of EEG theta/beta ratio research in ADHD: a meta-analysis. *J Atten Disord.* (2013) 17:374–83. doi: 10.1177/1087054712460087
95. Loo SK, Cho A, Hale TS, McGough J, McCracken J, Smalley SL. Characterization of the theta to beta ratio in ADHD: identifying potential sources of heterogeneity. *J Atten Disord.* (2013) 17:384–92. doi: 10.1177/1087054712468050
96. Ogrim G, Kropotov J, Brunner JF, Candrian G, Sandvik L, Hestad KA. Predicting the clinical outcome of stimulant medication in pediatric attention-deficit/hyperactivity disorder: data from quantitative electroencephalography, event-related potentials, and a go/no-go test. *Neuropsychiatr Dis Treat.* (2014) 10:231–42. doi: 10.2147/NDT.S56600
97. Janssen TW, Bink M, Geladé K, van Mourik R, Maras A, Oosterlaan J. A randomized controlled trial into the effects of neurofeedback, methylphenidate, and physical activity on EEG power spectra in children with ADHD. *J Child Psychol Psychiatry.* (2016) 57:633–44. doi: 10.1111/jcpp.12517
98. Bioulac S, Purper-Ouakil D, Ros T, Blasco-Fontecilla H, Prats M, Mayaud L, et al. Personalized at-home neurofeedback compared with long-acting methylphenidate in an european non-inferiority randomized trial in children with ADHD. *BMC Psychiatry.* (2019) 19:237. doi: 10.1186/s12888-019-2218-0
99. Gevensleben H, Holl B, Albrecht B, Vogel C, Schlamp D, Kratz O, et al. Is neurofeedback an efficacious treatment for ADHD? A randomised controlled clinical trial. *J Child Psychol Psychiatry.* (2009) 50:780–9. doi: 10.1111/j.1469-7610.2008.02033.x
100. Larsen S, Sherlin L. Neurofeedback: an emerging technology for treating central nervous system dysregulation. *Psychiatr Clin North Am.* (2013) 36:163–8. doi: 10.1016/j.psc.2013.01.005
101. Hurt E, Arnold LE, Lofthouse N. Quantitative EEG neurofeedback for the treatment of pediatric attention-deficit/hyperactivity disorder, autism spectrum disorders, learning disorders, and epilepsy. *Child Adolesc Psychiatr Clin N Am.* (2014) 23:465–86. doi: 10.1016/j.chc.2014.02.001
102. Arns M, Drinkenburg W, Leon Kenemans J. The effects of QEEG-informed neurofeedback in ADHD: an open-label pilot study. *Appl Psychophysiol Biofeedback.* (2012) 37:171–80. doi: 10.1007/s10484-012-9191-4
103. Arns M, Heinrich H, Strehl U. Evaluation of neurofeedback in ADHD: the long and winding road. *Biol Psychol.* (2014) 95:108–15. doi: 10.1016/j.biopsycho.2013.11.013
104. Van Doren J, Arns M, Heinrich H, Vollebregt MA, Strehl U, S KL. Sustained effects of neurofeedback in ADHD: a systematic review and meta-analysis. *Eur Child Adolesc Psychiatry.* (2019) 28:293–305. doi: 10.1007/s00787-018-1121-4
105. Leuchter AF, Cook IA, Hunter A, Korb A. Use of clinical neurophysiology for the selection of medication in the treatment of major depressive disorder: the state of the evidence. *Clin EEG Neurosci.* (2009) 40:78–83. doi: 10.1177/155005940904000207
106. Leuchter AF, Cook IA, Hamilton SP, Narr KL, Toga A, Hunter AM, et al. Biomarkers to predict antidepressant response. *Curr Psychiatry Rep.* (2010) 12:553–62. doi: 10.1007/s11920-010-0160-4
107. Arns M, Bruder G, Hegerl U, Spooner C, Palmer DM, Etkin A, et al. EEG alpha asymmetry as a gender-specific predictor of outcome to acute treatment with different antidepressant medications in the randomized iSPOT-D study. *Clin Neurophysiol.* (2016) 127:509–19. doi: 10.1016/j.clinph.2015.05.032
108. Widge AS, Bilge MT, Montana R, Chang W, Rodriguez CI, Deckersbach T, et al. Electroencephalographic biomarkers for treatment response prediction in major depressive illness: a meta-analysis. *Am J Psychiatry.* (2019) 176:44–56. doi: 10.1176/appi.ajp.2018.17121358
109. Leuchter AF, Cook IA, Lufkin RB, Dunkin J, Newton TF, Cummings JL, et al. Cordance: a new method for assessment of cerebral perfusion and metabolism using quantitative electroencephalography. *Neuroimage.* (1994) 1:208–19. doi: 10.1006/nimg.1994.1006
110. Cook IA, Leuchter AF, Witte E, Abrams M, Uijtdehaage SH, Stubbeman W, et al. Neurophysiologic predictors of treatment response to fluoxetine in major depression. *Psychiatry Res.* (1999) 85:263–73. doi: 10.1016/S0165-1781(99)00010-4
111. Cook IA, Leuchter AF, Morgan M, Witte E, Stubbeman WF, Abrams M, et al. Early changes in prefrontal activity characterize clinical responders to antidepressants. *Neuropsychopharmacology.* (2002) 27:120–31. doi: 10.1016/S0893-133X(02)00294-4
112. Leuchter AF, Cook IA, Witte EA, Morgan M, Abrams M. Changes in brain function of depressed subjects during treatment with placebo. *Am J Psychiatry.* (2002) 159:122–9. doi: 10.1176/appi.ajp.159.1.122
113. Cook IA, Leuchter AF, Morgan ML, Stubbeman W, Siegman B, Abrams M. Changes in prefrontal activity characterize clinical response in SSRI nonresponders: a pilot study. *J Psychiatr Res.* (2005) 39:461–6. doi: 10.1016/j.jpsychires.2004.12.002
114. Bares M, Brunovsky M, Kopecek M, Stopkova P, Novak T, Kozeny J, et al. Changes in QEEG prefrontal cordance as a predictor of response to antidepressants in patients with treatment resistant depressive disorder: a pilot study. *J Psychiatr Res.* (2007) 41:319–25. doi: 10.1016/j.jpsychires.2006.06.005
115. Bares M, Brunovsky M, Kopecek M, Novak T, Stopkova P, Kozeny J, et al. Early reduction in prefrontal theta QEEG cordance value predicts response to venlafaxine treatment in patients with resistant depressive disorder. *Eur Psychiatry.* (2008) 23:350–5. doi: 10.1016/j.eurpsy.2008.03.001
116. Leuchter AF, Morgan M, Cook IA, Dunkin J, Abrams M, Witte E. Pretreatment neurophysiological and clinical characteristics of placebo responders in treatment trials for major depression. *Psychopharmacology (Berl).* (2004) 177:15–22. doi: 10.1007/s00213-004-1919-2
117. Jaworska N, de la Salle S, Ibrahim MH, Blier P, Knott V. Leveraging machine learning approaches for predicting antidepressant treatment response using electroencephalography (EEG) and clinical data. *Front Psychiatry.* (2018) 9:768. doi: 10.3389/fpsyt.2018.00768

118. Appleton SL, Vakulin A, D'Rozario A, Vincent AD, Teare A, Martin SA, et al. Quantitative electroencephalography measures in rapid eye movement and nonrapid eye movement sleep are associated with apnea-hypopnea index and nocturnal hypoxemia in men. *Sleep.* (2019) 42:zsz092 doi: 10.1093/sleep/zsz092
119. Roemer RA, Cornwell A, Dewart D, Jackson P, Ercegovac DV. Quantitative electroencephalographic analyses in cocaine-preferring polysubstance abusers during abstinence. *Psychiatry Res.* (1995) 58:247–57. doi: 10.1016/0165-1781(95)02474-B
120. Jones HE, Herning RI, Cadet JL, Griffiths RR. Caffeine withdrawal increases cerebral blood flow velocity and alters quantitative electroencephalography (EEG) activity. *Psychopharmacology (Berl).* (2000) 147:371–7. doi: 10.1007/s002130050005
121. D'Rozario AL, Cross NE, Vakulin A, Bartlett DJ, Wong KKH, Wang D, et al. Quantitative electroencephalogram measures in adult obstructive sleep apnea-Potential biomarkers of neurobehavioural functioning. *Sleep Med Rev.* (2017) 36:29–42. doi: 10.1016/j.smrv.2016.10.003
122. Stevens D, Leong CWY, Cheung H, Arciuli J, Vakulin A, Kim JW, et al. Sleep spindle activity correlates with implicit statistical learning consolidation in untreated obstructive sleep apnea patients. *Sleep Med.* (2021) 86:126–34. doi: 10.1016/j.sleep.2021.01.035
123. Ip CT, Olbrich S, Ganz M, Ozenne B, Köhler-Forsberg K, Dam VH, et al. Pretreatment qEEG biomarkers for predicting pharmacological treatment outcome in major depressive disorder: independent validation from the NeuroPharm study. *Eur Neuropsychopharmacol.* (2021) 49:101–12. doi: 10.1016/j.euroneuro.2021.03.024
124. Kuroda N, Sonoda M, Miyakoshi M, Nariai H, Jeong JW, Motoi H, et al. Objective interictal electrophysiology biomarkers optimize prediction of epilepsy surgery outcome. *Brain Commun.* (2021) 3:fcab042. doi: 10.1093/braincomms/fcab042
125. Musaeus CS, Salem LC, Kjaer TW, Waldemar G. Electroencephalographic functional connectivity is altered in persons with Down syndrome and Alzheimer's disease. *J Intell Disability Res.* (2021) 65:236–45. doi: 10.1111/jir.12803
126. Mohammadi Y, Moradi MH. Prediction of depression severity scores based on functional connectivity and complexity of the EEG signal. *Clin EEG Neurosci.* (2021) 52:52–60. doi: 10.1177/15500594209 65431

Conflict of Interest: The authors declare that the research was conducted in the absence of any commercial or financial relationships that could be construed as a potential conflict of interest.

Publisher's Note: All claims expressed in this article are solely those of the authors and do not necessarily represent those of their affiliated organizations, or those of the publisher, the editors and the reviewers. Any product that may be evaluated in this article, or claim that may be made by its manufacturer, is not guaranteed or endorsed by the publisher.

frontiers | Frontiers in Psychiatry

TYPE Original Research
PUBLISHED 29 June 2022
DOI 10.3389/fpsyt.2022.876036

OPEN ACCESS

EDITED BY
Junpeng Zhang,
Sichuan University, China

REVIEWED BY
Sangtae Ahn,
Kyungpook National University, South Korea
Remko van Lutterveld,
University Medical Center Utrecht, Netherlands

*CORRESPONDENCE
Suh-Yeon Dong
sydong@sookmyung.ac.kr
Seung-Hwan Lee
lshpss@hanmail.net

SPECIALTY SECTION
This article was submitted to Neuroimaging and Stimulation, a section of the journal Frontiers in Psychiatry

RECEIVED 15 February 2022
ACCEPTED 16 June 2022
PUBLISHED 29 June 2022

CITATION
Kim S, Yang C, Dong S-Y and Lee S-H (2022) Predictions of tDCS treatment response in PTSD patients using EEG based classification.
Front. Psychiatry 13:876036.
doi: 10.3389/fpsyt.2022.876036

Predictions of tDCS treatment response in PTSD patients using EEG based classification

Sangha Kim[1], Chaeyeon Yang[2], Suh-Yeon Dong[1]* and Seung-Hwan Lee[2,3,4]*

[1]Department of Information Technology Engineering, Sookmyung Women's University, Seoul, South Korea, [2]Clinical Emotion and Cognition Research Laboratory, Inje University, Goyang, South Korea, [3]Department of Psychiatry, Ilsan-Paik Hospital, Inje University, Goyang, South Korea, [4]Bwave Inc., Goyang, South Korea

Transcranial direct current stimulation (tDCS) is an emerging therapeutic tool for treating posttraumatic stress disorder (PTSD). Prior studies have shown that tDCS responses are highly individualized, thus necessitating the individualized optimization of treatment configurations. To date, an effective tool for predicting tDCS treatment outcomes in patients with PTSD has not yet been proposed. Therefore, we aimed to build and validate a tool for predicting tDCS treatment outcomes in patients with PTSD. Forty-eight patients with PTSD received 20 min of 2 mA tDCS stimulation in position of the anode over the F3 and cathode over the F4 region. Non-responders were defined as those with less than 50% improvement after reviewing clinical symptoms based on the Clinician-Administered DSM-5 PTSD Scale (before and after stimulation). Resting-state electroencephalograms were recorded for 3 min before and after stimulation. We extracted power spectral densities (PSDs) for five frequency bands. A support vector machine (SVM) model was used to predict responders and non-responders using PSDs obtained before stimulation. We investigated statistical differences in PSDs before and after stimulation and found statistically significant differences in the F8 channel in the theta band ($p = 0.01$). The SVM model had an area under the ROC curve (AUC) of 0.93 for predicting responders and non-responders using PSDs. To our knowledge, this study provides the first empirical evidence that PSDs can be useful biomarkers for predicting the tDCS treatment response, and that a machine learning model can provide robust prediction performance. Machine learning models based on PSDs can be useful for informing treatment decisions in tDCS treatment for patients with PTSD.

KEYWORDS

tDCS, PTSD, EEG, therapeutics, stimulation, machine learning

1. Introduction

Traumatic experiences, such as the coronavirus disease 2019 (COVID-19) pandemic, are highly prevalent in modern society (1). Therefore, it is essential to understand how to best help those affected by traumatic events as well as informing effective interventions to reduce their psychosocial impacts (2). Many studies have sought to identify the optimal

way to prevent and treat post-traumatic stress disorder (PTSD) (3–5), a series of reactions that can occur after someone has experienced traumatic events.

Transcranial direct current stimulation (tDCS) is a possible alternative treatment modality for addressing PTSD. More specifically, tDCS is a therapeutic tool that normalizes brain function and relieves symptoms by sending weak direct current stimulation to the brain surface through electrodes located on the scalp in order to spontaneously activate nerve cells. This is a safe neuromodulation technique that has few adverse effects (i.e., loss of consciousness, convulsions, abnormal sensations) as compared to other brain stimulation modalities (6).

Previous research has demonstrated that tDCS shows great promise as a therapeutic intervention for treating clinical neuropsychiatric disorders, including PTSD, depression, and cognitive decline. Auditory verbal hallucinations are robustly reduced by tDCS (7). Another study recently suggested that tDCS may be a promising novel treatment for addressing impulsivity in attention deficit hyperactivity disorder (ADHD) (8). A small number of studies have reported clinically significant improvements following tDCS treatment with respect to a range of cognitive and emotional performance metrics in PTSD patients evaluated using electroencephalograms (EEG), event-related potentials (ERP), and alpha peak frequencies (APF) (9).

In the current study, although tDCS treatment resulted in clinical improvements in patients with PTSD, not all patients were positively impacted by tDCS. Several patients showed a clinical response, while others showed no difference or even a worsening of their symptoms. tDCS modulates spontaneous neuronal activity, and the amount and direction of its effects critically depend on the physiological state of the target neural structures. Since the effects of tDCS depend on the baseline status of the brain at the time of application, individual patients show considerable heterogeneity in treatment outcomes (10). Consequently, tDCS responses are highly individualized, and this critically affects the evaluation of tDCS responses (11).

Supervised machine learning methods (e.g., support vector machines; SVM) can be used to identify and predict individual clinical responses in electric field characteristics following tDCS treatment (12). Individual prognostic classifications of tDCS outcomes can provide important insights for future tDCS interventions. However, to the best of our knowledge, there are currently no studies utilizing machine learning strategies in patients with PTSD undergoing tDCS treatment.

EEG has been used as a biomarker for detecting and classifying brain dysfunction. Previous work has demonstrated that various forms of brain disorders, including PTSD (13), schizophrenia (14), major depressive disorder (15) and Alzheimer's disease, can be diagnosed by monitoring patients' EEG responses. Therefore, analyses using EEG responses have the potential to identify clinical responses to neuropsychiatric treatments, including tDCS. This study aimed to demonstrate the potential of evaluating EEG responses in order to classify responders and non-responders among patients with PTSD. The results of this study might inform appropriate individualized treatments that can be adequately introduced by selecting patients based on their characteristics and expected treatment effects.

In this study, we compared electrophysiological responses before and after tDCS treatment by analyzing 62-channel EEG readings in 48 patients with PTSD. We aimed to provide a tool for increasing the effectiveness of tDCS by building and validating a personalized therapeutic response classification model. A machine learning model was trained to determine the best performing EEG channels and frequency bands. These features were also used to predict the outcomes of tDCS treatment in patients with PTSD. We hypothesized that (1) a statistically significant difference in the specific channel and frequency band that can be observed by comparing EEG responses before and after treatment between responders and non-responders, and (2) therapeutic responders and non-responders could be predicted and classified using the EEG features identified in (1).

2. Materials and methods

2.1. Participants

Fifty-one patients with PTSD were enrolled in this study. Patients were diagnosed by an experienced psychiatrist using the Structured Clinical Interview for DSM-V (SCID) Axis I Psychiatric Disorders (16). The Clinician-Administered PTSD Scale for DSM-5 (CAPS-5) was used to evaluate psychiatric symptoms (17, 18). Participants aged <19 years or those with too many EEG artifacts due to body and eye movements were excluded from the current study. A total of 48 patients (23 males, age 50.81 ± 11.60 years [mean ± SD]) were ultimately enrolled. All participants signed a written informed consent form that was approved by the institutional review board of Inje University, Ilsan Paik Hospital (IRB no. 2015-07-025). This study was conducted in accordance with the principles of the Declaration of Helsinki and its later amendments.

Abbreviations: ADHD, attention deficit hyperactivity disorder; APF, alpha peak frequency; AUC, area under the ROC curve; CAPS-5, Clinician-Administered PTSD Scale for DSM-5; COVID-19, coronavirus disease 2019; EEG, electroencephalogram; ERP, event-related potentials; FDR, false discovery rate; ICA, independent component analysis; PSD, power spectral density; PTSD, post-traumatic stress disorder; ROC curve, receiver operating characteristic curve; SCID, Structured Clinical Interview; Sev, total severity score; Sx, total number of prevalent PTSD symptoms; SVM, support vector machines; tDCS, transcranial direct current stimulation.

We categorized the patients into responders and non-responders based on their CAPS-5 scores. For the clinical assessment, total severity scores (Sev) and the total number of prevalent PTSD symptoms (Sx) were obtained for each patient. These scores statistically significantly decreased in both groups after tDCS stimulation [Sev: $t_{(47)} = 6.33$, $p < 0.001$, Sx: $t_{(47)} = 6.89$, $p < 0.001$]. Patients whose PTSD scores (total Sev scores and total Sx scores) improved by more than 50% were designated responders. The remaining participants were designated non-responders. In total, 31 participants were designated non-responders and the remaining 17 participants were designated responders.

Demographic data for the participants in each group are presented in Table 1. We additionally conducted comparisons between responders and non-responders on the different sub-scales of the main PTSD symptoms. The sub factors of PTSD symptoms in CAPS-5, intrusions (B), avoidance (C), negative affect and anhedonia (D) and externalizing, anxious arousal and dysphoric arousal (E), were obtained for comparison. Independent *t*-tests were employed to compare age, educational attainment, and Sev and Sx scores and other main scales across groups. Sev and Sx scores and other scales include pre- and post-treatment values measured before and after treatment, respectively.

TABLE 1 Demographic and clinical characteristics of responders and non-responders.

	Responders ($N = 17$)	Non-responders ($N = 31$)	*p*
Age (years)	51.18 ± 10.84	50.61 ± 12.17.	0.874
Sex			0.489
Male	7 (41.2)	16 (51.6)	
Female	10 (58.8)	15 (48.4)	
Education (years)	10.59 ± 4.37	11.65 ± 3.27	0.348
CAPS-5			
Pre			
B Sev	11.76 ± 5.95	10.77 ± 4.92	0.539
B Sx	3.47 ± 1.70	3.58 ± 1.52	0.973
C Sev	5.71 ± 2.49	3.48 ± 2.42	0.004
C Sx	1.59 ± 0.62	1.19 ± 0.83	0.115
D Sev	13.65 ± 6.59	13.16 ± 6.16	0.8
D Sx	4.06 ± 1.52	4.10 ± 1.80	0.815
E Sev	11.65 ± 4.43	10.35 ± 4.56	0.348
E Sx	3.53 ± 1.07	3.52 ± 1.39	0.973
Total Sev	42.76 ± 16.22	37.42 ± 13.29	0.224
Total Sx	12.65 ± 3.69	12.26 ± 4.07	0.745
Post			
B Sev	2.29 ± 2.17	7.87 ± 3.86	<0.001
B Sx	0.65 ± 0.79	2.61 ± 1.54	<0.001
C Sev	0.53 ± 1.23	4.32 ± 2.69	<0.001
C Sx	0.24 ± 0.56	1.55 ± 1.12	<0.001
D Sev	2.88 ± 2.87	10.77 ± 5.70	<0.001
D Sx	0.71 ± 0.92	3.42 ± 1.84	<0.001
E Sev	4.24 ± 2.82	7.13 ± 3.42	0.005
E Sx	1.35 ± 1.00	2.48 ± 1.43	0.008
Total Sev	9.94 ± 6.02	30.1 ± 9.64	<0.001
Total Sx	2.94 ± 2.3	10.06 ± 3.56	<0.001

PTSD, post-traumatic stress disorder; CAPS-5, clinician-administered PTSD scale for DSM-5; Sev, severity; Sx, symptoms; B, intrusions factor of CAPS-5; C, avoidance factor of CAPS-5; D, negative affect and anhedonia factor of CAPS-5; E, externalizing, anxious arousal and dysphoric arousal factor of CAPS-5.

2.2. tDCS protocol and application

Each tDCS session was applied using two saline-soaked sponge pads, with the anodal electrode positioned over the dorsolateral prefrontal cortex (with a F3 electrode location selected according to the International 10/20 System) and a cathode electrode placed over the F4 electrode. The position of the anode (F3) electrode montage is important in patients with posttraumatic stress disorder (PTSD) as it is closely related to the left dorsolateral prefrontal cortex (DLPFC). DLPFC plays a central role in emotional processing by regulating fear expression through projections to the vmPFC (19) and lateralized DLPFC dysfunction could be the underlying cause of stress and memory problems shown in PTSD patients (20). In addition, patients with PTSD showed weakly connected and hypoactive central executive network (CEN) where DLPFC is involved as a major node (21). We further applied tDCS on athode (F4) as the position determines current intensity of stimulation at the left DLPFC by affecting neuromodulation under the anode (22). Therefore, considering (a) previous studies supporting the relationship between abnormalities found in PTSD patients and DLPFC dysfunction (23, 24) and (b) the efficacy of tDCS for PTSD on DLPFC (25), this study involved right and left DLPFC (F3 and F4) as the stimulation area of tDCS for patients with PTSD.

The active stimulation protocol involved applying 2.0 mA intensity for 20 min. Participants sat quietly during the stimulation session, while the researcher monitored and recorded tDCS electrode impedances. Each subject received 1 tDCS session per day during 10 days. Thus, total 10 session of tDCS were applied for a subject.

2.3. EEG data acquisition

For EEG acquisition, the participants were seated in a slightly dim room for 3 min with their eyes-closed and in a relaxed state. During the experiment, all the participants were told in advance not to move or sleep. EEG data were acquired using a NeuroScan SynAmps amplifier (Compumedics

USA, Charlotte, NC, USA), and a NeuroScan Quick-Cap with 62 Ag/AgCl electrodes was placed according to the extended international 10–20 system. All recorded EEG data were sampled at 1,000 Hz and filtered using a 0.1–100 Hz bandpass filter. The electrode impedance was kept below 5 kΩ, with ground and reference electrodes located on the forehead and Cz reference point, respectively.

2.4. EEG preprocessing

Raw EEG data from 62 EEG channels (excluding HEO, VEO, and EKG channels) were preprocessed using EEGLAB (26) and MATLAB R2020a software (MathWorks, Natick, MA, USA). EEG data sampled at 1,000 Hz were re-referenced according to the common average reference and the baseline data was removed. A Butterworth bandpass filter was used to filter the EEG data with cutoff frequencies of 1 and 50 Hz. Artifacts caused by movements, such as those of the muscles and eyes, were rejected using a independent component analysis (ICA). More specifically, all independent components were filtered by visual inspection and segments containing large artifacts were excluded. After pre-processing, EEG segments with a length of 150 s were prepared based on data from 48 patients.

For each segment, power spectral density (PSD) was extracted using Welch's method (27). Welch PSD values were obtained using the built-in method in MATLAB (28, 29). More specifically, data were divided into several 1 s segments with 50% overlap. Next, each segment was windowed using the Hamming window and the periodogram of each windowed semgent was obtained after a fast Fourier transform. Finally, all periodograms were averaged to obtain the Welch PSD values for each participant using the average powers in five specific frequency bands: delta (1–4 Hz), theta (4–8 Hz), low alpha (8–10 Hz), high alpha (10–12 Hz), and beta (12–30 Hz).

2.5. Feature extraction

Figure 1 summarizes the analytical procedure used in this study. First, we investigated treatment outcomes by comparing PSD values before and after tDCS treatment, as shown in the upper pathway in Figure 1. To assess differences, we computed PSD change rates after treatment. Changes in the frequency band power over the treatment period were calculated using the following equation:

$$P_{change}(f) = \frac{P_{pre}(f) - P_{post}(f)}{P_{pre}(f)} \quad (1)$$

where $P_{pre}(f)$ is the pre-treatment PSD in a certain frequency band, and $P_{post}(f)$ is the post-treatment PSD in the same frequency band. By comparing $P_{change}(f)$ between responders and non-responders, we attempted to identify frequency bands that exhibited therapeutic effects and used these bands to predict treatment responses.

To predict treatment response, only pre-treatment PSD was used to classify responders and non-responders. Pre-PSD was used as the input to the classifier, as shown in the lower path in Figure 1.

2.6. Statistical analysis

An independent *t*-test was used to evaluate the mean difference in PSD change rates between responders and non-responders. Since the number of responders was less than 30, we performed the Kolmogorov-Smirnov test for normality and Levene's test for equality of variance. If normality was not satisfied, we employed a Mann-Whitney *U*-test instead of a two-sample *t*-test as appropriate. Moreover, we used multiple EEG channels to compare PSD change rates between the two groups. *P*-values were adjusted using the false discovery rate (FDR) to control for Type I errors. All statistical analyses were performed using R Statistical Software (version 4.1.1; R Foundation for Statistical Computing, Vienna, Austria).

2.7. Classification

An SVM was used to classify responders and non-responders using the PSD of the pre-treatment phase. SVM is well-known as a classic supervised learning classifier (30). In this study, the radial basis function was selected as the kernel function in the SVM to model complex nonlinear relationships. We used the grid search method with a range of C and γ values (ranging from 0.001 to 100) to adjust the optimal combination of SVM parameters. One combination of hyperparameters with the best cross-validation accuracy was selected and used to train an SVM on the entire dataset (31). Using each EEG channel's average powers from five frequency bands, we first split the data into training and testing sets for five-fold cross validation. For each fold, a grid search was performed to identify the optimal parameter values producing the best predictive model. Model evaluation was based on evaluations of the area under the receiver operating characteristic (ROC) curve (AUC). We calculated classification performance using the AUC as well as sensitivity and specificity. To avoid imbalance between two classes and get reasonable conclusion, we also computed balanced accuracy which is based on two common metrics, sensitiviy and specificity.

More specifically, we evaluated classification performance based on readings from a single EEG channel for each frequency band. We then improved the SVM model using multiple channels, starting from a single channel and iteratively adding channels one by one. We added a channel that best improved

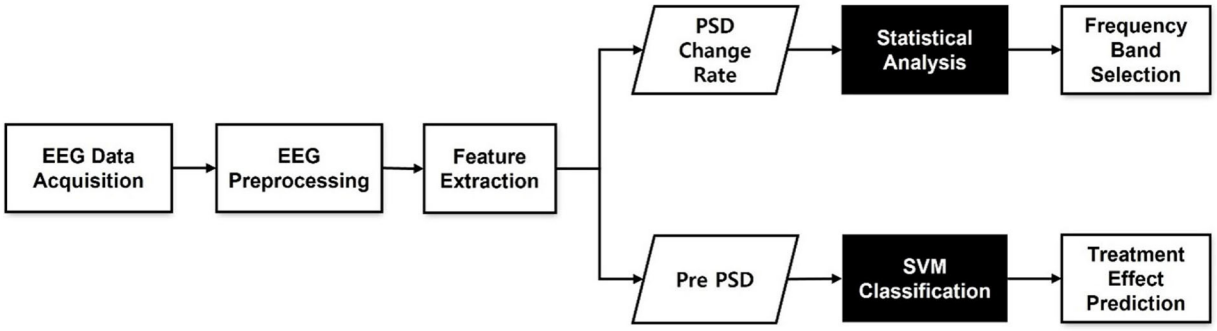

FIGURE 1
The flowchart of overall analysis procedure.

the model until all 62 channels were used for training. We aimed to design EEG channels for each frequency band to provide effective predictors of treatment outcomes. We also performed the cluster-based permutation test to deal with the multiple comparison problem in multi-channel EEG data. We produced 1,000 random permutations and *p*-values were obtained from the best SVM model which showed the highest AUC in multi-channel classification (32).

3. Results

3.1. Statistical analysis for treatment outcomes

To determine the frequency bands that could best select treatment outcomes following tDCS in patients with PTSD, we compared the rates of change in PSD values ($P_{change}(f)$) between responders and non-responders within five frequency bands. After FDR correction, some channels in the theta and beta bands showed statistically significant differences between groups. None of the channels in the remaining three frequency bands were found to be statistically significant. The theta band had six significant channels (F7, F8, FC6, FT8, P2, and POZ) and the beta band had 23 significant channels (AF3, AF4, F5, F3, F1, F2, F4, F6, F8, FC5, FC4, FC6, FT8, C3, C4, T8, CP3, CPZ, CP2, CP4, PZ, P2, and POZ) at a statistical significance level of 0.05. Although there were statistically significant differences of the rates of change in PSD values ($P_{change}(f)$) in those frequency bands, there were no existing significant differences in baseline power (pre-PSD). The F8 channel in the theta band [$t_{(39.348)} = -4.18$, $p < 0.001$] and the FC6 channel in the beta band [$t_{(42.95)} = -3.88$, $p < 0.001$] showed the strongest statistically significant differences. Figures 2A,B show the topographies of the averaged beta PSD change rates in responders and non-responders in beta frequency. As can be clearly seen in the figure, responders exhibited decreased beta PSD values within all 62 channels after treatment, with greater reductions especially in the frontal and centro-parietal regions. In contrast, in most non-responders, beta PSD values increased after treatment. Figure 2C illustrates the statistical significance of the topography of the logarithmic FDR-corrected *p*-values. Statistical significance was observed in the channels located in the frontal and centro-parietal regions. The FC6 channel in the frontal region, which showed the statistically strongest significant difference, showed a relatively large decrease of PSDs in responders (pre-PSD: 0.481 $\pm$ 0.32, post-PSD: 0.331 $\pm$ 0.172). On the other hand, it shows relatively large increase in non-responders (pre-PSD: 0.383 $\pm$ 0.286, post-PSD: 0.422 $\pm$ 0.355).

3.2. Prediction of treatment response

To determine whether pre-PSD reading could be used to predict treatment response, an SVM was trained to classify responders and non-responders. First, as a single-channel approach, the SVM model was trained for each channel and frequency band to identify the channels and bands that best represented the treatment response. SVM classification of all five bands accurately distinguished tDCS responders from non-responders, with AUCs ranging from 0.71 to 0.81 (delta: AUC = 0.81 at Cz; theta: AUC = 0.71 at FCz; alpha low: AUC = 0.72 at FC5; alpha high: AUC = 0.79 at FC2; beta: AUC = 0.78 at Pz). Figure 3 shows the topographies of the SVM classification performances in terms of the AUC for each frequency band.

Second, the multichannel approach improved the SVM classification between the two groups to a greater degree. More specifically, as shown in Figure 4, all five frequency bands usually demonstrate that the AUC increases for the first few channels and then continues to decrease as the number of channels increase. Therefore, the prediction accuracy reached its maximum in all frequency bands when using this multichannel approach. For the delta example, the single best prediction accuracy was 0.81 at Cz. However, adding the O1, FC2, FC1, and

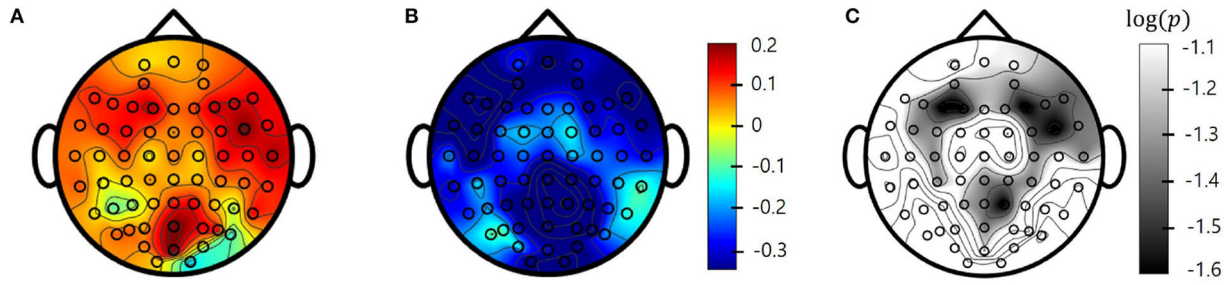

FIGURE 2
Topographies of beta band averaged power spectral density (PSD) change (pre-post) rates in **(A)** responders and **(B)** non-responders. **(C)** log-scaled adjusted *p*-values (corrected) from false discovery rate (FDR) obtained from two-sample *t*-tests also in Beta band. Values between electrodes are interpolated.

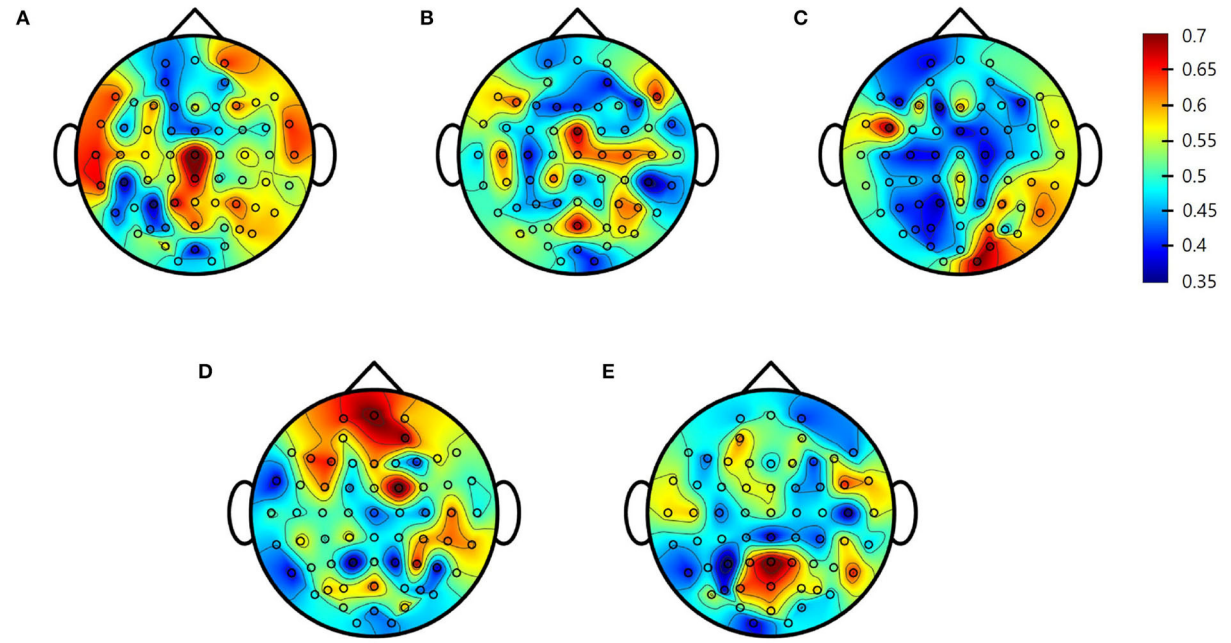

FIGURE 3
Single-channel support vector machine (SVM) performance (area under the receiving operating characteristics curve [AUC]) for each electrode. **(A)** Delta; **(B)** Theta; **(C)** Alpha Low; **(D)** Alpha High; **(E)** Beta.

F2 channels provided a much better performance at 0.93. Table 2 summarizes the prediction performance of the single-and multi-channel approaches in each frequency band.

4. Discussion

The present study investigated tDCS treatment responses using statistical analysis and machine learning techniques for EEG data in patients with PTSD. Each individual was defined as a responder or non-responder to tDCS treatment depending on psychiatric symptom changes assessed by the CAPS-5 evaluation. Since we acquired multi-channel EEG data before and after tDCS treatment, a comparison could easily be made to find the EEG feature best predicting responsiveness. Using the pre-delta PSDs for five selected channels (Cz, O1, FC2, FC1, and F2), the SVM model presented in this paper was able to predict an individual's tDCS responsiveness with an AUC of 0.93, despite the small size of the training data.

4.1. EEG for monitoring tDCS

Together with electrical stimulation, EEG monitoring can provide additional mechanistic information as well as

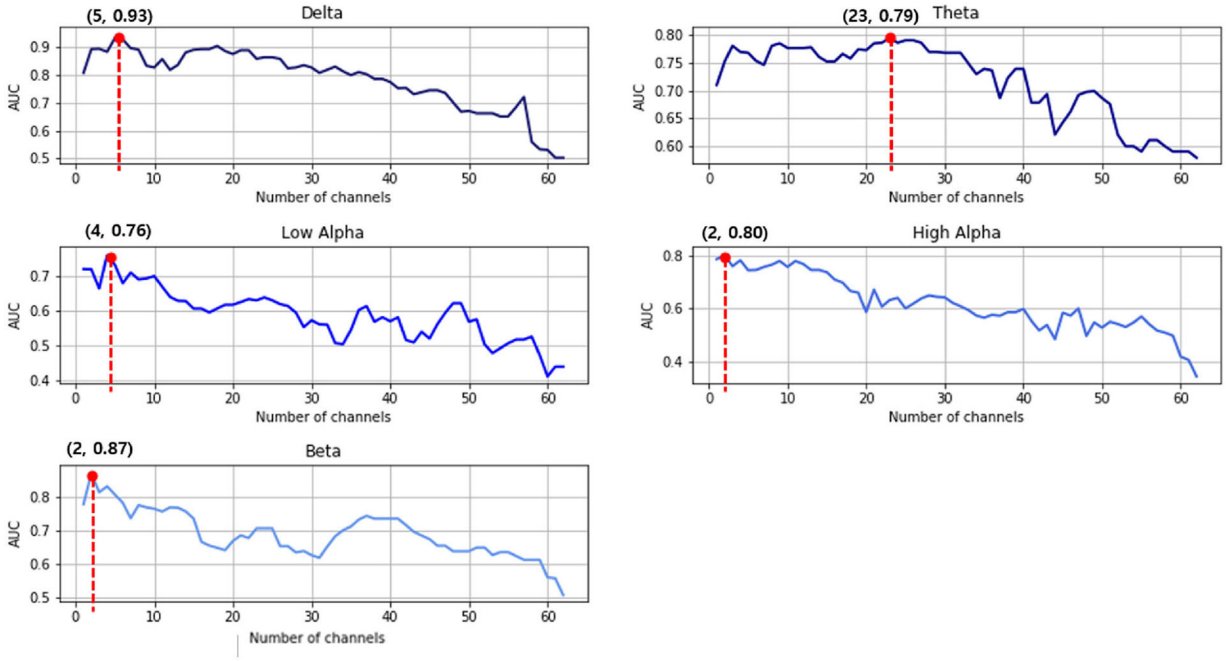

FIGURE 4
Support vector machine (SVM) prediction accuracy in the area under the receiving operating characteristics curve (AUC) for each frequency band. The red dots indicate the highest classification results of that frequency range.

TABLE 2 Support vector machine (SVM) classification results for the best channel per frequency range with pre-power spectral density (PSD) readings.

Frequency band	Single max					Multiple max					
	Channel	AUC	Sensitivity	Specificity	Balanced accuracy (%)	Channel	AUC	Sensitivity	Specificity	Balanced accuracy (%)	*p*-value
Delta	CZ	0.81	0.7	0.8	75.2	CZ, O1, FC2, FC1, F2 FCZ, POZ, CPZ, FZ, FC4, FC3, F6, FC1,	0.93	0.77	0.87	81.7	<0.001
Theta	FCZ	0.71	0.35	0.81	58.0	FC2, CP1, T8, AF4, CP2, CP4, F4, F2, C2, CZ, P6, CP5, FC5, P7, C6	0.79	0.12	0.97	54.2	0.006
Alpha Low	FC5	0.72	0.32	0.91	61.5	FC5, CP6, P2, PZ	0.76	0.13	0.93	53.3	0.011
Alpha High	FC2	0.79	0.53	0.87	70.2	FC2, P4	0.8	0.32	0.83	57.5	0.04
Beta	PZ	0.78	0.37	0.81	59.0	PZ, CP5	0.87	0.73	0.78	80.0	0.002

AUC, area under the receiver operating characteristics curve.

information regarding the clinical effects on brain function. EEG has been widely used to measure the cortical effects of tDCS. For example, Boonstra et al. (33) presented changes in mean frequency, demonstrating that the mean frequency was statistically significantly reduced after tDCS stimulation as compared to sham stimulation. Song et al. (34) observed a statistically significant increase in beta power during stimulation. Cavinato et al. (35) observed changes in cortical EEG oscillations, such as alpha and beta waves, in patients with disorders of consciousness. Similarly, we observed theta and beta power changes that were similar to other studies demonstrating spectral differences in PTSD patients with tDCS

treatment (36, 37). These two frequency bands, theta and beta, have been reported as the key observable indices for clinical effects of tDCS treatment related to major symptoms of PTSD, such as stress, depressive and anxiety. According to Palacios-García's study, the increase in psychosocial stress and stress-related anxiety was related to specific changes in beta-band (38). Dunkley also reported theta band plays a critical role in attentional, depressive and anxiety-related sequelae observed in PTSD populations (39). Therefore, our findings clinically suggest that the alleviation of PTSD symptoms, which is the effect of tDCS treatment, can be observed and monitored in patients' EEG.

Most of the aforementioned studies reported an increase in spectral power after stimulation, and this result was replicated in our study. However, when the participants were divided into responders and non-responders, this trend was observed only for non-responders. More specifically, the non-responders showed an increase, whereas the responders showed a decrease after treatment. As there were statistically significant group differences in PTSD Total sev and sx scores after treatment, as well as some sub scales of the CAPS (B, C, D and E), these spectral power differences could be related to clinical effects to PTSD in major symptoms such as intrusions, avoidance, negative affect and anhedonia. Especially in a key disease factor (avoidance, $P = 0.004$), the responder group differed significantly from the non-responder group, with a large effect size. Both groups present differently clinicaly at baseline. This avoidance factor in CAPS-5 is mainly related to the functional deterioration of the left frontal lobe (40, 41). The left frontal anodal tDCS performed in our study is a left frontal lobe activating protocol. Therefore, these numerical differences in the treatment responders suggest that the effect of tDCS treatment was clearly applied in the treatment responders.Since evaluating differences between responders and non-responders may help in identifying patients responsive to tDCS at early stages of treatment, it is crucial to compare patient groups through EEG monitoring.

4.2. Machine learning for predicting responsiveness

Owing to recent advances in machine learning, clinical outcomes can now be measured or evaluated using electrophysiological data. For instance, a study by Zandvakili et al. (42). presented an approach for predicting the clinical response to brain stimulation in mental disorders using resting EEG readings. Specifically, these researchers proposed an automated EEG classification to predict tDCS treatment outcomes in patients with major depressive disorder (MDD). Based on their proposed cognition labels, the evaluated machine learning classifier exhibited a high predictive performance (87%) using a single channel and an even higher predictive performance (92%) using multiple channels. Albizu et al. also reported an SVM model that could predict individual tDCS responsiveness with 86% accuracy (12).

Similar to the study conducted by Zandvakili et al, we evaluated prediction performance while comparing single channels and multiple channels. By comparing the performance of each of the five frequency bands, it was possible to identify specific channels and bands with high prediction performance. The proposed approach demonstrated that it is possible to predict therapeutic outcomes using resting EEG readings with relatively high performance and accuracy (AUC = 0.93). This result showed higher predictive performance than the case of logistic regression was performed with the baseline avoidance scale (AUC = 0.75), a key disease factor that showed a significant difference between the two groups in baseline. Furthermore, in each frequency band, EEG electrodes located in the middle line (e.g., FCZ, CZ, PZ) and electrodes placed in frontal region (e.g., FC5, FCZ, FC2) commonly showed the highest performance. The accurate prediction of tDCS response is meaningful because the efficiency of clinical treatment can be substantially increased given this information.

4.3. Study limitations

Despite the high performance of the predictions generated in this study, we acknowledge some limitations of this work. For example, the sample data were based on subjects who were diverse in age, with patients ranging in age from their 20s to their 70s. According to Bokszczanin's study, treatment outcomes may vary according to age and gender (43). However, differences in age-specific effects of tDCS treatment were not clearly observed in this study. In addition, the CAPS-5-based patient group assignments may not be divided clearly. As the degree of improvement varies substantially from person to person, some people are located near the boundary between response and nonresponse. We anticipate extending our study to a much larger and more comprehensive study population of patients with PTSD so that the therapeutic effects of tDCS can be comprehensively identified and predicted.

5. Conclusions

The current study investigated tDCS treatment responsiveness in patients with PTSD using EEG spectral power and machine learning-based prediction methods. In this study, the evaluated patients in the two groups showed statistically significant differences in EEG spectral power in the theta and beta frequency bands with respect to their treatment response. In addition, we demonstrated that machine-learning-based classifications can predict tDCS treatment outcomes

with considerable accuracy. From these results, it is possible to identify specific channels and bands that most accurately represent the tDCS response in patients with PTSD. Despite one of the aforementioned limitations (i.e., that we only considered two labels for CAPS-5), we conclude that these results have the potential to hold new insights as a basis for diagnosing and predicting the clinical response to tDCS treatment. These results could therefore provide critical information informing a meaningful approach for the early identification of patients who might be clinically affected by tDCS treatment, thus reducing the cost and time these patients would otherwise expend during the treatment process. Our findings inform future research directions, and, if confirmed, are expected to ultimately inform medical guidelines.

Data availability statement

The datasets presented in this article are not readily available because of ethical concerns. Requests to access the datasets should be directed to S-HL, lshpss@hanmail.net.

Ethics statement

The studies involving human participants were reviewed and approved by the Institutional Review Board of Inje University, Ilsan Paik Hospital (IRB no. 2015-07-025). The patients/participants provided their written informed consent to participate in this study.

Author contributions

SK: data analysis and writing-original draft. CY: data collection and writing-review and editing. S-YD: conceptualization, funding acquisition, and writing-review and editing. S-HL: conceptualization, supervision, and writing-review and editing. All authors contributed to the article and approved the submitted version.

Funding

This research was supported by KBRI Basic Research Program through Korea Brain Research Institute funded by Ministry of Science and ICT (22-BR-02-02), the Commercialization Promotion Agency for R&D Outcomes (COMPA) funded by the Ministry of Science and ICT (MSIT) (Commercialization of health functional foods by verifying the efficacy of functional ingredients and developing the selection method of appropriate content based on AI), and by Sookmyung Women's University Research Grants (1-2203-2006).

Conflict of interest

S-HL was employed by Bwave Inc.

The remaining authors declare that the research was conducted in the absence of any commercial or financial relationships that could be construed as a potential conflict of interest.

Publisher's note

All claims expressed in this article are solely those of the authors and do not necessarily represent those of their affiliated organizations, or those of the publisher, the editors and the reviewers. Any product that may be evaluated in this article, or claim that may be made by its manufacturer, is not guaranteed or endorsed by the publisher.

References

1. Kessler RC, Aguilar-Gaxiola S, Alonso J, Benjet C, Bromet EJ, Cardoso G, et al. Trauma and PTSD in the WHO world mental health surveys. *Eur J Psychotraumatol*. (2017) 8:1353383. doi: 10.1080/20008198.2017.1353383

2. Bisson JI, Olff M. Prevention and treatment of PTSD: the current evidence base. *Eur J Psychotraumatol*. (2020) 12:1824381. doi: 10.1080/20008198.2020.1824381

3. Shalev AY, Peri T, Canetti L, Schreiber S. Predictors of PTSD in injured trauma survivors: a prospective study. *Am J Psychiatry*. (1996) 153:219–25. doi: 10.1176/ajp.153.2.219

4. Wells A, Sembi S. Metacognitive therapy for PTSD: a preliminary investigation of a new brief treatment. *J Behav Ther Exp Psychiatry*. (2004) 35:307–18. doi: 10.1016/j.jbtep.2004.07.001

5. Ehlers A, Clark DM, Hackmann A, Grey N, Liness S, Wild J, et al. Intensive cognitive therapy for PTSD: a feasibility study. *Behav Cogn Psychother*. (2010) 38:383–98. doi: 10.1017/S1352465810000214

6. Brunoni AR, Nitsche MA, Bolognini N, Bikson M, Wagner T, Merabet L, et al. Clinical research with transcranial direct current stimulation (tDCS): challenges and future directions. *Brain Stimul*. (2012) 5:175–95. doi: 10.1016/j.brs.2011.03.002

7. Brunelin J, Mondino M, Gassab L, Haesebaert F, Gaha L, Suaud-Chagny MF, et al. Examining transcranial direct-current stimulation (tDCS) as a treatment for hallucinations in schizophrenia. *Am J Psychiatry*. (2012) 169:719–24. doi: 10.1176/appi.ajp.2012.11071091

8. Allenby C, Falcone M, Bernardo L, Wileyto EP, Rostain A, Ramsay JR, et al. Transcranial direct current brain stimulation decreases impulsivity in ADHD. *Brain Stimul*. (2018) 11:974–81. doi: 10.1016/j.brs.2018.04.016

9. Saunders N, Downham R, Turman B, Kropotov J, Clark R, Yumash R, et al. Working memory training with tDCS improves behavioral and neurophysiological symptoms in pilot group with post-traumatic stress disorder (PTSD) and with poor working memory. *Neurocase*. (2015) 21:271–8. doi: 10.1080/13554794.2014.890727

10. Woods AJ, Antal A, Bikson M, Boggio PS, Brunoni AR, Celnik P, et al. A technical guide to tDCS, and related non-invasive brain stimulation tools. *Clin Neurophysiol*. (2016) 127:1031–48. doi: 10.1016/j.clinph.2015.11.012

11. Hsu TY, Juan CH, Tseng P. Individual differences and state-dependent responses in transcranial direct current stimulation. *Front Hum Neurosci*. (2016) 10:643. doi: 10.3389/fnhum.2016.00643

12. Albizu A, Fang R, Indahlastari A, OShea A, Stolte SE, See KB, et al. Machine learning and individual variability in electric field characteristics

predict tDCS treatment response. *Brain Stimul*. (2020) 13:1753–64. doi: 10.1016/j.brs.2020.10.001

13. Kim YW, Kim S, Shim M, Jin MJ, Jeon H, Lee SH, et al. Riemannian classifier enhances the accuracy of machine-learning-based diagnosis of PTSD using resting EEG. *Progr Neuropsychopharmacol Biol Psychiatry*. (2020) 102:109960. doi: 10.1016/j.pnpbp.2020.109960

14. Kim JY, Lee HS, Lee SH. EEG source network for the diagnosis of schizophrenia and the identification of subtypes based on symptom severity–A machine learning approach. *J Clin Med*. (2020) 9:3934. doi: 10.3390/jcm9123934

15. Al-Kaysi AM, Al-Ani A, Loo CK, Powell TY, Martin DM, Breakspear M, et al. Predicting tDCS treatment outcomes of patients with major depressive disorder using automated EEG classification. *J Affect Disord*. (2017) 208:597–603. doi: 10.1016/j.jad.2016.10.021

16. Association AP. *Diagnostic and Statistical Manual of Mental Disorders: DSM-5 (AP Association Ed.)*. Washington DC: American Psychiatric Pub (2013).

17. Blake DD, Weathers FW, Nagy LM, Kaloupek DG, Gusman FD, Charney DS, et al. The development of a clinician-administered PTSD scale. *J Trauma Stress*. (1995) 8:75–90. doi: 10.1002/jts.2490080106

18. Weathers FW, Bovin MJ, Lee DJ, Sloan DM, Schnurr PP, Kaloupek DG, et al. The clinician-administered PTSD scale for DSM-5 (CAPS-5): development and initial psychometric evaluation in military veterans. *Psychol Assess*. (2018) 30:383. doi: 10.1037/pas0000486

19. Hartley CA, Phelps EA. Changing fear: the neurocircuitry of emotion regulation. *Neuropsychopharmacology*. (2010) 35:136–46. doi: 10.1038/npp.2009.121

20. Moran JK, Crombach A, Elbert T, Nandi C, Bambonyé M, Wienbruch C, et al. The individual contribution of DSM 5 symptom clusters of PTSD, life events, and childhood adversity to frontal oscillatory brain asymmetry in a large sample of active combatants. *Biol Psychol*. (2017) 129:305–13. doi: 10.1016/j.biopsycho.2017.09.014

21. Akiki TJ, Averill CL, Abdallah CG. A network-based neurobiological model of PTSD: evidence from structural and functional neuroimaging studies. *Curr Psychiatry Rep*. (2017) 19:1–10. doi: 10.1007/s11920-017-0840-4

22. Bikson M, Datta A, Rahman A, Scaturro J. Electrode montages for tDCS and weak transcranial electrical stimulation: role of "return" electrodes position and size. *Clin Neurophysiol*. (2010) 121:1976. doi: 10.1016/j.clinph.2010.05.020

23. Aupperle RL, Allard CB, Grimes EM, Simmons AN, Flagan T, Behrooznia M, et al. Dorsolateral prefrontal cortex activation during emotional anticipation and neuropsychological performance in posttraumatic stress disorder. *Arch Gen Psychiatry*. (2012) 69:360–71. doi: 10.1001/archgenpsychiatry.2011.1539

24. Zwanzger P, Steinberg C, Rehbein MA, Bröckelmann AK, Dobel C, Zavorotnyy M, et al. Inhibitory repetitive transcranial magnetic stimulation (rTMS) of the dorsolateral prefrontal cortex modulates early affective processing. *Neuroimage*. (2014) 101:193–203. doi: 10.1016/j.neuroimage.2014.07.003

25. Ahmadizadeh MJ, Rezaei M, Fitzgerald PB. Transcranial direct current stimulation (tDCS) for post-traumatic stress disorder (PTSD): a randomized, double-blinded, controlled trial. *Brain Res Bull*. (2019) 153:273–8. doi: 10.1016/j.brainresbull.2019.09.011

26. Delorme A, Makeig S. EEGLAB: an open source toolbox for analysis of single-trial EEG dynamics including independent component analysis. *J Neurosci Methods*. (2004) 134:9–21. doi: 10.1016/j.jneumeth.2003.10.009

27. Welch P. The use of fast Fourier transform for the estimation of power spectra: a method based on time averaging over short, modified periodograms. *IEEE Trans Audio Electroacoust*. (1967) 15:70–3. doi: 10.1109/TAU.1967.1161901

28. Hayes M. *Statistical Digital Signal Processing and Modeling*. 2nd ed. New York, NY: John Wiley & Sons (1996).

29. Stoica P, Moses RL. *Spectral Analysis of Signals*. Upper Saddle River, NJ: Pearson Prentice Hall (2005).

30. Suthaharan S. Support vector machine. In: *Machine Learning Models and Algorithms for Big Data Classification*. Boston, MA: Springer (2016). p. 207–35

31. Syarif I, Prugel-Bennett A, Wills G. SVM parameter optimization using grid search and genetic algorithm to improve classification performance. *Telkomnika*. (2016) 14:1502. doi: 10.12928/telkomnika.v14i4.3956

32. Park SM, Jeong B, Oh DY, Choi CH, Jung HY, Lee JY, et al. Identification of major psychiatric disorders from resting-state electroencephalography using a machine learning approach. *Front Psychiatry*. (2021) 1398:707581. doi: 10.3389/fpsyt.2021.707581

33. Boonstra TW, Nikolin S, Meisener AC, Martin DM, Loo CK. Change in mean frequency of resting-state electroencephalography after transcranial direct current stimulation. *Front Hum Neurosci*. (2016) 10:270. doi: 10.3389/fnhum.2016.00270

34. Song M, Shin Y, Yun K. Beta-frequency EEG activity increased during transcranial direct current stimulation. *Neuroreport*. (2014) 25:1433–6. doi: 10.1097/WNR.0000000000000283

35. Cavinato M, Genna C, Formaggio E, Gregorio C, Storti SF, Manganotti P, et al. Behavioural and electrophysiological effects of tDCS to prefrontal cortex in patients with disorders of consciousness. *Clin Neurophysiol*. (2019) 130:231–8. doi: 10.1016/j.clinph.2018.10.018

36. Mangia AL, Pirini M, Cappello A. Transcranial direct current stimulation and power spectral parameters: a tDCS/EEG co-registration study. *Front Hum Neurosci*. (2014) 8:601. doi: 10.3389/fnhum.2014.00601

37. Schestatsky P, Morales-Quezada L, Fregni F. Simultaneous EEG monitoring during transcranial direct current stimulation. *J Visu Exp*. (2013) 76:e50426. doi: 10.3791/50426

38. Palacios-García I, Silva J, Villena-González M, Campos-Arteaga G, Artigas-Vergara C, Luarte N, et al. Increase in beta power reflects attentional top-down modulation after psychosocial stress induction. *Front Hum Neurosci*. (2021) 15:630813. doi: 10.3389/fnhum.2021.630813

39. Dunkley BT, Sedge PA, Doesburg SM, Grodecki RJ, Jetly R, Shek PN, et al. Theta, mental flexibility, and post-traumatic stress disorder: connecting in the parietal cortex. *PLoS ONE*. (2015) 10:e0123541. doi: 10.1371/journal.pone.0123541

40. Berkman ET, Lieberman MD. Approaching the bad and avoiding the good: lateral prefrontal cortical asymmetry distinguishes between action and valence. *J Cogn Neurosci*. (2010) 22:1970–9. doi: 10.1162/jocn.2009.21317

41. Kelley NJ, Hortensius R, Schutter DJ, Harmon-Jones E. The relationship of approach/avoidance motivation and asymmetric frontal cortical activity: a review of studies manipulating frontal asymmetry. *Int J Psychophysiol*. (2017) 119:19–30. doi: 10.1016/j.ijpsycho.2017.03.001

42. Zandvakili A, Philip NS, Jones SR, Tyrka AR, Greenberg BD, Carpenter LL. Use of machine learning in predicting clinical response to transcranial magnetic stimulation in comorbid posttraumatic stress disorder and major depression: a resting state electroencephalography study. *J Affect Disord*. (2019) 252:47–54. doi: 10.1016/j.jad.2019.03.077

43. Bokszczanin A. PTSD symptoms in children and adolescents 28 months after a flood: age and gender differences. *J Traumatic Stress*. (2007) 20:347–51. doi: 10.1002/jts.20220

Frontiers in Psychiatry

Explores and communicates innovation in the field of psychiatry to improve patient outcomes

The third most-cited journal in its field, using translational approaches to improve therapeutic options for mental illness, communicate progress to clinicians and researchers, and consequently to improve patient treatment outcomes.

Discover the latest Research Topics

See more →

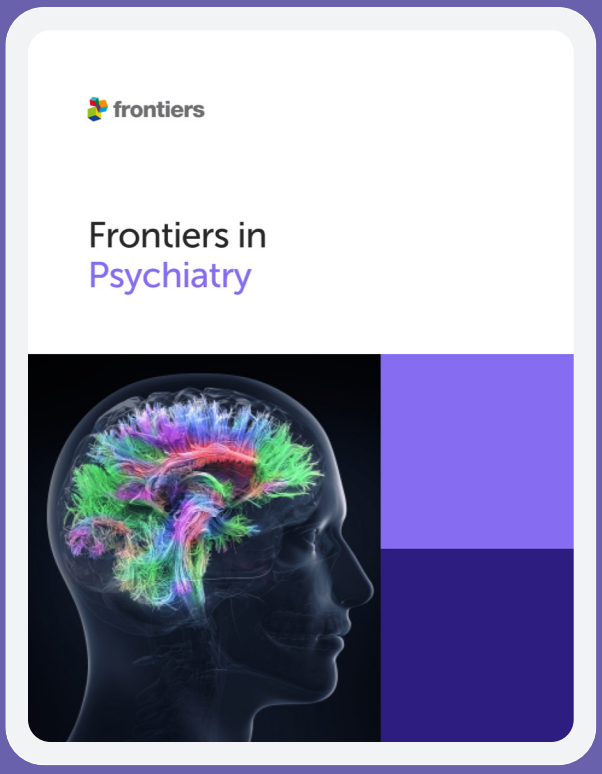

Frontiers

Avenue du Tribunal-Fédéral 34
1005 Lausanne, Switzerland
frontiersin.org

Contact us

+41 (0)21 510 17 00
frontiersin.org/about/contact